STUDIES OF CALCIUM ISOTOPE FRACTIONATION FOUND IN NATURE AND PRODUCED DURING ION SPUTTERING

Thesis by

William A. Russell

In Partial Fulfillment of the Requirements

for the Degree of

Doctor of Philosophy

California Institute of Technology
Pasadena, California

1979

(Submitted November 8, 1978)

Acknowledgments

I am grateful to the many people who have come into my life while at Caltech, both those who aided me with their scientific insight and technical abilities, and those who were simply pleasant to be around. I owe a great debt of gratitude to Tom Greenlee who, in his quiet way, persuaded me to come to Lake Avenue Congregational Church at a time when I was discouraged at not finding a fellowship of believers that I could really be at home with. There I met my Savior and Lord of many years, Jesus Christ, in a fresh new way. The burdens of working hard as a graduate student then became much more pleasant as I grew more and more aware of His daily care and love for me. Thanks to Him, interest in His Church was rekindled, and Kathy, my wife, and I found ourselves teaching delightful children about Jesus, singing praises to Him in the choir, and being involved in various other activities. He has been working in me for good, both at Lake and in my preparation at Caltech for a scientific career.

A number of people at Caltech have been particularly helpful and influential through their supervision, advice, patience, insight, and friendship. My professor, Tom Tombrello, is interested in so many different areas that it is easy to find interesting problems to work on with him. I appreciate his insight, personal and scientific, which are of so much importance when guiding students. I have always felt so lucky to have ended up with him as an advisor, especially since I was unsure as to what areas I wanted to work in, even after being at Caltech for a year and a half. Gerry Wasserburg was very kind in allowing a physics student to come into his geological environs and to take up a

project which, as initially conceived, was probably mostly of interest to a few physicists. He was always interested in keeping the research focussed in the most productive direction. The many hours spent with him in one-on-one sessions have been extremely useful and have instilled a heightened ability to think scientifically and critically which I hope is reflected to some degree in this document. His accessibility even on days when deluged with other business has been invaluable. Dimitri Papanastassiou, whom I have had the most contact with on a day-to-day basis, has helped me in many areas. I feel that he has successfully transmitted some fraction of his scientific paper-writing abilities, and this is perhaps one of the most useful things I have learned at Caltech. He allowed me to debate with him as an equal about the whole gamut of technical and scientific issues we encountered. He was willing to explain things about his and other people's work at times when a less patient person would have said, "Go read the paper." His aptitude at dogging problems with the mass spectrometers until they were solved, and at managing a lab with many people of diverse personalities is greatly appreciated by me and the other Lunatic Asylum inmates.

My loving wife Kathy is in so many ways responsible for the happiness of these years at Caltech. "A woman who fears the Lord is to be honored . . . is to be praised." Her sweetness and laughter are truly a joy.

I would like to thank my parents so much for their guidance and love. Though my dad is gone, I feel that he is in many ways responsible for this successful outcome. To my mother, from whom I have inherited a love of music, I am grateful for this priceless gift.

The National Science Foundation 14 years ago sponsored an experimental project whereby selected seventh grade students would learn an entire year's worth of high school biology, chemistry, and physics during successive summers. During the school years, high school and college mathematics were taught on Saturdays. These intensive programs gave me a first satisfying taste of science in a way which would have never been possible in a normal high school science class environment. Dr. Milton Saslaw, who later became director of the Dade County Board of Public Health, was responsible for this program. Caltech has a more modest Saturday program for high school students; I am convinced that the dividends from such programs are very high.

My good friend and undergraduate professor, George Alexandrakis, played a large role in helping me to find "a good place" to go to graduate school and has had continued interest in my welfare.

I would like to thank Dr. Sam Epstein for graciously allowing us to conduct some of our lunar soil experiments in his laboratory. Bob Lewis was most helpful in showing me how to use to advantage many of the capabilities of the SEM and X-ray analysis system. Many people at Caltech have provided valuable discussions. These include Alex Gancarz, Bob Weller, Typhoon Lee, Bob Kelly, Felix Oberli, Joe Griffith, and Dr. David Goodstein.

I would like to thank several people whom I met outside of Caltech and have grown very fond of: Doc Sam Allen, who is clearly right at home at Caltech (there is photographic evidence!), Stan and Martha Fedora, who are still honeymooners years after the fact, Anne

Dodge and family, Terry and Linda Wagner, Anita Brewer, Maryann Olofsson, Maybelle Allen, Bruce Leafblad, and Pastors Marvin Jacobs and Ray Ortlund.

The technical expertise of Jan Scott and Joanne Clark was indispensable for the production of this thesis. The cheeriness of Dr. Wasserburg's secretaries, Elizabeth Ball, Evelyn Brown, and Nan Orshan, was always amazing and appreciated.

The permission of the American Chemical Society and of Pergamon Press to reproduce the papers contained in Chapters 2, and 3 and 4, respectively, is gratefully acknowledged.

This research project has been supported in part by the National Science Foundation and the National Aeronautics and Space Administration.

Abstract

High precision analytical techniques have been developed for the measurement of calcium isotopic abundances in samples as small as 2×10^{-9} mole. Typical relative uncertainties for measurement of calcium isotope abundance ratios are $1 - 4 \times 10^{-4}$, and isotopic differences between samples arising from mass fractionation can be resolved to 1×10^{-4} per unit mass difference.

Variation of Ca isotope compositions in the solar system has been studied through analysis of meteorites, lunar samples, and terrestrial samples. Terrestrial, lunar, and meteoritic Ca isotopic fractionation ranges overlap and are about 2.5‰ for $^{40}Ca/^{44}Ca$. The small range of effects does not permit at present identification of the mechanisms leading to the isotopic fractionation.

Measurements were carried out for Ca leached with water from a lunar soil. Large O, Si, and S isotopic fractionation of components residing near the surfaces of the grains of this soil have been found previously. The Ca was found to be definitely mass fractionated, but only to a small extent. Either only small Ca fractionation is present, or bulk, unfractionated material was also removed and diluted the effects.

Sputtering by the solar wind is one mechanism which might have led to the thin, isotopically heavy coatings on lunar soil grains. This might occur either directly by the sputtering process or by escape from the lunar gravitational field of different fractions of the sputtered species. Experiments reported here show that substantial isotopic

fractionation arises directly from sputtering. Terrestrial samples were sputtered with relatively low current 130 keV N^+ or 100 keV N_2^+ beams. Sputtered Ca was collected over a wide range of angles and later analyzed. It has been found that at 130 keV, the first Ca removed is isotopically light, ranging from $\delta(^{40}Ca/^{44}Ca) = +11$ to $+13$ for the fluorite and apatite samples studied. Further sputtering causes the fractionation of the material being collected to decrease, achieving unfractionated and, for one sample, negative δ values. The initial fractionation behavior using 100 keV N_2^+ has not been thoroughly investigated, although initial sputtering of a plagioclase sample yielded $\delta(^{40}Ca/^{44}Ca) = +21$. Eventual achievement of unfractionated values is viewed as an attainment of equilibrium in which the surface of the target has become isotopically heavy by an amount sufficient to counter the positive fractionation produced by the sputtering. Two attempts have been made to measure the approximate thickness of this $\delta < 0$ surface layer by changing to a 100 keV N_2^+ beam after extensive sputtering at 130 keV. For a single crystal of CaF_2, the thickness was measured to be at least 1000 Å. A polycrystalline CaF_2 sample showed no evidence of such a thick layer. This may be caused by minor differences in target temperatures or by atomic mixing in the targets which proceeded to greater depths in the single crystal. SEM photographs, though, show no conclusive evidence of substantial heating by the beam of large areas of the targets. The data provide various indications that atomic mixing is important in controlling the effects. Mixing appears to be slow, and may not efficiently bring unfractionated material from the end of the ion beam range up into the very

near surface region.

Measurements show that there are large differences in the fractionation of Ca sputtered in different directions. These variations with ejection angle also change with increasing ion bombardment. The initial material sputtered had $\delta > 0$ at all angles, with a maximum at intermediate angles. After further sputtering at the same energy, the normally ejected material had $\delta > 0$, while the obliquely sputtered material had $\delta < 0$. In this case and in the case of Ca subsequently sputtered with 100 keV N_2, the total range of effects was 16 ‰ for $^{40}Ca/^{44}Ca$. It has been proposed that simple kinematic differences in the scattering of light and heavy isotopes off of each other at the target surface could account for similar effects which are seen with very low energy sputtering. Such differences could probably not have been important at the high beam energies used here; another mechanism must be responsible.

These sputtering experiments roughly simulate the solar wind conditions in terms of the beam energy per mass unit and in terms of the sputtering yields. The large effects indicate the likelihood that fractionation intrinsic to sputtering was a major mechanism contributing to the lunar soil isotopic fractionation.

TABLE OF CONTENTS

CHAPTER 1. INTRODUCTION

The use of various sites on the surface of the moon as observing stations for the study of physical phenomena was not implemented solely through the various instrument packages emplaced by the astronauts and by the unmanned probes. The returned lunar samples have as well afforded opportunities for such studies. Being a body with no atmosphere or strong magnetic fields, the moon is continually bombarded on its day-light side by low energy (few keV) hydrogen and helium atoms from the sun, the so-called solar wind. Sporadic flares on the solar surface cause large fluxes of high-energy (1 - 100 MeV) particles, primarily protons, to also bombard the lunar surface. Galactic cosmic ray particles, with energies ranging from 100 MeV - 10 GeV per nucleon mass, impinge on the lunar surface at a rate of about 1 $cm^{-2}\,sec^{-1}$ (cf. Taylor, 1975). Micron-sized micrometeorites or "cosmic dust" particles strike the lunar surface with a flux of about 1 $cm^{-2}\,yr^{-1}$; the rate for larger particles is much lower, being for example 2×10^{-6} $cm^{-2}\,yr^{-1}$ for those 100 μm in diameter (Schneider et al., 1973). The returned lunar samples represent a time-integrated record of the physical phenomena associated with these various bombardment processes, phenomena such as isotope production from nuclear reactions, track production, impact melting and volatilization, and mass fractionation. Hence, they provide valuable physical information complementary to that gathered from the limited-lifetime instruments placed on the lunar surface.

One of the interesting lunar sample observations which is thought to be directly related to some of these bombardment processes is that of

isotope mass fractionation in many of the lighter elements. Isotope fractionation refers to the alteration of the relative abundances of all isotopes of an element by means other than nuclear reactions. The term is usually used in the narrower sense of describing alterations in the relative isotope abundances which vary systematically with mass in such a way as to have changes in the ratios of pairs of isotope abundances dependent strongly on the mass difference between the pair, but only weakly dependent upon the actual isotope masses. In fact in nature, such fractionation is usually nearly independent of isotope mass and varies nearly linearly with the mass difference. For example, oxygen is an element consisting of three stable isotopes of masses 16, 17, and 18. Oxygen isotopic fractionation occurs in nature in such a way that changes in the ratio of the abundances of ^{18}O and ^{16}O are twice as large as the accompanying changes in $^{18}O/^{17}O$ and $^{17}O/^{16}O$:

$$\Delta(^{18}O/^{16}O) \simeq 2.0\Delta(^{18}O/^{17}O) \simeq 2.0\Delta(^{17}O/^{16}O) \quad (1)$$

What is striking about the isotopic fractionation in the lunar samples is that there are highly fractionated components which apparently reside within a distance of 1 μm or less from the surfaces of the material. This was first observed for oxygen and silicon in lunar soils (or "fines") by Epstein and Taylor (1971). In an extensive series of experiments (Epstein and Taylor, 1971, 1972, 1974, 1975; Taylor and Epstein, 1973) these workers demonstrated that the very first O and Si removed from soil samples during fluorine-stripping experiments were relatively enriched in the heavier isotopes ("isotopically heavy") by up to 50‰ and 25‰ respectively, i.e.

$$(^{18}O/^{16}O)_{first} / (^{18}O/^{16}O)_{bulk\ soil} = 1.050 \qquad (2)$$

and

$$(^{30}Si/^{28}Si)_{first} / (^{30}Si/^{28}Si)_{bulk\ soil} = 1.025 \qquad (3)$$

The per mil symbol "‰" means tenths of a percent. The observation that the $^{17}O/^{16}O$ and $^{29}Si/^{28}Si$ enrichments were correspondingly half as large demonstrated that the effects were indeed mass fractionation (Epstein and Taylor, 1971; Clayton et al., 1974). Epstein and Taylor demonstrated that the magnitude of the fractionation decreased as progressively greater depths in the lunar regolith were sampled. This was done by examining material taken from the bottom of a shallow trench dug by the astronauts and from some of the core (drive tube) samples. Furthermore, the magnitude of the isotopic fractionation in these samples was correlated with solar wind hydrogen content, suggesting that the fractionation was produced during long-term exposure to the various bombardment processes while the samples were residing on the lunar surface.

The oxygen and silicon isotope data for the lunar soils led to studies of a similar nature for other light elements. Thode and Rees (1971, 1976; Rees and Thode, 1972, 1974) found isotopically heavy fractionated sulfur in lunar soils. By observing, in cases in which the soil samples were divided into size fractions, that the measured fractionation increased as the grain size decreased, these workers demonstrated that the isotopically fractionated sulfur, also, was contained primarily near the soil grain surfaces. Potassium isotope studies on lunar soils (Barnes et al., 1973; Garner et al., 1975; Church et al.,

1976) have indicated that this element is probably also fractionated. However, analytical difficulties associated with the isotope measurements and the fact that the data do not show a large systematic offset between the $^{39}K/^{41}K$ of lunar soils and mare basalts make it hard to assess just how large the soil K fractionation really is. Other light elements such as H, C, and N have large isotope effects in lunar samples, but it is not possible to directly assess what portion is from mass fractionation since each element has only two stable isotopes. Not only are isotopes fractionated in the lunar samples, but elements as well are fractionated with respect to their bulk values. For example, O is depleted relative to Si in the outer layers of the soil grains (Epstein and Taylor, 1971, 1972; Taylor and Epstein, 1973). Data of Housley and Grant (1977), who used an ion sputtering and X-ray photoemission technique, indicate compositional changes in the major elements and in the outer few hundred angstroms of a lunar soil.

The isotope and elemental fractionation in these various elements was not anticipated for the lunar samples. The discovery has therefore led to a great interest in determining the actual physical mechanisms responsible for the fractionation. Epstein and Taylor (1971, 1972, 1974) discussed as possible mechanisms fractional vaporization from, or condensation onto, surface layers of the soil grains. They mentioned that bombardment by the solar wind might cause such fractional removal or condensation. Vaporization and condensation of material by the localized heating accompanying micrometeorite impacts has also seemed to be a plausible mechanism. Calculations by Switkowski et al. (1977) have

indicated that a cycling in the lunar gravitational field involving sputtering by the solar wind and subsequent redeposition could lead to isotopic fractionation in the material redeposited onto the soil grain surfaces. The calculated fractionation magnitudes were comparable to those actually observed in the O, Si, and S work.

Before describing this further, a brief description will be given of what is meant by "sputtering." Sputtering is a collisional process by which atoms are removed from a bombarded material, and proceeds as follows. The bombarding particles strike the surface and initiate a number of secondary collisions within the material. Energy from the primary particles is thus shared with the atoms in the material, which can then either vibrate with greater than thermal energies, or actually leave their lattice sites and collide with other atoms in the bombarded material. Viewed in a statistically-averaged way, there is a density of the deposited energy which varies with depth into the material. If enough of this energy is present at the surface, individual atoms can gain enough energy to break their chemical bonds, enabling them to leave the surface. The word "sputtering" aptly describes the process, since the energies of the removed particles are typically a few electron-volts, while the bombarding particles typically have energies 2 - 5 orders of magnitude larger.

Switkowski et al. (1977) noticed that the sputtered particle energies were close to those required for escape from the lunar gravitational field. Thus, with a spectrum of sputtered energies around the escape energy, some particles could escape while others would be redeposited onto the lunar surface. If the different isotopes of an

element all have the same sputtered energy spectrum, then different fractions of the various isotopes escape since the escape energies scale proportionally with the isotope mass (escape velocity is independent of mass). The calculations for this model therefore required knowledge of the sputtered particle energy distributions. A recent thesis by Weller (1978) demonstrated that the theoretically-derived spectrum used provides a reasonable fit to the energy spectrum of sputtered uranium.

If the sputtering process itself causes isotope fractionation, something which has not been known until now, the fractionation in lunar materials would exceed that caused by any gravitational selection alone. Sputtering is a complicated physical process, and the subject of whether isotope fractionation can occur has as yet resisted rigorous theoretical treatment. What has been clearly needed are well-conceived experiments which would clearly demonstrate the existence or non-existence of sputtering-produced fractionation. The demonstration that substantial effects can be produced would be of interest not only to those studying the lunar soil problem, but to those studying the basic sputtering process itself, a process which to date for multi-element targets is also far from being well understood. The purposes of the research in this thesis were to study these problems in the following ways: (a) to carry out laboratory sputtering experiments oriented towards learning whether the sputtering process itself produces isotope fractionation, (b) to carry out the experiments under bombardment conditions which approximately simulate those on the moon so that information learned from the sputtering experiments could be applied towards a

better understanding of the lunar soil fractionation mechanism, (c) to do the sputtering experiments for an element which was well-suited for the studies, and if this was an element previously unstudied in the lunar samples, to extend the existing base of data by probing the extent of its fractionation on the moon. Neither O, Si, nor S was especially well suited for this sputtering work, so a different element, calcium, was used. It turned out (Chapter 4) that the new data thus gathered for a lunar soil provided a serious disagreement with the Switkowski et al. model and cast some doubt as to whether such a simple description was realistic. However, an experimental complexity has clouded the interpretation of the data, which showed only small isotope fractionation while the model predicted large effects. Consequently, the sputtering simulations achieved additional importance: if large isotope fractionation was found, the probable presence of similarly large effects in the lunar samples would be indicated.

Calcium is a light element of atomic weight 40.076 which has six stable isotopes. Calcium was used for the following reasons: (a) it is only slightly heavier than sulfur, and therefore might be extensively fractionated on the moon; (b) the large percentage mass difference between ^{40}Ca and ^{48}Ca, the lightest and heaviest isotopes, allows the effective magnification of potentially very small degrees of isotopic fractionation per unit mass difference; (c) isotopic abundance measurements of calcium can be done with samples as small as 2×10^{-9} moles; (d) the large number of isotopes permits the use of the double isotopic tracer method for precisely distinguishing between isotopic

fractionation in a sample and artifacts introduced during the measurements. These various factors made calcium an ideal choice for these studies. The most abundant isotope is ^{40}Ca, which makes up $\sim 97\%$ of all calcium in nature. For precision measurement of the very low abundances in a sample of the other five Ca isotopes, careful attention has had to be paid to the development of adequate analytical techniques. These are described in Chapter 2 and have proven to be extremely effective in light of the low abundances of most of the isotopes. For instance, ^{43}Ca abundances can be measured to a precision of 5 parts in 10^4 with as little as 70 picomoles of ^{43}Ca loaded into the mass spectrometer. ^{46}Ca can be measured with a precision of 1% using as little as 3 picomoles.

After their development, these techniques were first tried out on a geochemistry problem for which conflicting results had been reported over the last fifteen years. Because of a variety of factors, it was not known to what extent calcium is fractionated between different rock types on the earth. Some authors reported extremely large effects while others found no effects within the precision of their measurements. A number of mechanisms for calcium terrestrial isotopic fractionation had been advanced in order to provide insight into what types of samples might prove most fruitful in a search for measurably large fractionation. The present contribution to this research is contained in Chapter 3. It was found that there was no evidence of large, wide-spread isotopic fractionation of calcium on the earth. This conclusion extended to other objects in the solar system through analysis of a number of meteorite and lunar whole-rock samples. Minor isotope fractionation of Ca was found

in a variety of terrestrial samples and in meteorites, but the effects were so small as to remove this as a problem of much current geochemical interest. After allowance for these small fractionation variations, a single isotopic composition of calcium was observed in all of these materials, and this sets apart as really remarkable the calcium and other-element anomalies recently found in a few small inclusions in the meteorite Allende (cf. Lee et al., 1978).

In Chapter 4 is contained a full description of the search for calcium isotope fractionation in a lunar soil which had been shown to have large O, Si, and S isotopic fractionation. The difficulty of this type of experiment is in the extraction of only the surficial, fractionated calcium. The attempts at doing this provided some internal indications that any dilution with unfractionated material from the interiors of the soil grains was not dominant, but this was still not very satisfying. It was clearly demonstrated though by this work that calcium is fractionated, albeit to a small extent, on the surface of the moon. What was unclear was whether the Ca isotopic fractionation of the soil grain surfaces was much larger than that indicated by the measurements, or whether the isotopic fractionation observed for all of the various elements is controlled by some chemical property such as volatility. Clayton et al. (1974) provided a discussion of the isotope fractionation effects in the light elements and considered a Rayleigh fractionation process as the mechanism. This implied either that as much as 20 - 30 % of the sulfur and potassium originally present in the soils had been lost by micrometeorite vaporization or solar wind sputtering, or that the soil grain surface enrichments were the result

of deposition of vapors which had been fractionated in the "atmosphere" subsequent to vaporization. It has been uncertain whether the refractory element calcium could be vaporized from micrometeorite impacts sufficiently well for large quantities of it to be cycled and fractionated in the lunar atmosphere (by some mechanism which has not been elucidated). The possible role of chemical volatility is further discussed in Chapter 4.

Although the Ca effects in the lunar soil were small compared to those for O, Si, and S, their presence well outside of experimental uncertainties allowed sputtering experiments involving Ca to be meaningful in relation to the lunar fractionation problem. If a large part of the 4‰ Ca fractionation was indeed caused by sputtering, then effects of similar magnitude should be expected in the laboratory, provided that the ion beam sufficiently simulates the solar wind bombardment. If no fractionation were observed in the laboratory, then the lunar Ca fractionation must have been caused in some different way. On the other hand, the observation in the laboratory of substantial isotopic fractionation would, when combined with the present observations of calcium fractionation on the moon, lead to the interpretation that sputtering fractionation is likely an integral part of the lunar mechanisms.

The calcium sputtering experiments are described and discussed in Chapter 5. The experimental goals were the following: (a) to determine whether calcium sputtered from a target is highly fractionated under a variety of conditions, (b) to determine approximately the thickness of any surficial layer of the target which might be fractionated in a direction complementary to that of the sputtered calcium, (c) to

determine if any isotopic fractionation of the sputtered material varies with the angle at which it was sputtered from the target, (d) to study any variations of sputtered calcium fractionation with increasing bombardment doses in order to obtain information about material transport within the target. The experiments thus designed proved conclusively that calcium is isotopically fractionated by large amounts in ion sputtering. The details of the fractionation data are complicated and not yet completely characterized in all respects, but still provide valuable information for the problems at hand. Relatively thick ($\sim$ 1000 Å) isotopically heavy layers on the bombarded surfaces have been observed. The data are first discussed from the point of view of learning about the sputtering process itself. The final section of Chapter 5 then discusses the relation of the results to the lunar soil fractionation phenomenon.

Chapter 5 includes a detailed discussion and photographic documentation of the radiation damage phenomenon of blistering which occurs in laboratory experiments. It is necessary to recognize that sputtered surfaces become complicated as roughness and blistering arise. Because of this, the theoretical domain in providing quantitative explanations of the data will probably be restricted to that of the effects observed prior to the onset of such complications. Interesting physics, for example material transport within the bombarded target, occurs during later stages of sputtering, but quantitative theories of these processes, if developed, will have to be applied with caution except when only minimal radiation damage is present.

CHAPTER 2. EXPERIMENTAL PROCEDURES OF PRECISION CALCIUM ISOTOPE ANALYSIS

The development of high precision, digital data acquisition mass spectrometers with ion optics that yield high transmission efficiencies (e.g. Wasserburg et al., 1969) has made possible techniques for precision isotopic analysis of nanomole and picomole quantities of many elements. The scientific information which has arisen from studies in the last ten years using these techniques has had major impact on a variety of disciplines in the fields of geochemistry and astrophysics. Described herein are the calcium isotope analysis techniques which were developed for the purpose of addressing the areas of inquiry dealt with in this thesis. Recently, though, these same techniques have been used to great advantage in studies of meteoritic material which provide highly interesting information about processes occurring prior to the condensation of the solar system (cf. Lee et al., 1978). The precision of the calcium isotope analyses has arisen in large part from the availability of these high-quality mass spectrometers.

The reader is first referred to the "Experimental Procedures," "$^{40}Ca/^{44}Ca$ Resolution," and "Appendix" sections of the paper which is reproduced in Chapter 3. This description documents the various procedures which were developed to measure absolute calcium isotopic compositions with high precision. The remainder of this chapter provides an expanded discussion of some of the points mentioned in these sections of the paper in Chapter 3.

Double Tracer Technique

The principle of this technique, which provides an internal standard for correction of instrumental fractionation, is easier to envision if one first considers an idealistic case in which ^{42}Ca and ^{48}Ca do not exist in samples to be measured. Assume also that the tracer is pure to the point of having no trace quantities of ^{40}Ca and ^{44}Ca. Any mixture of double spike and sample will then have (except for instrumental fractionation) $^{42}Ca/^{48}Ca$ and $^{40}Ca/^{44}Ca$ ratios equal to the ratios in the tracer and in the sample, respectively. If the double tracer had been prepared by mixing together two single tracers consisting of pure ^{42}Ca and ^{48}Ca, respectively, then the gravimetry involved in the mixing will provide a precise knowledge of the $^{42}Ca/^{48}Ca$ ratio in the mixed spike. Comparison of this value with the $^{42}Ca/^{48}Ca$ value measured during the above mixture analysis will then yield perfect agreement if the mixture is not isotopically fractionated in the mass spectrometer. In the presence of instrumental fractionation, comparison of these two values will yield a fractionation factor which can be used to correct the fractionated $^{40}Ca/^{44}Ca$ value measured in the mixture at the same time, thus yielding a measurement of the unfractionated (absolute) $^{40}Ca/^{44}Ca$ value.

Although this is the basic idea behind the double spike technique, it is in practice complicated by a number of factors. First of all, the technique does not actually provide absolute $^{40}Ca/^{44}Ca$ values. There is a bias of unknown size which is constant for all samples measured. For comparison between samples, though, this possible bias cancels out and is therefore unimportant for any of the work reported

here. The bias arises from three factors present during the mixing together of the single tracers. Neither tracer is pure, each containing traces of the isotope which is predominant in the other. The amounts of these impurities are measured by mass spectrometry, and hence the results are subject to instrumental mass fractionation. Second, the gravimetric calculation assumes that the individual tracer salts ($^{42}CaCO_3$ and $^{48}CaCO_3$) are stoichiometric and also free of any chemical impurities. Third, since calcium salts, particularly carbonates, are hygroscopic, the apparent weights may be somewhat greater than the weights of the carbonate salts themselves, even if precautions are taken to dry the salts in an oven. These various factors introduce an uncertainty into the $^{42}Ca/^{48}Ca$ ratio in the double tracer. The tracer composition in Table 3-1 represents a mass spectrometric analysis of the double tracer, corrected for instrumental fractionation by normalization to the $^{42}Ca/^{48}Ca$ value determined gravimetrically. The only important influence of this bias upon the present work was in its dominating the error in the atomic weight which is calculated from the data in Table 3-5 to be 40.076 ± 0.001.

From Table 3-1 it will be noticed that the double tracer has, as well as ^{42}Ca and ^{48}Ca, measurable quantities of the other calcium isotopes. Also, real samples of course contain small quantities of the two isotopes predominant in the spike. This significantly complicates the use of measured $^{42}Ca/^{48}Ca$ mixture ratios to provide instrumental fractionation corrections. The measured ratios may no longer be directly compared to the gravimetric value. Instead, the contribution of the sample to a measured $^{42}Ca/^{48}Ca$ mixture ratio must first be subtracted,

leaving a value for the tracer $^{42}Ca/^{48}Ca$ as fractionated at that time in the mixture run. Once done, a fractionation factor can be computed and used to correct the measured $^{40}Ca/^{44}Ca$ mixture ratio. Now, however, from this unfractionated value for $^{40}Ca/^{44}Ca$ in the mixture, an unfractionated value for this ratio in the sample must be obtained. This is done by subtracting from the $^{40}Ca/^{44}Ca$ mixture value the contribution from the double spike. The equations used for these two subtractions effectively unmix the tracer (T) and sample (S) isotope compositions from the mixture (MX) composition. Given a tracer composition (Table 3-1) and a sample composition, these equations compute the relative contributions of each in the mixture. The equations are

$$\left(\frac{42}{48}\right)_T = \left(\frac{42}{48}\right)_{MX} + \frac{\left[\left(\frac{42}{48}\right)_{MX}\left(\frac{48}{44}\right)_S - \left(\frac{42}{44}\right)_S\right]\left[\left(\frac{44}{48}\right)_{MX} - \left(\frac{44}{48}\right)_T\right]}{\left[1 - \left(\frac{44}{48}\right)_{MX}\left(\frac{48}{44}\right)_S\right]} \quad (1)$$

$$\left(\frac{40}{44}\right)_S = \left(\frac{40}{44}\right)_{MX} + \frac{\left[1 - \left(\frac{44}{42}\right)_{MX}\left(\frac{42}{44}\right)_S\right]\left[\left(\frac{40}{44}\right)_{MX}\left(\frac{44}{42}\right)_T - \left(\frac{40}{42}\right)_T\right]}{\left[\left(\frac{44}{42}\right)_{MX} - \left(\frac{44}{42}\right)_T\right]} \quad (2)$$

The left side of eq. (1) is interpreted as a measurement during the mixture run of the $^{42}Ca/^{48}Ca$ value of the tracer. The left side of eq. (2) is interpreted as a measurement during the mixture run of the $^{40}Ca/^{44}Ca$ value of the sample.

In this particular form, though, eqs. (1) and (2) are not of much use since they are only valid in the absence of instrumental fraction-

ation. To account for fractionation using the exponential power law (see the discussion in the appendix of the paper in Chapter 3), the above equations are rewritten in terms of the measured, rather than the fractionation-free, ratios using the following substitutions:

$$
\begin{aligned}
(42/48)_{MX} &\rightarrow (42/48)^{meas}_{MX}\ \{42/48\}^{p\sim} \\
(44/48)_{MX} &\rightarrow (44/48)^{meas}_{MX}\ \{44/48\}^{p\sim} \\
(40/44)_{MX} &\rightarrow (40/44)^{meas}_{MX}\ \{40/44\}^{p\sim} \\
(44/42)_{MX} &\rightarrow (44/42)^{meas}_{MX}\ \{44/42\}^{p\sim}
\end{aligned}
\qquad (3)
$$

where meas stands for measured and $p\sim$ is the fractionation factor for a set of ten mixture ratios (see below). Note that the sample isotopic ratios are left uncorrected for fractionation at this stage. With eqs. (3) substituted into (1) and (2), the mixture run fractionation parameter is solved for iteratively as follows. The iteration has two loops, one of which is an iteration within eq. (1) only, and the second of which involves single applications of eq. (2). To begin the iteration, $p\sim$ is set equal to zero in (1). The sample ratios used are grand means of the mass spectrometer data, uncorrected for any fractionation. The mixture ratios are means of a set of ten individual measurements. The entire iterative procedure is repeated for each set of mixture ratios. Such separate calculations are necessary since $p\sim$ changes during the mixture run. Equation (1) is then used iteratively to find a value for $p\sim$ which, when inserted in the right side of (1) along with the various means and grand means just described, will yield the unfractionated $^{42}Ca/^{48}Ca$ value of the tracer, as given in Table 3-1. The value for $p\sim$

thus found is then inserted in the right side of (2) to find in a single step a measurement of the unfractionated $^{40}Ca/^{44}Ca$ in the sample as measured by the mixture run. This two-step procedure is repeated for each set of ten mixture ratios and then the mean of the $(^{40}Ca/^{44}Ca)_S$ values calculated by (2) is formed. This mean provides the first "guess" of the absolute $^{40}Ca/^{44}Ca$ ratio in the sample. This result is then used to correct each measured ratio of the composition (S) data for mass fractionation. In other words, the $(^{40}Ca/^{44}Ca)_S$ "guess" enables fractionation factors for each composition run data set to be calculated, thereby allowing correction of the $^{42}Ca/^{44}Ca$ and $^{48}Ca/^{44}Ca$ measured values for fractionation prior to being used in the next iteration of eqs. (1) and (2). After these fractionation corrections, new grand means of the "corrected" composition data are then calculated and inserted into eqs. (1) and (2) so that the whole two-step iteration procedure can be repeated.

In practice, this procedure quickly converges to a self-consistent set of results after a few iterations. The stability of eqs. (1) and (2) is influenced by several factors. First, the terms in brackets are arranged so as to promote accuracy: large numbers of similar magnitude are not subtracted from each other, and the three bracketed factors in each equation together form but a minor correction to the other, main term. Secondly, the double spike is added to the sample in optimal amounts so that the tracer predominates at masses 42 and 48 while presenting only minor additions to the other isotopes. With $^{40}Ca_S/^{42}Ca_T \approx 7$ in the mixture, better than 90% of the atoms of each of the other isotopes arise from the sample, while better than 90% of the isotope

42 and 48 atoms come from the tracer. A variety of tests of the stability of these equations have been conducted using artificial mixture and composition "data" which is highly fractionated in both directions; "mixtures" ranging from $^{40}Ca_S/^{42}Ca_T$ = 3 to 12 were used for these tests. In all cases, the correct results were obtained after very few iterations by the computer programs which handled the calculations. There were no signs of instability.

Using this double spike technique, it was demonstrated by measurements of standards having known $^{40}Ca/^{44}Ca$ differences that fractionation differences could be reliably resolved to a level of 0.5‰ (i.e. 0.5 x 10^{-3}), or 0.13‰ per unit mass difference. This was first demonstrated with precision analyses of 10 μg aliquots of the standards (Table 3-2, Figure 3-1). Later, it was shown that this same precision could be attained when as little as 150 ng of calcium was loaded onto the mass spectrometer filament (Table 5-5).

Mass Spectrometry

The mass spectrometric techniques for calcium are adequately summarized in the account in Chapter 3. Two of the points mentioned there will be further discussed here.

In Figure 2-1 is shown a spectrum of the background signal levels in the calcium mass region. Such a record is generated on a chart recorder which monitors the amplified signal originating from the Faraday cup collector. The magnetic field is varied at a constant rate dB/dt. For the spectrum in Figure 2-1, the initial field value was at mass ∿48.5, and was decreased steadily, sweeping past isotopes 48, 46, 44, 43, 42, and stopping just as mass 40 was reached. It may be seen that the back-

ground--the heavy trace between each isotope peak--is not constant, but varies slowly and smoothly as a function of mass. The broad peak in the background at mass ~ 45.3 is from a reflection of the large ^{40}Ca beam off of one side of the mass spectrometer flight tube and into the Faraday cup. The maximum reflected beam is 10^{-4} of the primary ^{40}Ca beam. The background below mass 40 (not shown) continues at the same low level seen between masses 40 and 42. Below mass 38 though is seen a larger reflected peak similar to that shown in the magnesium spectra of Lee et al. (1977, Fig. 1). This peak is caused by a reflection of ^{40}Ca off the other side of the flight tube and has a maximum intensity of 10^{-3} of the primary beam. Being outside of the calcium mass region, this latter reflected peak was of no importance in the present work.

In Figure 2-1, the chart recorder scale was changed to prevent over-ranging as each peak (except ^{46}Ca) came into the Faraday cup. This is indicated by the breaks in the trace. The arrows indicate the magnetic field values used during data acquisition for measurement of the background on both sides of each peak. These correspond to 7.0 gauss offsets from the field values for each peak and were set for each run to within 0.1 gauss. Each pair of background measurements was averaged by the data-reduction programs to obtain the background under the peak. The background changed slowly enough with mass for this procedure to yield accurate results. As the background levels change with primary beam intensity, high precision measurements mandated the measurement of the background each time a peak was measured. Therefore, measurements of these "zeroes" were included during data acquisition in the automatic magnetic field cycling. This method is superior to that commonly used

in which background measurements are made only occasionally during the run.

Given the spectrum of Figure 2-1, it becomes clear why it was highly desirable to use for mass spectrometer sample filaments tantalum which was refined to a high enough degree as to have essentially no potassium present in it. Even after outgassing for periods of two hours at temperatures above 2000°C, filaments made out of tantalum stock which had previously been used in this laboratory showed ^{39}K intensities ranging up to $0.5 - 2.0 \times 10^{-10}$A at calcium running temperatures of about 1400°C. Such intensities are comparable to the ^{40}Ca intensity! This causes an additional reflected peak in the calcium mass region, this time centered around mass 44.3 instead of 45.3, causing enough background structure around ^{44}Ca to interfere with the precision measurement of this isotope. Also, as the potassium signal is highly unstable because of the elevated filament temperature, the background around masses 42, 43, 44, 46, and 48 becomes significantly noisier than shown in Figure 2-1, also causing decreased precision of measurement. (The noise of the background signals is represented by the width of the trace, and in Figure 2-1 corresponds to a current of approximately 10^{-14} A.) Using instead for filament material high purity tantalum which had been zone-refined, this source of difficulty was completely eliminated. With filaments made from this material, ^{39}K currents of 10^{-14}A were typically observed, with maximum levels observed in short-duration "spikes" being less than 10^{-13}A.

Fractionation Introduced During Chemical Purification of Samples

For the work reported in Chapters 3 and 4, it was necessary to use cation-exchange column techniques to separate the calcium, prior to its

isotopic analysis, from the other elements present in the sample. It was discovered during this work that even very short columns exhibited non-negligible differences in the elution patterns for the different isotopes. The heavier isotopes were preferentially eluted in the first fractions of the Ca-containing eluate, and the lighter isotopes were preferentially eluted in the final fractions. Therefore, if part of the calcium-containing eluate falls outside of the predefined column "cut" or collection range, perhaps from small changes in the elution speed of the calcium cations since the last time the cut was calibrated, the possibility exists that a net fractionation of the sample will be introduced. This source of error may be circumvented by using a cut wide enough to ensure that the column yield is in the 85% or better range, or by adding the double tracer to the sample prior to passing it through the column. In this latter case, any fractionation introduced by the column will be removed by the unmixing analysis (eqs. (1) and (2) above) just as if it were additional instrumental fractionation. (A negligibly small error might be introduced if the column fractionation law deviates from that used to correct the instrumental fractionation. This could only become significant if the fractionation introduced by the column were extremely large.)

On the third page following is reproduced a paper which was published in Analytical Chemistry. This more fully describes the observed cation column fractionation behavior.

Figure 2-1. Calcium mass spectrum. This is a chart recorder trace of ion current measured in the Lunatic I mass spectrometer Faraday cup collector. The magnetic field was decreased at a constant rate from the mass 48.5 value to that for mass 40. (The mass 44 region appears in both parts of the figure.) A background signal of approximately 1.3×10^{-14} A is seen at mass 48.5; the zero-signal reference level was measured with the ion beam turned off, and is shown at each end of the trace. The background is smooth, and attains a maximum of 3.8×10^{-14} A at mass 45.3. This broad maximum in the background is caused by scattering of the large ^{40}Ca beam from one side of the mass spectrometer flight tube into the Faraday cup, and is 10^{-4} of the primary beam intensity. For isotopes other than ^{46}Ca, the chart recorder sensitivity was decreased as each beam came into the cup, thereby preventing the top of the peaks from over-ranging. The spectrum was obtained with a source slit opening of 0.010 inch and a collector slit opening of 0.025 inch. The background was measured at the positions indicated by arrows; these correspond to ± 0.15 amu (atomic mass unit) offsets from the peaks.

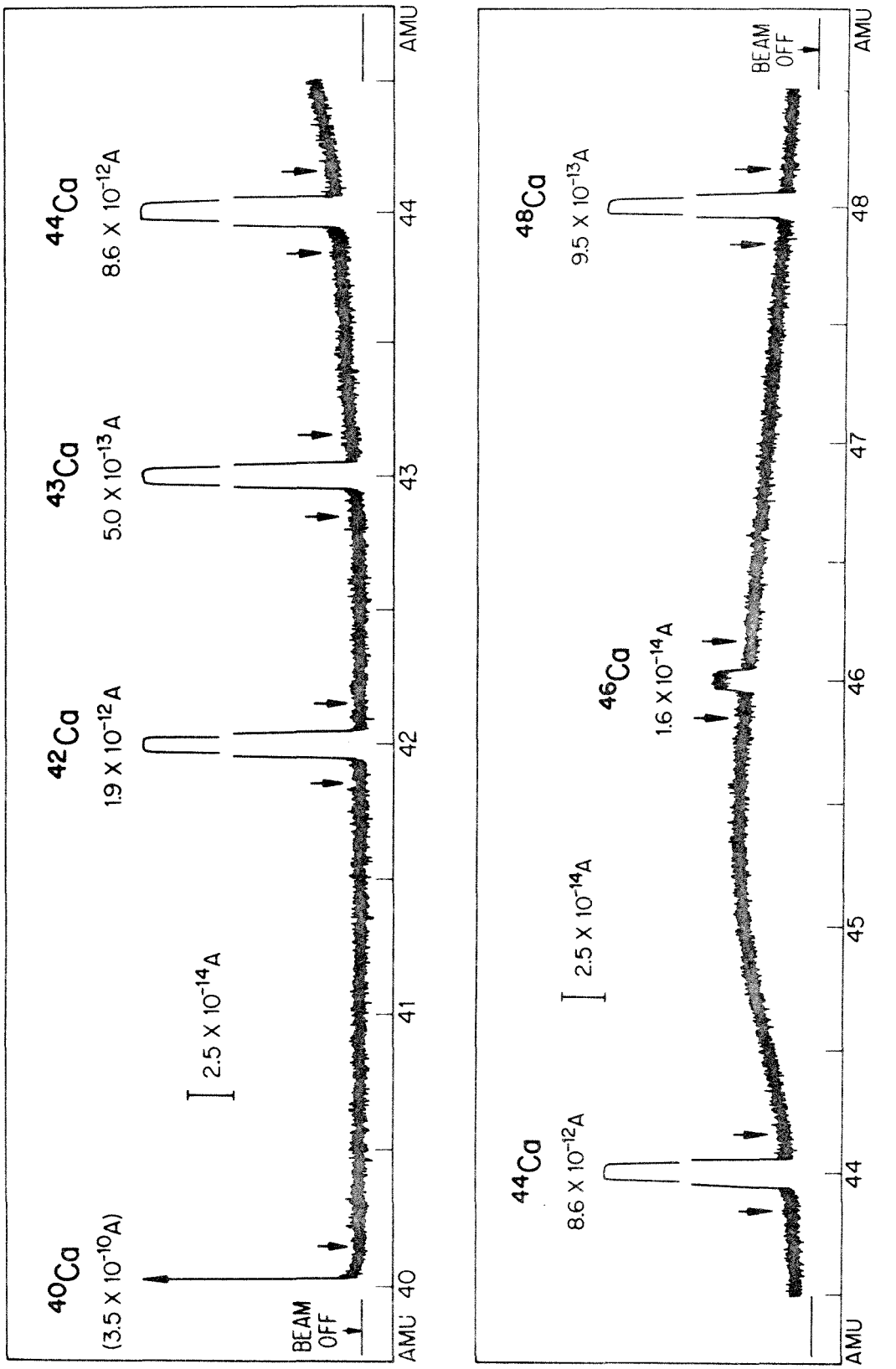
40Ca
(3.5 X 10-10A)
42Ca
1.9 X 10-12A
43Ca
5.0 X 10-13A
44Ca
8.6 X 10-12A
2.5 X 10-14A
BEAM OFF
AMU
40
41
42
43
44
44Ca
8.6 X 10-12A
2.5 X 10-14A
46Ca
1.6 X 10-14A
48Ca
9.5 X 10-13A
BEAM OFF
AMU
44
45
46
47
48

Figure 2-1

Calcium Isotope Fractionation in Ion-Exchange Chromatography

W. A. Russell

W. K. Kellogg Radiation Laboratory, Division of Physics, Mathematics, and Astronomy, California Institute of Technology, Pasadena, California 91125

D. A. Papanastassiou

The Lunatic Asylum, Division of Geological and Planetary Sciences, California Institute of Technology, Pasadena, California 91125

Volume 50, Number 8

Pages 1151–1154

Significant fractionation of the isotopes of calcium has been observed during elution through short ion-exchange columns packed with Dowex 50W-X8 resin. A double isotopic tracer was used to provide correction for instrumental fractionation effects. The absolute $^{40}Ca/^{44}Ca$ ratio is determined by this method to 0.05% and provides a measure of the fractionation of all Ca isotopes. It is found that the lighter isotopes are preferentially retained by the resin, with variations in $^{40}Ca/^{44}Ca$ between the first and last fractions of up to 1.1%. An estimate of the separation factor between batch solute and resin gives $\epsilon = 2.1 \times 10^{-4}$. Details of the chemical or physical mechanisms causing isotope fractionation of Li, Na, Ca, and other elements during ion-exchange chromatography are not yet clear.

Forty years ago, Taylor and Urey (*1*) investigated isotope separation in Li, K, and N during elution of LiCl, KCl, and NH_4^+ using long (9 to 34 m) columns which were packed with zeolites. For lithium, they observed up to 60% changes in the isotope ratio between the leading and trailing tails of the elution curve, with ^6Li being held more strongly than ^7Li. Changes in $^{39}K/^{41}K$ of up to 11% and in $^{14}N_2/^{14}N^{15}N$ of 10% were similarly observed by these workers, but in these cases the heavier isotopes were preferentially retained by the zeolite. These results created great interest in the possibilities of isotope separation using ion-exchange chromatography. A number of workers repeated the lithium experiments, but found only much smaller effects; a summary of this work is given by Lee and Begun (*2*). Part of the difficulty is that large fractionation of the isotopes occurs during thermal ionization in the mass spectrometer; hence, it is necessary to assess what portion of any observed effects actually represents artifacts of the measurement technique. Although particularly severe for lithium, this difficulty affects isotopic measurements for all elements which are analyzed using solid source mass spectrometry. Therefore, the results for potassium are open to question as well. In fact, the frequency with which isotope fractionation effects have been reported and later retracted is an indication of the analytical problems and of the lack of a theoretical working model for the prediction of isotope fractionation in cation exchange. Lee and Begun (*2*) used columns up to 1.5 m in length packed with Dowex-50 resin (sulfonated polystyrene–divinylbenzene copolymers) and observed variations of $^7Li/^6Li$ of ±10% with a reproducibility of ±5%. The regularity of the effects as a function of the fraction of Li in the eluate indicates that the observed fractionation is real. Lee and Begun (*2*) also observed that the lighter isotope of Li was held more strongly by the resin.

Using the radioactive isotopes ^{22}Na and ^{24}Na, Betts et al. (*3*) investigated the isotope fractionation of sodium eluted through a Dowex-50 column with 10^4 plates. The $^{24}Na/^{22}Na$ ratio in various eluate fractions was obtained by γ-ray counting, with the probable error estimated at ±0.4%. These workers found ~7% changes in $^{24}Na/^{22}Na$ between the first and last fractions of the eluate, with ^{22}Na more strongly adsorbed by the resin, when the resin was maintained at 5 °C or 25 °C; no significant fractionation was observed when the resin was maintained at the moderately higher temperatures 48 °C and 68 °C.

In this paper we report our observations of the large extent to which the isotopes of calcium are fractionated during elution through a cation-exchange column filled with Dowex-50 resin. In contrast to the work just reviewed, the effects reported here were obtained using much shorter columns for which it had been thought that isotope fractionation effects would be negligible. The effects were observed during the investigation of Ca isotope fractionation in terrestrial and extraterrestrial materials in several cases where a low yield of Ca was obtained. The fractionation introduced by cation-exchange chromatography when only ~60% of the eluted Ca is collected in the "Ca cut" is comparable to the range of fractionation in nature; ignoring this effect would have introduced serious artifacts in the data.

In this work, a ^{42}Ca–^{48}Ca double isotope tracer was used; this allows us to correct for fractionation occurring in the mass spectrometer during thermal ionization, and to determine the

Table I. Analytical Results

column	sample	eluate fraction, mL[a]	% Ca in fraction	$\Delta(^{40}Ca/^{44}Ca)$[b]
A	Abee[c]	67-72	1.6	−6.2 ± 0.6
		72-77	46.9	−1.6 ± 0.1
		77-82	49.1	+2.0 ± 0.1
		82-87	2.5	+4.8 ± 0.1
				+0.3 ± 0.1[f]
B	$CaCO_3$[d]	74.5-77	7.2	−4.4 ± 0.1
		77-79.5	27.1	nm[e]
		79.5-82	37.5	−0.4 ± 0.2
		82-87	26.9	nm
		87-92	1.2	+4.2 ± 0.1

[a] First 45 mL of the elution consisted of elution with 1.5 N HCl (see text) and has been included in the volumes listed here. [b] $\delta(^{40}Ca/^{44}Ca) = [(^{40}Ca/^{44}Ca)_{sample}/(^{40}Ca/^{44}Ca)_{standard} - 1] \times 10^3$; $\Delta = \delta_{fraction} - \delta_{total}$ where δ_{total} is the value for the original sample, as given in (*8*). [c] $\delta_{total} = 0.0 \pm 0.2$. [d] $\delta_{total} = 1.0 \pm 0.2$. [e] nm = not measured. [f] Weighted mean.

actual fractionation of Ca in a sample. Lindner (*4*) reported large variations in $^{45}Ca/^{40}Ca$ eluted through Dowex-50 resin; he measured this ratio by counting electrons from the β^- decay of ^{45}Ca to the ground state of ^{45}Sc, and by measuring ^{40}Ca gravimetrically. However, in a later personal communication to E. Glueckauf (*5*), these results were retracted.

EXPERIMENTAL TECHNIQUES

For this work we used two identical 1-cm diameter quartz columns (denoted A and B) packed with Dowex 50W-X8 (200–400 mesh) resin. In 4 N HCl, the resin height is 17 cm. An elution scheme for separating alkali and alkaline earth elements in this laboratory was described by Tera et al. (*6*) and used in this work. We carried out one set of measurements for each column using a Ca specpure salt and a meteorite sample. These samples simulate typical samples eluted through these columns. Both elutions were carried out at room temperature. The amounts of Ca eluted (0.320 mg and 1.05 mg, respectively) were far less than the ~50 mequiv capacity of the columns. The Ca in the eluate was collected in a series of 2.5- and 5.0-mL fractions. In spite of the coarseness of these fractions, the Ca in the leading and trailing tails was adequately isolated in order to permit investigation of the presence of large, and presumably complementary, mass fractionation effects. The Ca content of each fraction was determined using isotope dilution of a small aliquot of the fraction. The double tracer was then added in optimal amounts to the major aliquots of the eluate fractions. The spiked samples were analyzed on the Lunatic I mass spectrometer which has been described by Wasserburg et al. (*7*). The details of the measurement of fractionation of the Ca isotopes have been extensively discussed (Russell et al., *8*). Differences in $^{40}Ca/^{44}Ca$ between samples can be resolved to a level of 0.5‰ (per mil) corresponding to 0.13‰ per unit mass difference.

RESULTS

We list our analytical results in Table I. The deviation $\delta(^{40}Ca/^{44}Ca)$ measured for each eluate fraction is defined and listed in the table as the difference Δ from the $\delta(^{40}Ca/^{44}Ca)$ value of the original sample, which was reported previously (*8*). It is seen that large mass fractionation of the Ca isotopes occurs during elution. For column A, there was an 11‰ change in $^{40}Ca/^{44}Ca$ between the first 1.5% and last 2.5% of Ca collected; for column B, there was an 8.6‰ change between the first 7% and last 1% of Ca collected in the eluate. In both cases, the *lighter* isotopes of Ca are held more strongly by the resin and are enriched in the trailing fraction of the eluate. Figure 1 shows, for the two elutions, the Δ deviations of each fraction as a function of the cumulative percentage of the Ca being collected. The complementary nature of the isotopic

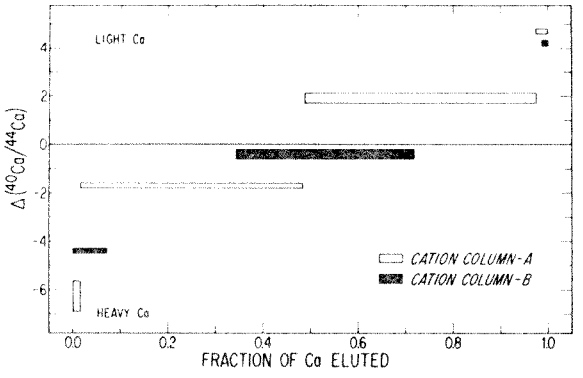

Figure 1. Per mil deviation Δ of $^{40}Ca/^{44}Ca$ of each eluate fraction from the $\delta(^{40}Ca/^{44}Ca)$ value for the original sample. Results for both column elution experiments are plotted as a function of the cumulative fraction of Ca eluted. A total variation in $^{40}Ca/^{44}Ca$ of $11^{0}/_{00}$ was observed for column A. A very similar pattern is seen for column B, with the total variation being $8.6\ ^{0}/_{00}$.

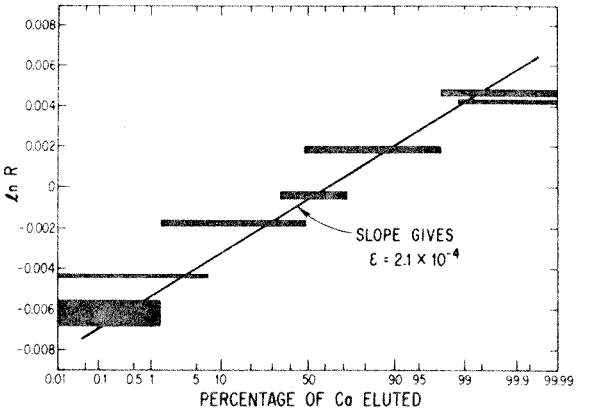

Figure 2. Data for isotopic variations in both column experiments plotted vs. the cumulative percentage of Ca eluted on a normal deviate (probability) scale. R is defined as $(^{40}Ca/^{44}Ca)_{fraction} \div (^{40}Ca/^{44}Ca)_{total}$. ln R is equal to $\Delta \div 1000$ to a high degree of precision. The line is a visual fit to the data. In the approximation where the slope of this line is equal to $\epsilon\sqrt{N'}$ (see text), where ϵ = batch enrichment factor and N' = number of theoretical plates in the column, we find $\epsilon = 2.1 \times 10^{-4}$

effects, as shown by the systematic progression from negative to positive Δ values, is apparent and also closely similar for the two columns.

As a check of the data, averages of the Δ values for each fraction, weighted by the amount of Ca in the fraction, may be calculated. By the definition of Δ, the average should be zero. Such a mass balance calculation for the column A elution yields a value for the total sample of $0.3 \pm 0.1‰$, which is in agreement with the measured value of $0.0 \pm 0.2‰$ (*8*). For the column B elution, it was only desired to verify the presence of highly fractionated Ca in the tails. Hence, two fractions were not measured, and a mass balance calculation cannot be carried out. However, since the central 37.5% fraction had $\Delta = -0.4‰$, the data are consistent with a Δ close to zero.

To be able to determine if the Ca isotope results given in Table I represent large or small enrichments per theoretical plate, we have attempted to estimate the number of plates (N') in the columns. The application of formulas for N' such as those derived by Glueckauf (*9*) requires some degree of caution because in the present experiment both 1.5 N and 2.5 N HCl were used in the elution procedure (*6*). The 1.5 N step was designed to separate the alkalis. However, there is no significant transport of Ca through these columns during the 1.5 N elution step, since the distribution coefficient for Ca at 1.5 N is a factor of 10 higher than at 2.5 N. The 45-mL volume of 1.5 N acid used therefore has not been included

in the calculation of N'. For both columns A and B, N' is calculated to be ~ 100. This indicates a plate height of 1.7 mm, which is about 20 times larger than plate heights that can be obtained with this resin. The elution of these columns using lower normality HCl, which would result in smaller plate heights, has not been necessary for the separation of Ca for mass spectrometry.

In Figure 2 we present a plot of column A and column B data which enable calculation of the enrichment factor, ϵ, the equilibrium ratio of $^{40}Ca/^{44}Ca$ in the solute to that in a well-stirred batch of resin. Figure 2 shows a plot of ln R against cumulative eluted percent on a probability abscissa. R is the ratio of $^{40}Ca/^{44}Ca$ in an eluate fraction to $^{40}Ca/^{44}Ca$ in the original sample. Since $R = 1 + \Delta \times 10^{-3}$, ln R is equal to $\Delta \times 10^{-3}$ to a high degree of precision. The analysis which leads one to expect the data to form a straight line array on this plot is given by Glueckauf (*10*). Although his derivation assumes a column consisting of thousands of plates, the actual approximations used in the derivation of his Equation 5 are fairly good for our case as well. From Figure 2 it may be seen that the data do approximately form a straight array, even though the Ca eluate fractions are rather coarse, making it difficult to obtain a well-defined fit. The line in Figure 2 has been drawn by inspection and corresponds to a slope of 2.1×10^{-3}. (The abscissa scale length in units of normal deviates is used in computing the slope. For example, the distance from 4.0% to 96.0% is 3.502.) Setting this value for the slope equal to $\epsilon \sqrt{N'}$ (*10*) and using $N' = 100$ yields $\epsilon = 2.1 \times 10^{-4}$. As a check, iterative solutions for ϵ using Glueckauf's more exact Equation 4 and various of the individual measurements in Table I give agreement within 15% of this value.

DISCUSSION

We have observed large and complementary fractionation of the Ca isotopes in Dowex-50 columns in the tails of the elution curve. These effects have been observed for short columns and could likely be amplified if the number of plates were increased, either by using longer columns or by using a lower normality acid so that the plate height would be decreased.

It has been of great importance to our work (*8*, *11*) to identify these columns as a source of isotope fractionation which may be introduced during the processing of samples in the laboratory. For the measurement of isotope fractionation in nature, the column effects can be excluded by either ensuring that the yields are 100% or, preferably, by adding the double tracer to the sample prior to its elution through a column. With this latter method, any fractionation in the column will affect both the double tracer and the sample identically; correction for such effects is automatically included in the data reduction.

In order to establish that these columns fractionate Ca, it has only been necessary to investigate a specific elution scheme. We have not attempted a full survey of what effects may be present when using (a) other elution schemes, (b) similar resins with different mesh sizes or degrees of cross-linkage, or (c) different types of resins.

It is not known at the present time what combination of physical or chemical processes is responsible for the fractionation. It does appear, though, that diffusion processes alone do not cause the effects. The length of time for cations in solution to come to equilibrium with the resin in a new plate is on the order of 0.5 to 2 s depending on whether the ion-exchange rate determining step is diffusion in a Nernst film or in the resin particles. It is therefore clear that, in either case, equilibrium is reached so quickly as to preclude the occurrence of diffusive isotope separation. These estimates are obtained from equations for half times for batch process ion exchange equilibrium under film or particle diffusion

controlling conditions. (See Ref. *12*, Equations 6-12 and 6-23. In these equations we take the bead radius to be 25 μm and the Nernst film thickness to be 10 μm.)

These considerations lead us to suspect that chemical isotope effects are an important factor contributing to the observed isotope fractionation. A simple model would be that all active sites in a resin grain are equally accessible, and that the lighter isotopes are more strongly held at these sites. However, since the attraction forces are thought to be electrostatic in nature, a mechanism for varying their magnitude as a function of mass is required. For example, hydration spheres around the cations may be partially stripped to differing extents, depending on the isotope mass, during transport into the resin. This could lead to equilibrium isotope partitioning between the resin and the eluate in a plate, as was suggested by Lee and Begun (*2*), who attempted to vary the degree of stripping by using resins with differing amounts of free water in them. To do this, they carried out experiments using Dowex-50 resins with various percentages of cross-linkage. However, a number of other parameters (mesh size, sample size, column dimensions, number of plates, eluting agent, and normality) were also varied simultaneously, making the data interpretation non-unique.

The possibility remains that isotope mass fractionation arising by mechanisms such as discussed here may be further enhanced by other means. For nitrogen, Spedding et al. (*13*) achieved a separation factor of $\epsilon = 2.6 \times 10^{-2}$. The large magnitude of this value was due to an equilibrium isotope-exchange reaction between NH_4^+ and NH_4OH, and enabled dramatic ^{14}N–^{15}N separations when Dowex-50 columns several hundred feet in length were used. The nitrogen band was maintained at a convenient length through the occurrence of reactions at the ends which have large equilibrium constants (10^9, 10^5); this caused both boundaries to be self-sharpening. Using Dowex-50 columns and ammonium α-hydroxyisobutyrate as the eluent, Aaltonen (*14*) observed isotope mass fractionation effects for Ca, Sr, Co, Y, and Sm. The ϵ value reported for ^{40}Ca–^{44}Ca separation is $\sim$2 times larger than our value. This may reflect additional isotope fractionation due to the Ca complexing, or analytical difficulties since the data reported by Aaltonen were not obtained using the double tracer technique. Fractionation of U isotopes observed in ion exchange using citrate or acetate eluents (cf. *15*) may also be due to complex formation.

CONCLUSIONS

A unique model adequately describing the observed isotope effects in cation-exchange chromatography is not yet apparent, despite the effects having been known for Li and Na for many years. In contrast to Li and K, the Ca data include an internally consistent correction for instrumental effects. Added work with Ca will be useful in elucidating the mechanism of the observed fractionation effects.

ACKNOWLEDGMENT

We have benefited from discussions with G. J. Wasserburg and other Lunatic Asylum inmates.

LITERATURE CITED

(1) T. I. Taylor and H. C. Urey, *J. Chem. Phys.*, **6**, 429 (1938).
(2) D. A. Lee and G. M. Begun, *J. Am. Chem. Soc.*, **81**, 2332 (1958).
(3) R. H. Betts, W. E. Harris, and M. D. Stevenson, *Can. J. Chem.*, **34**, 65 (1956).
(4) R. Lindner, *Z. Naturforsch. A*, **9**, 798 (1954).
(5) H. London, Ed., "Separation of Isotopes", George Newnes, London, 1961, p 218.
(6) F. Tera, O. Eugster, D. S. Burnett, and G. J. Wasserburg, *Proc. Apollo 11 Lunar Sci. Conf.*, **2**, 1637 (1970).
(7) G. J. Wasserburg, D. A. Papanastassiou, E. V. Nenow, and C. A. Bauman, *Rev. Sci. Instrum.*, **40**, 288 (1969).
(8) W. A. Russell, D. A. Papanastassiou, and T. A. Tombrello, *Geochim. Cosmochim. Acta*, **42**, No. 8 (1978), in press.

(9) E. Glueckauf, *Trans. Faraday Soc.*, **51**, 34 (1955).
(10) E. Glueckauf, *Trans. Faraday Soc.*, **54**, 1203 (1956).
(11) W. A. Russell, D. A. Papanastassiou, T. A. Tombrello, and S. Epstein, *Proc. Eighth Lunar Sci. Conf.*, 3791 (1977).
(12) F. Helfferich, "Ion Exchange", McGraw-Hill, New York, N.Y., 1962.
(13) F. H. Spedding, J. E. Powell, and H. J. Svec, *J. Am. Chem. Soc.*, **77**, 6125 (1955).
(14) J. Aaltonen, *Suom. Kemistil. B*, **44**, 1 (1971).
(15) A. Calusaru and F. Bunus, *Radiochim. Acta*, **18**, 23 (1972).

RECEIVED for review February 3, 1978. Accepted April 24, 1978. Work supported by National Aeronautics and Space Administration grant NGL 05-002-188. Division of Geological and Planetary Sciences Contribution No. 2967(263).

CHAPTER 3. CALCIUM ISOTOPE FRACTIONATION ON THE EARTH AND OTHER SOLAR SYSTEM MATERIALS

The development of high precision calcium isotopic analysis techniques was carried out in order to pursue investigations of fractionation caused by sputtering. However, the same techniques presented the opportunity to shed new light on an issue of geochemical interest which had been debated for some 15 years. At issue was whether natural processes occurring on the earth result in isotopic fractionation between such calcium reservoirs as igneous rocks, seawater, precipitated samples, or living organisms and their remains. Although the nature of processes which would cause substantial fractionation was unclear, a number of papers were published which claimed to have observed substantial isotopic fractionation. Such large effects contrasted sharply with the results of Hirt and Epstein (1964) who used a double spike method to precisely remove from the measurements the effects of mass fractionation from the mass spectrometer. Within their 8‰ precision of measurement of $^{48}Ca/^{40}Ca$, Hirt and Epstein (1964) observed no isotopic fractionation between many different types of terrestrial samples. Yet, as late as 1973, fractionations as large as -14.9 ± 9.1‰ for $^{48}Ca/^{40}Ca$ were being reported for some samples (Heumann and Lieser, 1973).

The paper which is reproduced in this chapter reports no evidence of any <u>substantial</u> isotopic fractionation in terrestrial samples. It is demonstrated that <u>small</u> effects of up to 2.5‰ for $^{40}Ca/^{44}Ca$ are present. In addition, calcium isotopic compositions of bulk lunar samples and of bulk meteorites of several different classes indicate

that no substantial calcium fractionation exists between major reservoirs in the solar system. This extends the observations of Hirt and Epstein (1964) who measured, in addition to their terrestrial samples, an L6 chondrite and a eucrite. The results presented here demonstrate for the first time what the real extent of calcium isotopic fractionation is in nature, and this then enables the beginning of serious consideration as to what mechanisms may be responsible. Also, it is shown here that there is a single isotopic composition of calcium in these materials after removal of the effects of the small naturally-occurring fractionation. Complementary to these results are the important observations for certain isotopically exotic inclusions in the carbonaceous chondrite Allende. In these very few cases both nuclear anomalies — enrichments or depletions of individual isotopes — and substantial isotopic fractionation were observed, and were attributed to processes occurring before and during the condensation of the solar system (cf. Lee et al., 1978).

The paper reproduced on the following pages originally appeared in Geochimica et Cosmochimica Acta. Some of the tables in the paper are referred to in other chapters of this thesis as "Table 3-x" where x is the number of the table as listed in the paper.

Geochimica et Cosmochimica Acta, Vol. 42, pp. 1075 to 1090
© Pergamon Press Ltd. 1978. Printed in Great Britain

0016-7037/78/0801-1075$02.00/0

Ca isotope fractionation on the Earth and other solar system materials

W. A. RUSSELL,* D. A. PAPANASTASSIOU† and T. A. TOMBRELLO*

(*Received* 23 *August* 1977; *accepted in revised form* 16 *March* 1978)

Abstract—It is demonstrated that differences in the $^{40}Ca/^{44}Ca$ ratio due to mass dependent isotope fractionation in nature are clearly resolvable to a level of 0.5‰. This precision is obtained (a) by using the double spike technique; (b) by using a mass-dependent law for correction of instrumental mass fractionation; and (c) by eliminating fractionation effects identified as due to differential elution of isotopes through ion exchange resins. We have determined the following uniform Ca isotopic composition after removing small natural fractionation effects: $^{40}Ca/^{44}Ca = 47.153 \pm 3$, $^{42}Ca/^{44}Ca = 0.31221 \pm 2$, $^{43}Ca/^{44}Ca = 0.06486 \pm 1$, $^{46}Ca/^{44}Ca = 0.00152 \pm 1$, $^{48}Ca/^{44}Ca = 0.08871 \pm 2$, where the errors correspond to the last figures shown. This yields an atomic weight of 40.076 ± 0.001. The data indicate the absence in the studied samples of detectable, distinct nuclear components in Ca similar to those observed for oxygen. In the samples studied, there is a distinct but small degree of Ca isotope fractionation. Overlapping ranges of fractionation of 2.5‰ for $^{40}Ca/^{44}Ca$ (four atomic mass units) are observed in meteorites, lunar, and terrestrial samples. Means by which isotope fractionation could arise for Ca are discussed, but the small range of effects and the lack of systematic variations do not permit at present the identification of the mechanisms responsible for the fractionation observed in the suite of samples. Ca in the biological cycle does not show fractionation effects larger than observed for non-biogenic samples. In contrast to these results, we have observed large effects of up to 13‰ for industrially purified Ca.

INTRODUCTION

WE REPORT on isotopic abundance measurements of calcium in meteoritic, lunar and terrestrial samples. These measurements have employed high precision mass spectrometric techniques and were carried out for the purpose of (a) precisely establishing the isotopic composition of Ca, and (b) identifying possible variations in the Ca isotopic composition due either to incomplete mixing of distinct nucleosynthetic materials or to mass dependent fractionation of the Ca isotopes in nature. Over the last 15 yr, a number of workers have attempted to determine the existence of mass dependent fractionation of Ca. Mass fractionation effects in nature could be enhanced in Ca because of the large relative mass difference of the isotopes (up to 20%). Discovery of Ca fractionation effects would provide important complementary data to well studied large isotopic effects in hydrogen, carbon, oxygen and sulfur. Mass fractionation is in principle possible due to chemical, biologic, or kinetic effects.

Mass spectrometric data are subject to instrumental fractionation effects. These effects are particularly serious for Ca because of (a) the large mass difference of the isotopes, (b) the low abundance of all Ca isotopes other than ^{40}Ca, which requires a high intensity ion beam for precise measurements. The use of a double spike as an internal standard has been a proven means of precisely correcting for instrumental mass fractionation effects. The technique was first used for Ca by HIRT and EPSTEIN (1964) who showed that, in nature, any mass fractionation effects in $^{48}Ca/^{40}Ca$ are less than ±8‰, corresponding to ±1‰ per atomic mass unit (amu). COLEMAN (1971) also used the double spike technique in his study of radiogenic ^{40}Ca formed by ^{40}K decay in pegmatitic micas. The double spike technique is not complicated. Yet, in contrast to these workers, other investigators have attempted to *reduce*, rather than to *remove*, instrumental mass fractionation effects by the use of a double or triple filament source for thermal ionization. For example, STAHL (1968) analyzed limestones, hydrothermal carbonates and ammonite shells and found no statistically significant variations. STAHL and WENDT (1968) did not find any variations in $^{48}Ca/^{40}Ca$ exceeding their error estimates of 11‰ during an experiment in which $CaCO_3$ was precipitated from solution in several steps. Within a quoted precision of 1‰ per amu, HEUMANN and LIESER (1973) found no Ca isotopic variations in carbonate and sulfate samples. However, six repeated analyses on one gypsum sample yielded results ranging from within the uncertainty of their normal $^{48}Ca/^{40}Ca$ value to over 3σ away from normal, indicating the possible presence of fractionated Ca. HEUMANN and LUECKE (1973) found no significant isotopic differences in carbonates and carbonatites within an uncertainty in $^{48}Ca/^{40}Ca$ of 8‰. These results do not support the existence of large Ca isotopic variations reported by

* W. K. Kellogg Radiation Laboratory, Division of Physics, Mathematics and Astronomy.
† Mail Code 170-25, Division of Geological and Planetary Sciences, California Institute of Technology, Pasadena, CA 91125, U.S.A. Contribution No. 2960.

MILLER *et al.* (1966), who used a triple filament source (effects up to 112‰) and by ARTEMOV *et al.* (1966), who measured a CaI^+ ion beam (effects from −50‰ to +80‰ for $^{48}Ca/^{40}Ca$). Using nuclear activation techniques, CORLESS (1966, 1968) and MESHCHERYAKOV and STOLBOV (1967) reported calcium fractionation effects corresponding to ~10‰ variations in $^{48}Ca/^{40}Ca$ ratios; the quoted errors of about ±2‰ appear to have been calculated from counting statistics alone, and may be lower than actual errors.

From the existing better-quality data it is certain that any Ca fractionation effects in nature are small (HIRT and EPSTEIN, 1964; HEUMANN and LUECKE, 1973). The reported effects for $CaSO_4$ (HEUMANN and LIESER, 1973) still provided the possibility of significant mass fractionation effects which, if indeed present, would be easily resolvable by state of the art measurements (WASSERBURG *et al.*, 1969). Whereas instrumental mass fractionation effects can be significantly reduced by standardization of sample filament loading and running techniques (SHIELDS, 1966) we consider the use of a double spike internal standard as the only reliable way of correcting for instrumental mass fractionation.

EXPERIMENTAL PROCEDURES

Double spike

The double spike technique has been extensively discussed by EUGSTER *et al.* (1969) in a search for Ba isotope fractionation effects in nature. We have used a double spike consisting predominantly of ^{42}Ca and ^{48}Ca. This choice provided a large mass difference for the tracer isotopes, so that uncertainties in the instrumental mass fractionation per amu during analysis of a spiked sample would be deamplified. The use of ^{46}Ca as a tracer was excluded. The presence of high levels of ^{46}Ca could possibly interfere at a later date in a search for Ca components of distinct nucleosynthetic origin. The ^{42}Ca–^{48}Ca spike (Table 1) was prepared in 1968 from solutions of $^{42}CaCO_3$ and $^{48}CaCO_3$ and has been used before for the determination of Ca concentrations in achondrites and in lunar samples (TERA *et al.*, 1970). From the gravimetry of the spikes we obtain $^{48}Ca/^{42}Ca = 0.192 \pm 0.002$ in the double spike. The error estimate is obtained from weighing uncertainties due to the hygroscopic nature of the Ca salts. The error estimate does not include the effect of possible lack of stoichiometry of the salts provided by the Oak Ridge National Laboratory. The double tracer technique provides correction of instrumental fractionation effects by normalization of the data to the $^{42}Ca/^{48}Ca$ in the double tracer (T). We note that an error in $(^{42}Ca/^{48}Ca)_T$ would shift *all* values for the isotopic composition of the samples by a uniform fractionation factor per amu. *Differences* in the isotopic composition of samples due to mass fractionation in nature would not be affected by this shift. In this work we report isotopic compositions of natural Ca which are subject to a possible constant bias in mass fractionation of up to ±2‰ per unit mass difference.

The double spike technique requires two mass spectrometer analyses for each sample: (a) measurement of the isotopic composition of the unspiked sample, and (b) measurement of a mixture of the sample and of the double spike. We shall refer to these as *composition* and *mixture* runs respectively. If *all* samples to be analyzed have Ca isotopic compositions which are identical except for mass fractionation, then it is sufficient to establish precisely the Ca isotopic composition for one sample and to use this composition for reduction of the mixture run data of all samples. In this case, only mixture runs need be performed for most samples.

Differences between samples in isotope fractionation are reflected in distinct values of $\delta(^{40}Ca/^{44}Ca)$, defined by

$$\delta(^{40}Ca/^{44}Ca) = [(^{40}Ca/^{44}Ca)_C/(^{40}Ca/^{44}Ca)_C^{STD} - 1] \times 1000$$

where STD refers to the CaF_2 standard and C denotes data corrected for instrumental fractionation.

The use of the double spike equations and the propagation of experimental uncertainties have been described by EUGSTER *et al.* (1969) and shall not be repeated here. Samples were spiked with optimal amounts of the tracer so that $^{42}Ca/^{48}Ca$ in the mixture was within 4% of $(^{42}Ca/^{48}Ca)_T$. This corresponds to $^{40}Ca_S/^{42}Ca_T \approx 7$ (S = sample, T = tracer). Using numerical examples of mixture runs it has been checked that the unmixing equations [cf. eqs. (1) and (2) in EUGSTER *et al.*, 1969] converge quickly to the *correct* sample composition for a wide range in $^{40}Ca_S/^{42}Ca_T$.

Fractionation in cation exchange resin

RUSSELL *et al.* (1977b) briefly described observation of large Ca isotopic fractionation between the initial and final fractions of the Ca from a sample eluted through a cation exchange column. The effects are as large as 3‰ *per mass unit*, and are described in a separate note (RUSSELL and PAPANASTASSIOU, 1978). Although isotopic fractionation produced in the chemical separation of some elements using cation exchange resins has previously been observed (cf. BETTS *et al.*, 1956; LEE and BEGUN, 1958) it is surprising to observe effects of such magnitude for short (17 cm) columns. If all of the Ca loaded on a column is recovered, there can be no net fractionation of the Ca due to the column processing. If the Ca double tracer is added to the sample *prior* to chemical separation, the standard way of reducing the data will correct for any mass fractionation occurring during chemical separation of the Ca. On the basis of our detailed measurements, we have found a shift in $\delta(^{40}Ca/^{44}Ca)$ of 0.5‰ for a yield of 80%. Some of our unspiked samples passed through the column show low yields. The reason for this is that, originally, narrow cuts were used in order to separate Ca and Sr (TERA *et al.*, 1970). Our measurements indicate that for our original Ca cuts, a ~15% shift in the elution curve would result in a ~50% loss of Ca, causing a corresponding shift in $\delta(^{40}Ca/^{44}Ca)$ of −0.9‰. The lighter isotopes of Ca are held more strongly by the resin and were depleted in the collected Ca fraction. Yields lower than 50% can lead to negative shifts of several per mil in $\delta(^{40}Ca/^{44}Ca)$ (e.g. Abee-1A and thinolite-A, Table 6).

These observations were made after much of this present work had been completed. Many samples had been spiked

Table 1. Composition of ^{42}Ca–^{48}Ca tracer

Isotope	40	42	43	44	46	48
Atom Percent	4.557	79.58	0.06328	0.5165	—	15.280

Mass spectrometer data were corrected for mass fractionation by using $^{42}Ca/^{48}Ca = 5.208$ as determined from gravimetry.

only after passage through the ion exchange column in order to obtain unspiked, separated Ca aliquots, without the need for separate processing through the column of different aliquots of the original sample. The yields for the various samples processed in this way are shown in Table 6. Those samples which were spiked *prior* to passage through the column are also indicated in the table.

Chemistry and mass spectrometry

Samples were dissolved and passed through a cation exchange column using standard procedures (cf. TERA *et al.*, 1970). Blanks were found to be negligible. For each sample, 5–10 μg Ca were loaded as either the chloride or nitrate on a single, oxidized, V-shaped tantalum filament. All analyses were performed on the Lunatic I mass spectrometer (WASSERBURG *et al.*, 1969). For this work, it was found necessary to use high purity, zone refined tantalum ribbon, produced pursuant to our requests, in order to eliminate substantial K signals. After outgassing, this material showed no significant K signal ($^{39}K < 2 \times 10^{-14}$ A) during the Ca analysis ($T \sim 1400$°C). Therefore, there was no direct interference at mass 40 from ^{40}K. In addition, a large ^{39}K signal would have resulted in a broad scattered beam significantly increasing the background in the Ca region (mass 41.5–48). Since any K beam is highly unstable at Ca analysis temperatures, a reflected ^{39}K beam would have increased significantly the noise of the Ca background and hence decreased the precision of the data.

The ^{40}Ca beam causes a small, broad reflected peak in the interval 42.5 to ~49 amu. This is due to scattering of the ^{40}Ca beam off of the mass spectrometer beam tube and into the Faraday cup. The Lunatic I was originally designed with a baffle to reduce significantly the reflected ion beam from ^{39}K during measurement of ^{40}K (WASSERBURG *et al.*, 1969). This design also results in the reduction of the effect of the ^{40}Ca reflected beam so that the maximum ^{40}Ca reflected beam in the Ca region is 10^{-4} of the primary beam. For Ca, 'zeroes' were measured at ±0.15 amu from each mass peak. Correction for the background can be made with adequate precision by averaging the zeroes for each peak.

For mixture runs, data were obtained by magnetic field stepping in the mass sequence (one cycle) 40, 42, 43, 44, (46), 48, 40 with zeroes measured on both sides of each isotope (lower mass zero first). All data were obtained using a $10^{10}\Omega$ feedback resistor on the Cary-36 vibrating reed electrometer. Data were grouped in sets of 10 cycles for calculation of instrumental mass fractionation. For composition runs, data were obtained in two different cycles. Cycle A was measured on the $10^{10}\Omega$ resistor and consisted of the sequence of isotopes 40, 42, 42, 44, 40. ^{42}Ca was measured twice to provide an extra time delay after the large ^{40}Ca beam and to check for the presence of long time constants in the electronics. Cycle B was measured with a $10^{11}\Omega$ resistor and consisted of the sequence 44, (46), 48, 42, 43, 44. Data were obtained in the following order: 3 A-cycles, 7 B-cycles, 3 A-cycles, etc., for a total of 23 cycles per data set. The feedback resistor was changed manually between A and B cycles within 30 sec. For composition runs the instrumental fractionation was calculated using $^{40}Ca/^{44}Ca$ of the A cycles. B cycles were corrected for instrumental fractionation by averaging the fractionation of the two adjacent A cycles. Typically, the change in fractionation between sequential A cycles was less than 0.3‰ per amu. This procedure of instrumental fractionation calculation results in minimal uncertainties for the described data cycles. The ^{39}K beam and the focussing of the Ca beam were monitored between data sets. Data were taken with $^{40}Ca^{+} = 1 - 4 \times 10^{-10}$ A, the lower intensities being sufficient for mixture runs. The means of the first and second $^{42}Ca/^{44}Ca$ measurements in cycle A differed by as much as 0.4‰, but the mean for the second $^{42}Ca/^{44}Ca$ in cycle A ($10^{10}\Omega$) agrees well with the mean of $^{42}Ca/^{44}Ca$ in cycle B ($10^{11}\Omega$) (Table 5). Therefore, the effects of the time constants of the system and of any nonlinearities are less than about 2 parts in 10^4.

Precise ^{46}Ca measurements required a separate procedure in order to spend sufficient time measuring this isotope. Data were obtained by cycling through ^{48}Ca, ^{46}Ca and ^{44}Ca. Instrumental fractionation was corrected by normalization of $^{48}Ca/^{44}Ca$ to the value obtained in the composition run (above), thus allowing correction of the measured $^{46}Ca/^{44}Ca$.

For samples for which both composition and mixture runs were made, data analysis proceeded as follows. The composition run data were used to obtain grand means for all isotopic ratios, subject to an *unknown* instrumental fractionation factor. These grand means were then used together with the double spike composition (Table 1) and each set of ten mixture ratios in order to calculate the instrumental fractionation during the *mixture* run from the measured $^{42}Ca/^{48}Ca$ in the mixture run. Using these instrumental fractionation factors, we calculated the true $^{40}Ca/^{44}Ca$ of the *unspiked sample* as measured by the *mixture* run. Using this value we corrected the remaining isotopic ratios of the *composition* run for the instrumental fractionation during the composition run. These corrected composition data were then used to iterate the calculation of the mixture run. For samples where only a mixture run was available, the Ca isotopic composition of the CaF_2 standard was used together with the mixture run data to obtain $^{40}Ca/^{44}Ca$ in the sample. Composition runs were made for enough samples in order to ascertain by this method the existence of no distinct nucleosynthetic components in lunar samples and in the meteorites analyzed. In principle, with the double spike used, we can compare $^{43}Ca/^{44}Ca$ in the sample obtained from a mixture run and from a composition run. In cases where the comparison can be made, no differences are apparent. However, ^{43}Ca data from a mixture run tend to be of relatively low precision (~1‰) due to the low abundance of this isotope and because data for mixture runs were obtained on the $10^{10}\Omega$ feedback resistor. We did not feel that this crosscheck justified additional data acquisition on the $10^{11}\Omega$ resistor during a mixture run.

Mass fractionation law

It is well known that isotope ratios measured using a thermal ionization source show variations because of mass fractionation in the source during a run. Correction for these effects requires knowledge of the functional relationship for the measured isotope ratios. The large mass range of calcium isotopes provides a sensitive test for particular mass fractionation laws. This implies also that a precise determination of the mass fractionation function is needed if we are to utilize effectively the high precision attainable on the Lunatic I mass spectrometer. We address in the Appendix the functional relationship between isotope ratios measured using a thermal ionization source. We demonstrate that neither a linear law nor a simple power law adequately describes the large instrumental mass fractionation effects in Ca. Based on the discussion presented in the Appendix, we have used an 'exponential' law for the correction of instrumental mass fractionation. This law provides for a progressively smaller mass fractionation correction as the mass increases from ^{40}Ca to ^{48}Ca. We note that the instrumental mass fractionation effects observed for Ca must also affect the measurements of other elements by thermal ionization mass spectrometry. The identification of such effects will depend on (a) the fractional mass difference for the isotopes of each element, (b) the precision with which isotopic ratios are determined, (c) the range of the mass fractionation parameters over which data are obtained, and (d) the extent of mass fractionation in nature. There is no reason why calcium isotopic fractionation in

nature would proceed according to the same fractionation function as the one appropriate to thermal ionization. It is clear that if large fractionation effects are found in nature, special care will be needed in reducing the data and in identifying the absolute composition of highly fractionated samples.

Voltage coefficient

For composition runs, the maximum voltage measured on the $10^{11}\Omega$ feedback resistor is 1 V (for ^{44}Ca); there is no significant voltage coefficient for the $10^{11}\Omega$ resistor at this level (EUGSTER *et al.*, 1969). Checks for drifts in the data due to a voltage coefficient for the $10^{10}\Omega$ resistor have shown no significant effects up to 4 V ($^{40}Ca = 4 \times 10^{-10}$A). As noted earlier, two sequential measurements of ^{42}Ca were obtained with the $10^{10}\Omega$ resistor (A cycles) to monitor the effect of the delay time after measuring the large ^{40}Ca signal. Since the background correction was obtained by averaging the background on either side of the peak, a fast, exponentially decaying signal from ^{40}Ca during measurement of ^{42}Ca would result in apparently lower ^{42}Ca intensity. The first measurement of ^{42}Ca ($\Delta t = 5.1$ sec between ^{40}Ca and ^{42}Ca peak measurement) on $10^{10}\Omega$ yielded $^{42}Ca/^{44}Ca$ lower than the second measurement ($\Delta t = 10.2$ sec) by as much as 0.4‰. However, the agreement of the second ^{42}Ca measurement on $10^{10}\Omega$ with the measurement on $10^{11}\Omega$ indicates that the two feedback resistors and the Cary-36 electrometer are not subject to significant nonlinearities, for signals corresponding to the Ca isotopes other than ^{40}Ca, for changes in measured voltages by a factor of ~10.

RESULTS

$^{40}Ca/^{44}Ca$ resolution

For every mixture run, we grouped ten sequential cycles into a data set and have corrected the set for instrumental fractionation using the means of the set. For most runs we obtained about 20 sets of data with a standard deviation for a set less than 0.2‰ for $^{i}Ca/^{44}Ca$, $i = 40, 42, 48$. The corrected $^{40}Ca/^{44}Ca$ from individual sets were averaged and we quote as uncertainties twice the standard deviation of the mean ($2\sigma_{mean}$) of these data sets. This uncertainty includes random errors (e.g. beam instability, electrometer noise, etc.). It may also include contributions either due to changing instrumental fractionation during data sets (PAPANASTASSIOU and WASSERBURG, 1969) or due to use of an imprecise law for correction for instrumental fractionation (see Appendix).

To demonstrate the precision with which we can resolve differences in $^{40}Ca/^{44}Ca$, we have prepared and analyzed standards enriched in ^{44}Ca. A ^{44}Ca tracer (98.5% ^{44}Ca; 1.4% ^{40}Ca) was added to $CaCO_3$ Standard-2 to produce solutions with *lower* $^{40}Ca/^{44}Ca$ ($\delta^G = -0.5$ and -1.9‰; G = gravimetry). The enriched standards were analyzed after being mixed with the double tracer. The results are listed in Table 2 and shown in Fig. 1. The gravimetric and mass spectrometric results on the enriched standards are fit by a straight line of unit slope and indicate that we can resolve changes in $^{40}Ca/^{44}Ca$ of 0.5‰. From replicate analyses of $CaCO_3$ Standard-1 (Fig. 6), we estimate that the $\delta(^{40}Ca/^{44}Ca)$ of most analyses calculated using the exponential fractionation law lie within ±0.34‰. Only two runs with highly fractionated Ca and limited precision are outside of this range. Using adequate care in the loading of samples on the mass spectrometer filament, and in the heating to Ca running temperatures, we were able to take data for mixture runs at high beam intensities *before* the samples had become depleted and highly fractionated. The results of replicate analyses and of enriched standards demonstrate that differences in the $\delta(^{40}Ca/^{44}Ca)$ values of samples can be clearly resolved by our techniques to a level of about 0.5‰. This represents a factor of ten improvement over the best previously published work. This precision of ~0.1‰ per amu is roughly equivalent to the precision obtained for oxygen and sulfur measurements, for which extensive analyses exist.

Table 2. ^{44}Ca enrichment of $CaCO_3$, Standard-2

δ^G Gravimetry	$(^{40}Ca/^{44}Ca)_C$	δ^S Mass Spectrometry
0.0	47.200±9	0.0±0.2
−0.46	47.164±5	−0.7±0.1
−1.86	47.094±5	−2.1±0.1

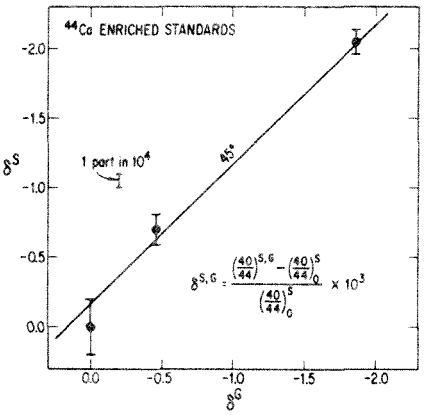

Fig. 1. Analyses of ^{44}Ca enriched standards. Measured amounts of a ^{44}Ca isotopic tracer solution were added to aliquots of a $CaCO_3$ standard in order to produce mixtures with lower $^{40}Ca/^{44}Ca$. Comparison of the spectrometric and gravimetric data shows that consistent results were obtained, as the data are fit well by a straight line of unit slope. Errors shown are $2\sigma_{mean}$ for individual mass spectrometer runs. If the uncertainty of the zero-enrichment standard were added to the enriched standard analyses the line would have been drawn through the origin.

Large effects

We discuss in this section analyses of samples which have effects in $\delta(^{40}Ca/^{44}Ca)$ very much larger than the resolution limit of 0.5‰. Such effects have been (a) induced by us, and (b) induced in the manufacture of Ca metal and of spectrographically pure $CaCO_3$.

We have evaporated CaF_2 onto stainless steel slides by heating in a vacuum. In Table 3 we present ana-

Table 3. Vacuum evaporation of CaF_2 Standard onto foils

		$(^{40}Ca/^{44}Ca)_C^a$	$\delta(^{40}Ca/^{44}Ca)$
Batch-A[b]	Foil-1	46.822±4	−7.0±0.1
	Foil-2	46.834±4	−6.8±0.1
Batch-B[b]	Foil-1	47.363±4	+4.5±0.1
	Foil-2	47.364±4	+4.5±0.1

[a] Corrected for instrumental mass fractionation. The errors correspond to the last figures shown and are $2\sigma_{mean}$.
[b] Foils in each batch were adjacent, with nearly identical geometries with respect to the evaporation cell.

lyses of Ca evaporated simultaneously for identical times on *adjacent* foils and then removed by rinsing with 1N HNO_3. The results show essentially identical $\delta(^{40}Ca/^{44}Ca)$ values of −7.0‰ and −6.8‰ for the two foils from evaporation Batch-A; these foils were exposed to the evaporating CaF_2 after the source had been allowed to become depleted. Two foils from a separate evaporation in which the source was not initially depleted *and* not heated to exhaustion of the CaF_2 have $\delta(^{40}Ca/^{44}Ca) = +4.5‰$. It is no surprise that vacuum distillation of Ca at ~1200°C results in mass fractionation, as this process is analogous to the fractionation in a thermal ionization source. The agreement of the data for pairs of foils expected to have identical $\delta(^{40}Ca/^{44}Ca)$ provides an independent confirmation of our precision.

We have also measured the Ca composition of spectrographically pure $CaCO_3$ provided by Johnson Matthey Chemicals, Ltd. This reagent, which we label $CaCO_3$ Standard-1, shows a large $\delta(^{40}Ca/^{44}Ca)$ of +12.8‰ (Table 4) as compared to the CaF_2 standard or effectively all other samples analyzed by us. The analyses of $CaCO_3$ Standard-1 include aliquots obtained from separate dissolutions of the salt, samples not passed through ion exchange columns, and samples spiked before or after passage through the columns. The large Ca effects in this standard provided additional impetus to this work, especially since Johnson Matthey first indicated that the $CaCO_3$ was obtained from chalk. However, further correspondence indicated that this particular spec-pure salt (Lot No. 4064) was prepared from Ca metal. One method used industrially to manufacture Ca metal involves an evaporation-distillation process! To check that in fact Ca metal may be highly fractionated, purified Ca metal from the J. T. Baker Chemical Co. was analyzed (Table 4); this sample has $\delta(^{40}Ca/^{44}Ca) = +6.8‰$. This value also is substantially different from the values of all naturally occurring samples. By comparison, $CaCO_3$ Standard-2 (Johnson Matthey, spec pure, Lot No. 9912) was obtained from Derbyshire chalk and has $\delta(^{40}Ca/^{44}Ca) = +1.0‰$. This is in much closer agreement with the CaF_2 standard and the other samples analyzed by us. The fractionation 'mirage' provided by Standard-1, Ca metal, and possibly other salts used by others as 'standards' may provide a reason for some of the Ca isotopic mass fractionation effects reported by other workers. It clearly shows that Ca produced industrially and possibly being cycled through organisms may not have an unfractionated initial composition.

Table 4. Commercial Ca reagents

	$(^{40}Ca/^{44}Ca)_C^a$	$\delta(^{40}Ca/^{44}Ca)$
CaF_2 Standard	47.153±3	0.0±0.1
	47.156±8	+0.1±0.2
$CaCO_3$ Standard-2[b]	47.200±9	+1.0±0.2
$CaCO_3$ Standard-1[c]	47.772±8	+13.1±0.2
	47.768±6	+13.0±0.1
	47.751±6	+12.7±0.1
	47.740±5	+12.4±0.1
	47.770±10	+13.1±0.2
	47.747±7[d]	+12.6±0.2
	47.762±7	+12.9±0.2
	47.718±6[e]	+12.0±0.1
	47.819±14[f]	+14.1±0.3
	47.803±6[f]	+13.8±0.1
Ca Metal[g]	47.472±7	+6.8±0.2

[a] See Table 3, footnote a.
[b] Johnson Matthey, Lot No. 9912.
[c] Johnson Matthey, Lot No. 4064.
[d] Passed through ion exchange column after adding double spike.
[e] Passed through ion exchange column before adding double spike.
[f] Highly fractionated run (see Appendix).
[g] J. T. Baker, Lot No. 6278.

Isotopic composition of Ca

The results of composition runs for Ca are listed in Table 5. For our work we show the $^{40}Ca/^{44}Ca$ determined using the double spike. For data of other workers we show the reported $^{40}Ca/^{44}Ca$. For the remaining isotopes, data were corrected for mass fractionation in nature (our data) or for instrumental fractionation (other work) through normalization, using the exponential law, to the $^{40}Ca/^{44}Ca$ value for the CaF_2 standard. This data presentation permits identification of possible nuclear effects in Ca independently of mass fractionation effects, and provides for direct comparison of analyses by different workers. We present data for two Ca terrestrial standards, two lunar samples and for four meteorites. Excluding the $CaCO_3$ Standard-1 discussed earlier, the samples in Table 5 show a range of 2.1‰ in $^{40}Ca/^{44}Ca$. After correction for this small natural fractionation, the data for the remaining Ca isotopes show no variations within the estimated errors of $2\sigma_{mean}$. For ^{42}Ca we present data obtained using the $10^{10}\Omega$ and $10^{11}\Omega$ resistors. The agreement of the second measurement on $10^{10}\Omega$ and that on $10^{11}\Omega$ indicates that any nonlinearities in the system have been reduced to the order of typical uncertainties for $^{42}Ca/^{44}Ca$ of 0.2‰.

There is good agreement within estimated uncer-

Table 5. Ca isotopic composition

	$\left(\frac{40}{44}\right)_C^{a,d}$	D[b]	$\left(\frac{42}{44}\right)^{c,d}$	$\left(\frac{42}{44}\right)^{c,e}$	$\left(\frac{43}{44}\right)^{c,e}$	$\left(\frac{46}{44}\right)^{c,e}$	$\left(\frac{48}{44}\right)^{c,e}$
This Work[f]							
CaF_2 Standard[g]	47.153 ±0.003	1.00000 ±0.00006	0.31205 ±0.00010	0.31219 ±0.00004	0.06487 ±0.00003	—	0.08874 ±0.00004
$CaCO_3$ Standard-1	47.751 ±0.007	1.01268 ±0.00015	0.31210 ±0.00005	0.31219 ±0.00004	0.06483 ±0.00002	0.00152 ±0.00001	0.08868 ±0.00002
70215 TR	47.108 ±0.005	0.99905 ±0.00011	0.31227 ±0.00010	0.31224 ±0.00005	0.06486 ±0.00003	—	0.08869 ±0.00003
15021 Res[g]	47.123 ±0.014	0.99936 ±0.00030	0.31223 ±0.00009	0.31225 ±0.00010	0.06484 ±0.00002	—	0.08869 ±0.00004
Orgueil	47.166 ±0.006	1.00028 ±0.00013	0.31215 ±0.00012	0.31222 ±0.00009	0.06485 ±0.00003	—	0.08873 ±0.00003
Murchison	—	—	0.31220 ±0.00008	0.31221 ±0.00002	0.06486 ±0.00002	—	0.08874 ±0.00002
Haverö	47.122 ±0.006	0.99934 ±0.00013	0.31220 ±0.00007	0.31218 ±0.00006	0.06486 ±0.00002	—	0.08869 ±0.00002
Guareña	47.082 ±0.005	0.99849 ±0.00011	0.31202 ±0.00008	0.31222 ±0.00003	0.06487 ±0.00001	—	0.08870 ±0.00002
Average	(≡47.153)	—	0.31215 ±0.00006	0.31221 ±0.00002	0.06486 ±0.00001	0.00152 ±0.00001	0.08871 ±0.00002
Earlier Work							
Nier (1938)	46.9 ±2.0	0.995 ±0.030	—	0.31 ±0.01	0.071 ±0.003	0.0016 ±0.0002	0.091 ±0.004
White and Cameron (1948)	45.5 ±0.9	0.965 ±0.019	—	0.31 ±0.01	0.063 ±0.003	0.0015	0.081 ±0.002
Backus *et al.* (1964)	45.7 ±0.9	0.969 ±0.019	—	0.314 ±0.006	0.0656 ±0.0015	0.00153 ±0.00008	0.092 ±0.003
Stahl (1968)	46.9 ±0.3	0.995 ±0.006	—	—	—	—	0.089 ±0.001
Coleman[h] (1971)	45.7	0.969	—	0.3143 ±0.0009	0.0624 ±0.0006	0.0016 ±0.0002	0.090 ±0.002
Heumann and Lieser (1973)	47.3 ±0.2	1.0031 ±0.0042	—	—	—	—	0.089 ±0.001
Barnes *et al.*[i] (1972)	46.480 ±0.087	0.98573 ±0.00185	—	0.3126 ±0.0011	0.0650 ±0.0009	0.0017 ±0.0005	0.08959 ±0.00055

[a] Corrected for mass spectrometer fractionation using the associated mixture run.

[b] $D = (40/44)_C/(40/44)_C^{STD}$; the CaF_2 analysis is used as the standard.

[c] The fractionation in nature between samples has been removed through normalization of $(40/44)_C$ to the value of the CaF_2 standard according to the exponential law.

[d] Measured on the 10^{10} Ω electrometer feedback resistor (this work).

[e] Measured on the 10^{11} Ω electrometer feedback resistor (this work).

[f] Errors quoted are $2\sigma_{mean}$.

[g] These values were calculated from the data used in RUSSELL *et al.* (1976) and differ slightly because the values were previously corrected for mass fractionation using a linear law and also because a distinct value for the tracer 42/48 was used in the previous work.

[h] The author normalized $^{40}Ca/^{44}Ca$ to the value of BACKUS *et al.* (1964).

[i] Errors estimated by the authors included uncertainties due to mass fractionation effects. The errors are probably smaller for the normalized ratios in the last four columns.

tainties between our results and those of NIER (1938) except for $^{43}Ca/^{44}Ca$ for which Nier's value is higher than ours by about twice the uncertainty estimated by Nier. There is also good agreement with the results of WHITE and CAMERON (1948) except for $^{48}Ca/^{44}Ca$ which is lower than our value by three times the estimated uncertainty. Our results are in agreement within uncertainties with more recent work of BACKUS *et al.* (1964). There is disagreement in $^{42}Ca/^{44}Ca$ and $^{43}Ca/^{44}Ca$ between our results and those of COLEMAN (1971). These disagreements are puzzling in view of the relatively high precision quoted by COLEMAN (1971). The description of the experimental procedure of COLEMAN (1971) is limited and provides no clues for this disagreement. There is good agreement between our work and the recent work of BARNES *et al.* (1972). It should be noted that the estimated errors quoted by Barnes *et al.* include uncertainties due to instrumental mass fractionation effects; therefore, for the normalized ratios in the last four columns of Table 5, the actual errors are probably smaller.

Samples

We have analyzed a variety of meteoritic, lunar and terrestrial materials; the following is a brief description of the samples:

A. *Meteorites.* The enstatite achondrite (aubrite) Norton County and the enstatite chondrite Abee (E4) were analyzed to check the possibility that these highly reduced materials contain fractionated Ca. In particular, the presence of CaS in these meteorites may indicate condensation at high temperature from a carbon-rich solar nebula parcel (C/O > 0.9) as discussed by LARIMER (1968, 1975). HULSTON and THODE (1965) and KAPLAN and HULSTON (1966) have also determined significant fractionation for sulfur in CaS in the enstatite meteorites they analyzed (Abee, Hvittis, Norton County). Two total meteorite specimens of Abee from different collections were analyzed; Abee-1 was obtained from the United States National Museum, while Abee-2 was obtained from the Nininger collection, Arizona State Univ. A sample of Abee-2 was also leached in cold water in order to extract the CaS for analysis; the leach contained about 44% of the Ca in the meteorite. The Norton County sample was also obtained from the Nininger collection; the sample analyzed consisted predominantly of large enstatite crystals. The Haverö ureilite was analyzed because it represents a rare and unique chemical class produced by significant chemical fractionation. In addition, Haverö contains trace amounts of CaS in carbon-rich veins (RAMDOHR, 1972); a total meteorite sample of 200 mg was dissolved and an aliquot was used for the Ca work. Total meteorite samples of Orgueil (C1) and Murchison (C2) were analyzed as representatives of 'chemically unfractionated', low temperature chondritic matter. The chondrite Guareña (H6) was analyzed as a representative of strongly metamorphosed chondrites; a total sample was obtained by crushing, with the metal phase being removed by use of a covered hand magnet. The eucrite Ibitira was analyzed for comparison with lunar and terrestrial igneous rocks.

B. *Lunar samples.* Ca from two mare basalts and a mare soil was analyzed. Basalt 70215 is an aphanitic, quenched magma, least subject to near-surface chemical fractionation. Basalt 75055 is a typical low-K coarse-grained sample from which mineral separates were obtained and analyzed. The soil 15021 was analyzed in a sequence of experiments described by RUSSELL *et al.* (1976, 1977a, b). The samples analyzed represent the bulk residue from mild leaching with water (and HNO_3 for 15021-B); less than 2% of the Ca was removed by the leaching in each case.

C. *Terrestrial samples.* The sample of seawater was collected near the Bahama Islands. The mid-Atlantic ridge tholeiite (VG295) and the carbonatite from Tanzania (OLC-1) have been previously analyzed by DEPAOLO and WASSERBURG (1976) for Sm–Nd and Rb–Sr; they are young igneous rocks which originated from distinct, ancient mantle reservoirs with very different REE patterns. The fluorite sample, also of igneous origin, is a cleavage fragment from the Stoddard mine in Westmoreland, N.H. The calcite from the Lucerne Valley in California is of nonmarine origin; no other details are known. The thinolite is from Mono Lake, California; thinolite is amorphous $CaCO_3$ precipitated from lake water as the result of the removal of CO_2 from the water by micro-organisms. The two gypsum samples are Lower Cambrian and Middle Jurassic, and have previously been isotopically analyzed for sulfur and oxygen (see Table 6) by THODE and MONSTER (1965) and SAKAI (1972). The seashell is from a specimen from the genus *Strombus.* The eggshell is from a domestic chicken. Ca in chicken eggshells, especially in case of dietary Ca insufficiency, is drawn partially from the skeletal structure. Since this egg came from a commercial farm, the Ca was probably dietary in origin. The squirrel tooth came from a squirrel taken in the high Sierras. This animal has been studied by ELIAS *et al.* (1977) and is expected to be least affected by industrial sources of Ca. The shark teeth came from a pregnant *Carcharhinus limbatus* caught near the Palau islands. The human tooth is an incisor made available to us shortly after removal from a 50 yr old female. The roots of the shark teeth and of the human tooth were analyzed as exchange with calcium in the bloodstream takes place in these regions.

Analytical results: mass fractionation

Fractionation results for these samples are shown in Table 6. For meteorites and lunar samples, these results are shown in Fig. 2; the results for terrestrial samples are shown in Fig. 3. The $\delta(^{40}Ca/^{44}Ca)$ values are shown relative to the CaF_2 standard. We have listed in Table 6 the measured column yields and have indicated which samples were spiked before elution through the column. For cases where the yields were not directly measured, we have provided estimates of the yields based on Ca concentration measurements in the literature. Two samples with extremely low yields (Abee-1A and thinolite-A) were spiked before column elution and reanalyzed. Historically, our attempt to duplicate the low $\delta(^{40}Ca/^{44}Ca)$ of these samples resulted in our identification of the Ca isotope fractionation during column elution. As discussed previously, $\delta(^{40}Ca/^{44}Ca)$ measurements are precise to 0.5‰ both for samples spiked before elution and also for samples which had elution yields greater than ~80% but which were not totally spiked. For yields between 80% and 50%, there may be systematic shifts in $\delta(^{40}Ca/^{44}Ca)$ of up to −0.9‰. The sign of the shift indicates that the low yields are due to the loss of the trailing part of the elution curve.

For the meteorites, there appears to exist a small range of natural fractionation of 2.5‰ for $^{40}Ca/^{44}Ca$. The more precise Abee data for the two different whole rock specimens are in excellent agreement. The Ca extracted from Abee-2B by leaching with water has an identical Ca composition to the Abee-2A total rock, and therefore provides no evidence for fraction-

Table 6. Analytical results

Sample	Weight (mg)	Column Yield (Percent)	$(^{40}Ca/^{44}Ca)^{a}_{C}$	$\delta(^{40}Ca/^{44}Ca)$
Meteorites				
Abee-1A (E4)	11	34	47.021±16	−2.8±0.4
			47.044±7	−2.3±0.1
Abee-1B	13[b]	SBC[c,d]	47.201±15	+1.0±0.3
			47.155±8	0.0±0.2
Abee-2A TR	12	96	47.143±7	−0.2±0.2
Abee-2B H_2O Leach[e]	25	83[f]	47.153±5	0.0±0.1
Norton County (aubrite)	21	SBC	47.193±6	+0.9±0.1
Orgueil (C1)	12	43[g,h]	47.166±6	+0.3±0.1
Guareña (H6)	50	56[h]	47.082±5	−1.5±0.1
Haverö (ureilite)	40	100[h]	47.122±6	−0.7±0.1
Ibitira (eucrite)	2	87[h]	47.146±9	−0.2±0.2
Lunar Samples				
70215	4	60-70[h]	47.103±8	−1.1±0.2
			47.108±5	−1.0±0.1
75055 Plagioclase	1	68[h]	47.126±8	−0.6±0.1
75055 Pyroxene	5	nm[i]	47.158±6	+0.1±0.1
15021-B Residue	9	62[h]	47.123±14	−0.7±0.3
15021-C Residue	106	SBC	47.181±9	+0.6±0.2
Terrestrial Samples				
Seawater	—	80-95	47.109±7	−1.0±0.2
		SBC	47.117±5	−0.8±0.1
Atlantic Ridge Tholeiite	8	nm	47.127±5	−0.6±0.1
Carbonatite (Tanzania)	5	nm	47.164±20	+0.2±0.4
Fluorite	3	96	47.165±10	+0.2±0.2
Calcite	4	87	47.123±6	−0.7±0.1
Thinolite-A	2	32	47.062±7	−2.0±0.2
			47.068±6	−1.8±0.1
Thinolite-B	17[b]	SBC	47.192±9	+0.8±0.2
Gypsum-1[j]	26	SBC	47.181±11	+0.6±0.2
Gypsum-2[k]	30	SBC	47.208±13	+1.2±0.3
Conch *(Strombus)* Seashell	7	95	47.170±6	+0.4±0.1
Chicken Eggshell	5	91	47.202±7	+1.0±0.2
Squirrel Tooth	36	>42[l]	47.240±14	+1.8±0.3
Shark Tooth, Mother (Root)[m]	2	SBC	47.193±6	+0.9±0.1
Shark Tooth, Fetus (Root)[n]	0.4	SBC	47.215±8	+1.3±0.2
Human Tooth (Root)	2	nm[o]	47.133±4	−0.4±0.1

[a] See Table 3, footnote a.

[b] Separate dissolution.

[c] SBC: Double spike added to sample before chemical separation of Ca.

[d] Measured Ca concentration is 0.794 ± 0.001% by weight, in fair agreement with 0.872% value of VON MICHAELIS *et al.* (1969).

[e] 44% of Ca in this total meteorite split was removed by a cold water rinse.

[f] Column yield *measured* by comparing Ca contents in sample aliquots prior to and after chemical separation.

[g] Yield estimate uncertain due to sample heterogeneity.

[h] Yield estimated using literature values for Ca concentrations: Orgueil (VON MICHAELIS *et al.*, 1969); Guareña (JAROSEWICH and MASON, 1969); Haverö (MARVIN and WOOD, 1972); Ibitira (WÄNKE *et al.*, 1974); 70215 and 75055 (DYMEK *et al.*, 1975); 15021 (RUSSELL *et al.*, 1977b).

[i] nm: not measured.

[j] Sample SL-120-T63-40 from H. G. Thode: $\delta^{34}S = 38.2‰$, $\delta^{18}O = 10.5‰$.

[k] Sample SL-91-9 from H. G. Thode: $\delta^{34}S = -23.3‰$, $\delta^{18}O = +3.1‰$.

[l] Because of the presence of significant amounts of organic material, the calculated yield is probably too low, as it was assumed that the tooth was comprised totally of calcium phosphate.

[m] Measured Ca concentration is 37% by weight.

[n] Measured Ca concentration is 50% by weight.

[o] Assuming root chip to be totaly comprised of calcium phosphate, a yield of only 18% is calculated. However, as this portion of the tooth appears to be primarily cementum rather than dentine, it probably has a Ca concentration much lower than phosphate.

ation between the oldhamite and the other Ca minerals. The enstatite achondrite Norton County yields a somewhat lighter Ca with $\delta = 1.0‰$. The two meteorites expected to be products of magmatic differentiation, Ibitira and Haverö, have slightly negative δ values of −0.2‰ and −0.7‰ which are similar to the values for lunar samples. The data on Guareña, which show the heaviest Ca, may reflect the low yield for this sample so that Guareña most probably has $\delta(^{40}Ca/^{44}Ca) \approx -0.5‰$. A similar argument for

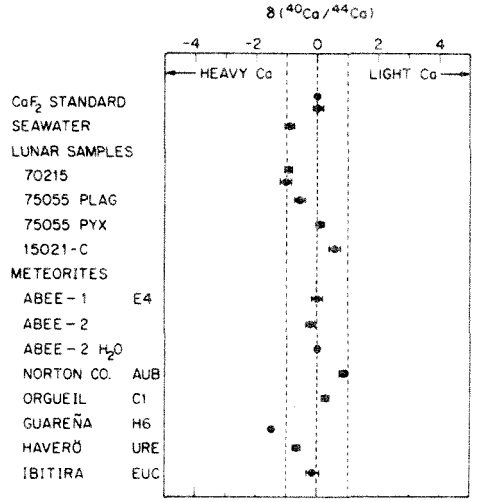

Fig. 2. Deviations of $^{40}Ca/^{44}Ca$ in per mil (relative to the CaF_2 standard) for lunar samples and meteorites. All data are within $\delta(^{40}Ca/^{44}Ca) = \pm 1.2‰$, corresponding to a fractionation range of $\pm 0.3‰$ per amu. Within this range distinct differences in $\delta(^{40}Ca/^{44}Ca)$ are obtained.

Orgueil would place it at $\delta(^{40}Ca/^{44}Ca) \approx 1‰$. Such possible small shifts do not change the general data display which demonstrates the existence of small distinct $^{40}Ca/^{44}Ca$ variations about a mean $\delta(^{40}Ca/^{44}Ca) \approx 0$, which are due to mass fractionation. The present data do not permit the identification of a systematic variation in $^{40}Ca/^{44}Ca$ with meteorite class.

The lunar samples (Fig. 2) also show small values of $\delta(^{40}Ca/^{44}Ca)$ and a total range less than 2‰. The small difference between the plagioclase and pyroxene

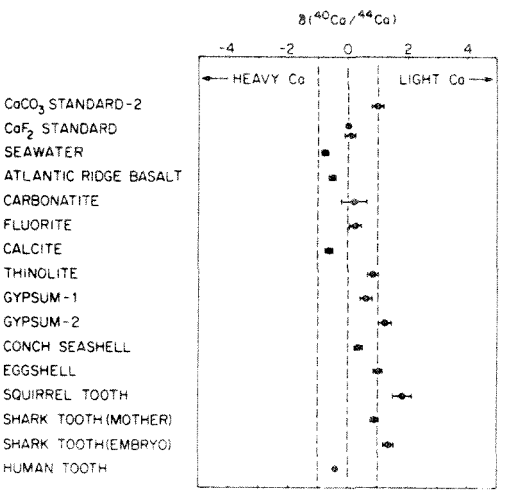

Fig. 3. Deviation of $^{40}Ca/^{44}Ca$ in per mil (relative to the CaF_2 standard) for terrestrial samples. A variety of samples, including igneous samples, evaporites and biogenic samples define a narrow range of fractionation from -1 to $+2‰$.

analyses of 75055 does not permit the establishment of a clear-cut fractionation between coexisting silicates because of small possible shifts due to the unknown column yield for the pyroxene analysis. The lighter Ca obtained for soil 15021 indicates that lunar samples do exhibit a range in $^{40}Ca/^{44}Ca$ of at least $\sim 1‰$.

In examining the terrestrial data, it may be seen that 2.1‰ of the total 2.6‰ range of $\delta(^{40}Ca/^{44}Ca)$ is observed for samples spiked prior to the column chemistry. These data demonstrate the existence on the earth of samples with distinctly fractionated Ca. The Ca in seawater provides the most negative δ value of all of our terrestrial samples. The Atlantic ridge tholeiite has a Ca composition overlapping the seawater value. This basalt has a Sr composition which is not contaminated by seawater Sr (DePAOLO and WASSERBURG, 1976), so our result is probably not due to contamination by seawater Ca. Two other igneous samples (carbonatite and fluorite) have δ values near zero. The δ value for the calcite crystal is close to the seawater value, although the calcite is of non-marine origin. The thinolite and the two gypsum samples have positive δ values from 0.6 to 1.2‰. The small, nearly identical δ values for the gypsum samples are in sharp contrast to the large $\delta(^{34}S/^{32}S)$ difference of 62‰ and $\delta(^{18}O/^{16}O)$ difference of 7‰. The Ca data clearly indicate the absence of significant Ca effects accompanying the large S effects associated with sulfate reduction. The aragonite from the *Strombus* shell is 1.2‰ lighter than our seawater Ca sample. The shark teeth also yield higher δ values. The 0.4‰ fractionation between the fetus and mother teeth is just at the limit of being significant. The chicken eggshell has $\delta(^{40}Ca/^{44}Ca) = 1.0 \pm 0.2‰$. The entire tooth of the squirrel has $\delta(^{40}Ca/^{44}Ca) = 1.8 \pm 0.3‰$ and is the highest value measured to date. Because of the uncertain column yield, the true value may actually be as much as 1‰ higher. However, it is to be emphasized that even if this were the case, all δ values for our samples still would be very small. The data presented here show no evidence at the present for much larger fractionation effects in Ca except in samples significantly modified by industrial processes.

DISCUSSION

Ca *isotope composition*

We have obtained precise isotope compositions of Ca in samples of various origins (Table 5). Within the experimental uncertainties of 0.2‰ for $^{42}Ca/^{44}Ca$, 0.5‰ for $^{43}Ca/^{44}Ca$ and 0.5‰ for $^{48}Ca/^{44}Ca$, a unique Ca isotope composition is observed after normalization which removes small differences due to mass fractionation in nature. The level of K in all samples analyzed in this study was so low as to preclude the presence of any detectable amounts of radiogenic ^{40}Ca. We have determined a uniform Ca composition in total meteorite samples after correc-

tion for mass fractionation. This is in contrast to oxygen, for which CLAYTON *et al.* (1976) find small but ubiquitous amounts of an ^{16}O-rich component in different classes of meteorites. For example, the Haverö ureilite is about 0.5‰ enriched in the ^{16}O component relative to the earth. Effects in ^{40}Ca, ^{42}Ca or ^{44}Ca as large as the ^{16}O effect would be easily resolvable for Haverö. Similar effects for the less abundant Ca isotopes might not be as easily resolvable. Although no nuclear isotope effects are observed in Haverö, a somewhat more sensitive test for an extra nucleosynthetic Ca component may come from analyses of L or LL chondrites, since they are depleted by ~2‰ in ^{16}O relative to the earth (CLAYTON *et al.*, 1976).

Recently, LEE *et al.* (1978) have reported Ca isotope anomalies in two Ca-Al-rich inclusions in the Allende meteorite relative to the Ca isotopic composition obtained here. These inclusions also show Ba and Nd isotopic anomalies (MCCULLOCH and WASSERBURG, 1978) and were chosen for analysis because they had been shown to contain Mg and O of a unique isotopic signature (WASSERBURG *et al.*, 1977; CLAYTON and MAYEDA, 1977). These data show the presence of isotope anomalies in rare Allende inclusions for a wide range in atomic number and will require in the future a more thorough search for anomalies both in Allende and in ordinary chondrites.

The precisely determined isotopic composition allows calculation of the atomic weight of Ca. Using isotope ratio average values tabulated in Table 5, we obtain an atomic weight of 40.076 ± 0.001. The dominant source of error is the uncertainty of ±2‰ per amu in the *absolute* isotopic composition of the double spike. This precise determination of the atomic weight is in good agreement with the value now in use of 40.08 ± 0.02 (error computed from WHITE and CAMERON, 1948).

Theoretical considerations

It is important to consider mechanisms leading to the Ca isotope fractionation effects reported in this paper. Over the years, predictions of the size of effects arising from equilibrium isotope exchange for chemical reactions in gasses have been based on statistical-mechanical calculations and have been quite successful. However, problems involving condensed phases are far more difficult because of the necessity to treat the continuous interactions between individual molecules and their neighbors. The problem is difficult even for a seemingly simple system such as water vapor and liquid water in isotopic equilibrium; there are no calculations which derive a theoretical expression for the oxygen fractionation in this important system. For the solid state, the situation is in principle somewhat clearer, providing that the solid is a perfect crystal. If enough is known about the potential energy function which describes the interactions between the various constituents of the unit cell, the phonon spectrum for the crystal can be calculated by numerical techniques. These normal modes for the unit cell then play the same role that vibrational energies of gas molecules do in calculations of gaseous isotope exchange. However, the assumed potentials always contain adjustable parameters so that it is not clear that fractionation effects can be truly predicted. For coexisting sulfides ($\Delta \sim 2$‰ for $^{34}S/^{32}S$), these difficulties have led to theoretical efforts of an approximate nature which have attempted to determine the order of decreasing $^{34}S/^{32}S$ among coexisting sulfide minerals (SAKAI, 1968; BACHINSKI, 1969).

To our knowledge, calculation of fractionation effects arising from non-equilibrium chemical processes have not been carried out. Such effects can be large, as is the case for S isotope fractionation during bacterial reduction of sulfate and sulfite (cf. HARRISON and THODE, 1958; KEMP and THODE, 1968). Although we have not made detailed calculations of Ca isotope fractionation effects, we list below several mechanisms by which small fractionation effects *may* arise in Ca.

(1) *Equilibrium isotope exchange between precipitated solids and aqueous solutions.* This process could possibly operate for multiple stages in nature, allowing isotope effects to be built up in, for example, evaporite deposits.

(2) *Isotope fractionation between coexisting calcium minerals.* Fractionation at the few per mil level for Ca in minerals crystallizing from a melt might be expected based on the experimentally measured sulfur isotope fractionation among coexisting sulfides (GROOTENBOER and SCHWARCZ, 1969; KAJIWARA *et al.*, 1969; KAJIWARA and KROUSE, 1971).

(3) *Diffusion out of mineral grains.* It is quite possible that appreciable isotope fractionation of Ca may arise because of diffusion, providing that bulk transport by an interstitial fluid is not dominant. These effects would be most evident for minerals originally rich in Ca from which the Ca has been extensively depleted. For a calcic plagioclase in which Ca has been replaced by Na at relatively high temperatures to yield albite, SENFTLE and BRACKEN (1955) estimate that, in a 100 yr cooling span, there will be a 5.6‰ per amu Ca isotope fractionation in millimeter-sized crystals.

(4) *Diffusion across membranes.* Possible examples of this mechanism, as operative in living organisms, would be the transfer of ingested calcium into the bloodstream and diffusion between the bloodstream and bones, teeth or shell. The precipitation exchange mechanism described above may also be operative in organisms. The extent to which organisms can amplify any calcium isotopic fractionation through multiple-stage processing is unclear.

(5) *Isotope fractionation of Ca in the solar nebula.* Recently, large mass dependent fractionation effects of up to 30‰ and 15‰ per mass unit have been found for Mg and O in two refractory-element-rich inclusions in Allende (see WASSERBURG *et*

al., 1977 and CLAYTON and MAYEDA, 1977). The mechanism for these large effects is not known but may be associated with plasma effects in the solar nebula (ARRHENIUS and ALFVÉN, 1971). The effects for Mg imply that *large* effects for the chemically similar element Ca are also possible.

(6) *Fractionation on planetary surfaces.* Extensive data on O and Si show large fractionation effects on surfaces of lunar soil grains. The effects have been interpreted as arising from the bombardment of the lunar surface by micrometeorites and/or the solar wind and subsequent isotope separation by the lunar gravity field (cf. EPSTEIN and TAYLOR, 1971; RUSSELL *et al.*, 1977b).

Ca *isotope fractionation in nature*

It is remarkable that for terrestrial and extraterrestrial samples representing distinct physical, chemical and biological processes there is only a small range of isotope fractionation in Ca and that there is nearly total overlap of the range of fractionation for the distinct planet reservoirs.

Meteorites. The meteorite data show small effects in $^{40}Ca/^{44}Ca$ with a total range of 2.5‰. In this range are included carbonaceous and normal chondrites, an enstatite chondrite and achondrite, and meteorites which are the product of magmatic differentiation. Unique among meteorites, the enstatites appear to have formed under reducing conditions. Models for their formation postulate the existence of regions in the solar nebula with distinct chemical conditions (LARIMER, 1975). From our data for Abee ($\delta = 0$‰) and Norton County ($\delta = +0.9$‰), there is clearly an absence of any *large* Ca isotope fractionation in these materials, either in the bulk samples or in the oldhamite (CaS). Therefore, it appears that the enstatites did not form in a region of the solar nebula in which there was highly fractionated Ca. A similar statement can be made for sulfur on the basis of the whole-rock isotope data (HULSTON and THODE, 1965; KAPLAN and HULSTON, 1966).

We now briefly review evidence for isotope fractionation of other elements in meteorites. Studies of oxygen isotope fractionation in meteorites by TAYLOR *et al.* (1965) showed the existence of significant variations which permitted the identification of three groups of stony meteorites. These attempts to group meteorites based on observed $\delta^{18}O$ have received a new interpretation based on the work of CLAYTON *et al.* (1976). The discovery of a ubiquitous ^{16}O-rich component and extensive work of CLAYTON *et al.* (1976) show that groupings of meteorites based on O reflect formation in parcels of the solar nebula with different oxygen isotopic composition due to admixture with oxygen of distinct nucleosynthetic history. Within each class of meteorites based on the three oxygen isotopes, there are much more limited variations due to mass dependent fractionation (CLAYTON *et al.*, 1976).

Isotopic studies using the double spike technique for Mo (WETHERILL, 1964) and Ba (EUGSTER *et al.*, 1969) have shown the absence of isotopic effects for these elements and that earlier reports of fractionation effects were incorrect. ROSMAN and DE LAETER (1976) have reported the presence of isotope fractionation in Cd; whole rock analysis of the H3 chondrite Brownfield gives $\delta(^{110}Cd/^{116}Cd) \div 6 = -2.3$‰. As repeated analyses of standards give a reproducibility of ± 1.6‰ per mass unit, the results for Brownfield may indicate a real effect. These workers report that Cd is considerably *enhanced* in this meteorite in comparison with other H chondrites, and speculate that the isotopic fractionation may be due to one of the mechanisms proposed by ARRHENIUS and ALFVÉN (1971) for volatile elements.

In contrast to these studies which indicate only small or no isotope fractionation effects in meteorites, recent magnesium work on two Allende inclusions shows large mass dependent fractionation of up to 30‰ *per amu* (LEE and PAPANASTASSIOU, 1974; WASSERBURG *et al.*, 1977). In addition, distinctive O isotopic compositions in the same two inclusions are compatible with fractionation effects for O (CLAYTON and MAYEDA, 1977). These large effects demonstrate that processes capable of producing large effects exist in nature and have affected major elements. The observation of uniform *and* highly fractionated Mg isotopic compositions within the coexisting minerals in the inclusions shows that the fractionation was a characteristic of the parent parcel of the solar nebula from which these inclusions condensed (WASSERBURG *et al.*, 1977). Recent measurements of Ca on these inclusions indicate that the Ca isotopes may also be fractionated by +1.8‰ per amu (LEE *et al.*, 1978). The effects in Ca involve enrichment of the lighter isotopes, in contrast to the Mg data which indicate preferential enrichment of the heavier isotopes. This disparate behavior of Ca and Mg may indicate that the large apparent fractionation effects in these samples are instead the result of the presence of large nuclear effects rather than evidence for mass fractionation (LEE *et al.*, 1978).

Terrestrial samples. The presence of extremely small mass fractionation effects as established in this work requires the use of the double spike technique. Therefore, we shall not discuss earlier reports of large effects in Ca obtained without the use of a double spike. Our results are in agreement with the work of HIRT and EPSTEIN (1964) who observed, using the double spike technique, no Ca isotopic fractionation effects within a precision of 1‰ per amu, or about ten times our precision. Recent work by WILLIAMS and GILETTI (1976), described in a brief abstract, claimed effects in $\delta(^{40}Ca/^{44}Ca)$ for various samples, ranging up to +11.3‰ for a human tooth. Comparison of our work with the double spike results of WILLIAMS and GILETTI (1976) must await publication of their work, in view of both the many technical problems discussed in this paper and of artifacts

present in industrially produced Ca 'standards'. It is clear that we cannot completely exclude the possibility of larger natural fractionation effects in types of samples *not* studied by us, but our analyses of a variety of teeth (human, squirrel, shark) show *no effects* comparable to their reported value.

There is an indication from the terrestrial data that Ca isotope fractionation may accompany precipitation of $CaCO_3$ and $CaSO_4$ from aqueous solutions, but not to an extent greater than $\sim 2‰$. The data on which we base this observation consist of the seawater and gypsum samples. It may be seen that the two gypsum evaporites are isotopically lighter than seawater by 1.4–2.0‰. If we assume that the Ca isotopic composition of the oceans has not changed with time, these data present an integrated fractionation of 2‰ for $^{40}Ca/^{44}Ca$ during precipitation as compared to the upper limit of 11‰ obtained by STAHL and WENDT (1968) from laboratory experiments.

It is interesting to consider the implications of the $\delta(^{40}Ca/^{44}Ca)$ value for seawater in the presence of Ca fractionation during precipitation of salts. If Ca is fractionated during precipitation, then for a steady state situation, the Ca precipitating out of seawater will have the same isotopic composition as the Ca influx to the sea, while the Ca in seawater will reach a distinct equilibrium value of $\delta(^{40}Ca/^{44}Ca)$ with respect to the Ca being added to and removed from seawater. Since the seawater has the *heaviest* Ca composition observed by us so far, this is consistent with a small *positive* fractionation effect in the precipitated salts of $\sim +0.5‰$ per amu.

Of the six biogenic samples analyzed (Table 6), three are from marine organisms. This presents the opportunity to observe if the biologic processing has resulted in any Ca isotopic fractionation beyond the fractionation observed for Ca salts inorganically precipitated from the oceans. The Ca in the sharks' teeth and in the conch shell yield $\Delta(^{40}Ca/^{44}Ca) \lesssim 2‰$ with respect to seawater. We are therefore not able to assign any portion of the effects to biologic processing over and beyond possible precipitation effects. The data show no large isotopic effects due to two processes occurring in biologic settings, diffusion through membranes or skeletal structure formation. It yet may be found that complex biochemical reactions involving Ca produce significant equilibrium or kinetic isotopic fractionation. In view of the evidence that industrially produced Ca may be highly fractionated, it will be necessary to exercise added care in the interpretation of data showing large biogenic effects. In passing, we note that FITZGERALD (1975), in order to explain certain features of the mechanical spectra of cancellous bone tissue, has proposed that there are preferential arrangements of ^{44}Ca within the calcium phosphate. To propose that only a single isotope (^{44}Ca) would form a regular lattice within such tissue seems to us to be wholly unrealistic and not supported by our data.

The small effects observed for Ca as compared to those observed for sulfur for the two gypsum samples reflect the very different chemical bonding responsible for the sulfur effects and the existence for sulfur of a mechanism for reduction of sulfates based on bacterial action (HARRISON and THODE, 1958; KEMP and THODE, 1968).

CONCLUSIONS

Three major conclusions can be drawn from the results of this paper: (a) no samples have been found in nature which have Ca fractionated by more than 2.5‰ for $^{40}Ca/^{44}Ca$; (b) meteorites, lunar and terrestrial samples show the same small range of $^{40}Ca/^{44}Ca$, indicating remarkable initial isotopic homogeneity in distinct planetary bodies; and (c) small Ca isotope fractionation to a level of $\Delta \approx 2.5‰$ *is* definitely present in nature, but further study will be necessary in order to determine what mechanisms are responsible. If the effects are due to multiple stage processing with only very small additional fractionation added at each stage, it may prove to be difficult to determine the nature of the mechanisms producing the Ca isotope fractionation.

Acknowledgements—We thank G. J. WASSERBURG for his interest and support of this work. H. A. LOWENSTAM shared his insight and enthusiasm on biological processes and provided us with interesting samples. We benefited from discussions with H. G. THODE, L. MARGULIS, S. EPSTEIN and G. R. ROSSMAN. A. J. GANCARZ provided valuable discussions about alternate fractionation laws. Meteorite samples were provided by F. BEGEMANN, K. KEIL, C. B. MOORE and P. PELLAS; H. G. THODE provided us with the two gypsum samples and R. ELIAS with the squirrel tooth. W. R. KELLY, R. LETOLLE, C. E. REES and S. M. SAVIN provided helpful suggestions regarding the manuscript. This work was supported by NSF grant PHY76-83685.

REFERENCES

ARRHENIUS G. and ALFVÉN H. (1971) Fractionation and condensation in space. *Earth Planet. Sci. Lett.* **10**, 253–267.

ARTEMOV Y. M., KNORRE K. G., STRIZHOV V. P. and USTINOV V. I. (1966) Ca^{40}/Ca^{44} and O^{18}/O^{16} isotopic ratios in some calcareous rocks. *Geochem. Intern.* **3**, 1082–1086.

BACHINSKI D. J. (1969) Bond strength and sulfur isotopic fractionation in coexisting sulfides. *Econ. Geol.* **64**, 56–65.

BACKUS M. M., PINSON W. H., HERZOG L. F. and HURLEY P. M. (1964) Calcium isotope ratios in the Homestead and Pasamonte meteorites and a Devonian limestone. *Geochim. Cosmochim. Acta* **28**, 735–742.

BARNES I. L., CARPENTER B. S., GARNER E. L., GRAMLICH J. W., KUEHNER E. C., MACHLAN L. A., MAIENTHAL E. J., MOODY J. R., MOORE L. J., MURPHY T. J., PAULSEN P. J., SAPPENFIELD K. M. and SHIELDS W. R. (1972) Isotopic abundance ratios and concentrations of selected elements in Apollo 14 samples. *Proc. Third Lunar Sci. Conf., Geochim. Cosmochim. Acta Suppl.* **3**, 1465–1472. M.I.T.

BETTS R. H., HARRIS W. E. and STEVENSON M. D. (1956) The partial separation of Na^{22} from Na^{24} by ion exchange chromatography. *Can. J. Chem.* **34**, 65–74.

CLAYTON R. N. and MAYEDA T. K. (1977) Correlated oxygen and magnesium isotope anomalies in Allende inclusions, I: Oxygen. *Geophys. Res. Lett.* **4**, 295–298.

CLAYTON R. N., ONUMA N. and MAYEDA T. K. (1976) A classification of meteorites based on oxygen isotopes. *Earth Planet. Sci. Lett.* **30**, 10–18.

COLEMAN M. L. (1971) Potassium–calcium dates from pegmatic micas. *Earth Planet. Sci. Lett.* **12**, 399–405.

CORLESS J. T. (1966) Determination of Ca^{48} in natural calcium by neutron activation analysis. *Anal. Chem.* **38**, 810–813.

CORLESS J. T. (1968) Observations on the isotopic geochemistry of calcium. *Earth Planet. Sci. Lett.* **4**, 475–478.

DEPAOLO D. J. and WASSERBURG G. J. (1976) Inferences about magma sources and mantle structure from variations of $^{143}Nd/^{144}Nd$. *Geophys. Res. Lett.* **3**, 743–746.

DODSON M. H. (1969) A theoretical study of the use of internal standards for precise isotopic analysis by the surface ionisation technique. Part II. Error relationships. *J. Sci. Instrum. Ser.* 2 (*J. Phys. E*) **2**, 490–498.

DYMEK R. F., ALBEE A. L. and CHODOS A. A. (1975) Comparative mineralogy and petrology of Apollo 17 mare basalts: samples 70215, 71055, 74255 and 75055. *Proc. Sixth Lunar Sci. Conf., Geochim. Cosmochim. Acta Suppl.* **6**, 49–77. Pergamon Press.

EBERHARDT A., DELWICHE R. and GEISS J. (1964) Isotopic effects in single filament thermal ion sources. *Z. Naturforschg.* **19a**, 736–740.

ELIAS R., HIRAO Y. and PATTERSON C. (1977) Impact of present levels of aerosol Pb concentrations on both natural ecosystems and humans. In *Symposium Proceedings of the International Conference on Heavy Metals in the Environment*, 1975. pp. 257–272.

EPSTEIN S. and TAYLOR H. P., JR. (1971) O^{18}/O^{16}, Si^{30}/Si^{28}, D/H and C^{13}/C^{12} ratios in lunar samples. *Proc. Second Lunar Sci. Conf., Geochim. Cosmochim. Acta Suppl.* **2**, 1421–1441. M.I.T.

EUGSTER O., TERA F. and WASSERBURG G. J. (1969) Isotopic analyses of barium in meteorites and in terrestrial samples. *J. Geophys. Res.* **74**, 3897–3908.

FITZGERALD E. R. (1975) Calcium-isotope effects in mechanical spectra of cancellous bone. *Med. Biol. Engr.* **13**, 717–719.

GROOTENBOER J. and SCHWARCZ H. P. (1969) Experimentally determined sulfur isotope fractionations between sulfide minerals. *Earth Planet. Sci. Lett.* **7**, 162–166.

HARRISON A. G. and THODE H. G. (1958) Mechanism of the bacterial reduction of sulphate from isotope fractionation studies. *Trans. Faraday Soc.* **54**, 84–92.

HEUMANN K. G. and LIESER K. H. (1973) Untersuchung von Isotopenfeinvariationen des Calciums in der Natur an rezenten Carbonaten und Sulfaten. *Geochim. Cosmochim. Acta* **37**, 1463–1471.

HEUMANN K. G. and LUECKE W. (1973) Calcium isotope ratios in natural carbonate rocks. *Earth Planet. Sci. Lett.* **20**, 341–346.

HIRT B. and EPSTEIN S. (1964) A search for isotopic variations in some terrestrial and meteoritic calcium. *Trans. Am. Geophys. Union* **45**, 113.

HULSTON J. R. and THODE H. G. (1965) Variations in the S^{33}, S^{34} and S^{36} contents of meteorites and their relation to chemical and nuclear effects. *J. Geophys. Res.* **70**, 3475–3484.

JAROSEWICH E. and MASON B. (1969) Chemical analyses with notes on one mesosiderite and seven chondrites. *Geochim. Cosmochim. Acta* **33**, 411–416.

KAJIWARA Y. and KROUSE H. R. (1971) Sulfur isotope partitioning in metallic sulfide systems. *Can. J. Earth Sci.* **8**, 1397–1408.

KAJIWARA Y., KROUSE H. R. and SASAKI A. (1969) Experimental study of sulfur isotope fractionation between coexistent sulfide minerals. *Earth Planet. Sci. Lett.* **7**, 271–277.

KAPLAN I. R. and HULSTON J. R. (1966) The isotopic abundance and content of sulfur in meteorites. *Geochim. Cosmochim. Acta* **30**, 479–496.

KEMP A. L. W. and THODE H. G. (1968) The mechanism of the bacterial reduction of sulphate and of sulphite from isotope fractionation studies. *Geochim. Cosmochim. Acta* **32**, 71–91.

LARIMER J. W. (1968) An experimental investigation of oldhamite, CaS, and the petrologic significance of oldhamite in meteorites. *Geochim. Cosmochim. Acta* **32**, 965–982.

LARIMER J. W. (1975) The effect of C/O ratio on the condensation of planetary material. *Geochim. Cosmochim. Acta* **39**, 389–392.

LEE D. A. and BEGUN G. M. (1958) The enrichment of lithium isotopes by ion-exchange chromatography—I. The influence of the degree of crosslinking on the separation factor. *J. Am. Chem. Soc.* **81**, 2332–2335.

LEE T. and PAPANASTASSIOU D. A. (1974) Mg isotopic anomalies in the Allende meteorite and correlation with O and Sr effects. *Geophys. Res. Lett.* **1**, 225–228.

LEE T., PAPANASTASSIOU D. A. and WASSERBURG G. J. (1978) Calcium isotopic anomalies in the Allende meteorite. *Ap. J. Lett.* **220**, L21–L25.

MARVIN U. B. and WOOD J. A. (1972) The Haverö ureilite: petrographic notes. *Meteoritics* **7**, 601–610.

MCCULLOCH M. T. and WASSERBURG G. J. (1978) Barium and neodymium isotopic anomalies in the Allende meteorite. *Ap. J. Lett.* **220**, L15–L19.

MESHCHERYAKOV R. P. and STOLBOV Y. M. (1967) Measurement of the isotopic composition of calcium in natural materials. *Geochem. Intern.* **4**, 1001–1003.

MILLER Y. M., USTINOV V. I. and ARTEMOV Y. M. (1966) Mass spectrometric determination of calcium isotope variations. *Geochem. Intern.* **3**, 929–933.

NIER A. O. (1938) The isotopic constitution of calcium, titanium, sulphur and argon. *Phys. Rev.* **53**, 282–286.

PAPANASTASSIOU D. A. and WASSERBURG G. J. (1969) Initial strontium isotopic abundances and the resolution of small time differences in the formation of planetary objects. *Earth Planet. Sci. Lett.* **5**, 361–376.

RAMDOHR P. (1972) The highly reflecting and opaque components in the mineral content of the Haverö meteorite. *Meteoritics* **7**, 565–571.

REES C. E. (1969) Fractionation effects in the measurement of molybdenum isotope abundance ratios. *Intern. J. Mass Spectrom. Ion Phys.* **3**, 71–80.

ROSMAN K. J. R. and DE LAETER J. R. (1976) Isotopic fractionation in meteoritic cadmium. *Nature* **261**, 216–218.

RUSSELL W. A. and PAPANASTASSIOU D. A. (1978) Isotope fractionation in ion exchange columns. *Anal. Chem.* **50**. In press.

RUSSELL W. A., PAPANASTASSIOU D. A. and TOMBRELLO T. A. (1976) Absolute Ca isotopic compositions in a lunar soil. In *Lunar Science* VII, pp. 752–754. The Lunar Science Institute, Houston.

RUSSELL W. A., PAPANASTASSIOU D. A., TOMBRELLO T. A. and EPSTEIN S. (1977a) Search for Ca isotopic fractionation and correlation of Ca and O effects. In *Lunar Science* VIII, pp. 823–825. The Lunar Science Institute, Houston.

RUSSELL W. A., PAPANASTASSIOU D. A., TOMBRELLO T. A. and EPSTEIN S. (1977b) Ca isotope fractionation on the moon. *Proc. Eighth Lun. Sci. Conf., Geochim. Cosmochim. Acta Suppl.* **8**, 3791–3805. Pergamon Press.

SAKAI H. (1968) Isotopic properties of sulfur compounds in hydrothermal processes. *Geochem. J.* **2**, 29–49.

SAKAI H. (1972) Oxygen isotopic ratios of some evaporites from Precambrian to recent ages. *Earth Planet. Sci. Lett.* **15**, 201–205.

SENFTLE F. E. and BRACKEN J. T. (1955) Theoretical effect of diffusion on isotopic abundance ratios in rocks and associated fluids. *Geochim. Cosmochim. Acta* **7**, 61–76.

SHIELDS W. R. (1966) *NBS Technical Note* 277. U.S. Government Printing Office, Washington, DC.

STAHL W. (1968) Search for natural variations in calcium isotope abundances. *Earth Planet. Sci. Lett.* **5**, 171–174.

STAHL W. and WENDT I. (1968) Fractionation of calcium isotopes in carbonate precipitation. *Earth Planet. Sci. Lett.* **5**, 184–186.

TAYLOR H. P., JR., DUKE M. B., SILVER L. T. and EPSTEIN S. (1965) Oxygen isotope studies of minerals in stony meteorites. *Geochim. Cosmochim. Acta* **29**, 489–512.

TERA F., EUGSTER O., BURNETT D. S. and WASSERBURG G. J. (1970) Comparative study of Li, Na, K, Rb, Cs, Ca, Sr and Ba abundances in achondrites and in Apollo 11 lunar samples. *Proc. Apollo 11 Lunar Sci. Conf.*, pp. 1637–1657.

THODE H. G. and MONSTER J. (1965) Sulfur-isotope geochemistry of petroleum, evaporites, and ancient seas. *Am. Assoc. Petrol. Geologists Mem.* **4**, 367–377.

VON MICHAELIS H., AHRENS L. H. and WILLIS J. P. (1969) The composition of stony meteorites—II. The analytical data and an assessment of their quality. *Earth Planet. Sci. Lett.* **5**, 387–394.

WÄNKE H., PALME H., BADDENHAUSEN H., DREIBUS G., JAGOUTZ E., KRUSE H., SPETTEL B., TESCHKE F. and THACKER R. (1974) Chemistry of Apollo 16 and 17 samples: bulk composition, late stage accumulation and early differentiation of the moon. *Proc. Fifth Lunar Sci. Conf., Geochim. Cosmochim. Acta Suppl.* **5**, 1307–1335.

WASSERBURG G. J., LEE T. and PAPANASTASSIOU D. A. (1977) Correlated O and Mg isotopic anomalies in Allende inclusions—II. Magnesium. *Geophys. Res. Lett.* **4**, 299–302.

WASSERBURG G. J., PAPANASTASSIOU D. A., NENOW E. V. and BAUMAN C. A. (1969) A programmable magnetic field mass spectrometer with on-line data processing. *Rev. Sci. Instr.* **40**, 288–295.

WETHERILL G. W. (1964) Isotopic composition of molybdenum in iron meteorites. *J. Geophys. Res.* **69**, 4403–4408.

WHITE J. R. and CAMERON A. E. (1948) The natural abundance of isotopes of stable elements. *Phys. Rev.* **74**, 991–1000.

WILLIAMS A. E. and GILETTI B. J. (1976) Natural variations of the stable calcium isotopes. *Geol. Soc. Am. Abstr. Prog.* **8**, No. 6, 1170–1171.

APPENDIX—MASS FRACTIONATION LAW

We address here the form of the fractionation law which best describes the instrumental mass fractionation effects during thermal ionization. EBERHARDT *et al.* (1964) studied the variations of the isotope ratios of Li, K and Rb as a function of time during a run, and found that the measured ratio approximately followed a Rayleigh distillation law during a substantial part of the run. However, complexities both in the early part of the runs as well as occasionally during the late stages prevented a firm conclusion as to the applicability of a Rayleigh law. REES (1969) has presented models to explain the instrumental variation of the measured $^{92}Mo/^{98}Mo$ ratio as the result of Rayleigh fractionation and of mixing of distinctly fractionated sample layers on the filament. For Li, K and Rb, there is only one isotope ratio available for study. In the present work we have precisely measured four isotope ratios during each run. We have attempted to develop a semiempirical function which describes both their temporal variations during a run and their variation between runs. These results have been presented briefly (RUSSELL *et al.*, 1977a).

Consider an element with at least three isotopes of masses m_i, m_j, and m_k. We assume that mass fractionation may occur during emission of the ions from the filament and that no fractionation is introduced either during extraction from the ion source or at the detector. The ion current for a given isotope may in general be written as a function both of its mass and of time, $f(m_i, t)$. As the sample reservoir on the filament is of finite size, the mass dependence of f implies that the isotopic composition of the reservoir and of the instantaneously emitted ions will change with time. We denote by $R_{ij}(t)$ the ratio of the ion currents of isotopes m_i and m_j measured at time t:

$$R_{ij}(t) = f(m_i, t)/f(m_j, t).$$

For ratios measured at the same time, the explicit time dependence can be suppressed:

$$R_{kj} = g(m_i, m_j, m_k, R_{ij}).$$

If the function g is known, then pairs of raw measured ratios can be corrected for instrumental mass fractionation. Common practice involves choosing a standard ratio R^C_{ij}, calculating a fractionation factor from a set of measured R^M_{ij} ratios, and then calculating corrected ratios R^C_{kj}. If the raw data are subject only to random errors, then for the correct function g, the R^C_{kj} ratios would be normally distributed and would converge to a mean value $\bar{R}^C_{kj}$. The most conclusive evidence that a wrong function g had been used would consist of a systematic drift of R^C_{kj} as a function of the magnitude of the fractionation correction provided by g. This arises because incorrect functions g will not closely follow the trend established by the collection of all sets of measured ratios (R^M_{ij}, R^M_{kj}).

We note that the exact dependence of the instrumental mass fractionation effects upon the isotope masses is not well known, especially for large effects. We have considered various specific functions g in an attempt to correct precisely for instrumental fractionation. For small effects, a commonly used approximation is that of a power law:

$$R^M_{ij} = R^C_{ij}(1 + \alpha)^{m_{ij}} \qquad \text{(A1)}$$

where $m_{ij} = m_i - m_j$; M stands for measured and C for corrected. Expanding equation (A1) we obtain:

$$R^M_{ij} = R^C_{ij}[1 + m_{ij}\alpha + \tfrac{1}{2}m_{ij}(m_{ij} - 1)\alpha^2 + \cdots]. \qquad \text{(A2)}$$

If we consider three isotopes, and specify here in order to avoid ambiguity that $m_i < m_j < m_k$, then we obtain to first order in α:

$$R^M_{jk} = R^C_{jk}\left[1 + \frac{m_{jk}}{m_{ij}}\left(\frac{R^M_{ij}}{R^C_{ij}} - 1\right)\right]. \qquad \text{(A3)}$$

A plot of R^M_{jk}/R^C_{jk} vs R^M_{ij}/R^C_{ij} using equation (A3) yields a straight line with a slope which is independent of R^C_{jk} and R^C_{ij}. For two Ca runs, we show in Fig. 4 $(^{44}Ca/^{48}Ca)^M/(^{44}Ca/^{48}Ca)^C$ vs $(^{40}Ca/^{44}Ca)^M/(^{40}Ca/^{44}Ca)^C$. The data are means of sets of ratios obtained at the same time and show a fractional variation in the isotopic ratios of five percent. For the isotopes shown in Fig. 4 the slope from equation (A3) is 1.0. It is clear that a straight line of this slope does not provide a good fit to the data. Use of a different set of $(^{40}Ca/^{44}Ca)^C$ and $(^{44}Ca/^{48}Ca)^C$ would displace the data points, without a change in slope, with respect to the line shown. A change in these values would therefore not improve the fit to the data. Also, either using equation (A1) directly or expanding it to higher order would not provide an improvement in the fit for the ratios shown. Since $m_{ij} = -4$ for both $^{44}Ca/^{48}Ca$ and $^{40}Ca/^{44}Ca$, we always obtain a slope of 1.0 using equations (A1) or (A3).

The application of equation (A1) results in the same mass fractionation constant α being used over the whole mass range, which for Ca is 8 amu (20% of the mass). For Ca, the observed instrumental fractionation effects are also large, so that it is not surprising that this model does not adequately describe the data. To improve the fit to the data, we have attempted to define a fractionation law which provides for decreasing mass fractionation correc-

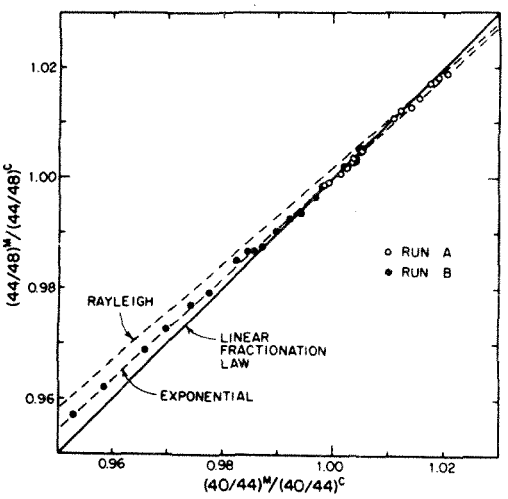

Fig. 4. Plot of $^{40}Ca/^{44}Ca$ and $^{44}Ca/^{48}Ca$ ratios measured (M) during two runs. The measured ratios have been normalized by the instrumental mass fractionation corrected values (C) found by double spike analysis. Each circle represents means for a set of cycles. Error bars are less than the size of the circles. For a linear fractionation law, the points would lie on the 45° line shown. The data are well-aligned instead with the exponential law curve, but are also nearly parallel to the Rayleigh law curve. Both of these laws provide fairly accurate corrections for the instrumental mass fractionation.

tions as the isotope mass increases. We have investigated two functions with the desired behavior:
(a) a Rayleigh-type distillation law, with a mass fractionation factor *assumed* proportional to $m^{-1.2}$;
(b) an 'exponential' law of the form

$$R_{ij}^{M} = R_{ij}^{C}\left(\frac{m_i}{m_j}\right)^{p}. \qquad (A4)$$

First we discuss the exponential law and then compare it to the Rayleigh distillation law. The exponential law has a relatively simple form which provides for ease in computations. Expanding equation (A4) we obtain:

$$R_{ij}^{M} = R_{ij}^{C}\left[1 + \frac{pm_{ij}}{m_j} - \frac{pm_{ij}^2}{2m_j^2} + \frac{p^2m_{ij}^2}{2m_j^2} + \cdots\right]. \qquad (A5)$$

If we place $p/m_j = \alpha$ we obtain:

$$R_{ij}^{M} = R_{ij}^{C}\left[1 + \alpha m_{ij} - \alpha\frac{m_{ij}^2}{2m_j} + \alpha^2\frac{m_{ij}^2}{2} + \cdots\right]. \qquad (A6)$$

The third term in this expansion is a term of first order in α not contained in equation (A2); this term reduces, by an amount inversely proportional to the mass, the total correction factor given by the linear or power laws. We now define the fractionation *per atomic mass unit* as

$$F_{ij} = (R_{ij}^{M}/R_{ij}^{C} - 1)/m_{ij}. \qquad (A7)$$

It is easily seen that the exponential law provides a smaller fractionation factor F_{ij} for the pair ^{48}Ca–^{40}Ca than for ^{44}Ca–^{40}Ca. For example, using equation (A4), $F_{44-40} = 0.0050$ amu^{-1} corresponds to $p = +0.208$ and $F_{48-40} = 0.0048$ amu^{-1}.

We now consider the Rayleigh distillation law. If we assume that the fractionation is proportional to $m^{-1.2}$, we obtain:

$$R_{ij}^{M} = R_{ij}^{C}\left(\frac{m_j}{m_i}\right)[h(m_j,t)]^{[(m_i-m_j)-1]} \qquad (A8)$$

where $h(m_j, t)$ represents the fraction of isotope m_j left on the filament at time t. The value of $h(m_j, t)$ may be determined from the pair of values $[R_{ij}^{M}(t), R_{ij}^{C}]$ and then used to correct the other measured ratios $R_{jk}^{M}(t)$. It can be demonstrated that, over a *limited* range of h, the Rayleigh distillation formula does *not* give strictly decreasing mass fractionation per mass unit as the isotope mass is increased. From $R_{44-40}^{M}/R_{44-40}^{C} = 0.986$ to 1.000, the magnitude of F_{48-40} is actually somewhat greater than the magnitude of F_{44-40}. However, over this range of R_{44-40}^{M}, the magnitudes of F_{ij} are too small for this to be of importance for the data correction.

We now compare the linear, Rayleigh and 'exponential' laws. Over the range of data in Fig. 4, curves derived from the latter two laws are nearly parallel to each other to within a few parts in 10^3. Furthermore, these two curves are nearly parallel to a smooth line drawn through the data. The Rayleigh formula implies that at all times during a run, no two ratios R_{ij}^{M} and R_{kj}^{M} are fractionated by exactly the same amount. Therefore equation (A8) does not pass through the point (1,1) in Fig. 4, in contrast to the exponential law which for $p = 0$ yields $F_{ij} = 0$ for all isotope pairs. The fact that the trend of the data in this figure is nearly parallel to the curves for the Rayleigh and the exponential formula is sufficient to ensure that the corrected $^{48}Ca/^{44}Ca$ ratios will not vary systematically to a significant extent with the fractionation correction provided by either of these two laws. This is illustrated in Fig. 5, which graphs the per mil changes of the $^{48}Ca/^{44}Ca$ ratios in run B of Fig. 4. Figure 5 has a time abscissa for simplicity; we note that for run B and for most runs, the fractionation parameters (α, p or h) are monotonic functions of time. In contrast to the linear law, least squares fits to exponential- and Rayleigh-corrected data shown in Fig. 5 yield slopes which are statistically consistent with lines of zero slope. However, in Fig. 4 the Rayleigh law appears to have a somewhat different slope than do the data over the more extensive fractionation range

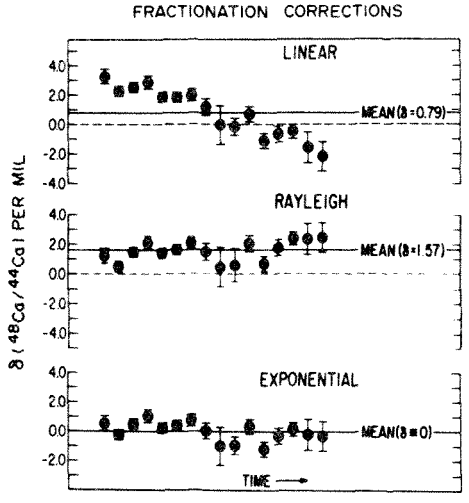

Fig. 5. Drifts in $^{48}Ca/^{44}Ca$ data for Run B of Fig. 4 which have been corrected for mass fractionation using different laws. A drift in the 'corrected' ratios of over $5‰$ occurs when the linear law is used. Least square fits to data as corrected by Rayleigh and exponential laws give lines of zero slope within statistics. The *shift* in the grand means when different laws are used is simply due to the facts that (a) the three laws do not intersect at a single point, and (b) the data do not lie symmetrically in Fig. 4 with respect to the intersections of the three laws.

of the two runs, considered together. Although the Rayleigh law can provide a good fit over the more limited fractionation range of either run considered separately, it appears to be slightly inferior to the exponential law when compared over the entire fractionation range represented in Fig. 4. It was shown above that the linear and power law formulas do not provide a good fit to the raw data. In Fig. 5 it may be seen that application of these laws leads to a 5‰ systematic drift in the *corrected* $^{48}Ca/^{44}Ca$ ratios.

Each of the three fractionation laws considered above yields a distinct, well-defined 44/48 correction for a given correction in 40/44. The array of data in Fig. 4 can be shifted with respect to these three functions if the $(^{40}Ca/^{44}Ca)^C$ and $(^{44}Ca/^{48}Ca)^C$ values are altered. The values used in Fig. 4 were obtained in a self-consistent fashion from analysis of a double spike mixture run using the exponential fractionation function. Therefore, the exponential curve is not displaced from the data array; by consistently using the Rayleigh formula, $(^{40}Ca/^{44}Ca)^C$ and $(^{44}Ca/^{48}Ca)^C$ assume slightly different values. This has the effect of shifting the plotted data array *parallel* to itself without a change of slope; the Rayleigh curve then overlays the data. Thus, use of either (A4) or (A8) does not lead to a large drift in the corrected data.

An important consequence of not being able to clearly choose between eqs. (A4) and (A8) is indicated in Fig. 5. The means of the $^{48}Ca/^{44}Ca$ data as corrected by the Rayleigh and exponential laws differ by 1.5‰. It can be demonstrated that if the mass spectrometer filament fractionated according to some given 'true' law, but the measured ratios were corrected by a different, erroneous formula which over the whole range of observed sample fractionation provides strictly *greater* 44/48 corrections than the true law, then the mean of the corrected 44/48 ratios derived by the erroneous formula is *less* than the actual value. We note that the Rayleigh law provides strictly greater 44/48 corrections than the exponential law over the range of data in Fig. 4, which explains the shift of $\bar{R}^C_{48\text{-}44}$ between the two laws.

The currently available precision in our measurements appears to favor somewhat the use of the exponential correction formula. Therefore, all results were corrected for instrumental mass fractionation using the double spike technique and the exponential law. Consistent use of *either* the Rayleigh law *or* the exponential law for different samples will in both cases yield the same value Δ_{ij}, where

$$\Delta_{ij} = \delta(^{40}Ca/^{44}Ca)_i - \delta(^{40}Ca/^{44}Ca)_j \qquad (A9)$$

for pairs of samples i, j.

Figure 6 illustrates the importance of correcting the data in this work by the appropriate fractionation function. This figure shows the results of many double spike mixture analyses of $CaCO_3$ Standard-1. The data from each run were reduced by all three fractionation formulas. It is clear that there is a much wider spread in the data when corrected by the linear formula than when corrected by the exponential formula. For the two runs labelled as highly fractionated, different Δ_{ij} values are obtained by each of the three laws. The data in these runs were taken with the samples nearly exhausted. The fact that all three fractionation laws give widely different results for these highly fractionated runs is an indication that their validity does not extend over an arbitrarily large range of instrumental fractionation. The 'laws' are only semiempirical approximations to the true fractionation behavior of the sample

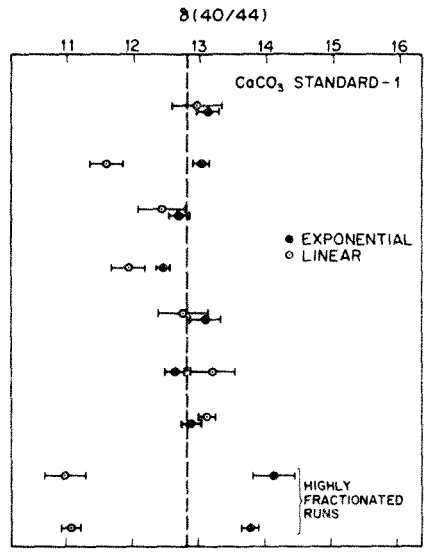

Fig. 6. Repeat analyses of $CaCO_3$ Standard-1, using the double spike, show reproducibility within ±0.34‰ in $^{40}Ca/^{44}Ca$ when the data are corrected by the exponential law (filled circles). Similar reproducibility is obtained when the Rayleigh law is used (not illustrated). By contrast, use of the linear law gives much poorer reproducibility of ±0.8‰. For data taken with the Ca on the filament nearly exhausted, the measured ratios are highly fractionated and none of the laws is adequate for precise reduction of the data.

in the ion source. We note that both DODSON (1969), in a theoretical error analysis, and COLEMAN (1971), in his Ca work using a double spike, indicated that the linear law provided a totally adequate description of the instrumental fractionation. The more precise data presented here show that the linear approximation is not valid.

It should be pointed out that the use of $\sqrt{(m_j/m_i)}$ in equation (A8), instead of some other function of the masses, involves the assumption that the filament behaves like a Knudsen cell. Only in this case is the interpretation of $h(m_j, t)$ as the fraction of isotope j remaining on the filament correct. However, measurements have not been made of the actual fraction remaining; comparison of directly measured values with the value of $h(m_j, t)$ computed from equation (A8) would be of great use in determining whether the filament does indeed behave like a Knudsen cell.

In a sample found to have *large* natural isotope fractionation, the process of correcting for instrumental fractionation requires extra care. This is because the natural fractionation may proceed by a function different from that appropriate to thermal ionization. In such a case it would be necessary to obtain, for the sample in question, unspiked composition data, to be used together with the associated mixture data in the double spike calculation of corrections for instrumental fractionation. This has not been necessary for the samples in this work.

CHAPTER 4. Ca ISOTOPE FRACTIONATION ON THE MOON

The use of calcium in this study of isotopic fractionation caused by sputtering made it useful to acquire data for the extent of its fractionation in lunar samples themselves. An extensive series of analyses was therefore carried out on an Apollo 15 surface soil which had previously been demonstrated to have very large O, Si, and S surface-correlated isotopic fractionation. The earliest attempts to remove Ca from the surfaces of the grains in this soil consisted of brief rinsings in water, 0.02 N HNO_3, or 0.02 - 0.1 N HCl. Even these mild treatments removed excessive fractions of the total Ca present in the grains, causing only very small amounts of isotopic fractionation to be measured. At that time then, firm conclusions could not be drawn about the presence or absence of fractionated calcium on the surfaces of these soil grains. Analyses of two Apollo 17 mare basalts indicated that the range of global Ca fractionation on the moon was very small.

A somewhat different technique was later tried in an attempt to increase the efficiency of removal from soil samples of the surface calcium relative to that in the unfractionated bulk. This consisted of short exposures of fresh portions of the above Apollo 15 soil to fluorine gas, exposures identical to those which liberated isotopically heavy O and Si from the same soil (Epstein and Taylor, 1972). This was an attempt to allow the freer removal of surface Ca in subsequent H_2O rinses by breaking some of the silicate bonds. It succeeded in removing calcium which was fractionated with respect to the bulk soil

by up to $\Delta(^{40}Ca/^{44}Ca) = -3.9‰$. It was therefore firmly established that calcium is fractionated in the lunar soils although by amounts small compared to those for O, Si, and S. The small magnitude of the fractionation had two possible interpretations: (a) calcium is not extensively fractionated in the lunar soils, and (b) although the fluorination technique allowed the preferential removal of enough of the surface relative to the bulk calcium to enable the presence of fractionation to be detected, the bulk material still dominated the calcium removed by the rinsing, causing a dilution of the surface-correlated fractionated Ca.

On the following pages is reproduced a paper which describes in detail the calcium measurements on this lunar soil, and which discusses more completely the observation of small degrees of isotopic fractionation. This paper originally appeared in the Proceedings of the Eighth Lunar Science Conference, Geochimica et Cosmochimica Acta Supplement No. 8.

Proc. Lunar Sci. Conf. 8th (1977), p. 3791–3805.
Printed in the United States of America

Ca isotope fractionation on the moon

W. A. RUSSELL[1], D. A. PAPANASTASSIOU[2], T. A. TOMBRELLO[1], and S. EPSTEIN[3]

[1]W. K. Kellogg Radiation Laboratory, Division of Physics, Mathematics, and Astronomy
[2]The Lunatic Asylum, Division of Geological and Planetary Sciences
[3]Division of Geological and Planetary Sciences
California Institute of Technology, Pasadena, California 91125

Abstract—We have measured Ca in a lunar soil in order to establish the presence of isotopically mass fractionated components. Ca was extracted by a series of water leaches after the soils were "activated" by brief exposures to fluorine gas. The O_2 obtained by this fluorination is found to have $\delta^{18}O = +21$ per mil and to be, therefore, significantly mass fractionated. Ca obtained in the leaches was analyzed using the double spike technique. We find very small Ca isotope fractionation in the leaches of this soil of up to 1 per mil per mass unit difference. The small Ca effects are in marked contrast to the measured $\delta^{18}O$ for the same sample and to large effects observed in many soils for oxygen, silicon, sulfur, and potassium. The data on Ca provide stringent constraints on models which attempt to explain the isotope mass fractionation effects in lunar soils.

INTRODUCTION

IN THIS STUDY we report on measurements of the Ca isotopic composition in easily leachable components of a mare soil in an attempt to establish whether Ca with a mass fractionated composition is present in lunar soils. Extensive work on other elements has established the presence in the lunar soils of highly fractionated isotopic compositions. Epstein and Taylor (1971, 1972, 1974, 1975) and Taylor and Epstein (1973) identified large enrichments of ^{18}O relative to ^{16}O and parallel enrichments of ^{30}Si relative to ^{28}Si for the first O_2 and Si extracted from soils by partial reaction with fluorine. These large effects are correlated with concentrations of H_2 of solar-wind origin (Epstein and Taylor, 1971, 1972) and the heavy oxygen and silicon are believed to reside on the surface coatings of the soil grains. Thode and Rees (1971, 1976) and Rees and Thode (1972, 1974) have reported S isotopic analyses of grain size separates of various lunar soils and observe enrichments in the heavier S isotopes which increase in magnitude systematically with decreasing grain size. They have interpreted their data as supporting a model in which the sulfur in a ~ 1.5 μm thick surface layer of soil grains is enriched in ^{34}S relative to ^{32}S by up to 20‰ when compared to the isotopic composition of S in lunar basalts. Two laboratories have reported $^{39}K/^{41}K$ values for lunar soils and rocks (Barnes *et al.*, 1973; Garner *et al.*, 1975; Church *et al.*, 1976). These workers observe lower $^{39}K/^{41}K$ values in bulk soils and in soil separates than the values for igneous rocks. In contrast to the O, Si, and S effects which are orders of magnitude larger than instrumental un-

certainties, the K effects range from null up to only four times the experimental uncertainties. Therefore, although the isotopic fractionation effects for these elements are at the percent level, we shall discuss the K effects separately from the O, Si, and S isotopic effects in a later section of this paper.

The reported isotopic effects for O, Si, and S have been shown to be of a mass fractionation character by Clayton *et al.* (1974), Epstein and Taylor (1971), and Rees and Thode (1972), respectively. Thus, no single isotope is enriched or depleted in any of these elements. In the absence of precise measurements on ^{40}K the effects in $^{39}K/^{41}K$ are assumed to be also due to mass fractionation. Isotopic variations in other light elements (H, C, and N, all of which originate principally from the solar wind) have been reported (see for example Epstein and Taylor, 1975; Kerridge *et al.*, 1975; Becker and Clayton, 1975) but it is not possible to ascertain which portion of these very large variations is due to mass fractionation effects similar to those observed for O, Si, S, and K.

As the mechanisms for production of the isotopically heavy O, Si, S, and K are not well known, it is not possible to predict with confidence whether fractionation effects should or should not be present in Ca. From the maximum size of the reported surface-correlated fractionation effects per mass unit difference for O (25‰), Si (13‰), S (10‰) there is an indication of a gradual decrease in the size of the effects as heavier elements are considered. Extrapolation of this trend to the mass 40 region indicates that one might well expect appreciable calcium mass fractionation effects in lunar soils. These heuristic arguments should be qualified by the following considerations:

(1) The data for the different elements may be particularly sensitive to the extraction techniques used. For example the maximum values for O and Si effects may not be directly comparable to the maximum S effects as the techniques used for extracting O and Si (partial fluorination) and S (extensive leaching of soil grain size separates) may probe different layers in the soil grains. Thus, while the existence of isotopic effects is manifest, the size of the effects observed for each element may depend strongly on the experiment design.

(2) It is thought likely that the sputtering of the lunar surface by the solar wind plays a role in the heavy isotope enrichment mechanism. However, there are many facets of the sputtering process which are poorly understood, and whose quantitative behavior must be known to extrapolate the isotopic effects to other elements:

(a) It is not well known which atomic or molecular species are dominantly emitted during ion sputtering of complex minerals although available experimental evidence suggests that aggregates of atoms may only comprise a few percent of the total material removed (cf. Gerhard and Oechsner, 1975). From the correlation of O and Si effects, Epstein and Taylor (1971, 1972) have placed general limits on the chemical Si and O species involved.

(b) We note that the theoretical treatment of ion sputtering in poly-

crystalline targets (Sigmund, 1969; see also Oechsner, 1975) predicts that the sputtering yield S per incident projectile: (1) is proportional to the stopping cross section for elastic atomic collisions, (2) is proportional to a function of the ratio of the "target" to the "incident particle" mass, and (3) is inversely proportional to the surface binding energy of the target material. On an atomic scale there may well be a distribution of binding energies due to non-equivalency of various chemical bonds in the material, which complicates the relation between sublimation and surface binding energies (Somorjai and Lester, 1967; Sigmund, 1969). However, these latter two parameters are certainly interrelated, so that the ion sputtering yield is influenced strongly by the volatility of the target material. The extent to which the volatility of a chemical species in a complex material is a critical factor for the production *also of isotopic* mass fractionation remains unclear.

(3) If, instead of ion sputtering, material is vaporized by micrometeorite impacts, then the resulting nearly total volatilization of the target area may actually minimize the importance of volatility as a factor in the complex processes resulting in isotopic mass fractionation.

(4) If the transport of nuclides on the surface of the moon and the mechanisms for loss of nuclides from the moon, coupled with vapor deposition back on the lunar surface, are important for isotopic fractionation, then the higher sputtering yield for volatile elements may result in the observation of larger effects for volatile elements due to an increase in the amount of isotopically heavier vapors of these elements being redeposited on the lunar surface.

From these considerations it is evident that it may not be possible to unambiguously predict whether Ca should show isotopic mass fractionation effects corresponding to those for O, Si, S, and K. We note that, depending on the model used to describe the isotopic mass fractionation effects, different parameters may become important. For example, if isotope mass fractionation is produced by ion sputtering, then volatility may be a less important parameter. Similarly, in the case of total removal of material from the target area, the observation of isotopic effects in the unsputtered material is, of course, precluded. The purpose of this study is to provide additional insights into the mechanisms for production of isotopic fractionation effects.

We have previously reported Ca isotopic analyses of a lunar soil (Russell *et al.*, 1976, 1977a) in an attempt to identify surface-correlated Ca which is enriched in the heavier isotopes in a manner analogous to the large enrichments observed for other light elements. We have concentrated our efforts on soil 15021, which has been shown to have large O, Si, and S effects.

In a first series of experiments, we attempted to preferentially remove surface layers of soil grains by a series of water and very dilute acid leaches (Russell *et al.*, 1976). We found that the acids readily leached small fractions of the total Ca from the soil and that the Ca in these leaches was not significantly

fractionated. However, we could not draw a firm conclusion about the absence of fractionation effects in Ca because of the possibility that small amounts of highly soluble, bulk phases were dominating the material leached from the soil. In this work, we have used the partial fluorination technique to attempt to break silicate bonds in the surface layers and effectively to "activate" Ca residing on or near the grain surfaces.

EXPERIMENTAL TECHNIQUES

Two fresh, 105 mg aliquots of 15021,73 (C & D) were placed in small stainless steel vials fitted with conical caps. Each vial was lowered into and eventually retrieved from the nickel reaction vessels used in the oxygen and silicon extraction apparatus for lunar samples (Epstein and Taylor, 1971). A hole in the conical cap enabled the sample to be freely exposed to the fluorine gas, but reduced the danger of Ca contamination from previous samples introduced in the reaction vessels. Aliquot C was fluorinated in 1/4 atmosphere F_2 for 30 min at 85°C; aliquot D was separately fluorinated for 35 min at 140°C. 20 μmole O_2 and 38 μmole O_2 were obtained from aliquots C and D respectively, and a total of 40 μmole Si was obtained from the two samples. Si isotopic analysis was not obtained because it was not possible for this experiment to purify the extracted Si. For the oxygen analyses it was necessary to combine the O_2 from both aliquots. The isotopic analysis yielded $\delta^{18}O = +21‰$ relative to SMOW. This demonstrated the existence and successful extraction of significantly isotopically enriched O from the actual soil sample used subsequently for the Ca experiment. The amounts of O_2 removed by partial fluorination also indicate that the exposure of aliquot C to fluorine was half as severe as was the case for aliquot D. Following the mild partial fluorination, each sample was removed from its stainless steel vial and then subjected to a ~3 ml reagent water rinse for approximately 10 min, during which time the sample was centrifuged. In order to remove any water remaining in the residue after removal of the supernate, the residues were rinsed and centrifuged in ~3 ml acetone. This acetone was mixed with the water leachate. Several weeks later, the two residues were leached for 30 min in water following procedures similar to those described above. The residue from soil aliquot C was then dissolved and processed using our standard techniques. All leach solutions were mixed with small amounts of HF and $HClO_4$ to ensure dissolution of any suspended fine grains or colloids. All samples were passed through a cation exchange column using standard techniques (cf. Tera *et al.*, 1970). Ca blanks were found to be negligible.

MASS SPECTROMETRY

In order to measure any naturally occurring Ca isotopic mass fractionation, we have removed instrumental mass fractionation effects by the use of a double spike consisting predominantly of ^{42}Ca and ^{48}Ca. The details of this technique have been extensively discussed by Eugster *et al.* (1969) and by Russell *et al.* (1977b). For every sample, the technique requires analysis of: (a) a mixture of the double spike and the sample; (b) the Ca isotopic composition of the sample. From a set of a mixture and a composition run, all Ca isotopic ratios in a sample are determined which are subject only to a uniform residual mass fractionation. If all effects in nature for the samples analyzed are of a mass fractionation character, then the Ca isotopic composition runs (b) above need only be obtained on one of the samples.

For Ca, the instrumental fractionation effects are large enough so that the use of either linear or power law functions which are characterized by constant

fractionation per mass unit throughout the 8 mass unit range has been found to be inadequate (Russell *et al.*, 1977a,b). All data reported here have been corrected using an "exponential" law defined by us as

$$R_{ij}^{C} = R_{ij}^{M}(m_i/m_j)^{p},$$

where R_{ij} is the ratio of isotopes of mass m_i and m_j, C = corrected, M = measured, and p is a constant for all ratios obtained at the same time. The ramifications of this law and of a Rayleigh law have been discussed extensively elsewhere (Russell *et al.*, 1977b).

Enriched Standards

In Fig. 1 we show results of analyses of enriched standards which demonstrate our resolution in $^{40}Ca/^{44}Ca$ using the double spike technique. A highly

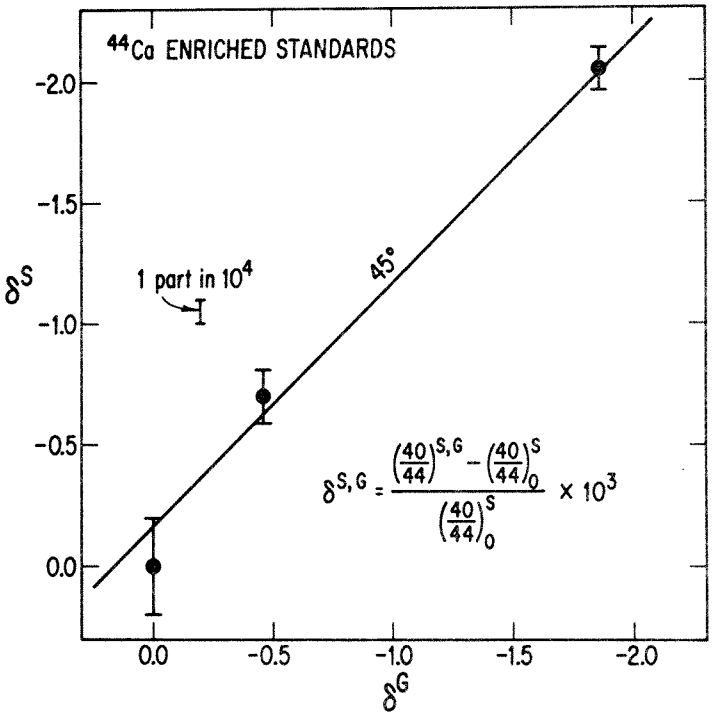

Fig. 1. Analysis of ^{44}Ca enriched standards. Measured amounts of a ^{44}Ca isotopic tracer solution were added to aliquots of a $CaCO_3$ standard in order to produce mixtures with lower $^{40}Ca/^{44}Ca$. Comparison of the spectrometric and gravimetric data shows that consistent results were obtained, as the data are fit well by the 45° line shown. We conclude that differences in absolute $^{40}Ca/^{44}Ca$ ratios of ~0.4‰, corresponding to fractionation of 1 part in 10^4 per mass unit difference, are clearly resolved.

enriched ^{44}Ca tracer solution was added to two aliquots of a standard prepared from reagent-grade $CaCO_3$ so as to *lower* the $^{40}Ca/^{44}Ca$ of the resultant mixtures from the value of the standard by about 0.5‰ and 2‰, respectively. These ^{44}Ca enriched mixtures were then spiked using the double spike and analyzed on the mass spectrometer. These ^{44}Ca enriched mixtures, when analyzed using the double spike, simulate samples with fractionated isotopic composition. Reduction of the mass spectrometer data (S) for the enriched standards, using the normal Ca composition of the original $CaCO_3$ standard, then yielded $^{40}Ca/^{44}Ca$ values for the enriched standards in excellent agreement with the values calculated from gravimetry (G). We interpret the data in Fig. 1 as showing that the double spike technique and the precision of the data obtained on the Lunatic I mass spectrometer (Wasserburg *et al.*, 1969) allow us to resolve natural fractionation of Ca samples to a level of 1 part in 10^4 *per unit mass difference.* We have also observed from repeat measurements of a standard that the data are consistent with this resolution in $^{40}Ca/^{44}Ca$ (Russell *et al.*, 1977b).

CHEMICAL MASS FRACTIONATION EFFECTS IN THE LABORATORY

The possibility has been recognized previously (cf. Eugster *et al.*, 1969) that isotope mass fractionation could be produced in the chemical separation of an element in the laboratory using cation exchange resins. If the chemical yield of a cation column is *unity*, this effect is non-existent. Similarly, if the double tracer is added to the sample *prior* to chemical separation, then the standard data reduction procedure will correct for any mass fractionation effects occurring during chemical separation. We recently have found that significant mass fractionation effects can be obtained during chemical separation through a cation exchange resin. As compared to the Ca composition of the original sample, we have measured a fractionation *per mass unit* of −1.6‰ for the first 1% of Ca eluted through a column; similarly, the first 50% of Ca yields a fractionation per mass unit of −0.4‰. A negative fractionation value indicates relative enrichment of the heavier isotopes and indicates that the *lighter* isotopes are held more strongly by the resin. The last 48% and the last 2% of eluted Ca yield mass fractionation effects *complementary* to those in the first cuts. These effects have important implications and will be described in detail in a separate note (Russell and Papanastassiou, 1977). It is clear that great care must be exercised in analytical procedures to avoid introducing artifacts in the data.

We have shown in Table 2 which samples were spiked prior to chemical separation. We have also listed the column yield for those samples spiked only after separation of Ca through the column when yields have been *measured* for the *actual samples* analyzed. We note that the reliability of our 15021 data has not been hampered by this effect, since the majority of the samples either were spiked prior to Ca separation through the column or had yields which were over 85%.

Table 1. Calcium isotopic composition.

Sample	$(40/44)_C$[a]	Δ[b]	$(42/44)_N$[a,c]	$(43/44)_N$[a,c]	$(48/44)_N$[a,c]
CaF_2	47.153 ± 3	1.00000 ± 6	0.31219 ± 4	0.06487 ± 3	0.08874 ± 4
70215 TR	47.108 ± 5	0.99905 ± 11	0.31224 ± 5	0.06486 ± 3	0.08869 ± 3
15021-B Res	47.123 ± 14	0.99936 ± 30	0.31225 ± 10	0.06484 ± 2	0.08869 ± 4
14163,159[d]	46.448	0.98505	0.312	0.0647	0.0884

[a]The data are corrected (C) for mass spectrometer fractionation using the associated mixture run. Errors correspond to last figures and are $2\sigma_{mean}$.

[b]$\Delta = (40/44)_C^{sample}/(40/44)_C^{CaF_2}$.

[c]For the purpose of establishing consistency of Ca composition within mass fractionation effects, fractionation between samples has been removed for these ratios (N) by normalization of $(40/44)_C$ to the value of the CaF_2 standard according to the exponential law.

[d]From Barnes *et al.* (1972).

Table 2. Ca analytical results.

Sample	Weight (mg)	Ca in leach (%)	Column yield (%)	$\delta(^{40}Ca/^{44}Ca)$[a]
Lunar				
70215	4		60–70[b]	−1.1 ± 0.2
				−1.0 ± 0.1
75055 Plag	1		68[b]	−0.6 ± 0.2
75055 Pyx	5		nm[c]	+0.1 ± 0.1
15021-A	62			
HCl	—	2.5	nm	−1.8 ± 0.2
15021-B	9			
H_2O	—	0.35	SBC[d]	−2.1 ± 0.4
HNO_3	—	1.2	SBC	−0.1 ± 0.2
Residue	—	95	62[e]	−0.6 ± 0.3
15021-C; F_2[g]	106			
H_2O	—	0.16	92[f]	−3.3 ± 0.3
H_2O	—	0.39	SBC	−2.6 ± 0.1
Residue	—	99.5	SBC	+0.6 ± 0.2
15021-D; F_2	105			
H_2O	—	0.37	85[f]	−1.4 ± 0.1
H_2O	—	0.98	nm	nm
Terrestrial standards				
CaF_2			—	≡0.0 ± 0.1
Seawater			SBC	−0.8 ± 0.1

[a]Corrected for instrumental fractionation using double spike.

[b]Yield estimated using Dymek *et al.* (1975) values for bulk Ca concentrations.

[c]nm = not measured.

[d]SBC: Double spike added to sample before chemical separation of Ca.

[e]Yield estimated using Ca weight percent value for soil aliquot C (see footnote g) and could in part reflect sampling inhomogeneities between the two soil aliquots.

[f]Column yield measured by comparing Ca contents in sample aliquots *prior to and after* chemical separation.

[g]Data on aliquot C yield a Ca concentration of 7.51 ± 0.01% (by weight).

RESULTS

In Table 1 we list the "absolute" Ca composition of a terrestrial standard and two lunar samples. Instrumental fractionation has been removed by the use of the double tracer so that the Ca compositions given are subject only to a uniform residual mass fractionation. The $^{40}Ca/^{44}Ca$ values given are those in the sample as calculated from the associated double spike plus sample ("mixture") run. In order to facilitate comparisons between the samples for all other isotopic ratios, we have normalized the $^{42}Ca/^{44}Ca$, $^{43}Ca/^{44}Ca$, and $^{48}Ca/^{44}Ca$ for the two lunar samples. For this normalization we calculated a mass fractionation factor Δ between samples by comparing the $^{40}Ca/^{44}Ca$ in each sample with the value in the CaF_2 standard. It then may be seen that, since the calculated isotopic ratios are identical within uncertainties for the normalized $(42/44)_N$, $(43/44)_N$, and $(48/44)_N$, there are no isotopic differences between lunar samples and the terrestrial standard except for the very small natural fractionation effects. Any residual isotopic effects would have indicated the presence of Ca with distinct nuclear anomalies. The results of Barnes *et al.* (1972) for Apollo 14 soil 14163 are also shown in the table and are in agreement with our results within a fractionation factor.

The results of all Ca isotopic analyses on 15021 to date are given in Table 2 and Figs. 2 and 3. In Table 2 we list $\delta(^{40}Ca/^{44}Ca)$, defined by

$$\delta(^{40}Ca/^{44}Ca) = [(^{40}Ca/^{44}Ca)_C^{\text{sample}}/(^{40}Ca/^{44}Ca)_C^{CaF_2} - 1] \times 1000$$

where C indicates that the ratio was corrected for instrumental mass fractionation using the double spike technique. This definition of δ is identical to that

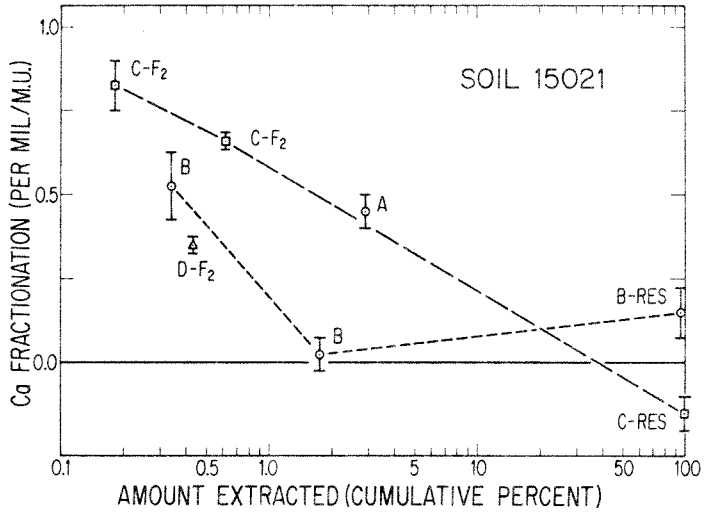

Fig. 2. Small Ca isotope fractionation in lunar soil 15021. We show values equal to $\delta(^{40}Ca/^{44}Ca)/4$ (see text for sign convention). Data for soil aliquots A–D are shown; F_2 indicates samples which were exposed first to fluorine. Data show generally decreasing effects as the amount of Ca extracted increases.

used for O and Si except for the sign convention. For negative $\delta(^{40}Ca/^{44}Ca)$ the heavier Ca isotopes are enriched. For the purpose of plotting and comparing the Ca results with the O and Si effects we have reversed the sign of $\delta(^{40}Ca/^{44}Ca)$ in Figs. 2 and 3.

For all samples we have measured the Ca content; this is easily obtained from the doubly spiked runs, since computation using either the ^{42}Ca or the ^{48}Ca component of the double tracer provides for a measurement of the Ca content in each sample by isotope dilution. For aliquot C of soil 15021 we have a complete set of Ca measurements on the leaches and the residue. We therefore obtain a Ca concentration in 15021-C of $7.51 \pm 0.01\%$ (by weight). Using this value we calculate the percent Ca in the leaches and in the residue for 15021-C and we estimate the percent Ca in all other leaches of the various 15021 aliquots (Table 2). In Figs. 2 and 3 we show the isotopic effects for each particular leach as a function of the *cumulative amount of Ca* extracted, which is defined as the Ca removed during the particular leach plus the Ca removed in all preceding leaches for each independent soil aliquot. For oxygen and silicon we also reproduce isotopic effects as a function of cumulative O extracted during successive fluorinations.

The Ca data show the existence in the leaches of soil 15021 of small fractionation effects of $\lesssim 1$ per mil per mass unit. In Fig. 2 we show a highly expanded view of the Ca effects. The estimated experimental uncertainties permit the identification of definite small isotopic effects for Ca. The data display a reasonable regularity as a function of Ca extracted so that the first leaches appear to show larger mass fractionation effects than the subsequent leaches. The fractionation effects indicate that Ca in the leaches is *heavier* than in the residues. The sign of the isotope fractionation effects for Ca is therefore consistent with the behavior of O, Si, S, and K. The leach data were obtained on samples either spiked before chemical separation or showing large column yields; therefore, we believe the small effects for the leaches are real. This is particularly the case for aliquot C where one leach and the residue were spiked before chemical separation. We note that the analysis of the residue from aliquot C is superior to the analysis of residue B because the latter sample was not spiked totally and showed a relatively low Ca column yield.

In Table 2 we also have shown results for rock 70215 and for mineral separates from 75055. These data show even smaller mass fractionation effects of less than 0.25 per mil per mass unit. For the mare basalt samples there is the possibility of mass fractionation during element chemical separation. Since we did not measure column yields, we do not believe that the data on the mare basalts demonstrate the existence of Ca fractionation effects during crystallization of these igneous rocks.

Figure 3 shows the striking contrast between the oxygen and silicon isotopic patterns and that obtained for calcium. The oxygen and silicon data are from Epstein and Taylor (1972). The maximum oxygen and silicon fractionations away from the bulk value are 22 and 12 per mil per mass unit, respectively; these effects are more than an order of magnitude greater than the Ca effects.

Table 3.

Sample	Extracted O_2 (μm)	Si (μm total)	Extracted Ca	
			Leach 1 (μm)	Leach 2 (μm)
15021-C	20	40	0.31	0.76
15021-D	38		0.73	1.93

μm = micromoles.

Table 4.

	Bulk[b]	Extracted (Aliquots C + D)
O/Si[a]	3.3	2.9
O/Ca[a]	14.8	31

[a]Atom ratio.

[b]Calculated using O and Si concentrations by Janghorbani *et al.* (1973).

DISCUSSION

We have demonstrated the presence of very small fractionation effects in Ca leached from a mare soil which shows much higher O and Si isotopic mass fractionation effects. The possible explanations of these data are:

(1) The range of Ca fractionation on the moon is far smaller than for O, Si, and S by at least an order of magnitude and for K by a factor of five.
(2) Our analytical procedures do not extract the significantly isotopically mass fractionated Ca.
(3) The mass fractionation effects are diluted by Ca extracted from easily soluble, bulk phases which show no isotopic fractionation.

The purpose of the experiment was to attempt to remove preferentially Ca from the surfaces of the soil grains. The fluorination technique involves a gas-solid reaction which attacks silicate bonds and releases O_2 and SiF_4. The presence of solar-wind implanted H_2 and of terrestrial adsorbed water may significantly affect the reaction mechanism; this may be especially important for the partial fluorination experiments during which it is assumed that the surface layers of the soil grains are preferentially attacked. It is likely that the fluorination reaction leaves a residue of Ca at the attacked sites which is in the form of CaF_2. The water leaching which we performed on partially fluorinated samples then was expected to remove this residual Ca. However, the leaching of Ca from bulk phases in the soil is also possible and such leaching cannot be prevented in

this experiment. Goldberg *et al.* (1976) have found some evidence that CaF_2 deposited on a glass substrate required leaching for ~10 min in hot water for complete removal. These leaching conditions are stronger than that of, for example, our first H_2O leach of 15021-C; however it is not clear to what extent the simulation experiments of Goldberg *et al.* (1976) are applicable to leaching of Ca from partially fluorinated lunar soil grains.

We note that neither the partial fluorination process nor leaching processes are well characterized or reproducible in detail. For example, in our partial fluorination of aliquots C and D (each weighing 105 mg) we extracted considerably more oxygen and silicon per milligram of sample than would have been expected from the original partial fluorination experiments of Epstein and Taylor (1972). It is possible that this is due to a difference of a factor of ~2 in the mean grain size of the soil subsamples used in the different experiments. Since we used much smaller sample sizes than for the extensive measurements of Epstein and Taylor (0.9 g), it is possible that different mean grain sizes apply to the different samples. At present we do not believe that the higher O and Si amounts extracted in this experiment are problematical. Whereas the details of the partial fluorination processes are not easily tractable, we believe that the observation of large $\delta^{18}O = 21$ per mil in our extracted O_2 demonstrates: (a) the existence of isotopically fractionated oxygen in the particular soil aliquot used for the Ca measurements, and (b) that these isotopically heavy oxygen layers were attacked during the partial fluorination in this experiment.

In Table 3 we have listed the amounts of O_2, Si, and Ca extracted from the

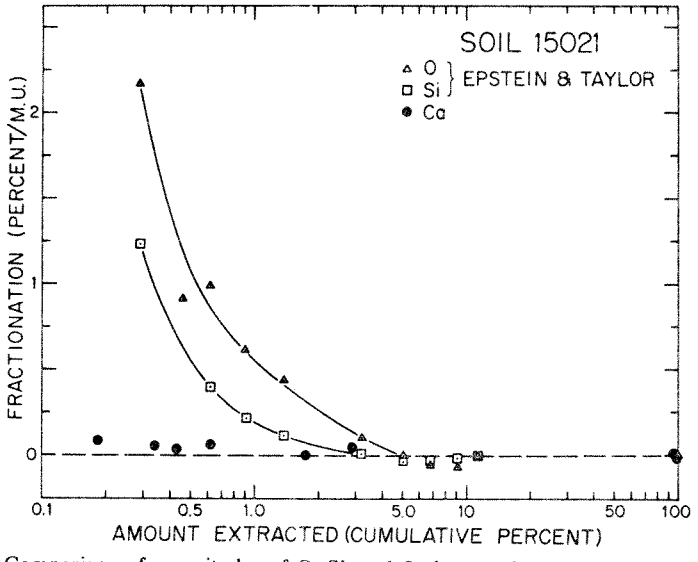

Fig. 3. Comparison of magnitudes of O, Si, and Ca isotope fractionation in 15021. The Ca data in this graph are the same shown in Fig. 2; the oxygen and silicon data are those of Epstein and Taylor (1972). The Ca mass fractionation effects are more than an order of magnitude smaller than the O and Si effects.

soil. We note that the amount of O_2 extracted from aliquot D is about twice as large as for aliquot C. The amounts of Ca extracted by *leaching* also show approximately a factor of two. This observation generally indicates that Ca extracted by leaching was obtained from sites *activated* by the fluorination process rather than from easily soluble phases in the soils. Insofar as the isotopic composition of the extracted oxygen shows a large effect, it is reasonable to assume that both the oxygen and the calcium analyzed were extracted from isotopically interesting and presumably surficial layers. A direct confirmation of whether in fact surficial layers of grains have been attacked is in principle possible by future careful SEM work on grains exposed to fluorine and then leached.

In Table 4 we have compared the amounts of O, Si, and Ca extracted from 15021 with their values in the bulk soil. For O and Si we note a smaller O/Si value in the extracted material than in the bulk soil. This has been observed by Epstein and Taylor (1971, 1972) and Taylor and Epstein (1973) in many partial fluorination experiments and has been interpreted as indicating that there are actual depletions of O relative to Si in the outer layers of the soil grains. The amount of Ca extracted by water leaching is about a factor of two depleted in the leach relative to the extracted oxygen. We do not consider this difference in absolute amounts to be of importance. Given our current understanding of the partial fluorination and leaching techniques, it may simply reflect different efficiencies of extraction.

We note that the amounts of Ca in the water leaches are not significantly limited by the solubility of Ca salts (presumably CaF_2) in water unless the kinetics of the dissolution process are very slow. We also note that possible "soluble" phases in the soil, e.g., whitlockite, are not significantly more soluble than CaF_2. We conclude that the fraction of Ca extracted from the soils by leaching is comparable to the fraction of the O_2 extracted by partial fluorination.

In contrast to the small mass fractionation effects observed for Ca, Barnes *et al.* (1973), Garner *et al.* (1975), and Church *et al.* (1976) have presented evidence for isotopic variations in $^{39}K/^{41}K$ of up to 0.9% in *bulk* samples. The observations in K are inherently limited by the lack of an *internal* isotopic standard which can be used to correct for instrumental and possible chemical element separation effects. Garner *et al.* (1975) have discussed in detail possible sources of instrumental fractionation which can affect measured isotopic ratios using a thermal ionization source. These workers have obtained data following a strict protocol in order to minimize the instrumental effects and have demonstrated under a variety of conditions that instrumental mass fractionation effects can be less than 0.2% for $^{39}K/^{41}K$. They have obtained a maximum $^{39}K/^{41}K$ variation of up to 0.89% between mare basalts and bulk soils while some bulk soils show no fractionation. Although it is clear that soils of different maturity may show distinct K effects (including null effects), these data do not show a well-defined systematic offset between $^{39}K/^{41}K$ in mare basalts and in soils, as has been pointed out by these workers. The work of Church *et al.* (1976) did not include measurements of $^{39}K/^{41}K$ in mare basalts to provide a direct comparison between

soils and mare basalts. These workers instead have used their value for the NBS prepared K standard SRM 985 for normalization of their data and comparison with the mare basalt data of Garner *et al.* (1975). Their observed $^{39}K/^{41}K$ differences for soil components are generally smaller than the differences between mare basalts and bulk soils. Although the K data provide no internal means of correcting for significant analytical and instrumental mass fractionation effects, and thus have larger experimental uncertainties, the effects seen for K are similar to those observed with much higher precision for O, Si, and S isotopes. Thus one might reasonably assume that the K isotopic effects reflect the action of the same enrichment processes that produced the effects in these other elements.

Considering that the $^{39}K/^{41}K$ effects at the level of 0.5% per mass unit difference are the result of isotope fractionating processes, these processes must affect K and Ca differently either because of differences in the volatility of these elements themselves or of distinct molecular species responsible for the effects. Epstein and Taylor (1971, 1972) have discussed possible molecular species involved in the correlated oxygen and silicon effects and showed that it was not possible to choose a specific molecular species involved in the production of the oxygen and silicon effects. The extent to which volatility is a dominant factor remains to be established. Housley and Grant (1977) have observed enhancements of Al, Mg, Ca, and Ti and depletions of Si and Fe produced on the surface of lunar soil 15301 by sputtering with Ar^+. These results demonstrate that volatility is an important parameter in sputtering (cf. Sigmund, 1969). However, the extent to which this parameter also controls which specific elements should or should not be highly isotopically fractionated remains unclear.

In interpreting the O and Si isotopic fractionation data, Epstein and Taylor (1971, 1972, 1974) discussed mechanisms of fractional vaporization of material from and/or fractional condensation onto surface layers of soil grains. They mentioned that bombardment by the solar wind was one candidate for the agent principally responsible for producing the observed mass fractionation. There are now data showing *elemental* fractionation from sputtering (Liau *et al.*, 1977). Wehner (1977) has reported isotopic effects for ion sputtered Mo of 6% for eight mass units. These results are not definitive because the use of a quadrupole mass spectrometer presents problems with sensitivity falloff with higher mass, as pointed out by Wehner (1977), which could result in mass fractionation artifacts. Wehner (1977) has not reported analyses of unsputtered, normal Mo by this technique.

The observation of extremely small mass fractionation effects on Ca is in sharp contrast to the O, Si, S, and K data. The Ca data provide an important constraint on theories which attempt to describe the mechanism for production of isotopically mass fractionated components in the lunar soils by ion sputtering or other processes (e.g., redeposition of vapors). The extent to which the Ca data can be reconciled with the O, Si, S, and K data is not clear at present. The extent to which large Ca isotopic effects are present on the moon but have not yet been detected remains to be seen. However, we believe that simulation experiments

which will demonstrate whether mass fractionation occurs for Ca and K during ion sputtering should lend direction to further experimentation with lunar soils.

Switkowski *et al.* (1977) and Haff *et al.* (1977) have presented a model for production of mass fractionated components in lunar soils. The model predominantly involves sputtering of elements and redeposition of some of the sputtered material onto the lunar surface. Calculations are presented which indicate that the isotopes are significantly fractionated both during the actual sputtering and also in preferential loss of the lighter isotopes from the moon. Their calculations of gravitational mass fractionation effects for O, Si, and S are in reasonable agreement (factor of two) with the maximum observed effects for these elements. However, these workers also predict an order of magnitude larger effects in Ca than observed. A major revision of this model is required if our interpretation of the Ca data as pertaining to Ca on the grain surfaces is correct.

Acknowledgments—We thank G. J. Wasserburg for his encouragement and comments. J. C. Huneke provided helpful suggestions regarding the manuscript. T. Wen helped in some of the laboratory work. This work was supported by NASA grants NGR-05-002-333, NGL-05-002-188, and NGL-05-002-190 and by NSF grant PHY-76-02724.

REFERENCES

Barnes I. L., Carpenter B. S., Garner E. L., Gramlich J. W., Kuehner E. C., Machlan L. A., Maienthal E. J., Moody J. R., Moore L. J., Murphy T. J., Paulsen P. J., Sappenfield K. M., and Shields W. R. (1972) Isotopic abundance ratios and concentrations of selected elements in Apollo 14 samples. *Proc. Lunar Sci. Conf. 3rd*, p. 1465–1472.

Barnes I. L., Garner E. L., Gramlich J. W., Machlan L. A., Moody J. R., Moore L. J., Murphy T. J., and Shields W. R. (1973) Isotopic abundance ratios and concentrations of selected elements in some Apollo 15 and Apollo 16 samples. *Proc. Lunar Sci. Conf. 4th*, p. 1197–1207.

Becker R. H. and Clayton R. N. (1975) Nitrogen abundances and isotopic compositions in lunar samples. *Proc. Lunar Sci. Conf. 6th*, p. 2131–2149.

Church S. E., Tilton G. R., and Wright J. E. (1976) Volatile element depletion and $^{39}K/^{41}K$ fractionation in lunar soils. *Proc. Lunar Sci. Conf. 7th*, p. 423–439.

Clayton R. N., Mayeda T. K., and Hurd J. M. (1974) Loss of oxygen, silicon, sulfur, and potassium from the lunar regolith. *Proc. Lunar Sci. Conf. 5th*, p. 1801–1809.

Dymek R. F., Albee A. L., and Chodos A. A. (1975) Comparative mineralogy and petrology of Apollo 17 mare basalts: Samples 70215, 71055, 74255, and 75055. *Proc. Lunar Sci. Conf. 6th*, p. 49–77.

Epstein S. and Taylor H. P., Jr. (1971) O^{18}/O^{16}, Si^{30}/Si^{28}, D/H, and C^{13}/C^{12} ratios in lunar samples. *Proc. Lunar Sci. Conf. 2nd*, p. 1421–1441.

Epstein S. and Taylor H. P., Jr. (1972) O^{18}/O^{16}, Si^{30}/Si^{28}, C^{13}/C^{12}, and D/H studies of Apollo 14 and 15 samples. *Proc. Lunar Sci. Conf. 3rd*, p. 1429–1454.

Epstein S. and Taylor H. P., Jr. (1974) Oxygen, silicon, carbon, and hydrogen isotope fractionation processes in lunar surface materials (abstract). In *Lunar Science V*, p. 212–214. The Lunar Science Institute, Houston.

Epstein S. and Taylor H. P., Jr. (1975) Investigation of the carbon, hydrogen, oxygen, and silicon isotope and concentration relationships on the grain surfaces of a variety of lunar soils and in some Apollo 15 and 16 core samples. *Proc. Lunar Sci. Conf. 6th*, p. 1771–1798.

Eugster O., Tera F., and Wasserburg G. J. (1969) Isotopic analyses of barium in meteorites and in terrestrial samples. *J. Geophys. Res.* **74**, 3897–3908.

Garner E. L., Machlan L. A., and Barnes I. L. (1975) The isotopic composition of lithium, potassium, and rubidium in some Apollo 11, 12, 14, 15, and 16 samples. *Proc. Lunar Sci. Conf. 6th*, p. 1845–1855.

Gerhard W. and Oechsner H. (1975) Mass spectrometry of neutral molecules sputtered from polycrystalline metals by Ar^+ ions of 100–1000 eV. *Z. Physik B.* **22**, 41–48.

Goldberg R. H., Tombrello T. A., and Burnett D. S. (1976) Fluorine as a constituent in lunar magmatic gases. *Proc. Lunar Sci. Conf. 7th*, p. 1597–1613.

Haff P. K., Switkowski Z. E., Burnett D. S., and Tombrello T. A. (1977) Gravitational and recoil contributions to surface mass fractionation by solar wind sputtering. *Proc. Lunar Sci. Conf. 8th.* This volume.

Housley R. M. and Grant R. W. (1977) An ESCA study of reduced Fe and other surface chemical alteration profiles in lunar fines (abstract). In *Lunar Science VIII*, p. 460–462. The Lunar Science Institute, Houston.

Janghorbani M., Miller M. D., Ma M., Chyi L. L., and Ehmann W. D. (1973) Oxygen and other elemental abundance data for Apollo 14, 15, 16, and 17 samples. *Proc. Lunar Sci. Conf. 4th*, p. 1115–1126.

Kerridge J. F. (1975) Solar nitrogen: Evidence for a secular increase in the ratio of nitrogen-15 to nitrogen-14. *Science* **188**, 162–164.

Liau Z. L., Brown W. L., Homer R., and Poate J. M. (1977) Surface layer composition changes in sputtered alloys and compounds. Submitted to *Appl. Phys. Lett.*

Oechsner H. (1975) Sputtering—A review of some recent experimental and theoretical aspects. *Appl. Phys.* **8**, 185–198.

Rees C. E. and Thode H. G. (1972) Sulfur concentrations and isotope ratios in lunar samples. *Proc. Lunar Sci. Conf. 3rd*, p. 1479–1485.

Rees C. E. and Thode H. G. (1974) Sulfur concentrations and isotope ratios in Apollo 16 and 17 samples. *Proc. Lunar Sci. Conf. 5th*, p. 1963–1973.

Russell W. A. and Papanastassiou D. A. (1977) Isotope fractionation in ion exchange columns. Submitted to *Anal. Chem.*

Russell W. A., Papanastassiou D. A., and Tombrello T. A. (1976) Absolute Ca isotopic compositions in a lunar soil (abstract). In *Lunar Science VII*, p. 752–754. The Lunar Science Institute, Houston.

Russell W. A., Papanastassiou D. A., Tombrello T. A., and Epstein S. (1977a) Search for Ca isotopic fractionation and correlation of Ca and O effects (abstract). In *Lunar Science VIII*, p. 823–825. The Lunar Science Institute, Houston.

Russell W. A., Papanastassiou D. A., and Tombrello T. A. (1977b) Ca isotope fractionation on the earth and other solar system materials. Submitted to *Geochim. Cosmochim. Acta.*

Sigmund P. (1969) Theory of sputtering. I. Sputtering yield of amorphous and polycrystalline targets. *Phys. Rev.* **184**, 383–416.

Somorjai G. A. and Lester J. E. (1967) Evaporation mechanism of solids. *Progr. Solid State Chem.* **4**, 1–52.

Switkowski Z. E., Haff P. K., Tombrello T. A., and Burnett D. S. (1976) Mass fractionation of the lunar surface by solar wind sputtering. Submitted to *J. Geophys. Res.*

Taylor H. P., Jr. and Epstein S. (1973) O^{18}/O^{16} and Si^{30}/Si^{28} studies of some Apollo 15, 16, and 17 samples. *Proc. Lunar Sci. Conf. 4th*, p. 1657–1679.

Tera F., Eugster O., Burnett D. S., and Wasserburg G. J. (1970) Comparative study of Li, Na, K, Rb, Cs, Ca, Sr and Ba abundances in achondrites and in Apollo 11 lunar samples. *Proc. Apollo 11 Lunar Sci. Conf.*, p. 1637–1657.

Thode H. G. and Rees C. E. (1971) Measurement of sulphur concentrations and the isotope ratios $^{33}S/^{32}S$, $^{34}S/^{32}S$, and $^{36}S/^{32}S$ in Apollo 12 samples. *Earth Planet. Sci. Lett.* **12**, 434–438.

Thode H. G. and Rees C. E. (1976) Sulphur isotopes in grain size fractions of lunar soils. *Proc. Lunar Sci. Conf. 7th*, p. 459–468.

Wasserburg G. J., Papanastassiou D. A., Nenow E. V., and Bauman C. A. (1969) A programmable magnetic field mass spectrometer with on-line data processing. *Rev. Sci. Instrum.* **40**, 288–295.

Wehner G. K. (1977) Isotope enrichment in sputter deposits. *Appl. Phys. Lett.* **30**, 185–187.

CHAPTER 5. LABORATORY SIMULATIONS OF SOLAR WIND EROSION ON THE LUNAR SURFACE

The discussion in the previous chapter indicates that the mechanisms leading to isotopic fractionation on the lunar surface remain poorly understood. This in large part is caused by the absence of experiments which simulate lunar surface exposure conditions and reveal the magnitude of isotope fractionation arising from the various proposed mechanisms. In this chapter are described the results of experiments in which calcium-bearing samples of terrestrial origin are sputtered with low-energy nitrogen beams. The calcium sputtered off of targets was itself collected and analyzed for isotopic fractionation. These experiments provide information about the bombardment of low-energy ions, from the sun, of planetary bodies, such as the moon, which lack atmospheres and strong magnetic fields. However, they also provide the first detailed experimental information about the sputtering of substrates containing several species, all of which have nearly identical surface binding energies. It will be shown here that large fractionation of the calcium isotopes occurred during these sputtering experiments. Earlier preliminary experiments attempted to measure directly the isotopic fractionation of sputtered substrates, but were inconclusive becuase of the difficulty in sampling only the potentially fractionated material; these measurements are briefly described in Appendix A. The present theoretical understanding of sputtering is inadequate for explaining the calcium fractionation variations. Binding energy variations between different calcium isotopes appear to

be too small to account for the effects (see Appendix B). Other calculations also yield predictions of null effects. Experimental information such as presented here will therefore be required if a better theoretical understanding of the sputtering of multiple-component targets is eventually to be gained.

The specific goals of these experiments were outlined in Chapter 1. In the following sections, the experimental apparatus and techniques will be described, the results of the fractionation measurements will be summarized, and then the results will be discussed. This discussion is divided into a number of areas: (a) sputtering theories and models of isotopic fractionation; (b) the development of surface roughness and blistering features in the bombarded targets; (c) the possible role of such radiation damage in isotopic or elemental fractionation studies; (d) atomic mixing and variations of fractionation with increasing bombardment; (e) isotopic fractionation results reported previously in the literature; (f) angular variations in Ca sputtering yields and isotopic fractionation; and (g) the relationship of the Ca sputtering data to processes occurring on the moon.

EXPERIMENTAL PROCEDURES

Sputtering Apparatus and Techniques

A rather unusual "catcher" surface geometry was adopted which afforded a number of advantages. The surface upon which the Ca would be deposited when it was sputtered was chosen to be cylindrical and coaxial with the incoming ion beam. The catcher's diameter was much larger than that of the ion beam, which passed down the axis of this

open cylinder prior to striking at normal incidence the target to be sputtered (Figure 5-1). The target was in a recess and was supported from the rear in an arrangement which allowed one end of the catcher tube to be positioned very close to the target without being interfered with by mounting hardware (Figure 5-2). This permitted Ca sputtered in directions nearly tangential to the target surface to be caught by the catcher tube. The sputtered material would deposit on the inside surface of the tube where it would remain until removed for isotopic analysis. The tube was long enough so that the angle subtended at the target by the end of the tube farthest from the target was a small angle, permitting material sputtered at angles greater than 5° from the normal to be collected by the tube. This geometry permits the loading of multiple catcher tubes into the vacuum chamber, each to be used at a different time during the experiment without cross-contamination caused by sputtering taking place at other times. It also allows collection of sputtered material exiting over a large range of sputtered angles. Each tube collects all material sputtered from the target at angles between roughly 5° and 70°. The catcher tubes are mounted side by side in a holder which is connected to a manipulator which allows for the change of catcher surfaces during an experiment. The length of travel of the linear-motion manipulator was such that six catcher tubes 0.660 inches in diameter could be accommodated at one time. A separate linear-motion manipulator was used to change targets. Up to four targets could be placed in the vacuum chamber at one time, although in practice, with the limited number of catcher tubes, fewer than this number of targets

were used; one of the positions was always reserved for a thin quartz disk which could be used for viewing the beam.

Both manipulators were electrically insulated from ground, which proved convenient for purposes of current integration. The catcher tube and target holders were electrically connected through a flexible copper wire and connected to external current integration apparatus via an electrical feed-through arrangement designed into one of the manipulators. With the two holders electrically connected and biased at +300 V with respect to ground, a good approximation to a Faraday cup would be obtained provided that any stray beam did not hit the catcher tube entrance, causing secondary electrons to be lost from the assembly. In addition, no slits were used upstream from the vacuum chamber, the beam size being limited primarily by the 7/16 inch aperture of the cold trap preceding the sputtering vacuum chamber. There was therefore probably no copious source of secondary electrons originating upstream which would have been attracted to the target apparatus by the +300 V bias. (For a description of the beam-line arrangement, see Weller, 1978.) The current integration was therefore probably accurate to within about 10%, although no direct confirmation of this was made.

It was of some concern to minimize charge build-up on the electrically insulating minerals which were being sputtered. Such positive charge build-up could cause arcing between the sample and the stainless steel target holder, even though every point on the target was within 0.23 inch of the circular edge of the target holder

recess. Such arcing could perhaps cause localized vaporization of Ca on the target, causing non-sputtered Ca to be deposited upon the catcher surface. In addition, charge build-up can degrade the effective energy of the primary ion beam, although in this particular experiment, where the beams had energies of either 100 keV or 130 keV (see below), charge build-up could not have been of a sufficiently great magnitude to have caused a serious ion energy degradation. In anticipation that arcing might be a difficulty, the catcher tubes were designed to accommodate annular apertures with a 7/16 inch diameter inner hole. The aperture would mount 7/8 inch inside the tube from the end nearest the target. Any stray beam hitting this aperture would generate secondary electrons which would strike the target and tend to minimize or neutralize the charge build-up. Use instead of an electron flooding gun was deemed too clumsy for the geometry of this experiment, and may have interfered with the current integration. In practice, arcing was not visually observed during the sputtering runs to occur more than occasionally, probably because fairly low beam currents were used which permitted the positive charges from the beam to drain off of the target at a sufficient rate. During some experiments the apertures were omitted without noticeably altering the rate of arcing--observed visually as sudden changes in the fluorescent patterns generated by the beam striking the target. Because of this and because in most cases the measured number of sputtered Ca atoms agrees rather well with that predicted by the Sigmund (1969) sputtering theory, vaporization of extra Ca due to

arcing was not considered to be a significant difficulty.

The sputtering experiments were carried out in the ultra-high-vacuum (UHV) chamber described by Gregg (1977). The target holder, the catcher tubes, apertures, and holder, and all miscellaneous hardware were made of stainless steel 304. Prior to each use, all pieces were electropolished, cleaned in boiling, reagent-grade, 8N HNO_3, and oven dried. Mineral samples were prepared by hand grinding on silicon carbide paper and polishing with 1 μm alumina powder; they were cleaned by ultrasonic rinsing in three separate reagent-grade methanol baths and were then warm-air dried. With these preparations, the vacuum chamber could be loaded with the apparatus and pumped to $\sim 4 \times 10^{-9}$ Torr base pressures using an ion pump backed up by occasional titanium sublimation. Sublimation was done only with the apparatus retracted to a position ~20 cm above the shielded top of the titanium filament in order to avoid any risk of coating Ti on the samples or catcher tubes. No sublimation was done during or after the sputtering. During sputtering, an in-line valve, used to isolate the chamber from the beam line, was open, but the chamber was isolated by an in-line liquid-nitrogen cold trap from the 5×10^{-6} Torr oil-diffusion-pumped beam line. With the beam on target, the sputtering chamber pressure, as measured by an ionization gauge attached to one port, was $1\text{-}2 \times 10^{-8}$ Torr.

Alignment of the catcher tube and target holders with the beam in the horizontal plane was done by visual sighting and was adjusted during chamber loading by means of the rotatable 6-inch

flange on the top of the chamber. Mated to this flange was a 6-inch flange upon which were mounted the two manipulators holding the sputtering apparatus. This pair of flanges could be rotated, thereby altering the angle between the catcher tubes' axes and the direction of the beam until it was approximately 0°. No provision was included to keep the apparatus mounted on the manipulators in mutual horizontal alignment, although some play was present due to the bellows-type design of the manipulator feedthroughs. However, visual inspection through two windows in the chamber itself, as well as through a port in the 31° mass-analyzing magnet upstream, indicated that the horizontal alignment with the beam of both the catcher tubes and the target holder was entirely satisfactory. Vertical alignment was maintained during catcher tube and/or target changing both by calibration markings on the manipulator micrometers and by visual inspection. The ion beam could be steered vertically on the target by means of small steering magnets and a quadrupole lens located upstream from the 31° magnet. (The quadrupole did steer the beam somewhat, probably because of imperfect alignment with the ion source Einzel lens and extractor beam-optics.) Horizontal steering could be accomplished by means of an orthogonal pair of steering magnets, the quadrupole lens, or by small adjustments of the 31° analyzing magnet field.

The catcher tubes could be adjusted in their holder so that the clearance between them and the target holder was as small as possible while still permitting free relative movement using the

manipulators. This clearance was between 1 mm and 3 mm and was not a uniform value for all tubes due to a slight machining inaccuracy which caused the target holder when mounted to have a few degrees vertical tilt. In addition to these clearances, the distance between a catcher tube end and its target was increased by the amount the sample was recessed into the target holder (0.5 mm to 1.5 mm, depending on whether a washer, used to help hold smaller diameter targets, was required). Although not of great importance insofar as affecting the experimental results, the small differences in the total clearances have been included in the estimates of angular range of collection listed in the tabulation of sputtering results (Table 5-3).

For one of the sequences of sputtering experiments, it was decided to incorporate means for measuring the isotopic fractionation of the sputtered material as a function of its angle of ejection from the target. Toward this end, a series of catcher tubes was constructed consisting of separable sections placed end to end. The sections had small "steps" at the ends by which they could snap onto adjoining sections without falling off. Careful machining enabled the assembled catcher tubes to present to the target an inside surface essentially uninterrupted by the joints. Estimates made during the design of these separable tubes indicated that satisfactory amounts of material could be collected on each section to permit separate isotope analysis when three sections were employed. To equalize the amounts of Ca deposited, the sections were of differing lengths, with the shorter sections being nearer to the target. Subsequently it was found that

Ca samples as small as 10^{-7} g could be analyzed for isotopic fractionation. Therefore, in the future perhaps four or five sections instead of three could be included within the same overall length. The apertures discussed above which were supposed to help minimize target charge build-up were omitted from these separable catcher tubes, as they had not been demonstrated as being helpful in minimizing what little (apparent) build-up was present.

In each of the sputtering runs, mass-analyzed nitrogen beams were used to sputter the calcium-bearing minerals. For some of the experiments, a single-energy beam was used during the entire sputtering. At other times, it was desired to study the fractionation pattern produced by first sputtering with one energy and then changing catcher tubes and sputtering the same target with a beam of higher or lower energy (longer or shorter range in the target). For this work, two beam energies were used; one was 50 keV, which corresponds to a 500 Å range in fluorite (CaF_2), and the other was 130 keV, which corresponds to a 1700 Å range in fluorite. The motivation behind the use of beams with differing ranges will be discussed later in this chapter. Because of the difficulty encountered in obtaining sufficient 50 keV $^{14}N^+$ currents from the ion source, 100 keV molecular $(^{14}N)_2^+$ beams were used instead. In these cases, the ion ranges for these beams depend strongly upon the energy per atomic mass unit (AMU) of the incoming beam but not as strongly upon the actual mass of the beam. This may be verified by calculating the ranges in the molecular and atomic cases using the Lindhard, Scharff, and Schiøtt (1963) ion range

theory, hereinafter designated LSS. This theory provides range estimates accurate in these single ion cases to ∿15%, which is sufficient for the estimates required in this chapter. For molecular ions, the calculated estimates are not highly accurate since the molecule can dissociate at any time. However, the accuracy is still probably sufficient to verify the present point. For beams of (a) nuclear charge 7, mass 14, and energy 50 keV and (b) charge 14, mass 28, and energy 100 keV, the LSS theory estimates the projected ranges in CaF_2 (average nuclear charge and mass 12.667 and 26) to be 489 Å and 414 Å. Since straggling in each case is calculated to be ∿500 Å, these two ranges are identical for all practical purposes. Therefore, the use of 100 keV $(^{14}N)_2^+$ and 130 keV $^{14}N^+$ beams succeeds in attaining the goal of having two highly different ion ranges available for these sputtering experiments.

Ion Source Operation and Analyzing Magnet Calibration

Prior to the commencement of a sputtering run, it was necessary to ascertain the value of the 31° magnet field which would bring the correct beam onto the target. The mass spectrum from the ion source revealed that many beams were present, so it was necessary to identify masses 14 and 28 with care. For the first two sets of sputtering runs (samples whose coded designation in Table 5-3 begins with a first number of 1 or 2) this was done by preparing a source gas bottle flushed and filled with dry-grade N_2 (10%) and He (90%). The mass spectrum was scanned with the beams incident on a quartz disk mounted in the target holder. Masses 1-4, 13-20, and 27-30 were

typically observed. Attempts to identify unambiguously masses 14 and 28 consisted of scaling readings of a Hall probe residing in the 31° magnet fringe field and of assigning masses on the basis of which beams had large currents. This was done in the following fashion. The Hall probe voltage for the clearly identifiable mass 4 helium beam would be noted. The following relation was used:

$$V_{Hall}(m_2) = V_{Hall}(m_1) \sqrt{m_2/m_1} \qquad (1)$$

where m_1 and m_2 are masses of the beam ions in amu and $V_{Hall}(m)$ is the Hall voltage observed when the magnet is correctly set to bring a beam of mass m onto the target. Setting $m_1 = 4$ and m_2 = various masses in the range 13 to 20, the calculated values of $V_{Hall}(m_2)$ for these masses could be compared with the actual observations, thereby enabling identification of the beams. In cases of doubt, the relative magnitudes of the beams were examined as well. The difficulty with accurately extrapolating V_{Hall} over too wide a mass range, for example 4 to 13, was that the fringe field was being measured rather than the main deflecting field. Therefore it was easy to become less certain of the identification of beams of masses 13 to 20 when several large beams were present in the sequence CH, N, NH, O, OH, H_2O. With C_2H_2, N_2, and N_2H present, a similar difficulty was present at mass 28.

Although at the time of the first two sputtering runs, the mass identification appeared to be clear, subsequent reexamination has indicated that these sputtering measurements were probably done using 130 keV $(^{14}NH)^+$ and either 100 keV N_2H^+ (probably) or $(^{16}O)_2^+$ (less

likely). The degree to which this may have been important to the interpretation of the results is discussed below. For the third and fourth sputtering runs, a more elaborate procedure was followed for calibration of the mass spectrum. What was called for was a clear identification of one of the masses observed within the 13-20 range. Consequently, a separate source bottle was filled with high purity neon, the only contaminant in the original bottle being He, which was in the tens of ppm concentration range. With this gas feeding the ion source essentially only masses 20 and 22 were observed, and almost in the proper isotopic ratio! This allowed unambiguous identification of all masses down through 14 and up through 28. Because of possible instabilities in the Hall probe electronics, which have subsequently been stabilized, and of hysteresis effects in the analyzing magnet, it is recommended that for any future sputtering experiments using this equipment and beams in the mass range 12-20, the magnet calibration always be checked against Ne as well as He.

In order to ensure that the mass 14 and 28 beams were in fact nitrogen primarily rather than some undesired molecular beam, efforts were made to use a source bottle containing as little water vapor and other gases as possible. To this end, the bottle was flushed with dry-grade nitrogen and thoroughly evacuated to 50-100 μm Hg several times prior to the final filling. Also, He rather than H, which could form molecular beams, was used to dilute the gas. The use of such a diluted source gas appears to promote the duoplasmatron filament life and stable operation of the source over extended lengths of time, but

is not very well understood. In the third and fourth sets of experiments, the dry-grade nitrogen used in the source bottle was further processed by passing it through a coiled copper line immersed in liquid nitrogen, the intent being to remove any small amounts of H_2O, CO_2, or O_2 which may have been present. This procedure resulted in a much "cleaner" mass spectrum. Previously, masses 14, 15, and 16, and 18 were fairly equal in intensity, with mass 17 five to ten times larger! Adopting this liquid nitrogen trapping procedure substantially reduced all beams other than mass 14; mass 17 was dramatically reduced to one-fourth the intensity of the mass 14 beam.

Monitoring of the beam focussing and steering during the sputtering of a target was done by visual means in addition to watching the ion current measured on target. Three ports were available for viewing the beam on target. One was in line with the beam behind the target. The target holder had been designed to permit rear viewing of transparent samples. Viewing through this port provided the easiest means of assessing where the beam was striking the target, the $\sim$1.2 cm diameter of which was comparable to the maximum possible beam diameter, but which was in fact several times larger than the beam. This rear viewing was possible for all samples but two, a poly-crystalline fluorite sample and a plagioclase sample. A second port in the target chamber permitted viewing of the target from one side. Despite the small catcher tube-target holder clearance of 1-3 mm, this view was useful in that it allowed confirmation of correct catcher

tube-target vertical alignment. For the two samples mentioned above it was also of great use in monitoring the steering of the beam, which could be slightly affected by changing conditions in the ion source. (The stable source usually required few such changes.) The third viewing port was located at the 31° magnet and permitted viewing along the axis of the beam tube between the magnet and the UHV chamber. Although the target was ∿3 m distant from this port, it was easy to tell whether or not the beam was adequately centered on the target and well-focussed. In the case of the two non-transparent samples sputtered, the beam was also monitored by interrupting the sputtering several times for a few minutes in order to allow the beam to be viewed from the rear while incident on the quartz disk.

Sputtered Sample Preparation and Mass Spectrometry

In order to adequately measure the Ca isotopic fractionation of the small amounts of Ca sputtered from the targets, means had to be devised for efficiently removing the Ca from the catcher tube inner surfaces. The technique tried after the first sputtering run proved entirely satisfactory. It involved use of ∿1 ml of 1N HNO_3 (double-distilled National Bureau of Standards grade) to flush the inside surface of the catcher tube. The acid was flushed into a teflon beaker and drawn up with a quartz pipette so that the same small quantity of acid could be used repeatedly until the entire rinsing was complete. The same technique and 1 ml of acid was used to rinse the catcher tube aperture, when used. Any blank (contamination) entering in the procedure from the acid would be minimized and the combined acid

plus beaker plus pipette blank would probably be small compared to that arising from the catcher surface itself. Measurement of the Ca on a catcher tube which had been in the vacuum chamber during sputtering but which was not itself used as the catcher for any of the sputtering yielded a blank of 18 ng Ca. This indicates excellent isolation from the neighboring catcher, which collected 445 ng Ca, and also shows that the blank was within tolerable limits. In reporting Ca concentrations of the sputtered samples, a nominal 15 ng blank has been adopted. For the separable-section catcher tubes, this blank has been apportioned among the three sections according to their relative surface areas. In rerinsings of some of the catcher tubes with 4N HCl, barely any Ca above this blank level was observed. From these measurements it is estimated that approximately 99% of the sputtered Ca was removed from the catcher tubes in the dilute nitric acid rinsing.

Although many of the sputtered samples were quite small in size compared to the samples discussed in Chapters 3 and 4, only minor modifications to the sample handling and mass spectrometric techniques were required in order to obtain satisfactory analytical precision. The samples required no ion exchange column processing, being washed from the catcher tubes as soluble calcium compounds contaminated primarily with some iron, nickel, and possibly chromium from the stainless steel. This contamination was minimized through use of dilute HNO_3 as the rinsing agent rather than HCl, which would have dissolved Fe from the catcher tube walls quite readily. Small 5-10%

aliquots of the sample solutions were mixed with ∿1 ml of a very dilute $^{42-48}Ca$ double tracer prepared from the concentrated tracer whose composition is given in Table 3-1; the concentration of this tracer was 10.8 ng ^{42}Ca/gram spike. Measurement of the resulting $^{40}Ca/^{42}Ca$ in the spiked aliquots then provided the concentration information required for optimal spiking of the remaining major aliquot. This sample was spiked with another dilute $^{42-48}Ca$ tracer prepared by another worker in the laboratory from the Table 3-1 concentrated tracer. Its concentration, as measured by isotope dilution with a normal of known concentration and fractionation, was 255.6 ng ^{42}Ca/gram spike. The composition of this tracer as measured on the mass spectrometer is given in Table 5-1. The composition was corrected for mass fractionation in a way which would permit identical corrected $^{40}Ca/^{44}Ca$ results to be obtained regardless of whether the sample was spiked with the concentrated or dilute tracers. This was done by treating the dilute spike as a mixture of concentrated spike plus contaminant Ca of normal composition; the "mixture" data plus the Table 3-1 tracer composition and a Ca normal composition were fed through the iterative double spike equations, enabling the calculation of $\delta_{blank} = 1.3‰$. The blank contamination was calculated to be 36 ng Ca/gram of dilute spike, a large value arising most likely from use of a bottle by this other worker which was slightly dirty, causing Ca to be leached into the solution.

In most cases the aliquoting and spiking of a sample was the only preparation needed prior to analysis on the mass spectrometer.

Amounts of Fe in the samples, when dried after spiking, were estimated visually to be tens of micrograms. However, most of this contamination, which had been leached from the catcher tubes with $\sim$1 ml of dilute nitric acid could not be redissolved with the $\sim 2 \times 10^{-3}$ ml of this same acid which was used for filament loading. Therefore the contamination on the filament was several orders of magnitude less, since the calcium, which is highly soluble in nitric acid, appeared to be picked up efficiently for loading even with this small quantity of acid. Although the resulting "loads" were often a dirty-brown color rather than the white color observed for a sample loaded with no contamination, the running behavior of the samples--their stability, rate of ion current growth, and ability to attain adequately large ion current levels--was not impaired. For these samples, mass spectra in the Ca mass region revealed no unusual background levels or other features, peak shapes were good, potassium levels were very low, and no ^{56}Fe peaks were observed at the filament temperatures used for Ca analysis. For one sample (4A-4-N, see the explanation of the sample designation code below) the apparent Fe levels were so high that it was decided to try to remove them by ion exchange subsequent to the double spiking. A small anion-resin column with a 2 ng Ca blank was prepared, and the sample was loaded onto and eluted through the column using 9N HCl. The Fe was retained by the 2cm x 0.2 cm resin bed with essentially no breakthrough, while the Ca was not held by the resin. However, much of the Ni in the sample also passed through the resin, being retarded only slightly. A second pass

through the column using a fresh batch of resin resulted in little further improvement. The sample was then passed through a small cation column. Much of the nickel was removed, but because of the small number of plates in this column, there was still some Ni eluted in the Ca cut. For future situations where it is desired to remove the Fe and Ni contamination, it would probably be sufficient to use one anion column pass and two passes through the small cation column. For very small samples, this would be preferable to the omission of the anion step and the use of a single large cation column pass, for which a larger blank (measured to be 17 ng Ca) would likely be obtained.

For the mass spectrometric analysis of these small sputtered samples, much of the data had to be taken using the $10^{11}\Omega$ simple collector feedback resistor. Heating the sample filaments to higher temperatures in order to obtain ion currents large enough to permit precise $10^{10}\Omega$ data to be taken often resulted in ion currents which became less stable and which increased at too fast a rate. Most data was consequently taken with $^{40}Ca^{+}$ currents of $1\text{-}5 \times 10^{-11}$ A. In order to avoid linearity problems in the $10^{11}\Omega$ resistor, the $10^{10}\Omega$ feedback resistor was used when the current increased to levels above 5×10^{-11}A, although because of the low ^{44}Ca and ^{48}Ca levels measured with this resistor, the precision was then somewhat lower until $^{40}Ca^{+}$ currents of $\sim 1.5 \times 10^{-10}$ A were achieved. Each resistor always yielded results consistent with those obtained on the other. Composition data for unspiked aliquots of the samples were not gathered; the small sample

sizes precluded in most cases the possibility of obtaining 2-4 x 10^{-10} A $^{40}Ca^{+}$ currents over the three-hour period required to obtain ∿100 composition ratios. However, on several occasions attempts were made to measure ^{43}Ca during the mixture runs. This was done either by including an extra time delay in the form of a "waiting" channel prior to the ^{43}Ca measurement, which was made between the ^{42}Ca and ^{44}Ca measurements, or by cycling through ^{43}Ca, ^{44}Ca, and ^{48}Ca only at some separate point in the mixture run; the second method provided $^{43}Ca/^{44}Ca$ analytical precision of about 1‰, and was sufficient to prove that the isotope effects were truly from mass fractionation rather than single isotope enrichment or depletion.

With these much smaller samples analyzed on the mass spectrometer, it was necessary to again assess the degree of resolution for samples having small differences in $\delta(^{40}Ca/^{44}Ca)$. In Chapter 2, it was shown that fractionation differences could be resolved to a level of ∿1 part on 10^{4} per unit mass difference. Another set of measurements on the ^{44}Ca-enriched standards has been made using 150 ng aliquots; the results listed in Table 5-2 still indicate a resolution of about 1 x 10^{-4} amu^{-1}.

The effect of a small but measurable blank upon $\delta(^{40}Ca/^{44}Ca)$ measured for a sample will now be examined. The effect of a blank in biasing the measured δ values is described by the equation

$$f\ \delta_{blank} + (1-f)\ \delta_{actual} = \delta_{measured} \qquad (2)$$

where f is the fraction of Ca in the sample arising from the blank.

It may then be seen that the magnitude of the bias ($\delta_{measured}-\delta_{actual}$) is increased either when f is increased (blank is a larger fraction of the sample) or when $\delta_{measured}-\delta_{blank}$ is increased. Since it is probably true that $\delta_{blank} \approx 0$ for this work, then only for the two plagioclase samples (Table 5-3), which were very small, would the bias of the measured δ for the samples be appreciable, although it would still be less than 2.5‰ . Even in the unlikely event of a highly fractionated δ_{blank} of, perhaps, 14‰ (the value of the $CaCO_3$ standard considered in Chapter 3) the bias would be appreciable only for one plagioclase sample (1B-2, Table 5-3); in this case, the blank correction makes the δ value even more negative by a few per mil, but for all of the other samples the blank correction would be less than 1‰ and hence unimportant.

ANALYTICAL RESULTS

Sampling

Five calcium-bearing mineral samples were used for these sputtering experiments. Those samples which were used in more than one experiment were carefully reground with 600 grit silicon carbide paper, polished with 1 μm alumina powder, and recleaned in three separate reagent-grade methanol ultrasonic rinses prior to reuse. The sample denoted Fluorite-1 was cleaved from a single crystal of unknown geologic origin or location. It is light purple in color and contains no impurities above the 1% level, as determined by electron microprobe analysis. $\delta(^{40}Ca/^{44}Ca) = 0.3\pm0.4$‰ was measured for a bulk

unsputtered chip of the sample. The sputtered plane was a polished (111) plane. The sample denoted Fluorite-2 was cleaved from a single CaF_2 crystal whose analysis was reported in Chapter 3 as $\delta(^{40}Ca/^{44}Ca) = 0.2\pm0.2‰$. It was sampled from a mine in Westmoreland, N.H., and was of light green color. The sputtered plane was again a polished (111) plane. As it was desired to compare sputtering of single crystals and of randomly oriented polycrystalline samples, a polycrystalline fluorite sample from the Fred Staats Fluorite Mine, located northwest of Lund, Utah, was prepared. This sample in bulk contained large quantities of what appeared to be carbon interspersed between the fluorite grains, but a large section consisting predominantly of randomly oriented fluorite grains was identified and polished. The resulting surface was fairly friable and contained a number of large fissures which could not be removed through further polishing without chipping off other parts of the surface, thereby producing other cracks or pits. A large single crystal of plagioclase was cleaved along an (001) plane and then ground and polished. The crystal was determined by microprobe analysis to have a modal composition of $Ab_{50}An_{50}$ (Ab = albite, $NaAlSi_3O_8$, and An = anorthite, $CaAl_2Si_2O_8$). The fluorapatite ($Ca_5(PO_4)_3F$) was sampled from Durango, Mexico, and consisted of a single crystal fragment. The crystal plane exposed to the sputtering beam was not documented and identified prior to grinding and polishing, with the result being that it was only subsequently identified by optical interference patterns as being either a $(10\bar{1}1)$ or $(10\bar{1}2)$ plane.

Sample Designation Coding

The sputtered sample designations in the second column of Table 5-3 have been given in a form which permits straightforward identification while reading the text describing and discussing the results of the calcium sputtering experiments. The first numeral in the code is an experiment number which refers to the particular ultra-high vacuum chamber loading batch. Therefore, "4" refers to an experiment occurring chronologically later than "1." Bombardment experiments carried out using different targets and catcher tubes loaded in the same vacuum chamber batch are labelled "A," "B," and "C" as appropriate. The last numeral in the sample code designates the order of collection of the sputtered calcium. A "1" therefore refers to the first calcium sputtered off, a "2" refers to the next collection interval, and so on. When referring to an entire irradiation sequence, the last digit in the coding is not included. For example, "the 2A sequence" means the irradiation sequence consisting of samples 2A-1, 2A-2, 2A-3, and 2A-4 (see Table 5-3). The various sections of each separable catcher tube are referred to in the text both individually and as groups assembled to form complete catchers. In connection with Table 5-3, they are referred to collectively, e.g., 4A-1. In conjunction with Table 5-4, though, the sections are referred to individually by an appended "-N," "-I," or "-O," which respectively stands for the normal, intermediate, and oblique angles of collection of the sputtered calcium.

Sputtering Fractionation Results

In Tables 5-3 and 5-4 are tabulated the experimental parameters and fractionation measurements for the various experiments. In Table 5-3 there are several lines of data for most of the targets listed. Each successive line indicates the results of successive sputtering of the sample. For example, sample 2A-1 contained atoms sputtered from the fresh surface of Fluorite-1, Chip A. Catcher tubes were then switched to 2A-2 and then 2A-3 while the sputtering was continued. Lastly, the beam was changed from 130 keV $^{14}N^+$ to 100 keV $(^{14}N)_2^+$ and the sputtering was continued using 2A-4 as the catcher. Catcher tubes were therefore in place during the complete sputtering of each sample, so that essentially all of the sputtered Ca was collected.

The first four entries in Table 5-3 show the results of prolonged sputtering of single crystal and polycrystalline fluorite (CaF_2) with 130 keV $^{14}N^+$. In each case, the initial Ca sputtered from the targets was isotopically "light," with $\delta(^{40}Ca/^{44}Ca)$ ranging from 12.7‰ to 11.1‰ . The 2A-1 bombardment was somewhat more extensive, with an estimated 0.06 range (100 Å) being sputtered as opposed to the 0.04 range (70 Å) sputtered initially in the cases of 4A-1 and 3A-1. The 11.1‰ value for 2A-1, being slightly less positive than the 12.5‰ for the other two samples, therefore is consistent with a decline in δ as the initial sputtering dose is increased. This type of decreasing trend is observed for each of these samples. For the 2A single crystal bombardment sequence, $\delta(^{40}Ca/^{44}Ca)$ decreased with

continued sputtering from 11.1‰ to -3.8‰ , while for the polycrystalline sample, the same type of general decrease was observed for similar bombardment doses. The final values in these cases, while negative, were however closer to being unfractionated, being -0.9‰ in one case and -0.2‰ in the other. The decreasing-δ pattern was similar in the total range of effects observed regardless of current density, a range of 1.4 - 8.9 $\mu A/cm^2$ (0.2 - 1.2 W/cm^2 power densities) having been used. This suggests that the fractionation observed was probably not dominated by beam-induced target heating. The sputtering yield, S_{Ca}, is a dimensionless number defined as the average number of calcium atoms which are sputtered per incident nitrogen atom. For molecular N_2 beams, each ion is regarded as two nitrogen atoms for the calculation of S_{Ca}. The major source of error in S_{Ca} is the beam current integration, as the amounts of Ca in the samples are measured very precisely by isotope dilution during the mixture analyses on the mass spectrometer. As the current integration was probably fairly accurate in a relative sense, variations in S_{Ca} between catcher tubes which exceed about 10-20% are considered significant. For the Fluorite-1 sample, S_{Ca} decreased 30% from 0.106 to 0.071 during the 130 keV bombardment. However, the polycrystalline sample bombardments showed no such systematic trend and appeared to be anomalously high for 3A-3.

After two of the three long, 130 keV irradiations, the beam was changed to 100 keV $(^{14}N)_2^+$ (i.e., 50 keV per nitrogen atom). After extensive sputtering with a longer range beam, during which the

lighter isotopes were being preferentially removed from the target, a surficial layer of some unspecified thickness with $\delta < 0$ might be expected to remain in the target. Certainly, at depths much greater than the ion range, the target will have been undisturbed and will retain its original isotopic composition. Even after the sputtering has proceeded for long periods of time, the isotopically heavy material cannot have become mixed down into the target to depths significantly greater than the primary-beam range. (In a later section, estimates will be presented for the extent of diffusion of such surficial material.) This fractionated material will then dominate the Ca isotopic composition of the sample near its surface. To sample the isotopically fractionated calcium from this surficial region, it was first sputtered extensively with a higher energy-long range beam (130 keV N^+). Then, a lower energy beam (100 keV N_2^+) of substantially shorter range was used in attempting the sampling of the surface layer established at 130 keV. Although for either energy the Ca is sputtered from the first few monolayers of the substrate, the shorter range beam will cause mixing only within its range which, if smaller than the depth of the fractionated layer, will cause all of the atoms eventually sputtered to have originated within this layer. This is important because unfractionated material "gardened" from depth would otherwise be sputtered eventually. The calcium sputtered from this isotopically heavy layer may, of course, undergo additional fractionation because of its being sputtered from the target. However, a sizable fraction of the material from this layer was sputtered (see

Table 5-3), so it is unlikely that a substantial, additional net fractionation would result.

In one of the two cases in which the beam was changed to 100 keV $(^{14}N)_2^+$ after extensive sputtering at 130 keV, $\delta(^{40}Ca/^{44}Ca)$ = -8.3‰ was observed. For this sample, 2A-4, an estimated 0.34 range or 580 Å was sputtered off by the 130 keV beam prior to sputtering of an additional 0.97 range or 485 Å by the 100 keV N_2^+ beam. It should be noted that, because of an experimental error, catcher tube 2A-4 was slightly contaminated during a repetition of the 1C experiment listed elsewhere in Table 5-3. A material balance calculation was therefore carried out using the measured 2A-4 $\delta(^{40}Ca/^{44}Ca)$ = -8.1±0.2‰ and the range of likely values for the contamination of -10.6‰ (cf. 1C-2) to -3.6‰ (cf. 3B-2). This resulted in only a small range of possible δ values for 2A-4 of -8.3±0.7‰ , so the fractionation of this sample is considered to be well established. This result is in contrast to the 4A-4 value $\delta(^{40}Ca/^{44}Ca)$ = -0.3‰ seen from the sputtering of 830 Å of the polycrystalline fluorite with a 100 keV $(^{14}N)_2^+$ beam subsequent to the sputtering of 980 Å (0.58 range) with a 130 keV $^{14}N^+$ beam. Possible explanations for these differing results will be advanced in a later section which discusses the sputtering fractionation results. The results of the experiments just described are summarized in Figure 5-3, which plots $\delta(^{40}Ca/^{44}Ca)$ as a function of the cumulative number of ion ranges sputtered from the target.

It was desired to verify that the $\delta(^{40}Ca/^{44}Ca)$ variations were really caused by mass fractionation of all of the Ca isotopes. There-

fore, careful $^{43}Ca/^{44}Ca$ measurements were made during the mixture run of sample 4A-4-0, which had $\delta(^{40}Ca/^{44}Ca) = -13.0\pm0.4$, or 3.3‰ per mass unit. These yielded $\delta(^{43}Ca/^{44}Ca) = -2.8\pm0.8$, in agreement with the 3.3‰ figure. This is a demonstration that the isotope effects reported in Tables 5-3 and 5-4 are in fact caused by mass fractionation as opposed to single isotope enrichments or depletions of ^{40}Ca or ^{44}Ca.

Isotopic fractionation variations were measured during the polycrystalline fluorite sputtering just described as functions of the angle at which the sputtered Ca left the target. An exiting angle of zero degrees, also referred to as normal exit, refers to the direction 180° opposite to that of the incoming primary ion beam. Since the ion beam was always normally incident to the target surface, the maximum exit angle was therefore 90°, also denoted as oblique exit; this refers to material sputtered in a direction parallel to the target surface. Angular isotopic fractionation measurements were carried out for three of the four irradiation periods in the 4A sequence--the initial and final 130 keV N^+ irradiations and the 100 keV N_2^+ irradiation. The $\delta(^{40}Ca/^{44}Ca)$ results discussed above for these samples and included in Figure 5-3 were calculated by forming averages of the δ values measured for each of the three sections of a catcher tube; the δ values were weighted according to the fraction of the Ca collected on the whole tube which was contained on the individual section. The results of the angular isotopic fractionation measurements are included in Table 5-4 and plotted in Figures 5-4, 5-5, and

5-6 as functions of the range in angles spanned by each catcher tube section. The δ angular distribution during the initial 130 keV sputtering bombardment (Figure 5-4) shows that Ca sputtered in all directions is isotopically light. It ranges from $\delta(^{40}Ca/^{44}Ca) = 13.3‰$ for the material exiting at small angles nearly normal to the target surface to a value of 8.0‰ for oblique exit, and has a peak of 17.3‰ for intermediate angles. After prolonged sputtering (Figure 5-5), the difference between normal and oblique exit δ values increased to 16‰, the peak at intermediate angles vanished, and the whole isotopic pattern shifted to heavier (less positive) δ values. The oblique exit material had a negative $\delta(^{40}Ca/^{44}Ca)$ of -10.6‰ , while the normal exit and intermediate angle sections still had positive, though smaller, values of 5.5‰ and 1.9‰ . An almost identical pattern (Figure 5-6) was obtained from the subsequent 100 keV N_2^+ irradiation, except that each of the three points was about 2‰ less than the corresponding values plotted in Figure 5-5.

The amounts of Ca found on each catcher tube are measured by isotope dilution and listed in Table 5-3 and 5-4. These values are considered accurate to about 1% for most samples, the isotope dilution itself contributing a few tenths of a percent, and the efficiency of removal of the Ca from the catcher tubes contributing an uncertainty of about 1%, as discussed earlier. For the smallest samples, the two ∿100 ng plagioclase samples, a 20% blank uncertainty would cause the blank-corrected concentration to be uncertain to 3%.

The amounts of Ca on each of the separate catcher tubes is

shown in Table 5-4 and plotted versus angle in Figure 5-7 in terms of the fractional amounts of the Ca on each catcher tube segment. The two angular distributions for the 130 keV sputtered Ca were similar, the 5-25° segments containing 44-50% of the Ca, the 25-41° segments containing 20%, and the 41-72° segments containing 31-35%. By contrast, the 100 keV sputtering produced a distribution much more sharply peaked toward the normal exit direction, with this section containing 69% of the sputtered Ca. The 24°-38° and 38°-66° segments contained 11% and 20% of the Ca, respectively.

A single, short, sputtering irradiation of the apatite crystal with a 130 keV $^{14}N^{+}$ beam yielded a result qualitatively similar to that observed and described above for fluorite. The sputtering proceeded to a depth of ~40 Å and yielded $\delta(^{40}Ca/^{44}Ca) = 11.5‰$. This initial isotopic fractionation is quite large, and may be compared with the initial large positive fractionation observed for the fluorite samples sputtered under similar conditions. In those cases, δ was 12.5‰ and 11.1‰ when 75 Å and 104 Å was sputtered. This suggests that the fractionation for fluorite may be somewhat greater than for apatite for a given depth of material sputtered away.

Large, positive initial fractionation of the sputtered Ca was observed not only when using 130 keV nitrogen beams, but for lower energy beams as well. Sputtering a plagioclase crystal to a depth of 140 Å with a 100 keV $(^{14}N)_2^{+}$ beam removed 118 ng of isotopically "light" Ca with $\delta(^{40}Ca/^{44}Ca) = 21.2‰$. Interestingly

though, this large initial fractionation behavior was not observed in experiments in which fluorite was sputtered with the same doses of 100 keV N_2. During two separate irradiation sequences, sputtering a fluorite crystal initially removed 460 Å and 225 Å of material (1.8 μg and 1.0 μg Ca) with $\delta(^{40}Ca/^{44}Ca) = -0.4$ and +0.3‰.

In the earliest sputtering experiment, the chief aims were to check out the apparatus and measure sputtering yields of calcium for a variety of minerals for the two beam energies which would be used subsequently. It was not felt to be necessary to follow the high-then-low-energy scheme described above because high energy irradiations which were long enough to sputter off a substantial fraction of a range could not be carried out precisely until the sputtering yields were known. The opportunity to study patterns of fractionation resulting from the lower-then-higher beam-irradiation sequence was therefore used, and the results were sufficiently interesting to merit continued study. Following the initial 100 keV $(^{14}N)_2^+$ sputtering of plagioclase and fluorite samples which were described in the above paragraph, each sample was sputtered with 130 keV $^{14}N^+$. The plagioclase then yielded $\delta(^{40}Ca/^{44}Ca) = -3.9$‰, a decrease of 25‰ from the initial value even though only 80 Å more of the target was removed by the sputtering. For the Fluorite-1 sample, different $\delta(^{40}Ca/^{44}Ca)$ values were obtained. In one case, $\delta = -10.6$‰ was observed after 460 Å and then 116 Å had been sputtered off in the low- and then higher-energy bombardment. In the other case, $\delta = -3.6$‰ was seen after 225 Å and then 94 Å had

been sputtered by the two irradiations. Although in the first case the 100 keV N_2^+ current density was a factor of 10 higher than in the second, the beam current densities in both cases were probably low enough to have prevented any serious heating of the target. The same irradiation sequence carried out with identical beam doses for the same crystal plane of another fluorite sample gave $\delta(^{40}Ca/^{44}Ca)$ = -2.2‰ after 165 Å and then 61 Å had been sputtered using fairly low beam current densities. Within errors there is no difference in the δ values for unsputtered, bulk specimens of these two fluorite crystals, so the -3.6‰ , -2.2‰ difference cannot be accounted for by a difference in the original bulk values. However, the estimated angular collection range for 4B-2 is 9° less at oblique angles than for 3B-2. Since it has already been shown that calcium sputtered from targets at oblique angles (albeit in a different beam-energy sequence) is isotopically heavier than that sputtered at smaller angles, the loss of 9° worth of material could conceivably account for 4B-2 being 1.4‰ lighter than 3B-2. However, the extra 10° of collection range for 1C-2 over 3B-2 probably could not have been responsible for the 7‰ difference in the isotopic fractionation for these two catcher tubes. This will be further discussed in a subsequent section.

DISCUSSION

Sputtering Theories and Isotope Fractionation

The sputtering theory advanced by Sigmund (1969) has been highly successful in describing rates of sputter-removal for a wide

range of target-ion pairs and of ion energies (see eq. 4, which is given in a later section of this chapter). In this theory, sputtering rates of random, single-component targets are described in terms of the beam-deposited energy density of the target at its surface. This energy density is a function of depth in the target, of time, of the initial ion energy, of the energy of the atoms in the target, and of the ion-target interaction cross section. The transport throughout the target of the deposited energy, which is gained from the incoming ion every time it collides with a target atom, takes place through the movements and further scatterings of those target atoms which have received, directly or indirectly, a fraction of the energy of the ion. It is assumed by this model that this "collision cascade" of target atoms behaves in a linear fashion. This means that there is essentially zero relaxation time, so that it does not matter what time interval separates the initial collisions of two ions incident at the same place on the target, or even if the two ions are bound as a molecule. The Boltzmann energy transport equation is thus linearized. It was solved by Sigmund using as the interaction differential cross section the same Thomas-Fermi model nuclear stopping power approximation used in the LSS ion range model (Lindhard et al., 1963). It has been pointed out by H. Andersen and Bay (1975) that the major shortcomings of the Sigmund theory in describing sputtering rates from single-component random targets, shortcomings which have only been important in some cases, are (a) the omission of the electronic contribution to the total stopping

power, (b) the absence of surface corrections in the theory, which treats semi-infinite media as though infinite, and (c) the use of linearized equations to describe experiments which are apparently not always linear in nature. Electronic stopping has been included by Winterbon (1972). For sputtering cases where the target-ion mass ratio A_2/A_1 is significantly greater than ~ 3, the absence of surface correction terms seems to be the cause of the model calculations exceeding the experimentally measured sputtering rates (Andersen and Bay, 1975); initial theoretical efforts in the area of surface corrections have been made by Bøttiger et al. (1971, 1973). The nonlinear nature of sputtering has been most evident in experiments which show a sharper-peaked energy dependence of the yield (e.g., Andersen and Bay, 1973; Sigmund, 1969) than predicted by the Sigmund model and in experiments in which molecular heavy-ion beams cause greater sputtering rates than observed in experiments identical in atomic dosage and in energy per ion (Andersen and Bay, 1975; see also Mitchell et al., 1975). These latter experiments observed nonlinearities for molecular beams of ions with masses greater than 70 amu, but not for lighter ions such as H and (perhaps) Cl.

Wehner (1955) was the first to point out the anisotropies in the angular distribution of material sputtered from crystals of metals such as Ag, Cu, and W. The patches or "Wehner spots" where the sputtered material is concentrated are characteristic of the particular plane bombarded (Wehner, 1955) and have been ascribed to lattice collisions which concentrate or focus some

fraction of the available kinetic energy into collisions along a lattice direction (Silsbee, 1957). When polycrystalline or amorphous targets are sputtered, the Wehner spots are smoothed into a continuous distribution; this may also occur when a crystalline target is sputtered for such a long time that the surface is made amorphous (Oechsner, 1975). In experiments where radioactive ^{198}Au was used to dope polycrystalline gold samples which were then sputtered with 5-8 keV Ar^+ or Kr^+, Patterson and Tomlin (1962) observed "over-cosine" angular distributions for the sputtered material. The term over-cosine refers to a distribution more peaked in the target normal direction than is a cosine distribution; if θ is not too oblique, say $\theta < 60°$, the distribution often may be approximated by $\cos^{\nu} \theta$, where $\nu > 1$. Patterson and Tomlin showed that the deviations from a cos θ distribution increased with bombarding energy and were less pronounced for Kr ($A_2/A_1 = 2.4$) than for Ar ($A_2/A_1 = 5.0$). As their targets were not flat on an atomic scale, they pointed out that the deviations from a cos θ distribution would be even larger for perfectly flat surfaces.

The reasonable success of the Sigmund sputtering theory and subsequent modifications does not extend to the detailed behavior of cases of multi-component materials. The model is simply not set up to handle such cases, which include even single element targets where the element is not monoisotopic. To do so would require keeping track of the energy densities of the various components (which of course means that the resultant transport equations will be

coupled) and of the compositional changes which will occur within the target as a function of depth if one component is sputtered more rapidly than another. The overcoming of these complications within the framework of a rigorous theory is a difficult problem the solution to which is only in a preliminary stage. N. Andersen and Sigmund (1974) have investigated the sharing of energy in multi-component targets, but their model (a) has not yet related the computed relative energy densities to rates of sputtering of the components, and (b) is unable to compute the changes in the energy sharing as the composition of the medium changes near the sputtered surface while remaining unchanged at depth. Nevertheless, it is illustrative to use their model to estimate energy sharing ratios within a target consisting of ^{40}Ca and ^{44}Ca in the ratio of 47.153:1. Define G_{40} and G_{44} as the numbers of ^{40}Ca and ^{44}Ca atoms moving per unit energy per unit depth in the target with speeds v_{40} and v_{44}. Also, define α_{40} and α_{44} as the fractional amounts of ^{40}Ca and ^{44}Ca present. Using as the power law cross section parameter a value $m = 1/2$, their equation 25b yields:

$$\frac{v_{40}\, G_{40}}{v_{44}\, G_{44}} \sim \frac{\alpha_{40}}{\alpha_{44}} \left(\frac{44}{40}\right)^{2m} = 47.153 \times 1.1 \qquad (3)$$

Therefore the number of ^{40}Ca atoms moving (with greater than thermal energies) within the target relative to the number of ^{44}Ca atoms moving exceeds the stoichiometric ratio of 47.153 by 100‰ . The products Gv have the dimensions of flux but cannot be integrated over energy and time to give sputtering yields as in Sigmund's (1969)

eq. 3; the depth and time variations of G were not included in this model.

These preliminary findings do indicate that one would expect the first calcium sputtered from a target to be isotopically "light," relatively enriched in the lighter isotopes, but the magnitude of the effect cannot as yet be predicted by this model. Using a simpler, diffusion picture of sputtering, Haff et al. (1977a) arrive at the result that the relative probabilities for sputtering isotopes are given in terms of the fourth root of the mass ratio. For calcium, the maximum ^{40}Ca-^{44}Ca fractionation of the sputtered material would then be $(44/40)^{1/4} - 1$ or 24‰ . However, more elaborate calculations by C. Watson (personal communication) have failed to indicate any substantial fractionation effects for fluorite or plagioclase. In these calculations, the fractionation was predicted to be $\delta \sim 0.2$‰ . The energy of the calcium isotopes near the sputtered surface was computed assuming the solid target to actually be an ideal gas. It was further assumed that calcium has only two isotopes and that ^{44}Ca cannot scatter off of itself, but only off of the more abundant ^{40}Ca or the non-Ca constituents, which are represented as a single component of some average weight. A surface binding energy for calcium to leave this "gas" was included.

As discussed in Appendix B, various complications make it difficult to rigorously attack the problem of isotopic differences in the surface binding energies of calcium atoms in a lattice. Any differences could directly cause isotopic fractionation during

sputtering, as inspection of eq. (4) below will reveal. However, estimates given in Appendix B indicate that any isotopic differences are far too small to cause substantial differences in the sputtering rates of the various Ca isotopes. It therefore appears that the isotope fractionation arises not because of binding energy differences, but through unequal sharing of the primary ion energy between the isotopes while still within the substrate.

No theoretical treatment has yet attempted to include a description of isotopic fractionation from perfectly flat planes as a function of ejection angle.

Observed Surface Roughness and Blistering of Sputtered Ca Targets

Having discussed the present state of theories which attempt to describe various phenomena associated with the sputtering of perfectly flat surfaces of crystalline or polycrystalline materials, it is now necessary to consider what complications might arise which may interfere with (a) the interpretation of the experimental results, or (b) theoretical modelling of the isotope fractionation process. Complications may arise from uneven sputtering which makes targets rough on a micron scale, from localized heating of the target surface caused by the stopping of the ion beam, and from "micro-gardening" of the irradiated surface by processes not directly connected with the collision cascades generated by the ion impacts. The latter two concerns can cause difficulties in assessing whether observed isotopic fractionation (a) is caused by the sputtering itself or in part by vaporization of heated target material (note the large vacuum

evaporation fractionations shown in Table A-2), (b) is diluted by the presence on the catcher surfaces of unfractionated chunks of material which were expelled from the target as radiation damage blisters formed and ruptured. This is more fully discussed below after it is demonstrated that many blisters indeed formed on the bombarded surfaces in the present experiments. The development of rough surfaces with or without the presence of blisters causes the measured fractionation to be averaged over that which would be obtained by sputtering to different uniform depths. Compared to the other two possible sources of difficulty listed above, though, this appears to be of minor importance. It was early recognized in this work that the targets should be examined after sputtering for signs of localized heating or blister development with chunk emission. All of the sputtered targets were examined under an optical microscope. Three of the sputtered targets were subsequently examined with a scanning electron microscope (SEM). Some of the resulting photographs are included herein and will be discussed in detail below. The main observations are: (1) extensive blistering occurred during bombardment of fluorite targets, and apparently began to develop after only small degrees of exposure to the beam; (2) such blistering though may not have been a major contributor to the surface roughness which developed during the sputtering of plagioclase; (3) some evidence that blistering fragments may have been dissociated from their original locations is present, although in most cases, the observed fragments appear to have remained fixed; (4) there is no

convincing evidence that blister chunks were a major component on the catcher tubes except possibly in two cases; (5) there is no evidence that localized heating dominated the sputtering, although its presence to a lesser degree cannot be completely ruled out. The phenomenon of blister development during ion bombardment is not yet well understood, but appears to be aided when the implanted species is a gas (cf. Erents and McCracken, 1973), especially if it is not "soluble" in the lattice, but tends to migrate to lattice vacancies (cf. Behrisch, 1972) where micro-bubbles or pockets of gas can form.

The three samples examined with the SEM were the Fluorite-1, polycrystalline fluorite, and plagioclase targets. Figures 5-8 through 5-14 and 5-16 through 5-19 were taken after the 3B, 4A, and 1B sputtering sequences, respectively. Figure 5-15 shows two optical micrographs of the Fluorite-1 sample taken prior to the carbon-coating of it for SEM work. The information contained in the field at the bottom of each SEM photograph shows the electron accelerating voltage, the magnification power, the length in microns of the solid white bar, the photograph number, and (for Figures 5-8 through 5-11 and 5-13 only) the length of the hatched bar which appears within the field of view itself.

Figures 5-8(a) and (b) show two regions of the polycrystalline fluorite which received minimal, if any, exposure to the ion beam. Figure 5-8(c) shows a similar region for the plagioclase sample. The regions in 5-8(a) and (c) were near the edges of the crystals whereas the region in 5-8(b) was somewhat closer to the bombarded region and

hence may have received minor beam exposure. Figure 5-8(a) shows that the initial target surface was in many places polished quite smoothly on a 1 μm scale, although because of the polycrystalline nature many deep pits could not be polished out without developing others in different locations. Figure 5-8(c), which is at higher magnification, shows the higher polish in some areas of the plagioclase. Figure 5-8(b) shows that in other locations of the fluorite many shallow 3-5 μm diameter "pock marks" were present in the initial surface. Closer examination of Figure 5-8(b) reveals another interesting feature, though. The initial development of subsurface, several-micron diameter blisters may be seen. This area could only have received a tiny fraction of the 5.8×10^{17} nitrogen atoms which bombarded target, most of them striking the target within the estimated 0.44 cm^2 central beam area. It can therefore be seen that blisters begin to develop at these energies even after only low bombardment doses. It will be shown below that these small features do not readily develop in regions shielded from the beam. Therefore, these developing blisters were probably not caused by the large bombardment dose in the middle of the target. Figure 5-9(a) shows that, closer to the center of the beam, the target has received a higher dose per unit area, with the result that a number of the blisters have come to the surface and ruptured. Figure 5-9(b) shows the same type of rupturing blisters for the plagioclase sample, although they are smaller in this case. Within the main sputtered area, the blisters have developed and ruptured in the polycrystalline

fluorite over nearly the entire surface, as can be seen in Figure 5-10. Figure 5-10(a) shows that the rupturing of the blisters leaves behind shallow craters 2-3 μm in diameter. From Figure 5-10(b) the depth of one of these craters appears to be ∿0.8 μm. A number of the craters in Figure 5-10(a) even appear to have ruptured twice, two examples being those immediately above the letters "F" and "O" in the lower center of the photograph. The closeup of one of the craters in the center of this photograph is shown in Figure 5-10(b). It is clear in this closeup that not only have 2-3 μm blisters developed in this region but that much smaller bumps on the order of 0.2 μm have developed as well. In Table 5-3 it may be seen that the average depth to which the sputtering removed material from the target was 980 Å for the 130 keV bombardment and 830 Å for the subsequent 100 keV N_2 bombardment. The total of 1810 Å or ∿0.2 μm is therefore comparable to the dimensions of these smaller features. Close inspection of Figure 5-10(b) shows that these smaller features are probably not blisters, but are actually high areas which the beam had not yet sputtered off. Also, none of these smaller features appear to have ruptured, which would have been expected had they been blisters.

Although the 2-3 μm blister craters appear throughout the heavily irradiated region of the polycrystalline fluorite surface, it is interesting that they appear to be absent in the heavily irradiated region of the plagioclase (Figure 5-10c). However, a rough surface did evolve with features whose dimensions are comparable

to the plagioclase blisters shown in Figure 5-9(b). If blisters which do develop in plagioclase (Figure 5-9b) are smaller, they could perhaps be annealed out more easily by the beam, causing them not to be observed in heavily damaged regions such as shown in Figure 5-10(c).

From Figure 5-11 it appears that the fluorite blistering craters occur in regions where the beam is directly incident, but not in locations which are very near to the beam but shielded from it. In Figure 5-11(a) is seen dense cratering around the edge of a deep 60 μm diameter pit in the sample. Reasonably enough, though, the cratering appears to be much less dense inside the pit which was at some locations partially shielded from the beam. Figure 5-11(b) shows a closeup of the bottom surface of the pit near the wall which forms the upper rim of Figure 5-11(a), an area which appears to have been partially shielded from the beam. (For the SEM photographs, the sample was tilted at 40° with respect to the electron beam, thereby permitting this particular view.) It may be seen that fewer craters per unit area are present. Although somewhat difficult to see, a number of craters are present in Figure 5-11(a) on the floor of this pit near the lower right corner. Their density appears to be higher than that observed in Figure 5-11(b), which is probably because of the more direct exposure of this area to the ion beam.

It is important to consider what happens to the target material at a location where a blister develops and ruptures. At such a location, the material either might fall back in upon itself or

there might actually be an "eruption," causing the transport of this material to other locations on the target or onto the catcher surface itself. In what follows, the latter possibility will be referred to as blister eruption or eruptive transport. Eruptive transport clearly has important implications for any sputtering experiment in which it is present to a significant extent. The possibility of its presence might well call for SEM work to be done for any experiment where such eruptive transport could alter the interpretation of the results. For the calcium isotope fractionation experiments described in this chapter, eruptive transport could affect the results in several ways. First of all, it provides a "gardening" process distinct from ion-beam-induced mixing. Erupted chunks are likely to have maximal dimensions comparable to the crater diameter or depth, in this case $\sim$1-3 μm. Eruption of material then leaves behind fresh, unsputtered surfaces which may be distinct from the isotopically heavy surficial layers which had been developing at that location up to that point. (The development of such isotopically heavy layers will be discussed in a later section.) Material subsequently sputtered from this fresh surface would then be isotopically lighter than that being sputtered simultaneously from other, non-cratered locations on the target surface. This would affect the δ value measured for the material sputtered from the surface, tending to keep it positive for longer periods of time than would be observed were eruptive cratering not to dominate. Second, if chunks erupted from craters were to be deposited upon the catcher

surface, the measured δ values would probably be smaller in absolute value. Such chunks would then dilute the apparent fractionation measured for the caught material. If the chunks were on average isotopically heavy, which seems unlikely, they would tend to bring the measured sputtering fractionation closer to this negative chunk value. Third, eruptive chunks which are deposited upon the catcher tubes would contribute toward higher sputtering yield values S_{Ca} (cf. Table 5-3) than would otherwise be the case. (For experiments which measure sputtered particle energy distributions, this could cause distortions in the low and high energy portions of the spectrum, since chunks likely erupt violently with reasonably high energies while those chunks which are initially deposited on the target surface and subsequently removed likely have low energies. In fact, it is not unreasonable to suppose that Gregg's disproportionately large numbers of $100\text{-}300 \times 10^6$ atom "sputtered" uranium chunks may have arisen from blister eruptions (Gregg, 1977). In summary then, if eruptive cratering were to dominate the target's irradiated surface area, quantitative comparisons between experimental results and sputtering models would become complicated for material sputtered after the onset of such cratering.

It would appear to be unlikely that very many erupted chunks would land elsewhere on the target instead of leaving the surface altogether. If one were to suppose that there is some electrostatic attraction of the erupted chunks back towards the surface, it would not be easy to see how the necessary charge exchange would be

accomplished; a chunk would probably be positively charged when it is first erupted, just like the surface. Examination of the SEM photographs does reveal a few instances where objects are observed which apparently are erupted blister fragments. In Figure 5-11(b) may be seen, especially near the wall of the pit which is at the top of the photograph, a number of chunks 0.2-1.5 μm in diameter. These objects appear white in the photograph. In Figure 5-11(a) the floor of this pit may be seen to contain a large number of such chunks, whereas they appear in this photograph to be absent for the most part from the surface surrounding the pit. Since they are smaller in size than the 2-3 μm craters, and appear to be concentrated in the pit where erupting material would have to clear the steep walls in order to escape, these objects seem to be prime candidates for chunks erupted from craters on the floor of this pit. However, although it appears unlikely, it cannot be ruled out that these chunks are fragments from the polishing of the surface which were not removed during the multiple ultrasonic rinses which were subsequently used to clean the surfaces. At least one instance was present where similar-looking objects were observed in a location where they had not been trapped. Figure 5-13 is an SEM photograph of a small section of the sputtered area of the plagioclase crystal. The smaller objects are 0.5-1 μm in size and may be blister fragments, perhaps rounded by thermal annealing (see below). These objects were not observed in most locations on the plagioclase surface; this is consistent with the observed low abundance of erupted blisters in this sample unless

one supposes, as pointed out above, that small blisters could have formed and been annealed or sputtered away.

It is important to note that in many instances, blister fragments were not erupted at all, but were merely partially detached from the surface. Examples of this are seen in Figure 5-12(b). They appear in this view as irregular-shaped gray or white objects 2-4 μm in diameter, and are in many cases clearly attached to the surface. Appreciable fractions of the polycrystalline fluorite surface contained such fragments, as may be seen in the lower-magnification view of Figure 5-12(a). In Figure 5-12(a), the white areas are somewhat overexposed, causing them to appear as larger white patches.

For the Fluorite-1 single crystal, thousands of more angular, oblong-shaped objects were found around and inside of the heavily-damaged region (Figures 5-14(a) and (b)). These objects ranged from 1-15 μm in length, were found on a surface highly populated with unbroken blisters (Figure 5-14(b) background), and appeared in a number of "colonies" such as is seen in Figure 5-14(a). Each colony has the appearance one would expect had it at one time been a single drop which later dried--the chunks nearest the edge are smallest in size. Despite this, Figure 5-14(c) clearly shows that at least the smaller objects in these colonies are attached to the surface, thereby suggesting that the fragments did not originate elsewhere, but are instead blister fragments still attached to their original sites. It is interesting that these chunks may have a chemical composition which is distinct from the bulk. They have small but

measurable amounts of chlorine which is not found on the main fluorite surface. The chlorine probably originated from contamination with HCl fumes in a room used to temporarily store the samples after sputtering. Chlorine is also observed in the chunks on the plagioclase sample (Figure 5-13) which was also kept in this room, but is absent in fragments (Figures 5-11 and 5-12) of the polycrystalline fluorite, which was not stored there. If the calcium in these objects had been altered during sputtering from the chemical form of the bulk (CaF_2 or $CaAl_2Si_2O_8$), it is possible that they may have been more reactive to small quantities of acid fumes. It is unknown whether any small HCl drops condensed and later dried on the surface of the Fluorite-1 sample, giving the appearance seen in Figure 5-14(a). However, the underlying surface appears no more attacked inside the colony shown in this photograph than outside of its border. It therefore seems rather unlikely that any macroscopic drops could have condensed onto the sample, which had been kept inside a plastic box inside of a drawer.

It has now been shown that under the present experimental conditions, blisters do develop and rupture. There does not appear in most cases to be strong photographic evidence of transport of blistered material long distances on the target surfaces, which might have been seen had material been spewed out during crater rupturings. It is now reasonable to try to understand something about the formation of blisters, in what ways they might erupt, and how hot an irradiated surface might become. The coalescing of ion-implanted gas

atoms into subsurface bubbles depends (a) upon whether or not the atoms are "soluble" in the host lattice so that they can be distributed to a large number of lattice sites, (b) upon whether the implanted atoms tend to stay fixed only at lattice vacancies, and (c) the implant energy, dose per unit area, and target temperature (cf. Behrisch, 1972). If the implanted atoms tend to migrate to vacancies or other lattice defects (some of which can be made during the actual bombardment) then small bubbles will form. However, it is not clear that these small bubbles which are tens of angstroms in diameter (J.P. Bibring, personal communication) need to migrate through the lattice in order to coalesce with others into larger bubbles. It may be that at least in some cases, they remain fixed, forming larger pockets of gas only when the density of bubbles becomes so large that they overlap (Erents and McCracken, 1973). The bubbles can have high internal gas pressures which, when they are at the surface, can cause them to burst, erupting fragments from the surface (Townsend et al., 1976, p. 85). Behrisch (1972) lists a number of references to blister formation when > 100 keV He^+ ions are implanted into Al and various metals at doses exceeding 10^{18} ions/cm^2. Erents and McCracken (1973) observed that blisters were found on polished polycrystalline Mo when irradiated with He^+ ions of lower energies in the range 7-80 keV. In this experiment, a focussed beam was electrostatically scanned on the target in order to allow uniform irradiation. Any gas released was analyzed using a quadrupole mass spectrometer. These workers found that the blisters

broke and released large quantities of the implanted He at reproducible implant doses which varied as a function of ion energy, target temperature, and micro-crystal orientation (which could sometimes be determined). This rupturing dose increased with increasing ion energy, ranging from 10^{17} cm^{-2} for 7 keV He^+ to 5×10^{17} cm^{-2} for 36 keV He^+. It may be that this dependence was caused by the larger depths over which the implanted He was distributed at higher energies. For much of their work, these workers kept the targets near room temperature.

It is interesting to roughly calculate the levels to which pressure from implanted gas molecules can build up within a bombarded target. Assume that the perfect gas law can be used for a first approximation. Then if 10^{17} ions are implanted in a 1 cm^2 area uniformly (because of straggling) up to a depth of 500 Å, the pressure is a very large value, 842 atmospheres for a target at room temperature. This figure is large compared to the yield strength of calcium metal, which is about 375 atm (Samsonov, 1968) although small compared to that for some other metals such as Mo (590-4400 atm) or various steels (2000-15,000 atm; Frocht, 1951). The yield strength is the stress that must be applied to a material before it begins to acquire a permanent set (Frocht, 1951) and is, roughly, the point at which plastic deformation begins. Because of the high pressures that can be built up within a bombarded target, general swelling can sometimes be observed even if blisters have not developed (M. Maurette, seminar). The observations of Erents and

McCracken (1973) indicated that the blisters which formed often fractured at their peripheries. The SEM photographs for calcium targets, however, do not always show a similar behavior, the initial fracturing sometimes taking place in the middle (Figure 5-9), the area which one would expect to perhaps be the weakest. The fragments seen in Figures 5-12(b) and 5-14(c) may have been caused by peripheral rupturing, though.

Looked at another way, a bombardment of 10^{17} cm^{-2} would implant one gas atom or molecule for every 2.4 CaF_2 molecules originally occupying the target to a depth of 500 Å. With such extensive bombardments, it may be that the sputtering isotope fractionation mechanism is influenced in some fashion by the effective change in the bombarded surface composition. The volume binding energies might be altered, affecting the rates at which the surface, down to a depth of about one range, can be stirred or micro-gardened by collision cascades or low-grade target heating. It should be mentioned that the diffusion constant of N in CaF_2 is probably so low at a bombarded target temperature of 200°C (see the below discussion of this temperature estimate) that very little implanted nitrogen will diffuse back towards the surface and be desorbed before blistering occurs. (A value for the N diffusion constant is not at hand. However, it may be similar in magnitude to that for ^{18}F in CaF_2, which is about 3.5×10^{-14} cm^{-2} sec^{-1} at 200°C [AIP Handbook, 1972]. An even smaller value might be appropriate if nitrogen can be trapped at radiation damaged sites [cf. Erents and McCracken, 1969].)

Under the sputtering irradiation conditions used for the present Ca isotope fractionation measurement, the targets were not severely heated in bulk by the energy loss of the beam. This can be seen in several ways. Wada et al. (1975) reported measurements of bulk temperatures during nitrogen implantation of silica glass disks 400 μm thick and 40 mm in diameter. From Table 5-3, it may be seen that the smallest and largest beam current densities for 100 keV $(N_2)^+$ were 2.2 μA/cm^2 (3B-1) and 18.3 μA/cm^2 (1C-1). With these current densities for 100 keV N_2, Wada et al. measured temperatures of the silica wafers to be 120°C and ∿400 °C, the latter value having been extrapolated here from their measurement at 11 μA/cm^2. From Table 5-3, the smallest and largest current densities for the 130 keV N^+ beams were 1.4 μA/cm^2 (3A-1) and 8.9 μA/cm^2 (2A-3), conditions under which Wada et al. measured substrate temperatures of 100°C and ∿330°C for their wafers. The samples used for the Ca measurements were all considerably thicker (0.2-1 cm) but of smaller diameter (∿1 cm) so that sample volumes were 0.2-3 cm^3 as compared to 5 cm^3 for the Si wafers. This heat-dissipating volume is probably not too important in determining the bulk temperature, though, as is seen below. The temperatures in the Table 5-3 samples may have been somewhat greater than the above estimates, but at any rate it is clear that the samples were not heated in bulk to temperatures above ∿500°C at most. However, measurements of temperature rises during the sputtering experiments of Liau et al. (1977) indicate that the maximum target temperatures achieved here may indeed have been far

less than 500°C. These measurements gave temperature rises $\leqslant$ 200°C for 20-80 keV noble gas beams with average current densities of 50 $\mu A/cm^2$. The substantially higher temperatures measured by Wada et al. (1975) under apparently similar conditions may indicate an error by Liau et al. or Wada et al. Lastly, the thermal conductivity of CaF_2 (AIP Handbook, 1972) is high enough compared to the heat capacity (see CRC Handbook, 1972, for Ca metal) that an appreciable thermal gradient near the bombarded surface will not be established. Instead, the bulk sample will be heated. Wada et al. (1975) concluded that their targets were mainly cooled by radiation rather than conduction. If this was the case here, then using the Stefan-Boltzmann law to estimate the bulk temperature gives 275°C for an input power of 0.5 watt (for the maximum beam current sample, 2A-4) using a rear radiating surface area of 1 cm^2. If conduction were important, the temperature would be even lower. The above 500°C figure should therefore at present be considered an upper limit, with the actual temperatures likely being much lower.

One of the SEM photographs appears to show evidence of very localized heating of the samples. Although the erupting blisters in Figure 5-9 and the debris in Figures 5-11(b) and 5-12 have rough edges, indicating that the blistering occurred at temperatures well below the melting point, there is one case where this is not so. Figure 5-13 shows many small fragments on the plagioclase surface which appear to be definitely rounded, as if they were partially molten when ejected. For this sample, a 100 keV N_2 beam current

density of 11 $\mu A/cm^2$ was used, which would give a bulk temperature of only 320°C using the data of Wada et al. (1975); the very low Ca "sputtering" yield measured for this 1B sample also argues against the presence of localized heating to the point of melting and then evaporating much calcium. At any rate, it has already been pointed out that the rounded objects shown in Figure 5-13 were rare for this plagioclase sample, so any localized heating caused by a temporary concentration of the ion beam into one spot was not extensive.

Despite these conclusions, though, a number of the photographs for the Fluorite-1 single crystal contain features which one might interpret as being caused by extreme heating by the nitrogen ion beams. This would require temporary concentration of the beam into small, localized areas, since bulk temperatures of only 120°C and 220°C are estimated using the data of Wada et al. (1975). These features will first be reviewed and then shown to have alternative interpretations. The optical micrographs in Figure 5-15 look convincingly like the products of molten calcium being removed from one position on the surface and "splatted" down in another. These areas were observed near the beam periphery, and were so thin that optical interference patterns were observed. By counting the number of interference rings, the maximum thicknesses of the two splats in Figures 5-15(a) and (b) may be inferred to be $\sim$4 wavelengths or, assuming a light wavelength of 5000 Å, $\sim$2 μm. A search for such features using the SEM proved surprisingly negative. It should be noted that the $\sim$0.5 μm range of 20 keV electrons in the SEM may have

rendered the very thin blisters unobservable. A number of 50-100 μm diameter irregular blisters were observed in this area, however (Figures 5-16(a) and (b)). In Figure 5-17, which shows a small portion of the heavily irradiated area, is seen a large, shallow pit which might at first appear to have been the site for such an "excavation." However, more careful examination of the rims of such "pits," another example of which is seen top center of Figure 5-14(a), showed them to be structureless discolorations. An optical micrograph which was taken of the area in Figure 5-14(a) soon after sputtering indeed showed this semicircular discoloration to be absent. Such features are then taken to be artifacts which developed prior to the subsequent SEM examination. Some of the elongated objects seen in Figures 5-14 and 5-17 appear to border on such discolored rims. Since calcium fluoride is rather hygroscopic, it may be that these structureless areas are caused by contamination of the sample surface with isolated tiny drops of water which dissolved any of the thin elongated objects they encountered.

Careful examination of Table 5-3 reveals a number of inconsistencies between the data and any extensive localized heating. It is first hard to understand how very much surface material could have become molten if the bulk crystal did not exceed 250°C. Second, the "sputtering" yield S_{Ca} would have been dominated by evaporating material, in which case much higher values should have been seen for the 1C irradiation sequence which had higher current densities than the 3B sequence but otherwise was similar. In fact, somewhat lower

S_{Ca} values were observed. Third, calcium evaporated from molten areas onto the catcher tubes would first be isotopically light ($\delta > 0$) and then heavy. One would then be forced to explain how the two polycrystalline fluorite irradiation sequences (3A and 4A) could exhibit such similar sputtering yields and fractionation patterns although the high current density sequence would presumably have led to much more material being evaporated onto the catcher tubes.

It will now be shown that although the precise origin of the features seen in Figures 5-14 through 5-17 remains unclear, it is not necessary to interpret them as arising from localized beam heating. The "splashes" and "molten areas" may actually be large blisters in various stages of development. Although the Figure 5-15 objects were not observed when the SEM was used, a number of large blisters were observed (Figure 5-16) well away from the area where the nitrogen beams had been concentrated. The shapes of these blisters did not appear to change, even when a high current density beam from the SEM was left on them for considerable periods of time. However, a number of other areas were observed which were extremely unstable under 10 keV electron beam bombardment. Typically they were 10-50 μm diameter circular or elliptical areas. When the electron beam was concentrated on them, they rapidly expanded in diameter. Figure 5-18(a) shows such an area during an early stage of its expansion, the starting diameter having been ∿60 μm. Several minutes later, this same area had expanded greatly, as is seen in Figure 5-18(b). Other blisters in these photographs had expanded a great deal as well;

the small blister above the final "E" in "BEFORE" (Figure 5-18a) had grown into the mound seen in the very center of Figure 5-18(b). These unusual observations clearly demonstrate that large areas of the surface had become extremely unstable during the ion bombardment. These areas and those in Figures 5-15 and 5-16 may therefore be pockets of implanted gas. It is proposed that such gas pockets could form by the implanted nitrogen freely moving laterally in the gaps between the (111) planes under the mild ion beam heating to areas at the periphery of the beam. It is unclear whether this type of implanted gas transport is realistic; it is proposed simply as a possible way for gas pockets to form in locations removed from the main areas of implantation. Now, notice that the originally smooth surface has become puffy and bumpy in Figure 5-18(b). It may be that these bumpy areas are the prototypes of the objects seen in Figure 5-14. Although it appears as though the larger chunks in Figure 5-14 are resting on the surface, the smaller chunks around the edges are actually attached to the surface, as pointed out before. Also, a few of the larger fragments on the right side of Figure 5-14(b) actually do appear to be attached to the underlying substrate. It then would be reasonable to suppose that the areas in Figure 5-14 were at one time blisters similar to that in Figure 5-18. The central area of such blisters is where most of the trapped gas is probably released since this is the area where the surface is the most bumpy and disturbed (Figure 5-18b). Beyond this, a very thin perimeter of the blister is seen in three corners of Figure 5-18(b); this perimeter

moved radially outward, often leaving very little bumpy material in its wake. Such a thin perimeter might have stopped expanding and formed into the smallest chunks seen growing out of the surface in Figure 5-14(a). The larger objects in the middle might have formed from the bumpy area near the eruption center. A second possibility is that the objects in these "colonies" are the results of smaller blisters which did not erupt but rather flaked apart in a fashion similar to that seen in Figure 5-12(b). However, although Figure 5-14(c) would appear to lend credence to such an idea, the radial fragment-size distribution in Figure 5-14(a) cannot be easily explained. A third possibility is that the entire area in Figure 5-14(a) might have been deposited from a blister eruption exterior to the field of view in this photograph. This possibility requires that the fragments which appear to have grown out of the surface around the perimeter of Figure 5-14(a) actually grew into the surface, which would mean the material was molten when deposited. From Figure 5-14(c) the elongated objects do not seem to have the appearance of material which was molten and then fused in the substrate; if the material were not molten, the radial size-distribution in Figure 5-14(a) cannot be explained by this third possibility.

Since bubble formation and blistering seem to be closely related, the ability to form blisters may depend greatly on the ion beam used. In the Experimental Techniques section above, it was mentioned that NH, N_2H, or O_2 may have been inadvertently used in the early experiments. The propensity to form bubbles would appear to be

about the same in each case; differences would have cast doubt on whether some of the experimental results could be directly compared.

One further point should be mentioned. There was no guarantee that the nitrogen beams used for sputtering had homogeneous profiles. With this in mind, attempts were made during the sputtering to steer the beam over as much of the target surface as practicable. It was hoped that inhomogeneities in current densities would then be averaged out to some extent so that the sample was sputtered more or less uniformly. Typically the beam would be steered several times during each irradiation to apparently different locations, these same areas being covered during subsequent collections as well. This was an uncertain procedure since the fluorescent pattern of the beam on the target could not reliably document the actual ion beam location and profile. Figures 5-12(a) and 5-19 indicate that the sputtering was not always uniform. Running through Figure 5-12(a) is an area without any of the blisters or flakes seen in Figure 5-12(b). This area appears to have been left largely unirradiated. Conversely, Figure 5-19(a) shows an isolated area where there was extensive sputtering. Figure 5-19(b) shows a closeup of this area the features of which appear similar to those (Figures 5-10b, 5-10c) attributed to uneven erosion by the sputtering beam.

The preceding discussion has shown that with 10^{17} - 10^{18} cm^{-2} nitrogen implantation doses: (a) blisters develop which may rupture; (b) initially smooth surfaces may become rough on a micron scale from both blistering and uneven sputtering; (c) blister rupturing may occur

through cracking and flaking, or perhaps may occur eruptively (although there is not strong evidence for this); (d) if blisters do erupt, transport of material from them probably occurs; (e) neither such transport nor localized melting with subsequent transport is required in order to explain the peculiar elongated objects in Figure 5-14; (f) wide-spread heating of samples during the sputtering irradiation was low and was not sufficient to evaporate significant amounts of calcium onto the catcher tubes; and (g) most of the blisters are micron-sized and stable, but some larger ones erupt to sizes of several hundred microns in diameter during SEM probing. It is clear from this discussion that micro-gardening from blistering will complicate comparisons of the isotope fractionation measurements with theories yet to be developed. However, the initial $\delta(^{40}Ca/^{44}Ca)$ values measured during a sputtering sequence will have been less subject to these complications and will therefore be more adaptable to such comparisons.

Sputtering Yields and Evaluation of the Possibility of Non-Sputtered Ca Contamination

Using the Sigmund (1969) model, expected values for calcium sputtering yields S_{Ca} may be calculated. In this section, these yields will be evaluated in order to see if there is any evidence of contamination of the catcher tubes with material (a) erupted from blisters on the target surface, (b) vaporized by beam heating of localized areas of the target surface, or (c) originating from outside sources. The calcium sputtering yield is calculated by first using

Sigmund's formula to find the total sputtering yield S, i.e., the number of target atoms sputtered per incident ion:

$$S(E) = 0.0420\ \alpha\ (A_2/A_1)\ s_n\ (E)/U \qquad (4)$$

where E is the beam energy, s_n is the nuclear stopping cross section (nuclear contribution to dE/dx divided by the target's number density), U is the surface binding energy, and α is a universal function which is an integral of the deposited energy distribution function satisfying the linearized Boltzmann transport equation. In the present calculations, α is obtained from Andersen's (1974) plot of experimental results. For U, the heat of sublimation of Ca from Ca metal is used; this value is 1.83 eV per atom (Gschneider, 1964). For s_n, the usual Thomas-Fermi cross section used in the LSS (Lindhard et al., 1963) range theory is used. Finally, in order to calculate S_{Ca} from S, it is assumed that the sputtering is stoichiometric, i.e., if one out of every ξ atoms in the target is calcium, it is assumed here that

$$S_{Ca} = (1/\xi)\ S \qquad (5)$$

Although a major point of this thesis is that sputtering is not stoichiometric, not for isotopes, and (by extension) certainly not for multicomponent targets each element of which has a substantially different surface binding energy U, this assumption is perfectly adequate at the 10-20% level considered here. Assessments then can be made as to whether major non-sputtering contributions to the

calcium on the catcher surfaces were present in these experiments.

For CaF_2 these calculations yield S_{Ca} = 0.6 and 0.3 at 50 keV (per nitrogen atom) and 130 keV. For $Ca_5(PO_4)_3F$ (fluorapatite), S_{Ca} = 0.4 and 0.2 at these two energies, while for $NaAlSi_3O_8$ + $CaAl_2Si_2O_8$ (plagioclase), S_{Ca} = 0.05 and 0.03. Better agreement with the S_{Ca} values tabulated in Table 5-3 is obtained when Winterbon's inelastic α, which includes electronic stopping (cf. Andersen and Bay, 1975), is used. In this case, the above numbers should be divided by two so that S_{Ca} = 0.3 and 0.16 for fluorite, 0.2 and 0.1 for apatite, and 0.025 and 0.015 for plagioclase.

The comparison of these values with those in Table 5-3 is complicated by the dual energy irradiations, so this will first be considered before attempting to identify samples with anomalously high S_{Ca} values. For the 130 keV irradiations of the fluorite and apatite samples, the measurements are lower than the calculations, but still within a factor of two in each case. These differences could be from surface binding energies being higher than those given by heats of sublimation or to overestimation of the nitrogen beam current due to loss of secondary electrons from the catcher tube-target holder assemblies. If the latter is true, the overestimate must be by a fairly constant factor as there is generally 10-20% reproducibility in S_{Ca} when the same targets were reused for similar experiments after repolishing. The sputtering yield calculations show that a factor of two higher value of S_{Ca} was expected when 100 keV N_2^+ was used as the sputtering beam. In fact, Table 5-3 shows that when comparisons of

S_{Ca}(100 keV) and S_{Ca}(130 keV) are made using in each case measurements for pristine targets, identical values in the range of 0.106 to 0.121 are obtained. The behavior appears to be somewhat more complicated when comparing yields measured at different energies during the same irradiation sequence of a target. When the lower energy beam sputtered a pristine fluorite target, S_{Ca} was only 10-15% higher than when measured for subsequent 130 keV bombardments. For the plagioclase sputtering, the 100 keV S_{Ca} value was 50% lower than the subsequently measured 130 keV value. In contrast to this, in the two fluorite cases where the opposite irradiation sequence was used so that 130 keV N^+ was the first beam, the subsequent 100 keV S_{Ca} values were 70% and 250% higher than the immediately preceding 130 keV values. Ignoring the 250% figure for a moment brings an interesting point into better focus: differences in sputtering yields measured at a variety of beam energies appear to be dependent upon the prior irradiation history of the sample. Although this could not be understood for single component targets unless the "sputtering" yields were dominated by blister chunks or target vaporization from beam heating, for multicomponent targets a possibility exists which is more attractive in light of the facts that blisters develop and break only after extensive sputtering and that there is no evidence for general target heating. (In fact, the 1C sequence gave lower S_{Ca} values than the 3B sequence, even though the latter was carried out using lower beam current densities.) This possibility is that atomic mixing or preferential lighter element sputtering with the longer

range-higher energy beam will tend to concentrate the heavier target constituents in a surface layer where they can be sputtered off in greater percentages by the subsequent low energy irradiation. One might at first also think that the higher energy beam should be able to break chemical bonds more easily than the lower energy beam so that greater numbers of calcium atoms can be sputtered in addition to the calcium-containing molecules. This would then cause some enhancement of sputtering yields at 130 keV relative to those at 100 keV, so that one could qualitatively understand why the yields at the two energies in the 1C and 3B sequences are nearly equal. However, typical energies required to break Ca bonds are greater than the 1.83 eV sublimation energy used in the above sputtering calculations; to break CaO, CaF, CaS, and CaCl bonds requires 4.7 eV, < 3.5 eV, 5.0 eV, and < 7.8 eV, respectively (Cottrell, 1954). As the deposited energy density shifts away from the target surface when higher energy-longer range beams are used, it then appears that even less energy would be available for dissociation at the surface. Returning to the atomic mixing possibility raised above, this mechanism could not cause any enhancement in S_{Ca} at 130 keV after a 100 keV N_2 irradiation, since the mixing depth of the lower energy beam is smaller (on the order of one range, probably) than that of 130 keV beam. Therefore, the 130 keV ions would "see" the same composition, averaged over the 1700 Å range, as if the sample had not been previously sputtered at lower energy. For the reverse sequence this need not be true, though. The initial higher energy bombardments, which might cause mixing over

a depth of up to one range, quite possibly might leave the top third (∿500 Å) of this layer with a composition distinct from the bulk. A subsequent lower energy irradiation would then sample only this material, with the result that the calcium sputtering yield would be higher if its concentration in this top layer exceeded that in the bulk. This mechanism cannot explain the virtual equality of sputtering yields for the two energies, each measured on fresh samples; this appears to be a discrepancy between the sputtering theory calculations and the experimental results. However, the mixing mechanism just described does probably help account for the substantially higher S_{Ca} values measured at 100 keV after sequences of higher energy irradiations.

From the preceding discussion, it should be clear that especially (but not only) for multielement targets, measurements of sputtering yields as a function of energy or bombarding ion should either provide means of making successive measurements on fresh targets or should be able to demonstrate that such a procedure is unnecessary.

Now, in examining the calcium sputtering-yield results tabulated in Table 5-3, it may be seen that only two values appear anomalously high, those for 3A-3 and 4A-4. It is for these two samples that the possibility of blister-eruption contamination of the catcher tubes must be given the most careful consideration. For the 3A-3 case, it seems reasonable to suppose that at most 50% of the sample is from blister fragment contamination. The measured

$\delta(^{40}Ca/^{44}Ca)$ is -0.2±0.2--quite small. A sample of the bulk, unsputtered polycrystalline fluorite was not measured for $\delta(^{40}Ca/^{44}Ca)$, but was considered likely to be very close to zero since (a) the range of calcium isotopic fractionation in terrestrial minerals is quite small, and (b) the sputtered fractionation patterns were similar to those obtained from the Fluorite-1 sample, for which $\delta_{Bulk} = 0.3\pm0.4$. If any cratering fragments deposited on the catcher tube had $\delta \approx 0$, the actual value of sputtered Ca would have been about -0.5‰, certainly not a serious discrepancy. If the fragments instead had been quite heavy, say -10‰ (the maximum negative value seen for any of the fractionation measurements), the sputtered δ would have been +10‰, which is completely out of line with the generally decreasing pattern shown in Figure 5-3. The δ value actually is probably less than the 2.7‰ observed for the previous point, and is therefore constrained to the range -0.5‰ to +2.5‰. This uncertainty will not alter any of the conclusions that will be made from the experimental results given in Table 5-3.

For the 4A-4 sample, a sputtering yield $S_{Ca} = 0.45$ was obtained for a total sample size of about 6 μg. This is in contrast to the $S_{Ca} = 0.12$ (2.4 μg) obtained for 2A-4, a similar sample obtained for the Fluorite-1 instead of the polycrystalline fluorite sample. Since 4A-4 was part of an angular fractionation experiment, the amounts of Ca on each catcher tube section may be examined (see Table 5-4). For the 4A-4 "intermediate" and "oblique" sections, the amounts are compatible with the range of 1.5-1.8 seen for 4A-1 and

4A-3 for the ratio of oblique-section Ca amount to intermediate-section Ca amount. If one assumes that the angular distribution of the sputtered material is roughly the same at both ion beam energies, then the "normal" (perpendicular) exit section 4A-4-N would be expected to have 1.4-1.9 μg Ca, based upon the amounts on the other two sections. This would give a total for 4A-4 of 3.3-3.8 μg of calcium, for a sputtering yield of 0.25 to 0.29 instead of the 0.45 value measured. Even so, this value is 2-2.5 times higher than that measured for the Fluorite-1 single crystal 2A-4 sample. For 4A-4-N, 4.1 μg Ca was observed, rather than the 1.4-1.9 μg "expected." One must question whether any localized heating or blister fragmentation and eruption could cause an anisotropic contamination of the catcher surface. This is not known. For localized heating at the surface, where the evaporating material is not restricted, the emission is probably fairly isotropic; this need not be the case though if material is vaporized from inside a blister but restricted by a crack in the top of the blister (see Figure 5-9). The angular pattern of blister eruption fragments cannot be predicted. If a blister erupts all at once, there may be an isotropic distribution of the fragments, but if it opens along a crack, which from Figures 5-9 and 5-12(b) seems to occur often, any fragments erupted may be carried preferentially in the direction of the gas passing out through the crack. The $\delta(^{40}Ca/^{44}Ca)$ values for the three sections of 4A-4 appear to be so reasonable, though, that it is somewhat difficult to believe that there is any non-sputtering contamination present at all. The δ-angular

pattern is just what was observed for the preceding 4A-3 130 keV sputtering, except that each point is 2‰ heavier. Were 4A-4-N to have been the primary recipient of contaminant calcium, its δ value would have been the only one subject to significant alteration. Assuming that the 4.1-1.4 = 2.7 μg "excess" was due to contamination of $\delta \approx 0$, the $\delta(^{40}Ca/^{44}Ca)$ of the 4A-4-N sputtered material would have been ∿10‰ . This would imply that the $\delta(^{40}Ca/^{44}Ca)$ weighted average for the three sections would have been ∿-0.7‰ , as compared to the -0.3‰ in Table 5-3. It appears unlikely that such a large amount of calcium contamination could have $\delta \neq 0$, particularly if the possibility of vaporization due to localized heating is discounted. If one assumes instead that all three catcher tubes are contaminated with $\delta \approx 0$ material, that the total amount of sputtered calcium is 2.4 μg (the 2A-4 quantity), and that the proportions of sputtered Ca on the three 4A-4 segments are similar to those measured for 4A-1 and 4A-3, then again the primary contamination is on the normal exit section 4A-4-N, and again the "corrected" weighted average is $\delta(^{40}Ca/^{44}Ca) = -0.7$‰ . Thus, it appears that there <u>is</u> a real difference between the δ values measured for 2A-4 (-8.3±0.7‰) and 4A-4 (-0.3 to -0.7‰).

There was some possibility that the double spike weight measured prior to its mixture with the 4A-4-N sample had either been recorded improperly or that the weighing itself was in error. As all the calcium sample amounts or weights are measured by isotope dilution during the main mixture run, such an error would cause the same

percentage error in the calculated calcium sample amount. An additional test was used to determine if such an error had been made. The ^{44}Ca spike used for preparing the enriched standards was added to the remainder of the main sample left after the mixture run. The fraction of the sample remaining had been roughly measured when the mixture run's fraction was withdrawn for loading. The change in $^{40}Ca/^{44}Ca$ between the mixture run and the mixture-plus-^{44}Ca-spike analysis enabled an independent calculation of the amount of calcium in the original sample; a result consistent with that in Table 5-3 was obtained.

The above arguments, which use measurements of "sputtering" yields to detect appreciable contamination of the catcher tubes, assume of course that in most cases there is no detectable contamination. Since isotopic variations are observed, it seems clear that the sputtered material is at least a major fraction of the Ca analyzed. It is useful to calculate how many blister fragments would have to be deposited on the catchers before their amounts exceed blank levels. Assuming that such chunks are 1 μm cubes yields a weight of 3×10^{-12} g per chunk. Therefore, 10^4 chunks would be required to be detectable. From Figure 5-10(a) it appears that there is a cratering density of up to 10^7 per cm^2. A complete survey of the surface was not performed in order to estimate what percentage of the surface is cratered to this extent. However, Figure 5-12 indicates that major areas were populated with fragmented, rather than erupted, blisters. If 20% of the irradiated surface area had erupted blisters

which deposited chunks on the catcher tubes, the Ca contamination would be ∿2.5 μg. Most of the sputtered samples have a total Ca concentration which is only a fraction of this. If blisters were erupting substantial numbers of chunks onto the catcher tubes, one would expect to see higher Ca contents per unit beam dose during the later bombardments. This is not observed, so it appears that such chunks did not heavily contaminate the catcher surfaces.

In summary, estimates indicate that if substantial fractions of the observed blisters erupted material onto the catcher tubes, it would have been easily detected. The general uniformity of the S_{Ca} values indicates that this was not the case except possibly in two instances. 4A-4 and 3A-3 are the only samples which suggest by anomalously high S_{Ca} values the possible presence of extensive quantities of cratering fragments or, less likely, of extensive vaporization from localized heating. It is not possible to tell if all the samples are affected by such "contamination" to minor extents. The main observations of greatly fractionated Ca and of the systematic changes in the δ values are not greatly compromised by this. Even if this requires a discounting of the 4A-4-N measurement, the total $\delta(^{40}Ca/^{44}Ca)$ still is in the range -0.3 to -0.7‰ for 4A-4, quite distinct from the value measured for the similar Fluorite-1 irradiation, 2A-4.

Isotopic Fraction of Ca during Sputtering

Large positive and negative $\delta(^{40}Ca/^{44}Ca)$ values have been observed for calcium collected onto catcher surfaces during the

sputtering of a variety of calcium-bearing minerals. In a number of cases, systematic variations in the observed δ values were observed with continued sputtering. Results obtained for similar sets of measurements were generally in agreement, and the few notable exceptions to this are discussed fully below. Fractionation of the calcium was observed to vary with the angle of exit from the target surface even though with prolonged sputtering the surface became rough on a micron scale. From the earlier discussion of theoretical models it is clear that a thorough understanding of the means by which the isotope fractionation is produced is not at hand. Nevertheless, insight into some aspects of the sputtering process may be obtained from these results, even though they are not completely well-characterized in all respects.

Initial Positive Fractionation. One of the striking features of the $\delta(^{40}Ca/^{44}Ca)$ fractionation data presented in Table 5-3 is that the first material removed is isotopically light when sputtering pristine fluorite and apatite surfaces with the higher energy 130 keV beam. In fact, this may be true for the lower energy ion beam as well, although the effect was observed for the plagioclase sample (1B-1), but not for the two fluorite samples (1C-1 and 3B-1). So much material was sputtered during these lower-energy bombardments that for the fluorite, the initial large fractionation may have already decreased to $\delta \sim 0$ in a fashion similar to that observed over a longer period of time at 130 keV (2A, 3A, and 4A irradiation sequences, see Figure 5-3). However, there also may be a complexity

here which cannot yet be adequately explained, since the plagioclase did show a large fractionation. Note that an order of magnitude fewer calcium atoms were sputtered from the plagioclase than from the fluorite samples. It seems quite reasonable to expect that the very first calcium sputtered from fluorite at this lower beam energy is also isotopically light. This can be tested in future experiments by sputtering fresh fluorite surfaces with $\sim 5 \times 10^{16}$ cm^{-2} doses of 100 keV N_2. Nevertheless, the present data indicate that the sputter removal of substantially fractionated, isotopically light calcium during the initial bombardment of a sample is apparently independent of (a) sample chemical composition, (b) calcium concentration, (c) beam current density, and (d) crystalline structure and orientation.

This type of initial isotopic fractionation behavior will likely be that which is most amenable to comparison with results of theoretical modelling. There is insufficient time for rough surfaces to develop which can cause geometric complexities to arise from the wide effective range of beam-incident angles. Neither will blistering and its attendant cratering have arisen to complicate the interpretation of the isotopic data. The use of isotopic fractionation data for comparison with yet-to-be-developed theoretical models of multicomponent target sputtering is to be preferred over elemental fractionation data, for which more data currently exist. This is because the surface (and volume) binding energies for different isotopes of an element are, for sputtering purposes, identical. For

different elements, any fractionation observed is caused not only by the different masses involved, as in the isotopic case. Substantial differences in binding energies also affect the relative sputtering rates (see eq. 4 above). For isotopes of moderate to heavy mass elements, substantial binding energy differences are not present (Appendix B). Even if the relative binding energies of the various elemental constituents are known or can be estimated for bulk materials, it is usually unknown how they change in amorphous, non-stoichiometric surface layers produced by preferential sputtering of some of the components. For the isotopic data, though, comparisons with models can be made without undue complications until the surface roughness or radiation damage blisters arise to a significant extent. Detailed models will have to account for surface layer isotopic changes. For data such as that in Table 5-3, an accounting may also have to be made for elemental composition changes in the surficial layer, as this may affect the energy sharing. This can be done though via a set of measurements (perhaps obtained using the sputtering-ESCA technique of Housley and Grant, 1977) rather than having to be parameters calculated by the model. On the other hand, the use of elemental fractionation data to test quantitatively any sputtering models would require the calculation of these parameters, which may be much more difficult than for the isotope case because of the binding energy uncertainties described above.

In comparing the Table 5-3 results with the model of Haff et al. (1977a) which was discussed in an earlier section of this

chapter, it should be noted that there is no evidence to indicate whether the experimental values are the maximum that can be attained for these target-ion beam combinations; the model predicts maximal effects attainable and yields results which are in qualitative agreement with the measurements presented in the table. However, as the reasonably detailed calculations of Watson (personal communication) fail to predict any substantial fractionation, it is clear that little fundamental understanding of the large initial fractionation effects is at hand.

Atomic Mixing. Information about the role of ion-beam-induced atomic mixing during target bombardment may be obtained from Table 5-3. To see this, it is constructive to first consider the thought experiment where a liquid which has zero vapor pressure (to avoid confusing the results) is sputtered. Any isotopic fractionation which is then observed for the first material sputtered will be observed for all successive times as well, providing that the liquid is continuously well stirred and that the volume of liquid is large enough to avoid significant depletion of any isotope. If one instead sputters a solid material and observes isotopic fractionation which changes during the course of the bombardment, an assessment should be made when interpreting the data as to whether the changes are caused simply by the inability of the solid to stay "well stirred." If so, then the measurements not only contain useful information about the actual fractionation mechanism, but also (more indirectly) about the extent and means of any significant moving or mixing of target atoms in the

substrate which might be occurring during ion beam bombardment. In this section, the calcium isotopic fractionation results will be assessed in terms of their ability to shed light upon the extent of any such mixing and the mechanisms by which it might occur.

Any mixing which occurs can be produced either by the collision cascades or by enhanced diffusion from beam heating. Haff et al. (1977b) discussed the first of these using a diffusion model to describe the effect of the collision cascades in a simplified way. This model considers a target consisting of two thick layers, each with a different composition, and calculates the extent of mixing across the interior interface when the top layer is bombarded by an ion beam. Significant mixing across this interface is predicted to occur during the course of experiments which have beam doses of the order of 10^{17} cm^{-2} or more. Such doses were used in the calcium experiments described herein. The calcium isotope fractionation data in Table 5-3 will be shown in the discussion below to be consistent with the presence of mixing during sputtering, but it is unclear whether such mixing occurred primarily through the collision cascades or through enhanced diffusion arising from low-grade target heating. The extent and efficiency of this mixing, as reflected in the isotopic patterns, will be assessed.

First, though, an assessment needs to be made of the reliability of the data in Table 5-3 which give the amounts of material sputtered as fractions of the amounts contained within a depth equal to the ion range. Each such value is calculated from

the measurement of the calcium amount collected on the catcher tube and from the apparent sputtered area. The sputtered area is taken to be the area of significant radiation damage, as measured under a microscope in reflected light. This measurement is subject to the following uncertainties: (a) beam inhomogeneities cause certain areas to be sputtered more than others, although radiation damage may have been produced in each of the areas; (b) radiation damage may be produced outside of the primary ion beam area by electron trapping or by the secondary ion collision cascades. Also, stoichiometric compositions of the surface layers of the samples are assumed so that the number of target atoms sputtered can be calculated from the number of calcium atoms. For these various reasons, it is considered that the calculated average depth of sputtering for each bombardment provides only a qualitative basis for comparisons. Used in this way without too much regard for the absolute numbers, it proves to be a useful parameter for indexing the extent of sputtering in each case.

When an initially isotopically homogeneous target is first sputtered, the first material to be removed is isotopically light ($\delta > 0$), as was seen in the previous section. For the very first material removed, it may then be expected that a surficial layer a few monolayers deep, from which the sputtered atoms were ejected, will be correspondingly heavy ($\delta < 0$) by an amount sufficient for material balance. With increased sputtering, this thin, isotopically heavy layer <u>may</u> be mixed down into the substrate so that a much thicker $\delta < 0$ layer is eventually produced. Suppose that the

fractionation of the material initially sputtered is +F. As the top few monolayers become isotopically heavy, the sputtered δ values will decrease, but a net +F fractionation above the present substrate layers will be maintained. If isotopic equilibrium is eventually established, a surficial layer of the sample will have an isotopic fractionation of -F, and the material sputtered from the equilibrium layer will then have $\delta = 0$, identical to the initial target composition and to that still present at depth in the sample. With atomic mixing, isotopically heavy material may extend deep into the target--perhaps to a depth on the order of the range of the incident ions. From these considerations, it can be seen that there may be clues in the isotopic fractionation measurements as to the extent to which atomic mixing actually occurs in the investigated energy regime.

If atomic mixing were not occurring during the sputtering experiments, one might expect no net isotopic fractionation to have been observed. This is because the amount of Ca collected on any of the catcher tubes represents the sputtering of many monolayers worth of material. In fluorite, for example, one monolayer equals a 5.5 Å depth in the target. For the 3A-1 initial bombardment of polycrystalline fluorite, 13 monolayers were removed; the estimated depth to which the 130 keV initial sputtering proceeded was least for this bombardment, which was one of three for fluorite samples. When one considers that the majority of sputtered atoms originate from within a 5-10 Å (one-two monolayers) distance from the surface (Sigmund, 1969), it might be thought that in the absence of atomic mixing, any

fractionation would be completely averaged out to zero during experiments which collect material representing the sputtering of many monolayers.

Numerical modelling of the time dependence of sputtering-produced fractionation shows that in fact the fractionation is not quickly averaged out to zero. In these calculations, a limited-size reservoir consisting of one monolayer's worth of calcium is allowed to be depleted by sputtering. It is assumed that the calcium consists solely of ^{40}Ca and ^{44}Ca, and that the sputtering introduces an isotopic fractionation factor of $(44/40)^{1/4}$. As the reservoir is depleted, it is replenished with unfractionated material. Several cases of replenishment have been considered: (a) an on-going, continuous replenishment such as considered by Haff (1977), and (b) replenishment which occurs at discrete intervals whenever the reservoir becomes depleted by some specified percentage. Particularly if the sputtered particles can originate from within the top few monolayers instead of the very top one, which seems likely, then in the absence of mixing, appreciable depletion of the sputtered layer may be able to occur before any of the underlying, unfractionated material is sputtered. In these numerical models, the fractionation is averaged from the onset of sputtering at time $t = 0$ to some final time T by weighting the fractionation of the material sputtered during a short interval of time dt by the number of atoms sputtered during this interval. The resulting calculations are shown in Figure 5-20. Plotted on the ordinate is this average fractionation, and the final

time T is plotted on the abscissa. T, measured in seconds, has been scaled using the formulas of Haff (1977, eqs. 8 and 9) to correspond to typical parameters for the samples in Table 5-3: $S_{Ca} = 0.1$, I = beam particle current density = 3×10^{13} particle/cm^2-sec, Δx = depth of sputtered layer = 5 Å, and ρ = target density = 1.6×10^{22} Ca atoms per cm^3 of CaF_2. With these parameters, it takes about 400 sec to sputter away 1 monolayer. Two cases are shown in Figure 5-20, one corresponding to continuous replenishment of the reservoir, and the other to the case where the reservoir is depleted by 50% before the unfractionated material is added. Figure 5-20 shows that similar trends are obtained in both cases. From this figure it is clear that even with no beam-induced admixture of unfractionated material, the overall fractionation of material collected during the sputtering of several monolayers will not average out to a value very close to zero. Appreciable positive fractionation is still observed after four monolayers worth of calcium has been sputtered, although it then quickly becomes negligible with further sputtering. The similarity of the fractionation patterns in the two cases shown in Figure 5-20 do not allow conclusions to be drawn about the presence of mixing solely on the basis that non-zero fractionation is observed initially.

With the present data though, it is apparent, since so many monolayers were sputtered initially while still yielding highly positive fractionation, that larger reservoirs (i.e., larger Δx) would be more appropriate in the above models. This is an indication

that atomic mixing probably did play an important part in the fractionation experiments. Additionally, two other facets of the data in Table 5-3 suggest that mixing was important: (a) the initial plagioclase sputtering, which was with a 100 keV N_2 beam, showed a large positive fractionation after one-fourth of a range was sputtered, something not seen for similar-dose experiments with fluorite; (b) short bombardments of samples at the higher beam energy after extensive lower-energy sputtering produced negative δ values. Point (b) and the observation about larger reservoirs seem to suggest strongly that mixing plays a significant role in controlling the isotopic fractionation. Point (a) will briefly be considered below. Later, attempts to measure thicknesses of the isotopically heavy surficial layers of two fluorite targets will be discussed. These measurements provide more direct evidence that mixing was present to a significant extent. However, the present data do not permit distinguishing between mixing generated by collision cascades and that occurring through diffusion of the calcium at the somewhat elevated target temperatures.

Regarding the first point, notice that the sputtering of a given number of monolayers represents a less extensive depletion of the reservoir if Δx is increased; this means that it takes a longer time to deplete the reservoir and to cause the fractionation to decrease to a given level. Increasing Δx then has the effect of compressing the scale of the abscissa in Figure 5-20: every point on the abscissa then corresponds to a larger time value. Calculating

the values of Δx (Haff, 1977, eqs. 8 and 9) which will compress the abscissa enough to bring it into agreement with the elapsed beam-times (not shown in Table 5-3) for each fractionation measurement yields Δx = 20-30 Å for the 2A 130 keV sequence and 40-60 Å for both the 3A and 4A 130 keV sequences; the model does not adequately fit the 2A-3 point, about which more will be said below. This is therefore suggestive of the presence of mixing in these samples. Although the technique used above for computing Δx is crude, it probably is sufficiently accurate to indicate that Δx is larger than a few monolayers but smaller than one range. Since computed Δx values much greater than one monolayer were found, this indicates that mixing was apparently operative to some extent.

Attempts to more directly measure Δx will be discussed later, but if the distances Δx are indeed much smaller than the 1700 Å beam range, they are in sharp contrast to the calculation of Haff (1977) that $\Delta x \sim 1$ range for the elemental fractionation of Liau et al. (1977). This may indicate that the use of this simple mixing-model to describe isotopic fractionation is unjustified, that the fractionation factor, the fourth root of the mass ratio, is incorrect for calcium, or that an artifact exists in the measurement of Δx by Liau et al. With either of the first two possibilities, one would have supposed that the elemental fractionation data would not be fit well by the simple model either, whereas they do appear to be. The possibility that the large Δx values of 400-1200 Å observed by Liau et al. (1977) were an artifact of their experimental technique may probably be discounted.

If their alloying together of separately evaporated elemental films did not proceed to completion, diffusion coefficients and mobility of the constituents during the sputtering could have been enhanced since many bonds would not have formed. This would enable easier mixing, with the results that Δx would be larger while the dose of sputtering ions required to achieve sputtering equilibrium would be lower; the equilibrium dose was used by Haff to calculate a value for Δx which then favorably compared to the measured value. Liau et al. (1977) did not verify that their annealing procedures did more than produce a composition uniform within the 100 Å backscattering resolution limit. However, the annealing in most cases probably did proceed to completion since the techniques were those of others who, using diffraction methods, verified the chemical structures inferred from backscattering compositions (cf. Campisano et al., 1975; Poate and Tisone, 1974). Liau et al. did not document the reliability of the Au-Ag, Au-Cu, or Ge-Si annealings. It should be noted that Braun and Färber (1975b) have claimed that phase diagrams of Ag-Cu alloys imply that some individual grains may consist of nearly pure Ag or Cu; however, they imply that this is not the case in Ag-Au alloys (Braun and Färber, 1975a).

The data on sputtering of plagioclase starting with 100 keV N_2 provides some indication about the possible presence of beam-induced atomic mixing during sputtering, although a non-mixing explanation cannot be ruled out completely. For sample 1B-1, the sputtering was estimated from the collected calcium concentration to have proceeded

to a depth of 140 Å, or 0.27 range. A large positive $\delta(^{40}Ca/^{44}Ca)$ was measured, in contrast to the fluorite cases where the initial value measured was much smaller. For example, the fractionation for fluorite was +0.3‰ for 3B-1 after the removal of only 60% more material. It appears as though the number of Ca atoms removed by sputtering, rather than the total number of target atoms removed, is the important parameter in determining the extent to which the isotope fractionation decreases from its initial value. In order for this to be true, calcium atoms which find themselves within a few monolayers of the surface cannot all be sputtered, or there would be no large fractionation; those which remain must in some way exchange with other Ca atoms in a "reservoir." The larger this reservoir, the less fractionated it will be after a given number of atoms are removed from it. This was also seen above where Δx had to be much larger than 5 Å in order for the initial collected Ca to be extensively fractionated. A larger reservoir here will result in those Ca atoms which <u>are</u> removed representing a surface composition which is not yet highly fractionated. Two ways for such a reservoir to actually exist are that the calcium would have to become concentrated in the upper few monolayers as the surface was excavated, or that the calcium in the top few monolayers would mix down into the target. In the first case, mixing need not be operative. For Ca to be concentrated near the surface, its sputtering yield would have to be lower than that of Si and O, the major constituents in plagioclase. The relative binding and bond dissociation energies of Ca, Si, and O (Gschneider, 1964; Cottrell,

1954) lead one to expect that Ca would be sputtered more easily, though. However, ESCA (Electron Spectroscopy for Chemical Analysis) data of Housley and Grant (1977) for some samples sputtered with 1 keV Ar do show surface enrichments of Ca relative to Si. The presence of such surface concentrations of Ca in the present plagioclase sputtering therefore cannot be ruled out, and provides a non-mixing means for having a reservoir of size sufficient to support the large positive isotopic fractionation. However, the Housley and Grant (1977) data also showed the surface enrichment/depletion layer to be a few hundred angstroms thick. It would not then be inconsistent to suppose that a surface layer at least as thick as this was established with the higher energies used in this plagioclase experiment. Mixing either by the collision cascades or by enhanced diffusion seem to be plausible means by which such a thick layer could be generated.

In order to be tenable, though, such mixing must be shown to be consistent with the much smaller isotopic fractionation values measured for the similar 100 keV bombardments of fresh fluorite samples, 1C-1 and 3B-1. The rate at which atomic mixing by the collision cascades proceeds is clearly determined in part by the number of ions striking the surface per unit area per unit time. Regardless of whether the calcium in a target is a major or minor component, there will be the same amount of calcium mixing per sputtered calcium atom, so that the isotope effects should be the same. However, if the sputtering yield for calcium in a sample is lower in comparison with other samples, stoichiometric factors being

accounted for, there will be more calcium mixing per sputtered Ca atom. As was seen above, more efficient mixing increases the size of the reservoir (Δx) so that it takes longer for the fractionation to decrease to $\delta = 0$ isotopic equilibrium. For plagioclase, a minor Ca component sample where one atom in 26 is calcium, the mixing was indeed somewhat more efficient than for fluorite. In fluorite, one atom in three is Ca, and the 100 keV N_2 sputtering yields S_{Ca} ranged from 0.11-0.12. Multiplying this by 3/26 gives a stoichiometric "prediction" for S_{Ca} in plagioclase of 0.013-0.014, which is a factor of two greater than the 0.007 value observed. This would mean that the reservoir size in plagioclase was proportionately larger and hence less depleted per unit depth of sputtering excavation. Smaller percentage depletions of the reservoir mean that it will be less isotopically heavy, so that the sputtered calcium will have a more positive $\delta(^{40}Ca/^{44}Ca)$.

The isotopic evidence for atomic mixing is of course indirect, and can cause arguments such as the one above to be less than convincing. For this particular plagioclase sputtering, for example, it remains hard to see how sputtering which was at most half as extensive as for fluorite (0.27 ranges removed as opposed to 0.45 for 3B-1) and only slightly more efficient in mixing can lead to a 21‰ to 0.3‰ fractionation difference. As pointed out above, this is a complexity in the data which cannot as yet be convincingly explained. Only the consistency or inconsistency of the fractionation data with respect to atomic mixing can be tested, of course, and cannot prove

that mixing is present. However, direct or indirect observation of a thick isotopically heavy surface layer would strongly suggest that it was produced by collision-cascade or diffusion-generated mixing.

A third aspect of the fractionation data also provides indirect evidence of a thick isotopically heavy surface layer, and readily lends itself to an explanation in terms of mixing. This deals with the observation that $\delta(^{40}Ca/^{44}Ca)$ quickly turns from positive or zero values obtained during initial 100 keV N_2 sputtering to negative values when the beam energy per nitrogen atom is increased to 130 keV (samples 1B-2, 1C-2, 3B-2, and 4B-2). If mixing was not present, so that the isotopic fractionation of the sputtered Ca was controlled totally by the fractionation of the first few monolayers, then there should have been no change in δ when the beam energy was changed, since in both cases the ion range was large compared to the depth of a monolayer, and since it is very unlikely that the fractionation is in any direct way dependent upon the beam energy.

An attempt will now be made to explain the direction of this change in δ. This will provide information about the rate of the mixing, which according to the above argument apparently does exist. Consider the product of the fraction of target atoms displaced per unit volume by the cascade atoms, denoted f, and the number of cascade atoms, n, present at a given time. If mixing within the target is indeed driven by the collision cascades, then this product should reflect the efficiency of mixing at the particular beam energy under consideration. Haff et al. (1977b) present an estimate that f is

proportional to the nuclear stopping power, $(dE/dx)_n$. It is precisely this stopping power which accounts for the energy differences in the calcium sputtering yields calculated in an earlier section, so it may be seen that both in the fluorite and plagioclase cases, $(dE/dx)_n$ is a factor of $\sim$1.7 lower at 130 keV than at 50 keV/N. Therefore, f is also probably lower by a similar factor. However, as the calcium sputtering yields in Table 5-3 illustrate, sputtering yields do not always follow the $(dE/dx)_n$ energy dependence, so it may be too much to expect mixing efficiencies to do any better. Weller (1978) has presented a simplified mathematical analysis of the time evolution of the density within a target of collision cascade atoms. However, this model is insufficiently sophisticated to address the question of how n might change as the beam energy E_o is increased (Weller, personal communication). Also, the WSS (Winterbon et al., 1970) theory of energy deposition does not directly address this point. However, it is intuitively clear that a higher energy incident ion will require more collisions in order to slow down, and this means more target atoms will be part of the collision cascades. Thus, n increases with energy. Since the exact energy dependence is not known, though, it is unclear how the product, nf, and therefore the mixing efficiency, changes with incident ion energy. It seems reasonable to suppose that the near-surface mixing efficiency is lower at higher energies because the cascades are generated for the most part deeper within the target; it is there, near the end of its range, that an incident ion loses most of its energy and undergoes most of the

collisions.

The fractionation data do, in fact, lend themselves to the interpretation that the mixing depth is greater, and that the near-surface mixing efficiency is lower, at higher energies. Suppose that the 100 keV N_2 initial sputtering established a surficial region with $\delta < 0$. The thickness of this layer will depend upon the degree to which mixing occurred. The δ value of the sputtered material and of the surface region depends upon the isotopic fractionation factor for material sputtered from a fresh surface, whether the sputtering dose was sufficient for isotopic equilibrium to be set up, and the mixing efficiency, if equilibrium has not been established. After the surface layer has reached an equilibrium isotopically heavy composition at 50 keV/N, negative δ values will be observed during subsequent sputtering at 130 keV since a reduced mixing efficiency will reduce the quantities of unfractionated calcium being brought up into the surface layer per unit time.

It is clear that the mixing is a rather slow process, at least at the higher energy. If it were instead to proceed so quickly that unfractionated material could be brought up to the surface from deep within the sample before any significant quantity of atoms could be sputtered, then the greater mixing depth which we suppose exists for the higher energy beam would cause an immediate dilution of the isotopically heavy layer. This would have the effect of producing positive sputtered δ values when the beam energy is increased to 130 keV. As this is not observed, the mixing rate must indeed be

relatively slow. Since at issue is the rate at which bulk quantities of Ca may be transported within the sample over distances of hundreds of angstroms, it is reasonable to suppose that at both energies there may be an appreciable time delay between the onset of mixing and the arrival at the surface of unfractionated material transported from depth; only at the surface can such material dilute the isotope fractionation of the material being sputter-removed. The more efficient the mixing, the smaller this time delay will be. The negative δ values observed during short 130 keV bombardments which follow long irradiations at lower energy could then be understood if (a) the lower energy sputtering had previously established an isotopically heavy layer which was at least twice as thick as the 60-120 Å estimated depth to which the 130 keV sputtering subsequently eroded the surface (such a thick layer would indicate the presence of a mixing mechanism), and (b) the time lag increased from the value at 50 keV/N and was greater than or comparable to the time required for the 130 keV sputtering. In this case, unfractionated material would not have come near the surface at the rate it did during the lower energy bombardment, with the result being that the $\delta(^{40}Ca/^{44}Ca)$ of the top few monolayers was not maintained at the previously established value.

If an appreciable time delay can exist, there are interesting ramifications for the isotopically heavy surface "layer." If the mixing was very fast compared to the sputtering rate, this layer would have a uniform isotopic composition down to the end of the

mixing range. If generated by the collision cascades, this mixing depth conceptually would appear to be limited to a depth approximately equal to the projected primary ion range. (In contradistinction to the path length of the ions which are multiply-scattered as they travel in the target, the projected range is the perpendicular depth in the sample to which the ions penetrate. The values given in Table 5-3 are projected ranges.) If one considers straggling of the beam, some smooth transition region can be imagined to exist at the bottom of the mixing range. This transition region would have fractionation varying with depth from the value of the surface layer to that of the bulk sample. If the mixing is not efficient, so that appreciable time lags become important, the surface "layer" itself will not have a uniform isotopic composition. This is because material at the surface will exchange and mix only with the next few monolayers. Those will mix only with the next few, and so on. Thus, fractionated material at depth will be that which is mixed most readily with unfractionated material, and so the fractionation will be more diluted than for material closer to the surface, which exchanges directly with only other fractionated material. In the case of mixing proceeding via slow diffusion at somewhat-elevated target temperatures, the situation would be similar except that the mixing depth would not be limited by the range of the beam.

To calculate approximately what shape the fractionation, $\delta(z)$, will have as a function of distance z into the target, the diffusion equation will be considered to approximate the mixing

transport (cf. Haff et al., 1977b). Thus

$$\frac{\partial^2 N_i}{\partial z^2} = \frac{1}{D} \frac{\partial N_i}{\partial t} \tag{6}$$

where N_i is the fractional amount of isotope i and D is the effective diffusion constant. For the steady-state case, the right-hand side of this equation is zero. In solving this for the steady state, the boundary conditions are taken to be that at z = 0 the isotopic fractionation is so negative that the sputtered material will have $\delta = 0$, and that at some depth d at the end of the mixing range, the composition will be that of the bulk, $\delta = 0$. In considering a medium of finite thickness d, rather than a semi-infinite slab, the reasonable approximation is being made that the mixing has a definite range beyond which no transport will occur. Consider for simplicity a calcium two-isotope system of masses 40 and 44; assuming that the surface isotope fractionation factor is $(44/40)^{1/4}$, the boundary conditions are then

$$\begin{aligned} N_{40}(z=0) &= 0.97874 \equiv n'_{40} & N_{44}(z=0) &= 0.021257 \equiv n'_{44} \\ N_{40}(z=d) &= 0.97923 \equiv n_{40} & N_{44}(z=d) &= 0.020767 \equiv n_{44} \end{aligned} \tag{7}$$

Note that $n_{40}/n_{44} = 47.153$ and $n'_{40}/n'_{44} = 47.153 \times (40/44)^{1/4} = 46.043$. The steady state solution is

$$\begin{aligned} N_{40}(z) &= n'_{40} + (n_{40} - n'_{40})(z/d) \\ N_{44}(z) &= n'_{44} + (n_{44} - n'_{44})(z/d) \end{aligned} \tag{8}$$

The function $\delta(z)$ is then found to be extremely close to being linear in z, ranging from $\delta(z = 0) = -23.5‰$ to $\delta(z = d) = 0‰$. This calculation is clearly approximate, but does illustrate that it is an oversimplification to speak of the surface layer as if it were isotopically homogeneous.

An alternate interpretation will be briefly considered for the data from the lower-then-higher-energy sputtering sequences. This deals with another mechanism by which atoms from the first few monolayers might be sputtered. This mechanism, though, will be shown here to have probably not been important in the calcium experiments. Chapman et al. (1972) have discussed the direct recoiling of surface atoms when struck by an incident ion. While it is kinematically impossible to have the struck atom recoil in the backwards direction (away from the target), such an energetically recoiling particle may be able to glance off of another atom at the surface and then recoil in the backwards direction. In the calcium experiments, if there is a greater propensity for this to occur at the higher beam energy, then isotopically heavy material near the surface could be directly sputtered and collected, yielding $\delta < 0$ values. Chapman et al. (1972) state, though, that since the number of primary recoils is small compared to the number of collision cascade atoms, the contribution to the sputtering yield may be expected to be quite small. For their 10-40 keV Ar on Au sputtering experiments, Chapman et al. estimate that only a few percent of the total sputtering yield, measured at 90° from the beam, is from such surface recoils.

This is the most favored direction for observing direct recoils. The collectors in the calcium experiments span an angular range from 5°, where direct recoils are nearly forbidden, to 60 - 80°, where the direct recoil contribution is at most a few percent of the atoms coming off in this direction. Therefore, there seems to be no reason to suppose that direct recoils could have played a significant role in the calcium measurements.

It is surprising that the subsequent 130 keV irradiations in the 1B, 1C, 3B, and 4B sputtering sequences discussed above do not yield more reproducible results. The $\delta(^{40}Ca/^{44}Ca) = -10.6‰$ value obtained for 1C-2 represented a -10‰ change from the value obtained during the 100 keV bombardment. The 100 keV beam dose of 1.25×10^{17} N_2 ions was a factor of two more extensive than the 100 keV initial sputtering dose used for the other two fluorite experiments. Nevertheless, it is not clear how this could be responsible for the ∿7‰ difference in the fractionation subsequently measured at 130 keV since $\delta \sim 0$ isotopic equilibrium was achieved during the 3B-1 bombardment as well as that for 1C-1. In comparison with the 3B and 4B fluorite experiments, the -10.6‰ value for 1C-2 therefore appears to be an outlier. The plagioclase was sputtered the same day under nearly identical conditions, and also had a very big swing in δ values of -25‰ between the two bombardments. It cannot be decided from the present data whether these differences originated somehow (a) in the factor of ∿10 higher 100 keV beam currents used when the larger effects were observed, (b) in the inadvertent use of N_2H^+ as the

100 keV beam in these early experiments (see the Experimental Procedures section of this chapter), or (c) from something else. This can be explored in future experiments. It is important to emphasize that the foregoing discussion of mixing and mixing efficiencies is not affected by this point. Only the main observation was of interest in establishing that some mixing mechanism had been operative during the sputtering; this was the observation that all four of the sputtering sequences yielded δ values considerably more negative than the values obtained in the prior lower energy bombardments which in three of the four cases had apparently proceeded to isotopic equilibrium. The variations in the magnitudes of the negative $\delta(^{40}Ca/^{44}Ca)$ values were therefore unimportant for that discussion.

Single Crystal-Polycrystalline Differences. One aspect of the calcium fractionation data which appears puzzling has to do with the three series of prolonged 130 keV irradiations of fluorite targets. For the polycrystalline fluorite target, two separate sequences (3A and 4A, see Table 5-3 and Figure 5-3) yielded zero or slightly negative δ values from the time 0.152 ranges (258 Å) had been sputtered (in the 3A sequence), through to the end of the more extensively irradiated 4A experiment, in which a total of 0.578 ranges (983 Å) was sputtered off with the 130 keV beam. By contrast, for the Fluorite-1 single crystal target, $\delta(^{40}Ca/^{44}Ca) = -2.0‰$ was observed by the time 0.291 ranges (495 Å) had been sputtered, and this decreased further to -3.8‰ for the next 0.052 ranges (88 Å) sputtered; the Fluorite-1 2A sequence was therefore not as extensive

as the one polycrystalline experiment, but yet yielded significantly negative δ values at times when the polycrystalline sample was yielding $\delta \approx 0$. It should be cautioned that since no SEM photography of the Fluorite-1 target was made after the 2A sputtering sequence, no assessment can be made of whether cratering was present as extensively as for the polycrystalline sample. If the surface of the Fluorite-1 sample was less extensively blistered and cratered than the surface of the polycrystalline sample, one would perhaps prefer to explain the $\delta \approx 0$ results of the latter as being from catcher tube "contamination" with bulk, crater-erupted material. However, the SEM photographs discussed earlier in this chapter included some for the Fluorite-1 sample after a different experiment (3B); these figures showed that there were large quantities of micron-sized blisters plus larger areas where many of these blisters "flaked" off of the surface (see Figure 5-14c). For the more extensively sputtered 2A sequence presently under discussion, it is then reasonable to suppose that the radiation damage of the surface was at least as severe as in the 3B experiment. Indeed, there is no reason to think that the surface damage was not similar to that seen in the polycrystalline fluorite photographs. Furthermore, although the S_{Ca} sputtering yields were somewhat higher for the polycrystalline target, this was observed even during the earliest bombardments, and is therefore thought to reflect a real difference in yields, rather than the added presence of blister-erupted material. As was pointed out in an earlier section, the one exception to this for 130 keV sputtering was the

3A-3 point, but since it falls in an intermediate dose range with the points for 4A-2 and 4A-3 plotting farther along the abscissa of Figure 5-3, it can be discounted without consequence. In the discussion below, then, the isotopic differences between the single crystal and polycrystalline fluorite sputterings will be treated at face value as arising from something more fundamental than blistering.

The first thing that should be pointed out is that negative $\delta(^{40}Ca/^{44}Ca)$ values for the sputtered material are incompatible with a simple diffusion-equation description of atomic mixing if isotopic equilibrium can eventually be established. If the diffusion coefficient and boundary conditions are constant, the diffusion equation cannot yield "underdamped" solutions for the sputtered fractionation as a function of time, solutions which start out positive, go negative, and then return to zero. With different boundary conditions, the diffusion equation can yield physically meaningful solutions which are "underdamped" and overshoot the steady-state value. Such solutions are analogous to those for thermostatically-controlled room heating systems (cf. Carslaw and Jaeger, 1959). In such cases though the boundary conditions are time-varying and excite solutions with a similar behavior. In the present problem, the only ways such modes could be excited are if the net isotopic fractionation factor at the surface were not a constant like $(m_1/m_2)^{1/4}$, but varied with the isotopic composition of the surface, or if the diffusion constant D could vary with isotopic

composition. (Note that this latter case was treated above to some degree in connection with the discussion of Figure 5-20. There it was seen that a relatively high frequency pulsed type of variation of D with time could not produce a solution which yielded $\delta < 0$ for some times.)

From the above considerations, it can be seen that if the negative δ values observed for the 130 keV experiments have arisen from something more fundamental than blistering, then (a) the diffusion equation of Haff et al. (1977b) does not accurately model the real physical situation, or (b) the net surface fractionation factor is not constant, or (c) atomic mixing near the surface does not proceed at a constant rate (D varies). Because of (b) and (c), it would be useful to investigate analytically whether such variations still permit an equilibrium with $\delta = 0$ to be achieved.

The possibilities raised in the last paragraph will perhaps become better defined with some further theoretical work in the area of mixing processes. It is not yet clear why, in the present set of experiments, the single crystal sample yielded negative fractionation values while the polycrystalline samples did not. This will be further discussed below. However, additional experimental evidence using other single and polycrystalline samples and other minerals would be most useful in confirming and extending the observations of negative fractionation during sputtering with a single beam energy. Isotopic, as opposed to elemental, fractionation studies will be potentially quite useful in research into mass fractionation and

mixing mechanisms. For such measurements, a few per mil isotopic fractionation is a big number well outside of experimental uncertainties (for calcium), whereas few per mil changes in elemental fractionation are not resolvable with current state-of-the-art techniques other than isotope dilution.

The above discussion pointed out some possible implications of the negative $\delta(^{40}Ca/^{44}Ca)$ values which arose from the 130 keV sputtering of a fluorite single crystal. It is now interesting to speculate about the reasons a similar negative δ pattern was not observed for the polycrystalline fluorite sample as well. Two possible mechanisms will be discussed here, the first of which, though, does not appear to be adequate for the present context. This deals with the possibility of having a significant degree of channelling of the primary ions which bombard the single crystal. The target mounting arrangement was not rigidly controlled so as to have the (111) bombarded surface exactly perpendicular to the beam, but it is still reasonable to suppose that appreciable fractions of the ion energy could have been focussed into collision cascades along the two sets of (112) planes which perpendicularly intersect the surface. (This is referred to as the $\langle 111 \rangle$ direction.) If this was indeed the case, then the collision cascades would have extended on average much deeper into the target for the Fluorite-1 sample than for the polycrystalline sample. In the polycrystalline sample, the individual crystals could not be identified under low magnification using reflected light, and have therefore been estimated to have typical sizes no larger than

$\sim$100 μm; therefore, any channelling effects in these randomly oriented crystals were quite probably negligible because of both the large number of individual, randomly-oriented crystals and the relatively large size of the beam. (From the Figure 5-11b view of the unpolished floor of a large pit in the surface of this sample, it appears that the small grains making up the surface are actually individual, equigranular microcrystals 0.2 μm in diameter.) With some appreciable fraction of the ion energy channelled deep into the Fluorite-1 target, there would have been a lesser number of random collision cascade participants near the surface and therefore slower rates of atomic mixing near the surface. However, this means that the sputtering rate would be proportionately lower, too, so that the amount of calcium mixing per sputtered calcium atom is the same regardless of channelling. Therefore, it does not appear that channelling could have affected the fractionation patterns. Additionally, the high bombardment doses, for example $6.3 \times 10^{16}/0.26$ cm^2 for 2A-1, likely turned the lattice structure near the surface into an amorphous state. These doses are comparable to those of Bibring et al. (1974), who found that 10^{17} cm^{-2} doses of 12 keV He were sufficient to produce amorphous rinds $\sim$800 Å thick in minerals such as pyroxene.

An alternate mechanism considers the possibility that the diffusion constant appropriate for mixing (see eq. 6 above) decreases as the lattice structure is damaged and changed into an amorphous state down to a depth of perhaps 1700 Å. This decrease would cause a decrease in the rate of mixing of unfractionated material into the

top few monolayers, causing more-negative δ values to be observed. This mechanism implies that with further sputtering, an isotopic equilibrium consistent with the lower mixing rate will eventually be established. Therefore, if the change in D, considered here for simplicity to be a step function change, occurred near the time when isotopic equilibrium was originally being reached, further sputtering would cause values of $\delta < 0$ to be observed until a new equilibrium with $\delta = 0$ was reached. From Table 5-3, it is reasonable to suppose that sputtering a fresh fluorite crystal with twice the 130 keV flux used for 2A-1 and 2A-2, i.e., $6.4 \times 10^{17}/0.26$ cm^2 or 2.5×10^{18} cm^{-2}, would be sufficient to reestablish isotopic equilibrium.

The suggestion might be made that the single crystal could have had a "Wehner spot" pattern (Wehner, 1955) with a large fraction of the material in a spot at $\sim 0°$ from being lost from the far end of the catcher tube. If this material were isotopically light (see the discussion below on angular fractionation effects), then the calcium which <u>was</u> collected could have been isotopically heavy even though isotopic equilibrium had been established. However, it is probably true that any such marked anisotropies had been removed well before the time the eventual ion beam dose of $10^{17} - 10^{18}$ cm^{-2} had been reached. Also, such an explanation is inconsistent with the progression of $\delta(^{40}Ca/^{44}Ca)$ towards more and more negative values in the 2A sputtering sequence; achievement of a constant negative, or increasingly <u>less</u> negative, value would instead have been expected.

<u>Isotopically-Heavy Surface Layer Depth</u>. On an earlier page

an attempt was made to calculate, using a simple model of the transport of unfractionated material within a target, the approximate depth Δx to which the isotopically heavy surface region extended. In two cases, attempts were made to directly sample material from the surface regions by sputtering with an ion beam the energy of which was adjusted so that the range was small compared to a reasonable pre-experiment guess for Δx. The above calculations of Δx were not very believable, but were also smaller than the $\sim$500 Å range of the lower energy 100 keV N_2 beam used for probing the surface regions. Accordingly, if significantly "heavy" ($\delta < 0$) calcium were observed in the subsequent lower energy measurements, it would confirm the presence of a "heavy" region at least as thick as the sum of the beam range plus the depth to which the sputtering progressed. On the other hand, a $\delta(^{40}Ca/^{44}Ca) \approx 0$ measurement would have two possible interpretations. One would be that any isotopically heavy surface region either did not exist or else that it had a thickness smaller than this sum. The other possibility would be that the positive fractionation of the material sputtered cancelled the negative fractionation that was present in the surface layer, causing a net $\delta = 0$ to be observed. If the isotopically heavy layer established at 130 keV was many times thicker than the mixing range at 50 keV/N, then sputtering an appreciable fraction of it would introduce <u>no</u> additional fractionation (cf. Figure 5-20). However, if the mixing depth at 50 keV/N is, for instance, only a factor of three less, then sputtering two thirds of the isotopically heavy layer will

cause an added positive fractionation perhaps as large as ∿8‰ (Figure 5-20 value at 800 sec).

The two 50 keV/N measurements, 2A-4 and 4A-4, followed extensive 130 keV bombardments of the Fluorite-1 single crystal and of the polycrystalline fluorite samples, respectively. While in the former case a large negative fractionation was observed from the low energy bombardment, in the latter case essentially no fractionation was observed. For the Fluorite-1 experiment, then, the existence of an isotopically heavy surface layer at least 500 + 485 ≈ 1000 Å thick appears to have been confirmed. This is much larger than the estimates for Δx above, and is comparable to the 500±250 Å projected range of 50 keV/N ions in fluorite. On the other hand, the polycrystalline measurement showed no fractionation when an apparent depth of 500 + 830 ≈ 1350 Å was probed. Taken at face value, this indicates that Δx was not nearly so large in the polycrystalline case. It does not seem likely that the fractionation of the surface in the polycrystalline case could have been very much smaller than for the single crystal sample, causing any fractionation added by the 50 keV/N step to have cancelled out the effects in the polycrystalline case only. In an earlier section of this chapter where the calcium sputtering yields were discussed in detail, the possibility was raised that the 4A-4-N section of the catcher tube might have been seriously contaminated. It was shown though that even if this had been the case, the effect on the total $\delta(^{40}Ca/^{44}Ca)$ = -0.3‰ value would have been inconsequential, amounting to -0.4‰ or less.

Therefore, if the contamination were indeed a problem, the consequences for the above statement about the polycrystalline Δx value would be minimal; in that event, the polycrystalline fluorite measurement showed no fractionation when an apparent depth of $500 + 230 \approx 750$ Å was sputtered. (The 230 Å figure was computed from the 0.97 ranges sputtered in the Fluorite-1 2A-4 experiment, adjusted for sputtered area and beam dose differences.) In either case, for the polycrystalline fluorite sample where $\delta \approx 0$ isotopic equilibrium had apparently been established during the 130 keV bombardment, there is no evidence for the establishment of an equilibrium isotopically heavy layer of thickness comparable to the 1700 Å ion projected range. In contradistinction to this, for the Fluorite-1 sample, it is not clear that an equilibrium was reached, but a 1000 Å-thick isotopically heavy layer was observed.

This difference is a puzzling result. The more extensive bombardment of the polycrystalline target (0.58 as opposed to 0.34 ranges sputtered off) did not apparently establish nearly so thick a surface layer. As there is a great deal of confidence in the two measured $\delta(^{40}Ca/^{44}Ca)$ values, a non-trivial explanation for the differences should be sought. One possibility deals again with the channelling of the primary ions and the existence of focussed collision cascades, but, unlike before, it might still be operative even after the surface region has become amorphous. This idea has also been mentioned by Winterbon et al. (1970), and is vaguely similar to that of "anomalous diffusion" along channelling directions (cf.

Kornelsen et al., 1964). Suppose that some relatively low energy collision cascade calcium atoms receive their energy near the current bottom of the amorphous layer and enter into a channel. The likelihood that they will not be dechannelled immediately is proportional to the angular range of acceptance for that channel. This is shown below to be quite large. If these atoms are not dechannelled, they could then quite conceivably be transported deep into the target. Furthermore, having originated in the amorphous region which is mixed to some extent by the random collision cascades, this material could well be isotopically heavy. This scenario could then account for a deeper isotopically heavy layer in the single crystal target. Other reasons why the model is unrealistic may come to light, but the calculation below shows that the $\langle 111 \rangle$ (and other) fluorite channels do in fact have rather large angular acceptance ranges.

The angular range extends from zero degrees (perfect alignment with the channel) to a critical angle Ψ_{crit}, estimates for which have been given by Lindhard (1965; see also Van Vliet, 1973). Define E' by

$$E' = \frac{2Z_1 Z_2 e^2 d}{a^2} \tag{9}$$

where Z_1 is the nuclear charge of the particles entering the channel, Z_2 is the average nuclear charge of the target atoms, d is the spacing between lattice rows along the channelling direction, and a is the Thomas-Fermi screening distance, commonly defined as

$$a = \frac{0.885\ a_0}{\left(Z_1^{2/3} + Z_2^{2/3}\right)^{1/2}} \tag{10}$$

with a_0 being the Bohr radius, 0.53 Å. The above equation can be written in a more convenient form by replacing $e^2/2a_0$ by the Rydberg energy, E_R, which is 13.6 eV. Then

$$E' = \frac{4Z_1 Z_2 a_0 d E_R}{a^2} \tag{11}$$

There are two formulas for Ψ_{crit}, depending on the energy E of the particles entering the channel:

$$\Psi_{crit} = \left[\frac{\sqrt{3}\, a}{d}\left(\frac{2Z_1 Z_2 a_0 E_R}{Ed}\right)^{1/2}\right]^{1/2} \quad (E < E')$$

and (12)

$$\Psi_{crit} = \left(\frac{4Z_1 Z_2 a_0 E_R}{Ed}\right)^{1/2} \quad (E > E')$$

For fluorite, it can be shown that the spacing between lattice rows along the $\langle 111 \rangle$ channelling direction is 5.46 Å (the lattice parameter) divided by $\sqrt{3}$. This can be demonstrated by using an Euler angle transformation matrix to find the coordinates of the calcium and fluorine atoms in a system where two of the axes are in the (111) plane; the projection of these coordinates perpendicular to the plane then can be found by inspection. Ψ_{crit} can now be evaluated, using

$$\begin{aligned} Z_1 &= 20 \quad \text{for the Ca cascade atoms} \\ Z_2 &= \tfrac{1}{3}(20 + 9 + 9) = 12.667 \\ E &= 50 \text{ eV} \quad \text{for the cascade atoms} \end{aligned} \tag{13}$$

Calculating E' = 1.3 MeV, it can be seen that the first of the two formulas for Ψ_{crit} should be used. The result for 50 eV cascade atoms

is then found to be $\Psi_{crit} = 34°$.

A simpler and more appealing mechanism than that above postulates that the very large values of Δx are not caused by cascade-driven mixing, but rather are the results of diffusion over short distances caused by low-grade target heating by the beam. If the single crystal was even only moderately hotter (as little as 70°C) during its bombardment than the polycrystalline sample was, then the differences in Δx could be caused by differences in the diffusion constant, which varies exponentially with temperature. To see this, the length over which appreciable amounts of calcium could have diffused will be estimated, using as the diffusion coefficient the values experimentally determined for radioactive ^{45}Ca diffusing in Ca polycrystalline metal (CRC Handbook, 1972, p. F-48). The diffusion constant is $D = 1.4 \times 10^{-17}$ cm^2 sec^{-1} for a 200°C target, $D = 2.7 \times 10^{-15}$ for a 270°C target, and $D = 1 \times 10^{-10}$ for a 500°C target. The characteristic diffusion length L is $\sqrt{4 D T}$. For the typical sputtering times T of 10^4 sec, it may be calculated that

$$L = \begin{cases} 75 \text{ Å} & \text{for a 200°C target} \\ 1000 \text{ Å} & \text{for a 270°C target} \\ 2 \times 10^5 \text{ Å} & \text{for a 500°C target} \end{cases} \qquad (14)$$

It is therefore quite conceivable that appreciable fractions of isotopically heavy calcium could have diffused from the surface to depths of 500 - 1000 Å even if the substrate temperature was relatively low, $\lesssim$ 270°C. Of course, the diffusion constant in fluorite will be

somewhat different from that in calcium metal, but this is not likely to be of importance to this argument. If in fluorite the diffusion distances actually were 500-1000 Å, then a diffusion coefficient lower in polycrystalline material by a factor of 4 or more would have decreased Δx by at least a factor of 2. However, it seems much more likely that the differences in Δx between these two samples were caused by small temperature differences arising from small differences in the beam current densities (see Table 5-3). This can be checked in future work by using a liquid-nitrogen-filled cold finger to keep the target cool.

It should be noted, however, that the previous discussion of the solutions to the diffusion equation still seems to be valid. It therefore does not appear possible to explain the negative δ values observed during the 130 keV sputtering solely on the basis of a slightly hotter target and a longer characteristic diffusion length.

Summary. The main points raised in this section on atomic mixing and isotopic fractionation of calcium during sputtering were: (a) quite large, systematically-varying isotopic fractionation of calcium is observed during sputtering with moderately-high-energy nitrogen beams; (b) the first calcium which was removed using 130 keV nitrogen doses of $\sim 10^{17}$ cm^{-2} was fractionated by +11‰ to +13‰ ; (c) the first calcium removed from fresh targets using 100 keV molecular N_2 beams was unfractionated for fluorite; a similar dose for the plagioclase sputtering removed far fewer calcium atoms, and the fractionation observed was +21‰ ; (d) positive initial fractionations

may be observed during sputter-removal of a few monolayers from a target, even if no atomic mixing is present; (e) the results are consistent with mixing having been present and important in controlling the isotopic fractionation patterns; (f) the characteristic times for mixing may be rather long, implying that an isotopically fractionated surface region would have a decreasing, rather than approximately constant, fractionation as a function of depth; (g) a simple diffusion-equation description of atomic mixing in the target appears to be inadequate in describing the negative isotopic fractionations observed during single-energy sputtering sequences; (h) differences in the isotopic results obtained during such sputtering of polycrystalline and single fluorite targets do not appear to be from any experimental problems; a possible mechanism based on the changing of the single crystal's lattice into an amorphous form was advanced in order to explain why similarly negative $\delta(^{40}Ca/^{44}Ca)$ values were not observed in both cases; (i) a channelling-type of mechanism and a diffusion mechanism involving small target temperature differences were alternatively proposed in order to account qualitatively for the apparent difference observed for the thicknesses of the isotopically heavy surface layers in the crystalline and polycrystalline samples.

Previous Observations of Isotope Fractionation from Sputtering

Very few observations of sputtering-induced isotopic fractionation have been reported in the literature. The first paper on the subject was by Fluitt et al. (1961) who attempted to measure

the fractionation, if any, of lithium sputtered from lithium metal targets using 5 keV to 20 keV ^{40}Ar beams of 20 to 100 μA intensity. The purpose of their search was to provide information about whether sputtering was primarily an evaporative process, which would lead to isotope fractionation, or a "momentum interchange" process, which was thought would not lead to large effects. Using Ar doses of 10^{17} cm^{-2}, ∿18‰ relative enrichments in $^{6}Li/^{7}Li$ were observed. However, these results are far from convincing insofar as demonstrating whether the Li was truly fractionated. Fluitt et al. (1961) provided no numerical estimate of the precision of their results, and instead simply referred to the ∿6‰ fluctuations in the tabulated analyses. Lithium is very hard to analyze precisely since it is subject to substantial instrumental fractionation, even in multiple-filament thermal ionization sources such as used by Fluitt et al. For this reason, it seems particularly serious that these workers did not attempt to handle some of their standards in a fashion similar to the sputtered samples: there is no indication that the standards were analyzed in the 0.1 μg quantities used for the sputtered samples. With no further documentation of the analytical precision and of the reliability of their methods in minimizing fractionation biases between samples and standards, these results should be considered to be inconslusive.

The next paper on this subject, by Arai et al. (1976), dealt with isotopic fractionation of sputtered magnesium, although it has not been demonstrated that Mg is fractionated in lunar soils. The

Mg was deposited on mass spectrometer filaments and then sputtered *in situ* using ~35 $\mu A/cm^2$ 2.1 keV H^+ beams and total doses of 10^{18} cm^{-2}. The fractionation of the Mg remaining on these filaments was then measured. For reasons which are not clear, Arai *et al.* (1976) used an ion-counting mass spectrometric technique, even though the pre-sputtered samples contained ~4 μg of magnesium and should have easily yielded large, stable ion currents. In estimating analytical uncertainties, only $\sqrt{N}$ counting errors were considered. However, 130‰ deviations in $^{24}Mg/^{25}Mg$ *corrected* ratios were observed by these workers in seven analyses of a single Allende meteorite sample (Kobayashi *et al.*, 1975), indicating other very large systematic errors in the technique. With one-sigma error bars, it appeared that there was perhaps a mass fractionation effect of $\delta^{26}Mg$ = -50 to -90‰ , but with more realistic 2σ error bars, the measurements are found to be consistent with $\delta = 0$.

Wehner (1977; Wehner *et al.*, 1977) reported substantial isotopic fractionation in Mo, Cu, and U sputtered by a 100 eV Hg^+ plasma created in a triode discharge. (These two papers will be referred to collectively as Wehner, 1977a,b.) Isotope measurements of the sputter-removed material were carried out by outside vendors using Secondary Ion Mass Spectroscopy (SIMS) for Mo and Cu and standard mass spectrometry for U. Tantalum strips were used to collect material sputtered over a wide angular range and were cut into three sections, giving one isotope fractionation measurement at 0° (perpendicular exit from the target) and two at similar oblique angles.

For Mo, the many isotopes enabled a determination that the fractionation was approximately linear in the mass difference. There was a ∿70‰ decrease in $^{92}Mo/^{100}Mo$ from normal to oblique exit, with the oblique material having a composition close to normal. For Cu, the $^{63}Cu/^{65}Cu$ decreased by ∿9‰ from normal to oblique exit. The Wehner et al. (1977) paper on uranium reported changes in ^{234}U and ^{235}U atomic abundances. From these, $^{234}U/^{238}U$ and $^{235}U/^{238}U$ ratios may be deduced. The analytical precision for the measurement of these ratios was ±18‰ and ±2‰ , respectively. The $^{235}U/^{238}U$ ratio decreased ∿24‰ from normal to oblique exit, with the normally ejected material about 19‰ lighter and the obliquely ejected material 5‰ heavier than normal. Wehner (1977a,b) did not attempt to follow any changes in the isotope ratios with increasing sputtering doses, and did not provide information as to the amounts of material sputtered or the integrated Hg doses used. It was stated that the films deposited by the sputtering were at least several microns thick. Although the SIMS instruments did not provide uniform sensitivity for all isotopes (Wehner, 1977) the changes in the isotope ratios between the normal and oblique exit samples, as well as the use of standard mass spectrometry techniques for the U analyses demonstrates that the observations were real and apparently not caused by experimental artifacts.

Wehner (1977a,b) did not provide estimates for the extent of the angle-integrated fractionation. Since it is not clear how extensive the sputtering was, a rough estimate of the total Hg doses

used in the sputtering will be given here and based upon stated geometric parameters. Taking a deposited Cu film thickness of 3 μm (Wehner, 1977) and the surface area the Ta strip would have had had it covered a full 2π solid angle, then by assuming for simplicity an isotropic deposition of sputtered material, a calculated total of 0.27 gm or 2.5×10^{21} atoms of Cu is obtained. Wehner (1977) lists the 100 eV Hg sputtering yield of Cu as 0.15, so this implies a total Hg bombardment dose of 1.7×10^{22} atoms or $9.6 \times 10^{21}/cm^2$ (the Cu targets were 1.5 cm in diameter). The amount of copper sputtered formed a layer on the original target 170 μm thick. Wehner's sputtering results therefore give the isotopic patterns that are formed after extremely extensive bombardment. It is then likely that the fractionation results, when integrated over all angles of ejection, would have given $\delta = 0$. Without any SEM photographs or other evaluation of the condition of the sputtered surfaces after these bombardments, the question should be raised as to whether the fractionation is from the sputtering itself, or is influenced strongly or even dominated by radiation damage of the surface. Very little is known about blistering and other forms of radiation damage at low energies (Behrisch, 1972). For Hg sputtering, blistering probably does not occur, although lattice defects are surely produced since appreciable sputtering does occur. Rough surfaces might also conceivably develop.

Wehner (1977) has proposed that the angular fractionation is caused by kinematic effects. For very low energy sputtering,

relatively few collisions can be involved. "Direct reflection" of lighter isotopes or elements at the surface off of heavier ones immediately beneath could lead to their preferential sputtering normal to the surface (Wehner, 1977). Olson and Wehner (1977) and Wehner et al. (1977) have observed similar elemental effects during low energy sputtering of various alloys. For high energy sputtering, it has been considered that the more extensive collision cascades would cause a dilution of the contribution of directly reflected atoms to the sputtering yield, thereby minimizing or eliminating any angular fractionation effects (Wehner, 1977).

In summary then, the Li and Mg fractionation results are inconclusive because of a lack of analytical sensitivity. Wehner (1977a,b) has reported large, and apparently real, angular fractionation effects in Mo, Cu, and U after very extensive sputtering. It is unclear how radiation damage may have affected the results. If the fractionation observed is really that produced by the sputtering itself, it would represent the fractionation occurring at isotopic equilibrium. It is not stated by Wehner whether or not the angle-integrated results are then consistent with a $\delta = 0$ isotopic equilibrium. The state of affairs before the calcium work described here was undertaken was therefore considered to be poorly characterized and in need of more definitive demonstrations as to what effects really existed and were caused directly by sputtering.

To learn more about whether the sputtering itself produced the angular fractionations reported by Wehner, a series of measurements

of δ as a function of ejected angle were made during the calcium experiments.

Angular Variations of Calcium Isotopic Fractionation and of Sputtering Yields

In interpreting the differences in the $\delta(^{40}Ca/^{44}Ca)$ values and in the sputtering yields observed for different sections of the catcher tubes an assessment first needs to be made of whether the observed values truly reflect the fractionation of the calcium coming from the target in the inferred direction. Specifically, the possibility exists that some of the calcium might first strike one section of the catcher tube but not "stick," thereby ending up on a different section. For the cylindrical geometry of the catcher surfaces used in this experiment, a variation in the sticking fraction of calcium incident at various angles onto stainless steel would cloud the interpretation of the results as the true variation of $\delta(^{40}Ca/^{44}Ca)$ with angle of sputtering ejection. In order to determine if there are indeed such variations in the relative calcium sticking fractions, they could be measured by sputtering a series of fresh targets, catching the sputtered calcium on flat surfaces inclined at various angles. However, it does not appear as if the effective sticking fractions in the present experiments could have varied significantly with angle. This is because the inside surfaces of the catcher tubes were not polished, and hence were rough on an atomic or even a micron scale. A sputtered atom striking this "mountain range" would therefore have a range of angles

of incidence independent of the macroscopic ejection angle. It is therefore quite likely that the trapping probabilities were uniform and independent of ejection angle.

Sticking fraction problems have not only the potential of disturbing the angular fractionation measurements, but the angle-integrated $\delta(^{40}Ca/^{44}Ca)$ results as well. This could occur if the calcium bounces or is desorbed one time or several times within the catcher tube in such a way as to finally exit from the end opposite the target. If this occurred to any significant degree in the present experiment, the measured calcium sputtering yields would have been lower than the actual values and the δ values might have been biased somewhat, probably a little heavier than the true values. However, it is very important to emphasize that the changes in the measured δ values with progressive sputtering clearly demonstrate that the isotopic fractionation of the sputtered material was changing. In addition, the eventual attainment of $\delta \approx 0$ for the polycrystalline fluorite experiments appears to show that any bias present was at the level of less than 1‰ .

Trapping Probabilities for Other Elements. In the absence of calcium sticking fraction data, it is appropriate here to briefly mention results observed for other elements. These results suggest that the Ca trapping probabilities were quite high in the present experiments. Measurements by Griffith et al. (1978) of the sticking fraction of ^{235}U sputtered by 80 keV ^{40}Ar onto aluminum indicate that 97% of the ^{235}U sticks to the catcher surface. Measurements of

the sticking fraction of ^{235}U as a function of energy have been attempted (R. Weller, private communication); preliminary results show a sticking fraction of 95% at 1 eV, 90% at 2 - 3 eV, and a rise toward 100%, which was measured at 29 eV. As 30% of the ^{235}U sputtered had energies between 1 eV and 10 eV (see Figure 15 of Weller, 1978), which is the energy range corresponding to the minimum sticking fraction, the possibility persists that calcium may be similarly affected. However, a 90% Ca sticking fraction appears high enough to have avoided any serious difficulties. The U measurements were carried out under conditions in which the sputtered uranium struck the first catcher surface perpendicularly. That which did not stick was deposited upon a second catcher, and the relative proportions on each were measured. These measurements are presently unable to provide information about sticking probabilities when the sputtered material strikes the first catcher surface at other angles.

Some work on the sticking fractions of alkali metal atoms sputtered from targets in a charged state (Hurkmans et al., 1976a,b) has shown that in these cases, sticking fractions do vary with the angle of incidence. However, the measurements were carried out at the elevated surface temperature of 1200°K for the tungsten catcher surfaces used; this was done to ensure a high ionization efficiency of ∿95% for the sputtered atoms when they left the tungsten surface. The elevated surface temperature makes it impossible, in view of the lack of adequate models for trapping probabilities, to relate the data of Hurkmans et al. (1976a,b) to trapping probabilities at room

temperature, which was used for the catcher surfaces in both the Ca and U experiments.

It is not yet clear how sticking fractions change as appreciable concentrations of the sputtered species collect on the catcher surface. M. Weller (personal communication) has attempted to measure such changes during the sputtering of Nb, but the experimental uncertainties do not at present permit a firm conclusion, as the effects would be expected to be reasonably small, on the order of 10% perhaps.

In the absence of definitive information about sticking fractions for calcium, the angular sputtering yields and $\delta(^{40}Ca/^{44}Ca)$ measurements will be discussed here with the possibility in mind that the trapping probabilities may not have been unity at all energies. Future work on calcium sticking fractions may be able to provide a firm estimate as to whether this can cause a major or minor perturbation of the true angular variations. At the present time, it does not appear to be a source of major difficulty. Also, it is demonstrated below that the present data definitely reveal the presence of large changes in $\delta(^{40}Ca/^{44}Ca)$ with the angle of sputter ejection.

Angular Variations of Sputtered Ca Yields. Shown in Figure 5-7 are the fractions of the total collected calcium which were found on each of the three segments of the separable catcher tubes. These separable tubes were used during only one of the polycrystalline fluorite sputtering sequences, but provided three sets of measurements

during the course of this bombardment. Although each section spans a large angular range, a rough idea of the angular distribution can still be gained from the three angular ranges for which yields were measured during each of the collection intervals. Contained also on the plots in Figure 5-7 are shaded areas corresponding to calculations of what the sputtering yields for each of the catcher sections would have been had the sputtered material been ejected from the target with a cosine-raised-to-a-power angular distribution. It should be noted that sputtering theories have to date not provided firm predictions of the angular distribution of sputtered material. Therefore, a few of the experimental determinations of angular distributions of sputtered material will be mentioned here. For 100-1000 eV Hg incident on various heavy metals, Wehner and Rosenberg (1960) found "under cosine" patterns, meaning relatively more (less) material was sputtered at large (small) angles than given by a cosine distribution. (If the observed distribution can be approximated by $\cos^{\nu}\alpha$ for some fixed power ν, then "under cosine" refers to a value in the range $0 < \nu < 1$.) For 5-10 keV Ar or Kr incident on Au, Patterson and Tomlin (1962) found "over cosine" patterns. Their distributions can be fit reasonably well by various powers of $\nu > 1$, providing that angles larger than $\sim 70°$ are not considered; for larger angles, the Patterson and Tomlin data approach a cosine distribution. Fits of the Patterson and Tomlin data with $\cos^{\nu}\alpha$ require increasingly larger values for ν, up to 1.5, for the more extensive bombardments. Gregg (1977) has shown that for 40-50 keV H^+ and H_2^+, and for

120 keV He^+, the uranium sputtered by these beams has a very flat angular distribution, which he approximately fit using $\nu = 0.25$. The shaded areas in Figure 5-7 therefore have been chosen to span the range of ν which was thought likely to include the value or values appropriate for these calcium experiments; the range 0.25 to 5/3 (an arbitrary value larger than the maximum for the Patterson-Tomlin data) was then chosen. Defining θ_1 and θ_2 as the angular limits of a catcher tube section, and Ψ_1 and Ψ_2 as the angular limits of the entire catcher tube, then Figure 5-7 shows in the shaded regions the values taken on by

$$F \equiv \int_{\theta_1}^{\theta_2} \cos^{\nu}\alpha \, d\alpha \Big/ \int_{\Psi_1}^{\Psi_2} \cos^{\nu}\alpha \, d\alpha \qquad (15)$$

for the range of ν values. In Figure 5-7, the arrows between the two 130 keV plots indicate that F increases as ν increases for the two lower-angle sections, and decreases as ν increases for the high-angle (obliquely sputtered material) section.

Comparison of the measurements with the shaded areas in Figure 5-7 shows that no single power ν provides a good fit to the data. Larger powers appear more appropriate for the low-angle measurements and intermediate values more appropriate for the high-angle data, while no value adequately fits the intermediate-angle data. More calcium was found on two of the low-angle (normal ejection) sections than is "predicted" by cosine distributions with any reasonable power ν. Less material was found on each of the middle

sections than is expected from the calculations. For the two 130 keV plots, a range of F values around the values measured for the high-angle section was obtained. The dashed lines in the 100 keV plot in Figure 5-7 show the results of assuming that all but 1.4 μg of the calcium on the low-angle section was non-sputtered contamination from blister eruptions or some other source. (A detailed assessment of the likelihood of this was made in an earlier section of this chapter.) In either case, the 100 keV measurements show a deficiency in the middle section with respect to the calculated values. These results are compatible with two alternate interpretations: (a) the sputtered material did not follow a $\cos^{\nu}\alpha$ pattern; (b) the collected material was redistributed, because of sticking fractions less than unity, from the middle- and perhaps the high-angle sections to the low-angle section.

As an aside, Figure 5-21 is a plot of the angular cosine distributions integrated from zero to some angle θ, as normalized by the distributions integrated from zero to 90 degrees (Ψ values of 5-72° and 5-66° were used for the normalizations in Figure 5-7). If the sputtered calcium does indeed follow a $\cos^{\nu}\alpha$ distribution, Figure 5-21 can be used to easily find the fraction of material sputtered between angles θ_1 and θ_2 by subtracting the ordinate value corresponding to θ_1 from that corresponding to θ_2.

Angular Variations of Sputtered Ca Fractionation. Three things are convincingly demonstrated by the angular variations in $\delta(^{40}Ca/^{44}Ca)$ shown in Figures 5-4, 5-5, and 5-6. First, it is

clear that there are real variations of δ with the angle of sputtering ejection. The differences of up to 16‰ in the fractionation of the calcium found on the low- and high-angle sections are so large that it is wholly unrealistic to suppose that they could be accounted for solely by trapping probabilities less than unity which are isotope-dependent. Second, it may be seen that the change in the angular fractionation pattern from that of Figure 5-4 to that of Figures 5-5 and 5-6 is sufficiently large to clearly show that the angular fractionation patterns can change during the course of a sputtering bombardment in ways other than by shifts only in the absolute numbers, shifts which otherwise leave the patterns unchanged (Figures 5-5 and 5-6). The difference in fractionation between the two higher-angle sections is 3‰ larger in Figure 5-5 than in Figure 5-4. Even more striking though is the fact that the low-angle section is 4‰ heavier than the middle section in Figure 5-4, but 3.6‰ lighter in Figure 5-5. There is no basis for an explanation of these changes in terms of sticking fractions which are not only isotope-dependent but also dependent upon any minor differences in catcher surface roughness characteristics which may have been present. Third, it is interesting to observe that when $\delta \approx 0$ isotopic equilibrium is achieved, the angular pattern (Figure 5-5) is not one in which $\delta = 0$ is observed at all angles. These main observations appear to be assignable directly to the sputtering process itself and not to any subsequent redistributions on the catcher surface.

If isotopic equilibrium is to be reached, the angular

fractionation must also achieve an equilibrium pattern. The similarity of the fractionation patterns in Figures 5-5 and 5-6 suggest that an equilibrium pattern was indeed obtained, one in which "heavy" Ca is found at oblique angles and "light" Ca is found where the material is sputtered in directions nearer to perpendicular to the target. There is no indication from the data that an angular pattern in which δ is equal to zero at all angles will be obtained with more extensive sputtering.

The observation of extensive isotopic fractionation variations with angle is interesting because it is unexpected on several accounts. Wehner (1977) stated that any kinematic effects leading to the angular variations observed during low energy sputtering should be insignificant at higher energies. The energies used in the present experiments are two to three orders of magnitude larger in energy, and even higher if the energy per mass unit of the incident beam is considered. Second, Wehner et al. (1977) considered the possibility that kinematic fractionations were of small magnitude, and had been amplified through multiple resputtering; the catcher as well as the target was exposed to the Hg plasma. Here, all Ca collected represents a single sputtering, so such amplification was not possible. Third, the sputtered surfaces are rough on a 500 Å scale. It is therefore not clear why angular variations are simply not averaged out for such surfaces. (Note that 500 Å--the beam range of 100 keV N_2--is approximately the distance represented by one of the small checkered marks making up the 510×10^{-9} m bar in Figure 5-10b.) The

basic mechanism behind these angular isotopic fractionation variations therefore remains unknown. It is not clear how kinematic effects could be responsible, and this means either that the low energy observations are caused by something else, or that there are two mechanisms which lead to similar effects in different energy regimes.

Isotope fractionation which varies as a function of angle means of course that the isotopes are sputtered in somewhat different angular patterns. It is interesting to speculate on some of the implications of this. Of particular interest is the peak in the fractionation observed for the middle section of 4A-1 (Figure 5-4). At least two interpretations can be advanced to explain this feature. One is that it is reflective of the fact that the target is polycrystalline rather than amorphous. It is difficult to see how there could have indeed been a preferred orientation of the individual constituent crystals; if there were, it could be argued that a change at the target surface from a polycrystalline to an amorphous state might have caused the change in the angular fractionation patterns seen by comparing Figures 5-4 and 5-5. In such a case, the peaked pattern in Figure 5-4 might reflect an isotopic "Wehner spot" (cf. Wehner, 1955). An alternate interpretation of the Figure 5-4 peaked pattern is that it simply reflects the differences in the angular patterns for the isotopes. If this is true, there is a constraint placed on $\cos^{\nu}\alpha$ distributions which might be used in an attempt to fit the data. Assume that isotope A has the angular

distribution $N_A \cos^{\nu}\alpha$, where N_A is the normalization constant found by requiring that the amount of isotope A which is sputtered is equal to the angular distribution integrated over all possible angles. For isotope B, if the distribution is taken to be $N_B \cos^{\nu+\Delta\nu}\alpha$, where $\Delta\nu << \nu$, then the decreasing-type of isotopic patterns seen in Figures 5-5 and 5-6 can be reproduced reasonably well for suitable ν and $\Delta\nu$ values. However, a peaked distribution such as in Figure 5-4 cannot even be qualitatively reproduced. All this really says is that the differences in the isotope angular patterns cannot be fit initially by different powers of cosines. However, it does suggest that caution should be used in assigning very much significance to $\cos^{\nu}\alpha$ distributions themselves, at least until further theoretical results are in hand.

Whatever the angular distribution functions may be, the possibility is present that they may introduce a unique kind of isotopic mass fractionation function. There is no a priori reason why the differences in the angular distributions should yield fractionations which are linear in the isotope mass difference. Wehner's (1977) molybdenum results showed approximately linear patterns, but the SIMS precision (1‰ claimed by Wehner et al., 1977) was low compared to that which probably can be obtained by mass spectrometry; the SIMS instrument also had a non-uniform sensitivity which decreased with increasing isotope mass (Wehner, 1977). Nonlinearities in the fractionation function may be greater for calcium, which has not only a lower mass but also a larger mass

range (10% change between ^{40}Ca-^{44}Ca and ^{44}Ca-^{48}Ca, as opposed to the 8% change from ^{92}Mo to ^{100}Mo). In the present experiments, the quantities of calcium sputtered were in almost all cases insufficient to permit precision isotopic composition analyses in addition to the double-spiked mixture runs. (Unless at least 1 μg of Ca can be used in the mass spectrometer for a composition analysis, experience has shown that the only beam currents which can be obtained by the present techniques are insufficiently large, stable, and long-lived to permit precision measurements.) Such analyses would have shown whether any large nonlinearities exist in isotopic fractionation caused by sputtering. Only for the 4A-4 catcher tube was enough calcium present on the low- and high-angle sections to have permitted a comparison of any fractionation nonlinearities which were a function of the sputtered angle, but unfortunately this was realized only after the samples had been totally spiked. However, this leaves open the possibility that such comparisons can be made in a few cases in future experiments without extensive revision of the mass spectrometric analysis techniques.

It is interesting to compare the magnitudes of the angular fractionation differences observed for calcium in this work and for Cu, Mo, and U by Wehner (1977a,b); for the Ca data, the comparison will be made on the basis of the "equilibrium" pattern on Figures 5-5 and 5-6, where there is a 16‰ difference between the low- and high-angle sections. For all four elements, the material is isotopically lighter at normal ejection than at more oblique angles. For Ca and U,

the normally ejected material is isotopically lighter than the bulk value while the obliquely sputtered material is also isotopically heavier than the bulk. In contrast to this, the obliquely sputtered Mo and Cu were both reported to have essentially their bulk isotopic compositions. No mention is made by Wehner (1977a,b) of exactly what angular ranges comprised the "normal" and "oblique" catcher surface sections, or of whether this was even standardized in all cases, so it is somewhat difficult, in view of the large change of δ with angle, to compare the magnitudes of the ranges of the angular effects observed for the four elements. Nevertheless, the magnitudes are so different in the four cases as to warrant a comparison even without knowledge of the specific angular ranges used for Cu, Mo, and U. For Ca, there is a 16‰ difference in $^{40}Ca/^{44}Ca$ between the low- and high-angle sections; an alternate way of looking at this is that it is a difference of 4‰ per amu. The $^{63}Cu/^{65}Cu$ differences of 9‰ may be regarded as 4.5‰ per amu; for Mo, the $^{92}Mo/^{100}Mo$ changes of 70‰ are ∿9‰ per amu. The $^{235}U/^{238}U$ decrease of 24‰ may be regarded as 8‰ per amu. The uranium effects, if proven to really be this large, might well prove to be of great technological importance; Wehner's results are for <u>equilibrium</u> which means that a 19‰ enrichment of ^{235}U relative to ^{238}U in the normally sputtered direction may be obtained in a <u>single</u> step. The implications of this for atomic energy appear to be very important and call for confirmation of these results. Sputtering separation may be simpler to implement on a plant-sized scale than existing diffusion or electromagnetic methods. Further

study would be required in order to assess if this method could provide an economically feasible alternative means of uranium enrichment.

Considering how heavy uranium is, it is hard to see at the present time how it could have such extensive fractionation effects. Yet, considering the isotope differences given above for Ca, Cu, Mo, and U in terms of the magnitude of the effects per atomic mass unit, they became larger as the mass of the element was increased. Of course, it may not be quite justified to include calcium in this comparison since the beam energies used were so much higher and resputtering was not possible. Nevertheless, the fact that the fractionation effects do not decrease systematically with increasing mass is a key observation which will have to be included in future theoretical descriptions of the nature of the mechanisms leading to angular variations of isotopic fractionation induced by sputtering.

The Relation of Sputtering Simulations to Lunar Surface Processes

Having demonstrated that large isotopic fractionation of calcium occurs in terrestrial ion-sputtering experiments, it remains to assess to what degree the results provide insight into the real processes which have produced the isotopic fractionation in lunar surface soils.

The accuracy with which the solar wind sputtering conditions on the lunar surface were simulated will first be discussed. The solar wind is composed almost totally of hydrogen (cf. Geiss et al., 1970), with helium being present at the 5% level (Robbins et al., 1970).

Solar wind energies are approximately 1 keV per nucleon mass (cf. Robbins et al., 1970). The present experiments were carried out with nitrogen beams of somewhat higher energies per nucleon mass, being 3.6 keV (for 100 keV N_2) and 9.3 keV (for 130 keV N). Even use of nitrogen beams of 1 keV per amu would cause a departure from lunar conditions in that the sputtering rates are a factor of 20 higher than for 1 keV protons and a factor of 7 higher than for helium, according to calculations for fluorite obtained using the Sigmund formula given in an earlier section. The use instead of heavier beams such as 40 keV argon, often used in sputtering work, results in sputtering rates a factor of 100 higher than for 1 keV protons. As the projected ranges for 1 keV per mass unit H, He, N, and Ar are all about the same ($\sim$80 Å in fluorite), sputtering yields differing by factors of 20-100 could well result in differences in isotopic fractionation patterns. This could come about through differences in the amount of atomic mixing per sputtered atom. For this reason, isotope fractionation sputtering experiments carried out with heavier 1 keV per mass unit beams can provide only qualitative information about the extent of fractionation which would be observed with kilovolt protons. For the higher energy nitrogen beams used in this experiment, the projected ranges are factors of 6 and 20 larger than for 1 keV H; the sputtering rates, though, are only factors of 13 and 7 higher than for 1 keV protons, and factors of 4.5 and 2.5 higher than for 4 keV alphas. As such, the efficiency of atomic mixing within the target may be somewhat closer to that for lunar conditions. This cannot be

demonstrated at the current time though, so again it is best to only use the present data to provide qualitative insight into the fractionation capability of the solar wind. The total sputtering doses of $5.8 \times 10^{17}/0.44$ cm^2 for the 4A polycrystalline fluorite sputtering sequence and $6.5 \times 10^{17}/0.26$ cm^2 for the 2A Fluorite-1 sequence are the equivalent of $1\text{-}3 \times 10^{18}$ ions/cm^2. On the lunar surface, where the flux is 10^8/cm^2-sec (Geiss et al., 1970) a soil grain would have to have a residency time of 300-1000 yr to receive a dose equivalent to this. Soil grains are thought to have much longer surface residency times than this, and so would have received even larger solar wind doses. The beam currents used for sputtering simulations can clearly not be as low as for the solar wind; in these experiments, the rates of bombardment were $0.8\text{-}6 \times 10^5$ times higher than those on the moon. It is possible then that on the moon, the lower particle fluxes might enable the radiation damage produced by the solar wind ions to be annealed out to some degree by the elevated temperatures of the surface. For this reason, it is not clear that blistering could ever be an important factor in the lunar environment. However, since large fractionation of the first calcium sputtered during the simulations was observed, it is clear that blistering is not an integral part of the mechanism producing fractionation during sputtering.

From these various considerations, it appears that the simulation of lunar sputtering conditions was only approximate. Even so, a major conclusion is inescapable: it appears to be highly likely

that sputtering by the solar wind was a major means by which the isotopic fractionation in the lunar soil grains took place. It is difficult to believe that any of the differences discussed above between the lunar and laboratory sputtering conditions could be sufficient to totally eliminate the fractionation of calcium. It seems that since large (20‰ to -10‰) values of $\delta(^{40}Ca/^{44}Ca)$ were observed in the laboratory, similarly large effects could be produced by the solar wind. However, this cannot be directly verified by the present results. In Chapter 4, measurements of calcium fractionation in a lunar soil were presented and discussed. It was shown that calcium is isotopically fractionated in this lunar soil, which had been shown by other workers to have large O, Si, and S effects. However, it was not definitively established that the 4‰ fractionation of $^{40}Ca/^{44}Ca$ was the maximum extent of the effects in this soil, or if the measurements had been diluted by the leaching of unfractionated bulk Ca phases from the interiors of the grains. The sputtering results suggest but do not prove that some dilution did indeed take place. The laboratory sputtering shows that the initially sputtered material is isotopically light, and that isotopically heavy surface layers are apparently established. These observations are consistent in sign with the isotopic fractionation of O, Si, S, K, and Ca on the soil grain surfaces.

This work does not provide insight into whether other mechanisms proposed in order to explain the lunar soil fractionation are indeed contributors to the isotope effects. These mechanisms

are discussed in the paper reproduced in Chapter 4. It has been clearly demonstrated herein that sputtering can cause large fractionation in non-volatile elements such as calcium. It has yet to be shown how the magnitude of the isotopic fractionation varies between volatile and non-volatile elements. It is clear that volatility strongly controls the gravitational mass separation model proposed by Switkowski et al. (1977), provided that less volatile species have higher surface binding energies. For instance, a change from U = 1 eV to U = 3 eV would cause the $\delta^{18}O$ gravitational effects to decrease from 25‰ to 9‰ . Whether volatility is a controlling parameter in any fractionation produced by micrometeorite impacts is not yet known. Thus, the current knowledge is insufficient to predict how a property such as volatility might influence the relative contributions of these various mechanisms to the isotopic effects. However, this present work has clearly demonstrated that sputtering is quite likely a mechanism responsible in large part for the lunar soil fractionation.

Table 5-1. Dilute ^{42}Ca-^{48}Ca Tracer Composition[a]

Isotope	40	42	43	44	46	48
Atom Percent[b]	0.14253	0.71302	0.000704	0.006778	---	0.13696

[a]Prepared from concentrated ^{42}Ca-^{48}Ca tracer (Table 3-1). Measured concentration is 255.6 ng ^{42}Ca/gram spike.

[b]Calculated from the following isotope ratios, corrected for mass fractionation in a way permitting identical $\delta(^{40}Ca/^{44}Ca)$ values to be obtained for samples spiked with either the dilute or concentrated tracers: $^{42}Ca/^{48}Ca = 5.20596$, $^{44}Ca/^{48}Ca = 0.04949\pm2$, $^{40}Ca/^{44}Ca = 21.029\pm9$, $^{43}Ca/^{44}Ca = 0.1039\pm2$. The errors are $2\sigma_{mean}$ and correspond to the last figures shown.

Table 5-2. Analysis of Micro-Quantities of ^{44}Ca-Enriched Standards

δ Gravimetry	δ [a,b,c] Mass Spectrometry	$(^{40}Ca/^{44}Ca)_C$ [a,d]	δ [b,d] Mass Spectrometry
$\equiv$ 0.0	0.0±0.2 [e]	nm [f]	nm
-0.46	-0.7±0.1 [e]	47.167±0.016 [e]	-0.7±0.3
-1.86	-2.1±0.1 [e]	47.087±0.016 [g]	-2.4±0.3

[a] Corrected for instrumental fractionation using the double spike.

[b] Zero enrichment standard had $(^{40}Ca/^{44}Ca)_C = 47.200$. This value was used here to compute δ.

[c] Values previously measured using 10 µg aliquots loaded onto the mass spectrometer filament (see Table 3-2).

[d] Values measured using 150 ng aliquots loaded onto the mass spectrometer filament.

[e] Concentrated ^{42}Ca-^{48}Ca double tracer used (Table 3-1).

[f] nm: not measured.

[g] Dilute ^{42}Ca-^{48}Ca double tracer used (Table 5-1).

Table 5-3. Isotope Fractionation of Ca Sputtered by Nitrogen

Target[a]	Catcher Tube[b]	Range (Å)[c]	Current (μA)	Dose[d] (x 10^{17})	Area[e] (cm^2)	Ranges Sputtered[f]	S_{Ca}[g]	Angular Range[h]	Amount Ca(ng)	δ(40/44)[i]
Fluorite-1[j] Chip-A	2A-1	1700	1.7	0.63	0.26	0.061	0.104	5°-79°	436	+11.1±0.3
	2A-2	1700	2.0	2.55	0.26	0.23	0.095	5°-66°	1617	-2.0±0.2
	2A-3	1700	2.3	0.80	0.26	0.052	0.069	5°-72°	367	-3.8±0.2
	2A-4	500	5.2	2.5	0.26	0.97	0.12	5°-69°	2018	-8.3±0.7[k]
Polycrystal. Fluorite Chip-A	4A-1[ℓ]	1700	2.7	0.67	0.44	0.044	0.121	5°-72°	540	+12.5
	4A-2	1700	2.9	2.5	0.44	0.49	0.150	5°-63°	2486	+0.1±0.2
	4A-3	1700	3.0	0.63	0.44	0.044	0.128	5°-72°	531	-0.9
	4A-4	500	3.4	2.0	0.44	1.66	0.447	5°-66°	5996	-0.3
Polycrystal. Fluorite Chip-A	3A-1	1700	0.67	0.63	0.48	0.042	0.134	5°-72°	559	+12.7±0.7
	3A-2	1700	0.69	0.63	0.48	0.033	0.104	5°-79°	437	+2.7±0.2
	3A-3	1700	0.70	0.62	0.48	0.077	0.246	5°-79°	1024	-0.2±0.2
Apatite ($10\bar{1}1$) or ($10\bar{1}2$)	1A-1	1500	1.5	0.69	0.58	0.025	0.061	5°-60°	279	+11.5±0.3
Plagioclase	1B-1	525	4.6	2.5	0.43	0.27	0.007	5°-66°	118	+21.2±0.2
	1B-2	1750	1.4	0.69	0.43	0.046	0.014	5°-69°	66	-3.9±0.2

Table 5.3. (cont'd.)

Target[a]	Catcher Tube[b]	Range (Å)[c]	Current (μA)	Dose[d] (x 10^{17})	Area[e] (cm^2)	Ranges Sputtered[f]	S_{Ca}[g]	Angular Range[h]	Amount Ca(ng)	δ(40/44)[i]
Fluorite-1 Chip-A (111) plane	1C-1	500	4.4	2.5	0.24	0.92	0.106	5°-72°	1762	-0.4±0.3
	1C-2	1700	1.7	0.73	0.24	0.068	0.092	5°-79°	445	-10.6±0.3
Fluorite-1 Chip-A (111) plane	3B-1	500	0.47	1.25	0.21	0.45	0.121	5°-66°	1005	+0.3±0.3
	3B-2	1700	1.1	0.56	0.21	0.055	0.109	5°-69°	416	-3.6±0.1
Fluorite-2[m] (111) plane	4B-1	500	0.72	1.25	0.33	0.33[n]	--	5°-60°	--	--
	4B-2	1700	0.79	0.58	0.33	0.036	0.094	5°-60°	360	-2.2±0.3

Table 5-3. (continued)

---

[a]Lines of data grouped together refer to sequential sputtering irradiations of the target.

[b]See text for a description of the catcher tube sample designation code.

[c]130 keV $^{14}N^{+}$ has a range in fluorite of 1700±600 Å, in apatite of 1500±550 Å, and in plagioclase of 1750±575 Å. 100 keV $(^{14}N)_2^{+}$ has a range in fluorite of 500±250 Å and in plagioclase of 525±275 Å. Values calculated using Lindhard et al. (LSS) model and average atomic weights and charges of 26.0 and 12.667 for fluorite, 24.02 and 11.91 for apatite, and 20.79 and 10.31 for plagioclase.

[d]For 100 keV N_2 bombardments, equivalent atomic N dose is given.

[e]The sputtered area was estimated, using optical microscopy of the sputtered targets, as the area of significant discoloration.

[f]Calculated from measured amount of Ca collected on the catcher tube, the calculated ion range, and the estimated sputtered area.

[g]Calcium sputtering yield, defined as the ratio of Ca atoms sputtered to the atomic nitrogen dose. It is assumed that the number of Ca atoms sputtered is well-approximated by the number collected on the catcher tubes.

[h]Range of angles subtended by the catcher tube at the center of the target.

[i]Corrected for instrumental fractionation using a double spike. Value refers to the average for all Ca collected on the catcher tube.

Table 5-3. (continued)

---

[j] δ_{Bulk} ($^{40}Ca/^{44}Ca$) = 0.3±0.4 ‰.

[k] Error given is an estimate of possible range of values, taking into account contamination of this catcher tube with a small amount of other sputtered material (see text).

[ℓ] Individual measurements of Ca amounts and $\delta(^{40}Ca/^{44}Ca)$ for each catcher tube section are listed in Table 5-4.

[m] δ_{Bulk} ($^{40}Ca/^{44}Ca$) = 0.2±0.2 ‰.

[n] Catcher tube not analyzed. This estimate calculated from primary ion dose and $S_{Ca} \simeq 0.108$.

Table 5-4. Angular Variations of Ca Sputtering Yield and Isotopic Fractionation[a]

Catcher Tube	Normal[b]		Middle[b]		Oblique[b]		Total[d]	
	Amount[c]	δ	Amount	δ	Amount	δ	Amount	δ
4A-1	263	+13.3±0.2	108	+17.3±0.3	169	+8.0±0.3	540	+12.5
4A-2	--	--	--	--	--	--	2486	+0.1
4A-3	229	+5.5±0.3	110	+1.9±0.4	192	-10.6±0.2	531	-0.9
4A-4	4125	+3.5±0.3	655	-0.9±0.4	1216	-13.0±0.4	5996	-0.3

[a]Measured during polycrystalline fluorite sputtering with 130 keV N (samples 4A-1 through 4A-3) and then 100 keV N_2 (sample 4A-4).

[b]NORMAL refers to the calcium collected on the 5°-25° section, MIDDLE refers to the 25°-41° intermediate section, and OBLIQUE refers to the 41°-72° section. These angles, correct for catcher tubes 4A-1 and 4A-3, are actually 5°-24°, 24°-38°, and 38°-66° for 4A-4.

[c]Amount of Ca in 10^{-9} grams as measured by isotope dilution.

[d]Total calcium amounts and weighted averages of $\delta(^{40}Ca/^{44}Ca)$, listed also in Table 5-3.

Figure 5-1. This is a schematic representation of the apparatus used in the calcium sputtering experiments. The targets (maximum of 4) are mounted in a holder which, using Manipulator B, can be moved up and down with respect to the ion beam, thereby allowing the sputtering of several different targets prior to unloading the ultrahigh vacuum chamber. The beam is incident from the left in this view and passes unimpeded along the axis of one of the cylindrical catcher tubes until it strikes the target. Calcium sputtered from the target is collected on the inside surface of the catcher tube. The catcher tube ends come within 1 - 3 mm of the face of the bombarded-sample holder, allowing material sputtered at oblique angles up to 79° to be collected. This also minimizes cross-contamination of the catcher surfaces. The 8.3 cm length of the catcher tubes is sufficient to allow collection of material sputtered at angles greater than 5°. The catcher tubes (maximum of 6) are mounted in a holder. Using Manipulator A, this holder can be moved up and down, allowing different tubes to be used during the course of an experiment.

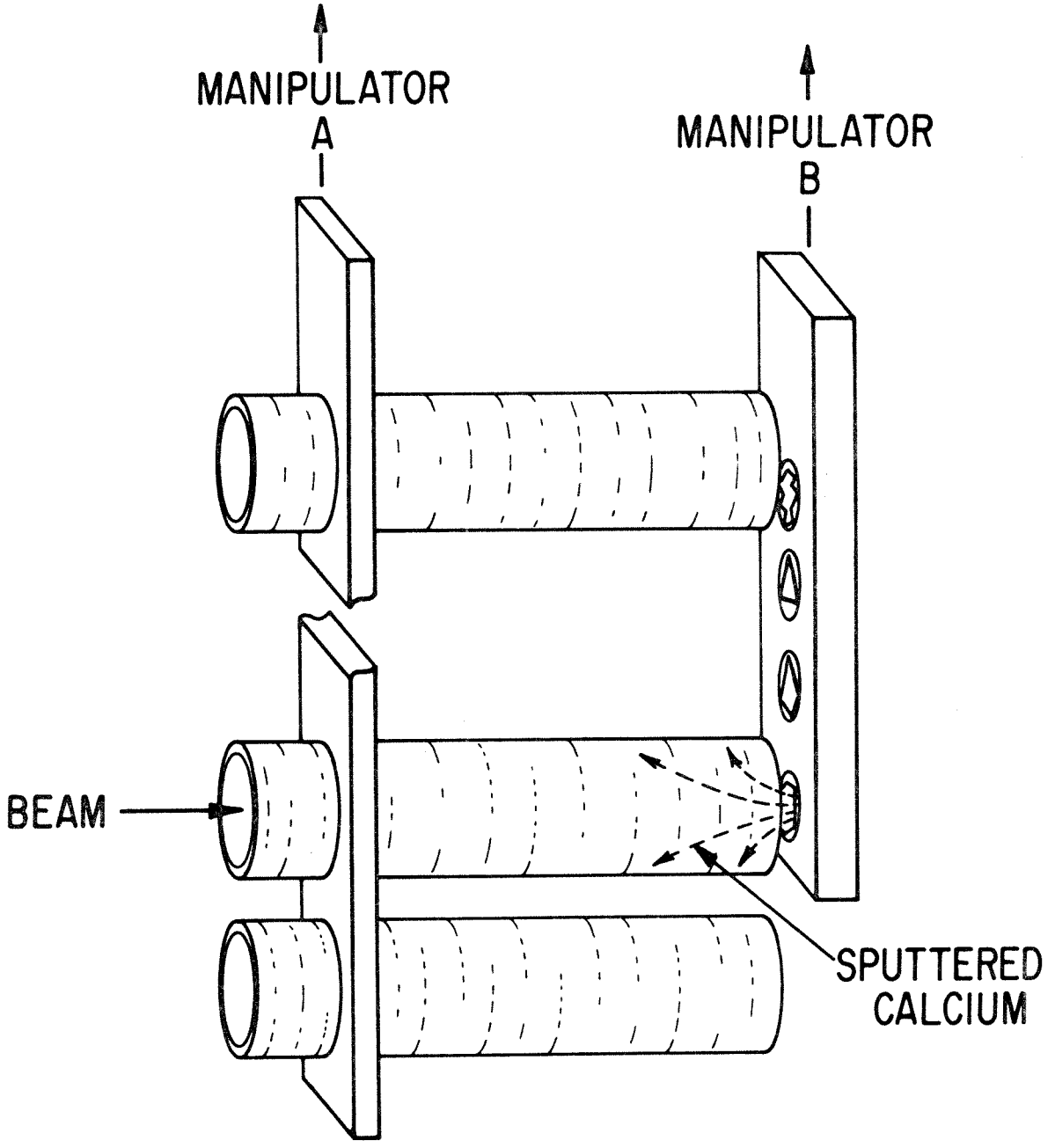

Figure 5-1

Figure 5-2. A more detailed view of part of the target holder in Figure 5-1; this shows the target mounting arrangement. The sample is held, polished surface down, inside of a cylindrical recess, and the beam strikes it from below through a shallow hole of diameter slightly smaller than the recess. With a washer and three screws, the sample is held against the lip thus formed in the recess. The hole in the separate small plate at the top allows viewing of the sample from the rear during its ion bombardment. In actual use, the target holder is mounted vertically as indicated in Figure 5-1.

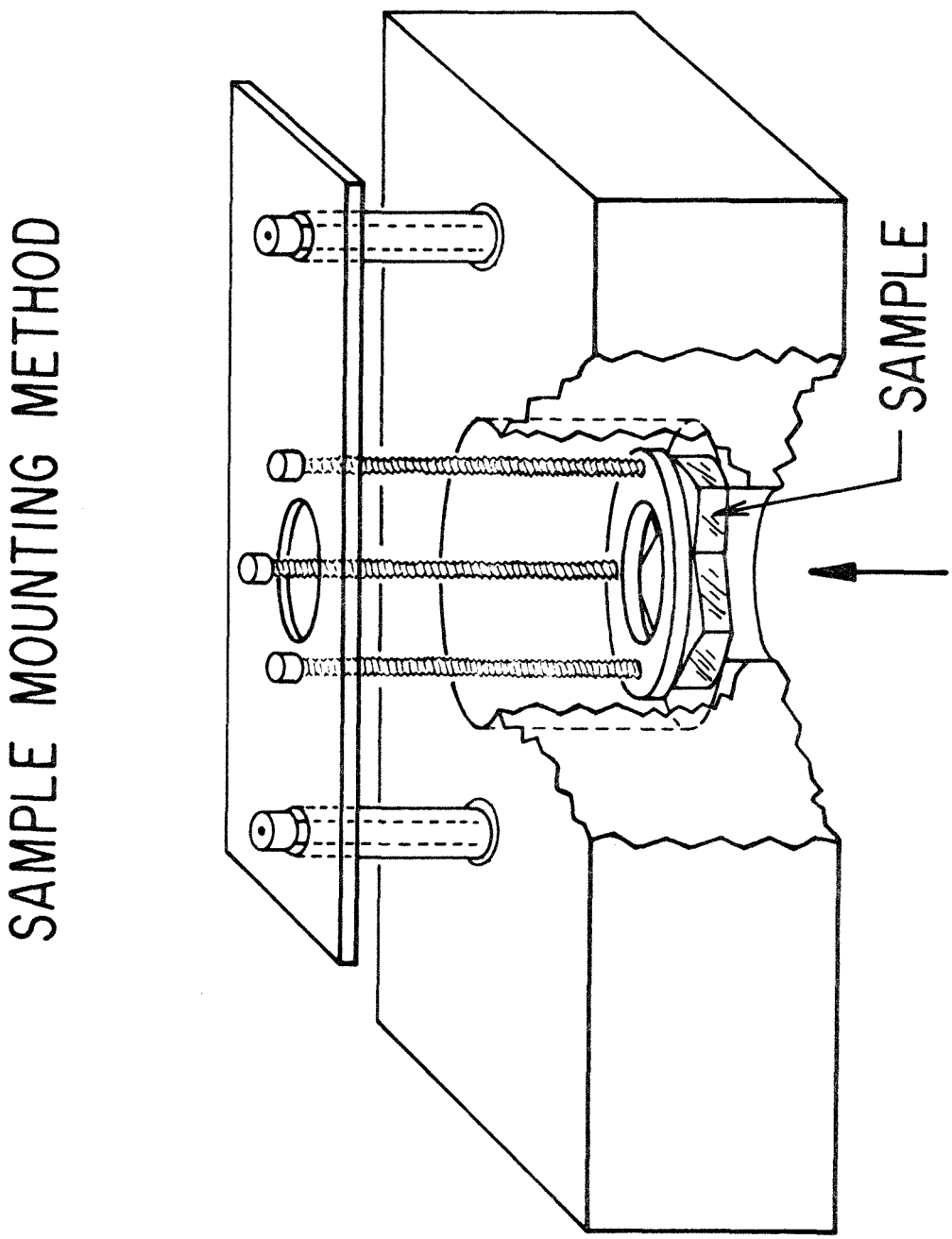

Figure 5-2

Figure 5-3. Isotopic fractionation of calcium sputtered from apatite and fluorite targets as a function of cumulative depth of excavation. For example, for the polycrystalline fluorite, Ca sputtered from 0 to 0.04 range is shown at 0.04; Ca sputtered from 0.04 to 0.08 is shown at 0.08. These depths were calculated from the amounts of Ca collected, the target chemical composition, the apparent beam area, and the target density. Because of various uncertainties in these factors, this depth to which the sputtering removed material is considered to be a qualitative measure only. The initial sputtering of each target was with 130 keV N^+. For the fluorite samples, this was continued for appreciable lengths of time. The open symbols are the measurements of the fractionation during this time. Each represents the calcium fractionation integrated from the time of the previous measurement. The upward- and downward-pointing triangles represent separate bombardments of polycrystalline fluorite samples (the 4A and 3A sequences in Table 5-3). After extensive 130 keV bombardment, a 50 keV/N (i.e. 100 keV N_2^+) beam was used to sputter the same targets. These measurements are represented by the two filled symbols. They are plotted along the abscissa correctly for the depth of excavation (top scale). However, the lower scale, which is the depth of excavation divided by 1700 Å, is not valid for the two filled symbols, since the beam range at 50 keV/N is only 500 Å. This figure clearly shows the initial large fractionations of ~ 12 ‰, the systematic decrease in fractionation with continued sputtering, and the differences in the isotopic patterns observed for single and polycrystalline fluorite samples.

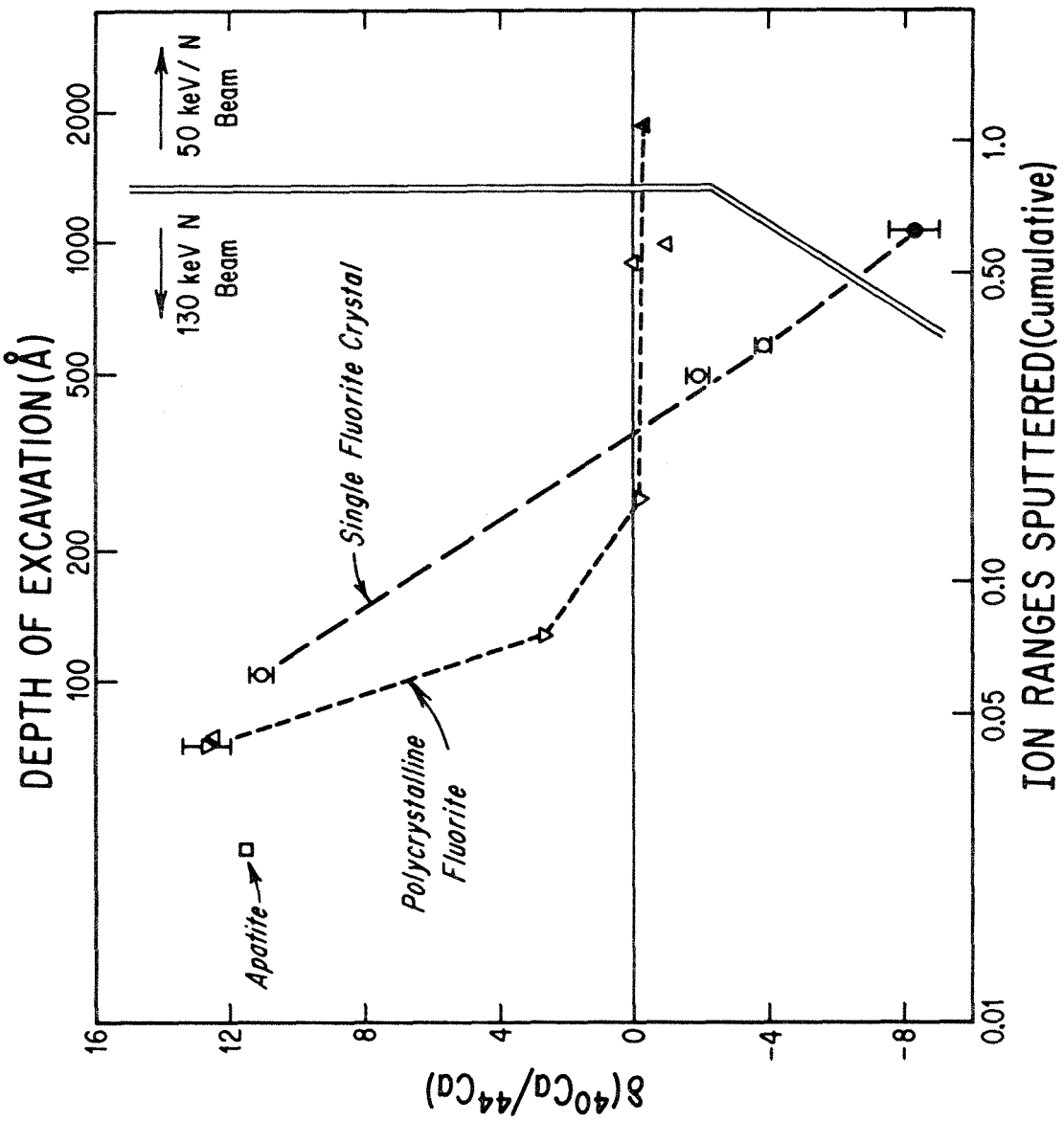
DEPTH OF EXCAVATION(Å)
100
200
500
1000
2000
50 keV / N
Beam
130 keV N
Beam
Single Fluorite Crystal
Polycrystalline
Fluorite
Apatite
16
12
8
4
0
-4
-8
δ(40Ca/44Ca)
0.05
0.10
0.50
1.0
0.01
ION RANGES SPUTTERED(Cumulative)

Figure 5-3

Figure 5-4. Calcium isotopic fractionation of material sputtered from a fresh polycrystalline fluorite target at different angles. This is a graph of the data in Table 5-4 for sample 4A-1. The ion beam used was 130 keV N^+. After the experiment, the catcher tube was separated into its three sections, and Ca from each section was analyzed separately. The mean of these measurements was computed, each measurement being weighted by the amount of Ca found on that section of the catcher tube. This mean is shown as the dashed line, and is also listed in Table 5-3 and plotted in Figure 5-3. The angular distributions of the Ca found on the catcher tube sections are plotted in Figure 5-7. The angular variations of fractionation plotted here show that (a) each section of the catcher tube had Ca which was substantially isotopically light, (b) there is a peak in fractionation at intermediate angles. This initial sputtering fractionation pattern is different from that seen in Figures 5-5 and 5-6, and therefore reflects substantial changes in the relative angular distributions of the Ca isotopes with more extensive sputtering.

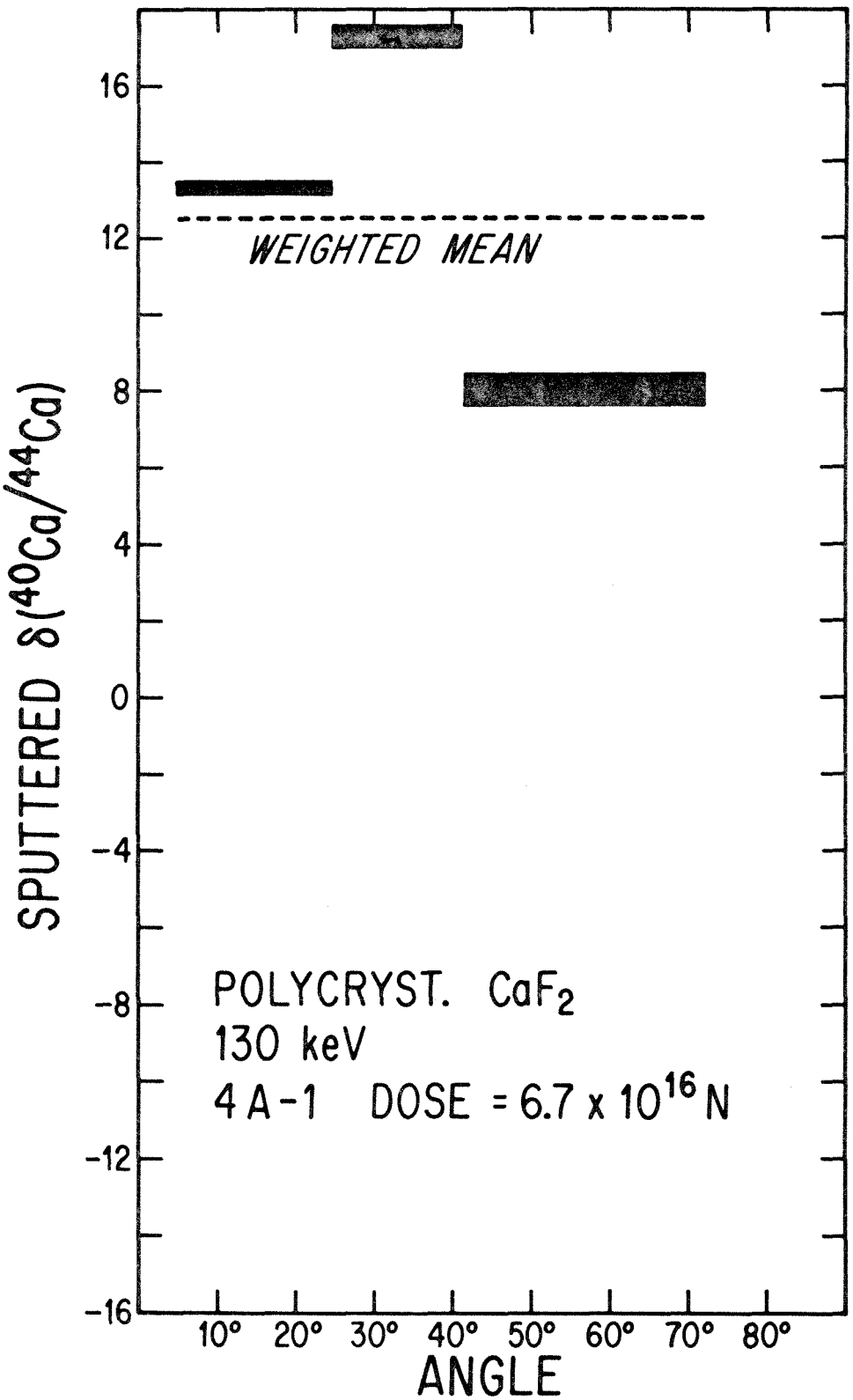
16
12
8
4
0
-4
-8
-12
-16
SPUTTERED δ(40Ca/44Ca)
WEIGHTED MEAN
POLYCRYST. CaF2
130 keV
4 A-1 DOSE = 6.7 x 10^16 N
10° 20° 30° 40° 50° 60° 70° 80°
ANGLE

Figure 5-4

Figure 5-5. This is a plot similar to Figure 5-4. The data shown were obtained after extensive sputtering of polycrystalline fluorite at 130 keV. The collection interval itself was short, though, and was approximately the same as for Figure 5-4. The material sputtered between the time of Figure 5-4 and this figure was collected on a standard, non-sectioned catcher tube, and is listed in Table 5-4 as sample 4A-2. The present data are listed in the table as sample 4A-3. At every angle, these data have appreciably smaller δ values than the corresponding points in Figure 5-4. The pattern itself has also changed substantially, having, instead of a peak at intermediate angles, a monotonic decrease in δ with increasing angle. Whereas in Figure 5-4 isotopically light ($\delta > 0$) values are observed at each angle, here the obliquely sputtered material had $\delta(^{40}Ca/^{44}Ca) = -10.6 \pm 0.2$ ‰.

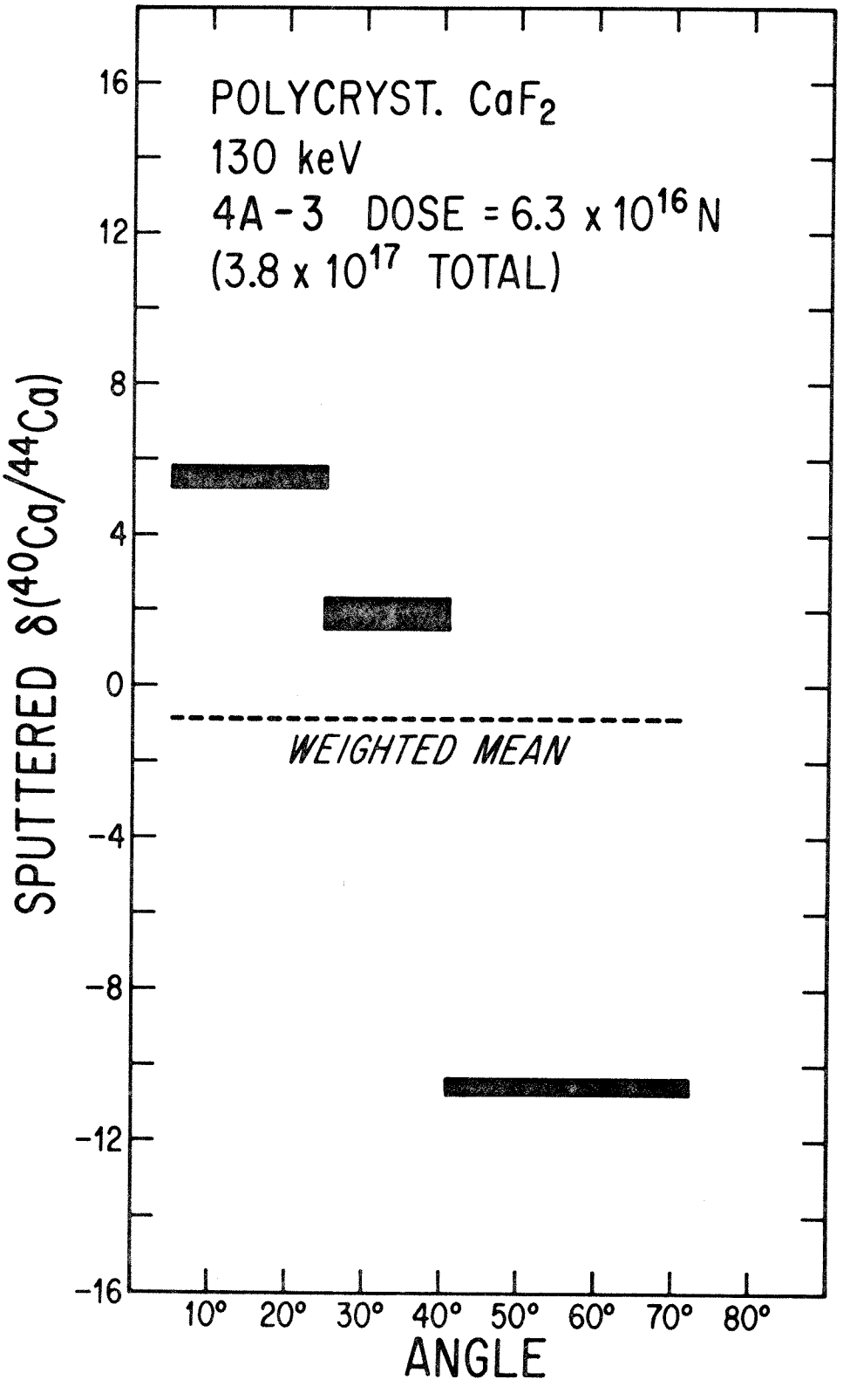
POLYCRYST. CaF_2
130 keV
4A-3 DOSE = 6.3×10^{16} N
(3.8×10^{17} TOTAL)
WEIGHTED MEAN
SPUTTERED $\delta(^{40}Ca/^{44}Ca)$
16
12
8
4
0
-4
-8
-12
-16
10°
20°
30°
40°
50°
60°
70°
80°
ANGLE

Figure 5-5

Figure 5-6. This is a graph similar to Figures 5-4 and 5-5. After extensive bombardment of the polycrystalline fluorite sample with 130 keV N^+ to a dose of 3.8×10^{17} (with estimated beam area of 0.44 cm^2), the sample was bombarded with 1.0×10^{17} N_2^+, for an equivalent atomic nitrogen dose of 2.0×10^{17}. The calcium sputtered during this lower energy bombardment was collected on catcher tube 4A-4, and the results of the separate analyses of each section are shown here and also listed in Table 5-4. The fractionation pattern seen here is similar to that of Figure 5-5, having a monotonic decrease in δ with increasing angle. In fact, each measurement is 2‰ less than the corresponding one in Figure 5-5. This indicates that at isotopic equilibrium, the angular isotopic pattern achieves a constant form which has substantial fractionation at small and large angles instead of $\delta = 0$ for all angles.

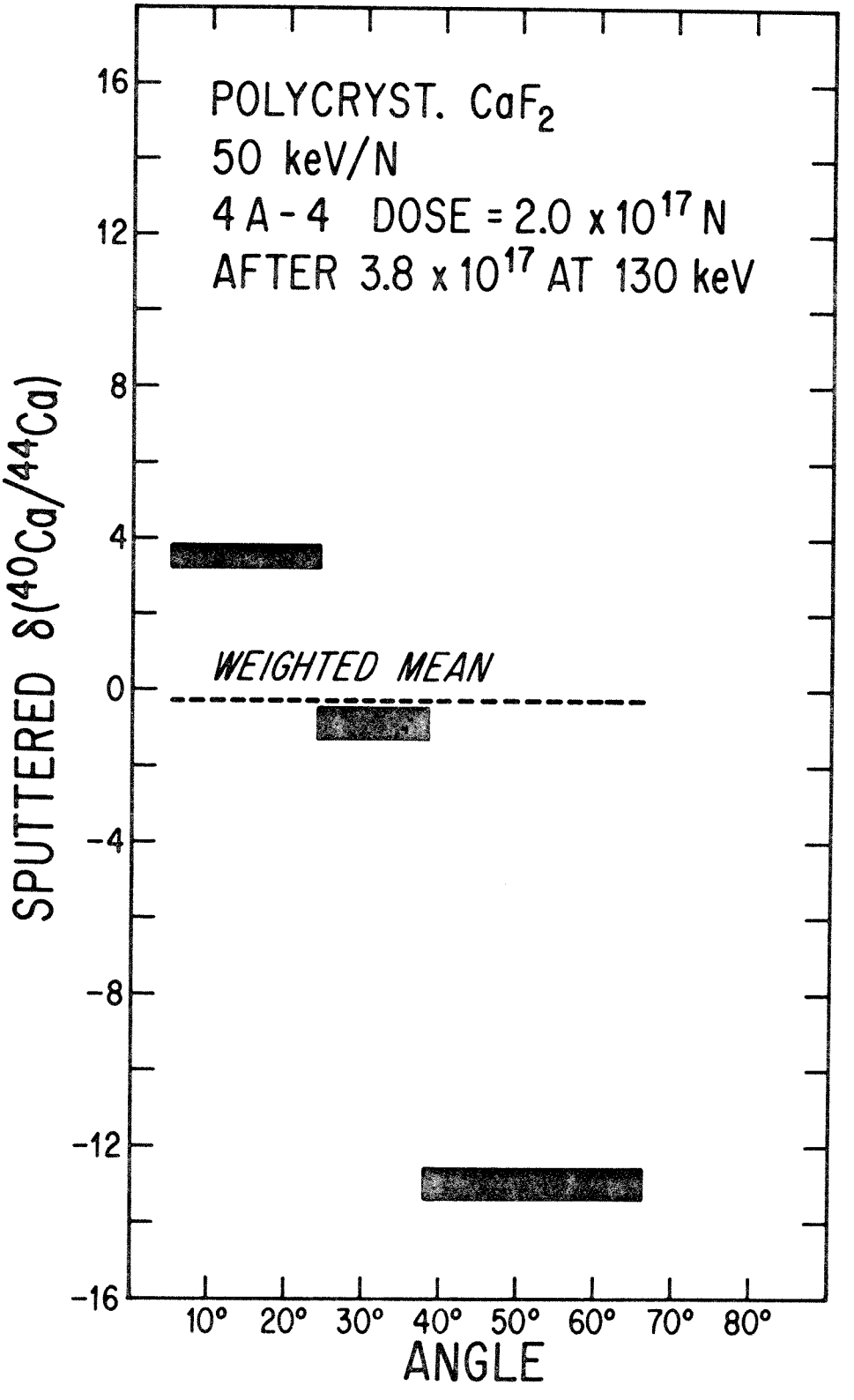
POLYCRYST. CaF_2
50 keV/N
4 A - 4 DOSE = 2.0×10^{17} N
AFTER 3.8×10^{17} AT 130 keV
WEIGHTED MEAN
SPUTTERED $\delta(^{40}Ca/^{44}Ca)$
16
12
8
4
0
-4
-8
-12
-16
10°
20°
30°
40°
50°
60°
70°
80°
ANGLE

Figure 5-6

Figure 5-7. Angular distributions of sputtered material. This figure contains three graphs of measurements during the 4A bombardment sequence. The top graph shows data for the 4A-1 sample (see Figure 5-4 and Table 5-4), the middle graph shows data for 4A-3 (Figure 5-5), and the bottom graph displays the data for 4A-4 (Figure 5-6). The ordinate of each graph gives the fraction of the total Ca collected on the three sections of the catcher tube which was collected on each individual section, i.e. the amount of Ca on an individual section normalized by the total Ca collected over all angles. These data are plotted as functions of the angular range spanned by the sections, and are shown as the solid, heavy, horizontal lines. For comparison, the hatched areas show calculations of the distributions had they followed a $\cos^{\nu}\theta$ angular variation (see Chapter 5, equation 15). The top boundary of the low- and intermediate-angle hatched areas corresponds to $\nu = 5/3$, whereas the bottom boundary of the high-angle hatched area corresponds to $\nu = 0.25$. It is seen then that no power of ν provides an adequate fit to the data. All powers of ν predict less Ca on the low-angle section than is observed, and more Ca on the intermediate-angle sections. The dashed lines in the bottom graph are the results of assuming that part of the Ca on the low-angle section is from blister fragment contamination (see text); even then, an adequate fit is not obtained for any reasonable power of ν. The angular distributions of the sputtered material might be altered because of trapping probabilities which vary with angle. However, as the catcher surfaces were relatively rough, this is thought to probably not have been a major difficulty

in the present experiment. Measurements with greater angular resolution would be desirable, but these data apparently indicate the presence of angular distributions which are not fit well by $\cos^{\nu}\theta$.

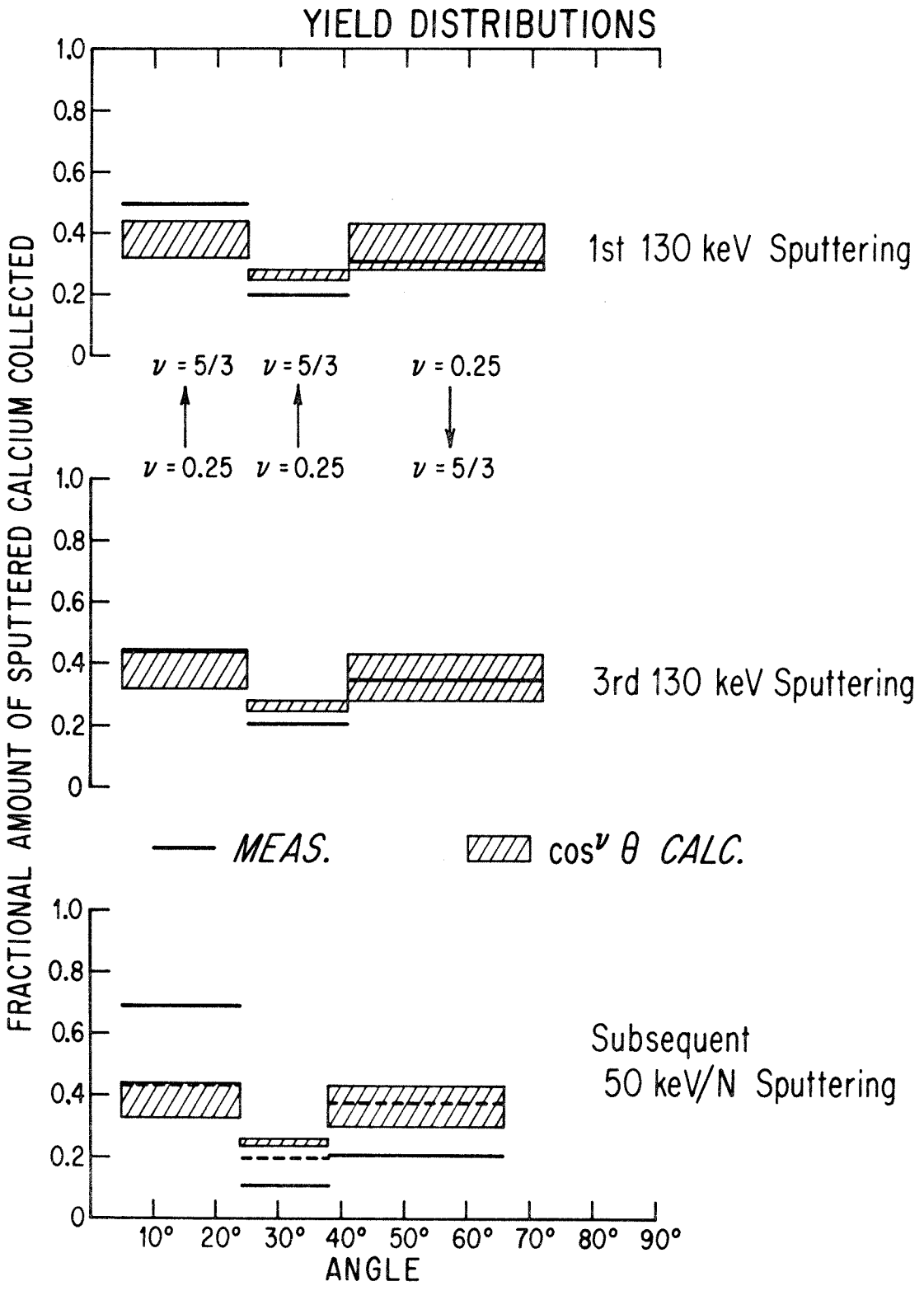
YIELD DISTRIBUTIONS
FRACTIONAL AMOUNT OF SPUTTERED CALCIUM COLLECTED
1.0
0.8
0.6
0.4
0.2
0
1st 130 keV Sputtering
ν = 5/3
ν = 5/3
ν = 0.25
ν = 0.25
ν = 0.25
ν = 5/3
3rd 130 keV Sputtering
MEAS.
cos^ν θ CALC.
Subsequent
50 keV/N Sputtering
10° 20° 30° 40° 50° 60° 70° 80° 90°
ANGLE

Figure 5-7

Figure 5-8. Three Scanning Electron Microscope (SEM) photographs of regions on the polycrystalline fluorite and plagioclase targets which had minimal or no exposure to the nitrogen ion beam. The information in the alphanumeric fields includes the accelerating voltage, the magnification power, the length in microns of the solid white bar, the photograph number, and the length in microns or nanometers of the hatched bar. Photograph (a) demonstrates the smoothness of the polished surface at locations not pitted with cracks or holes. As mentioned in the text, this surface was friable, and further polishing only caused other pits to be exposed. Photograph (b) shows the same sample at a location somewhat nearer to the region bombarded by the beam. Many pits 2 μm in diameter are seen. Notice also that the surface has developed a blistered texture. This is clearly seen in the lower left corner. The blisters have not developed and ruptured. This region received only minor exposure to the ion beam; if it is assumed to have received $\sim$1% of the fluence in the heavily irradiated region, this would indicate that such blisters develop with nitrogen fluences of 10^{16} N/cm^2. Photograph (c) was taken at higher magnification, and shows the high polish given to some areas of the plagioclase surface. This area was shielded from the beam by the target holder, and contrasts greatly with areas receiving substantial bombardment (e.g. Figures 5-9b and 5-10c).

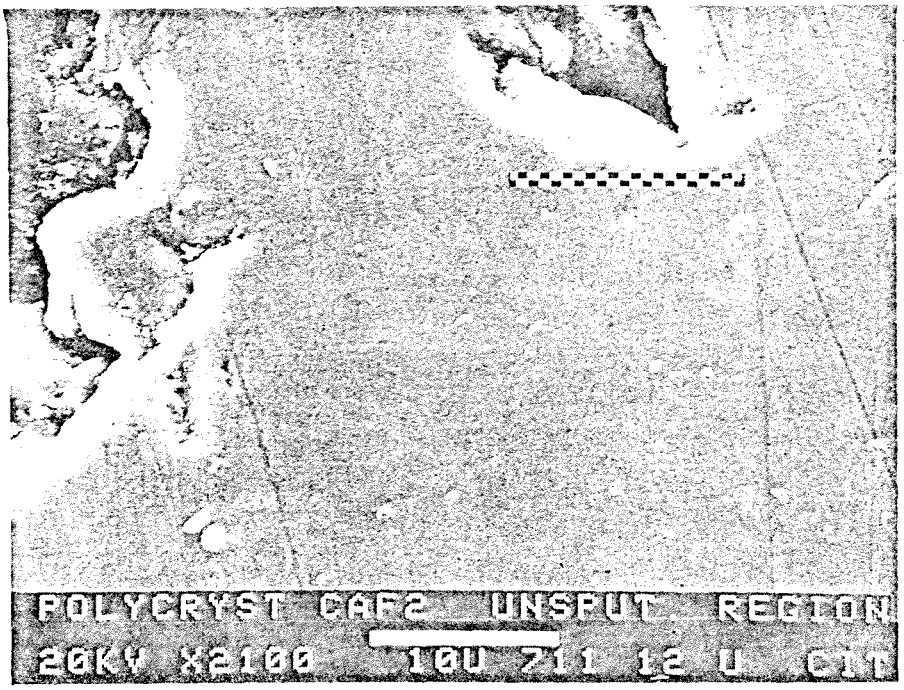

Figure 5-8(a)

Figure 5-8(b)

Figure 5-8(c)

Figure 5-9. These two SEM photographs show bombarded regions of the polycrystalline fluorite and plagioclase targets after the 4A and 1B irradiation sequences, respectively. All of the SEM photographs of these targets (Figures 5-8 through 5-13 and 5-19) were made after these irradiation sequences. These two photographs show regions near the intensively irradiated regions. The development of blisters from the bombardment is clearly seen, and it appears that in many cases the blisters which rupture do so in the middle rather than at their peripheries. This is in contrast to the type of rupturing seen in Figure 5-12(b). The blisters in photograph (a) are ~ 2 μm in diameter, while those in (b) are ~ 0.5 μm in diameter.

Figure 5-9(a)

Figure 5-9(b)

Figure 5-10. Regions of the polycrystalline fluorite and plagioclase targets which were heavily irradiated by the beam. SEM photograph (a) shows that the fluorite surface was heavily populated with craters from ruptured blisters. The plagioclase, though, only developed a rough surface, as is seen in photograph (c). This roughness is in contrast to Figure 5-8(c), which was taken at the same magnification. It may be that small plagioclase blisters such as seen in Figure 5-9(b) were annealed with more extensive bombardment into the bumpy features seen here in photograph (c). Photograph (a) shows no sign of fragments from the blisters. This may be because of eruptive transport of the fragments to areas outside of the field of view, or to annealing of the fragments into the surface. Photograph (b) is a closeup of one of the craters near the center of (a). The hatched bar represents a length of 5100 Å. The rough features seen in this view may be caused by uneven sputtering, and do not appear to be very small blisters 1000 Å in diameter.

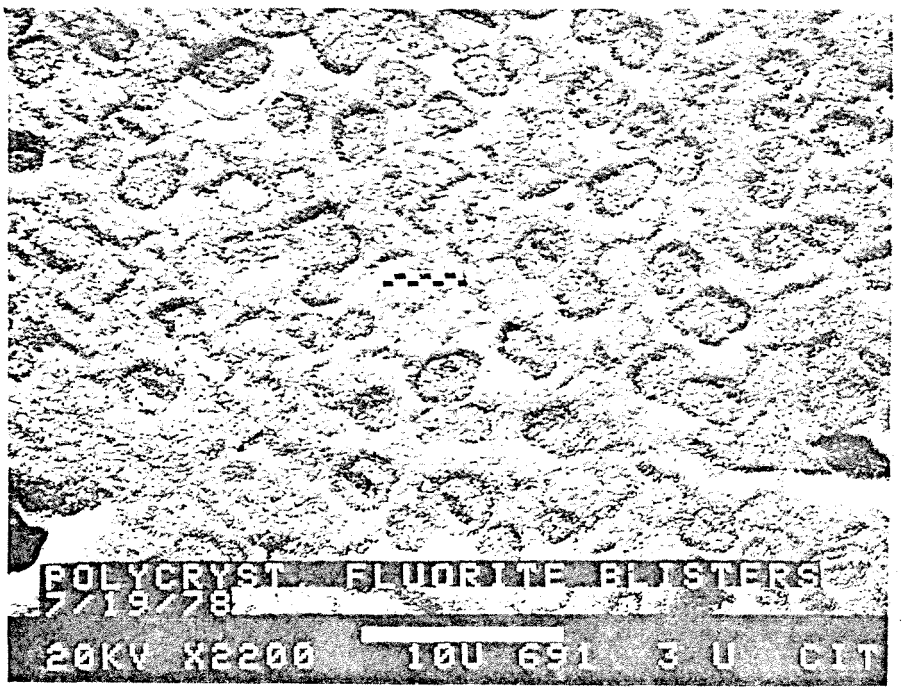

Figure 5-10(a)

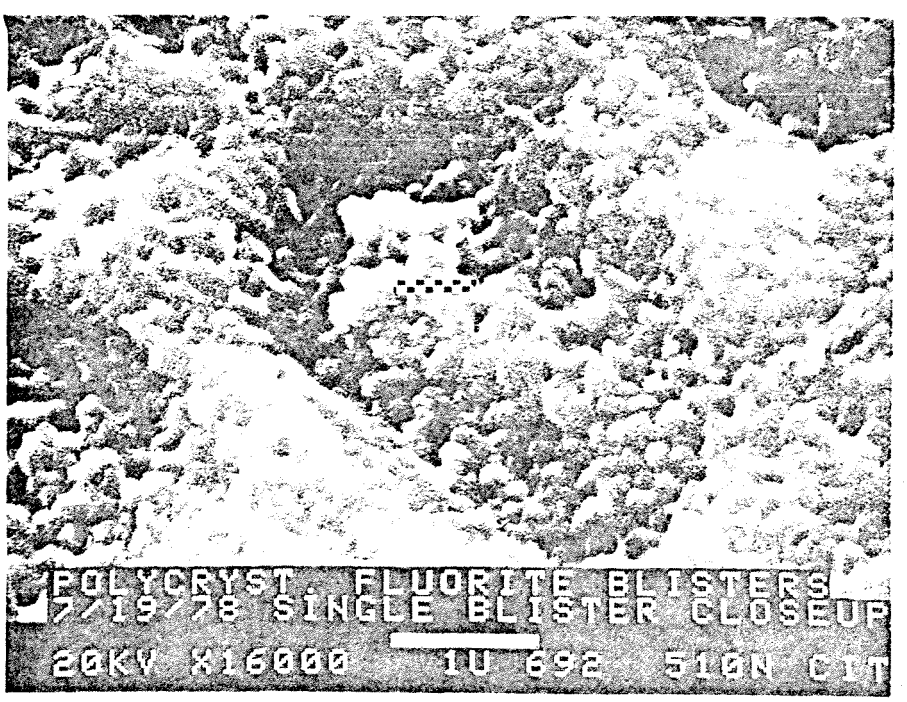

Figure 5-10(b)

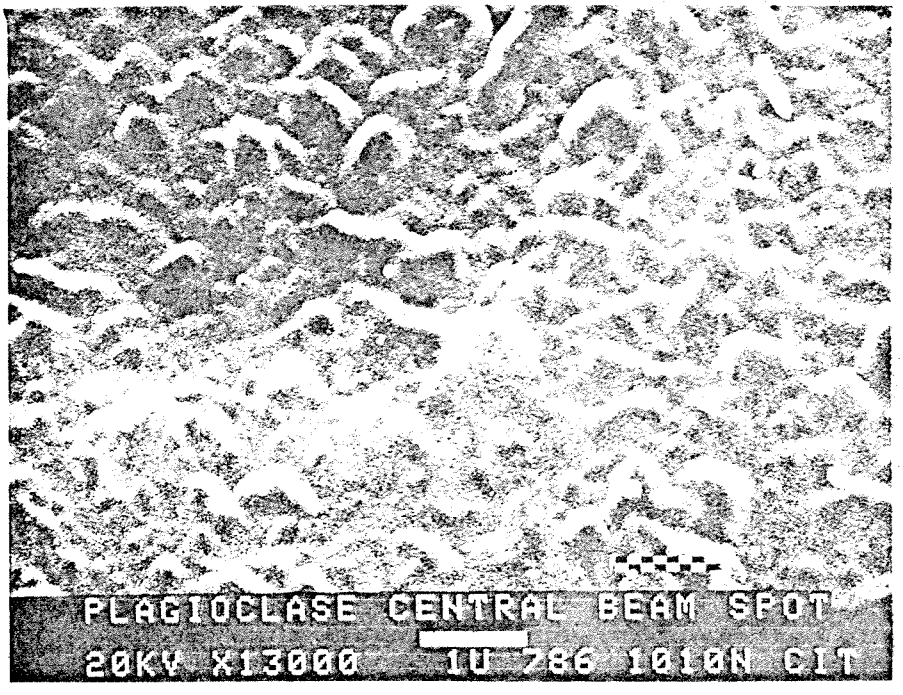

Figure 5-10(c)

Figure 5-11. Two SEM photographs of a large pit in the polycrystalline fluorite surface. This area of the target was heavily irradiated by the nitrogen ion beam. Photograph (a) shows the cratered surface outside of the pit. In addition, a number of craters may be seen on the floor of the pit in the lower right corner. For all of the SEM photographs (Figures 5-8 through 5-14, 5-16 through 5-19), the target surface was tilted at 40° with respect to the electron beam. In this figure, the tilting enabled examination of sections of the floor of the pit which had been shielded from the nitrogen ions by the overhanging, steep wall. Photograph (b) shows such an area, which is located at the top center of photograph (a). Here the cratering density appears to be less, indicating that blisters of this size can form only from local bombardment, not from bombardment of another region of the target. The whitish objects near the top of photograph (b) are discussed in the text as possible candidates for fragments erupted from blisters. Photograph (a) shows that such objects are found over the entire floor of the pit.

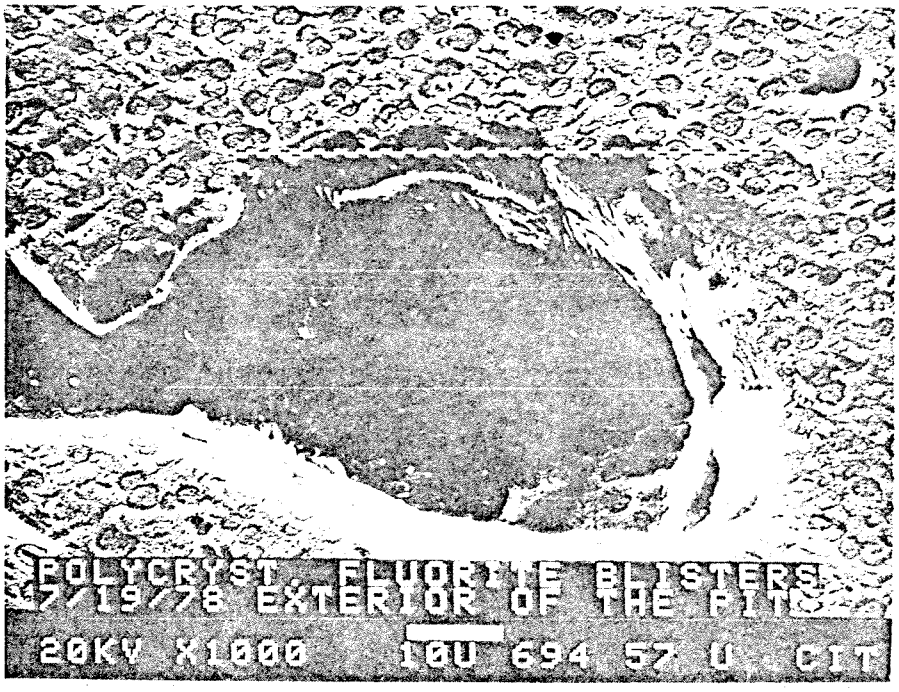

Figure 5-11(a)

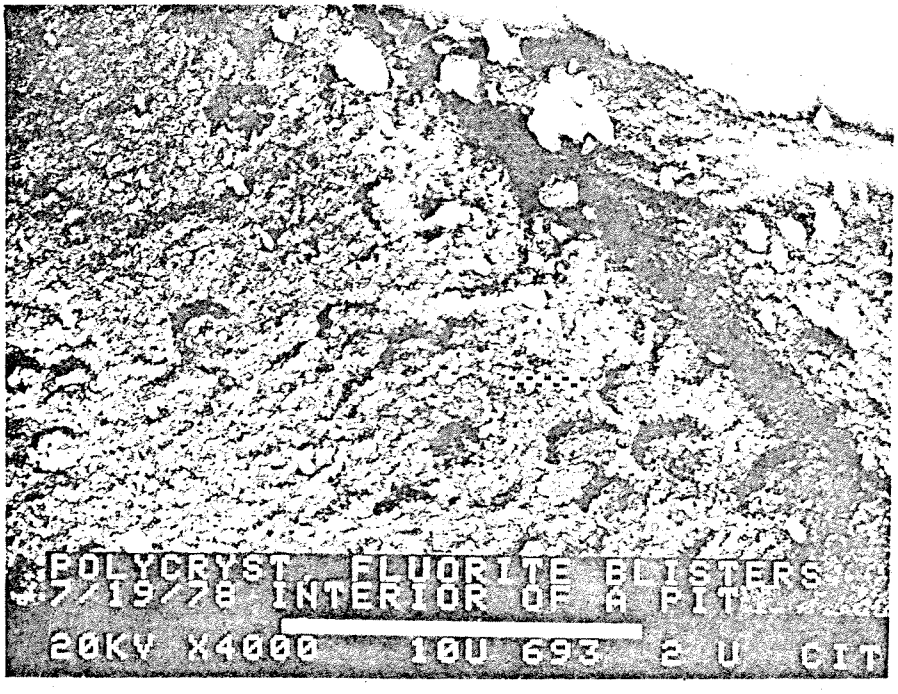

Figure 5-11(b)

Figure 5-12. These are two SEM photographs of another portion of the heavily irradiated area of the polycrystalline fluorite surface. Photograph (b) is a higher magnification view of the center of photograph (a). In (b) there may be seen many blisters which have ruptured by fracturing around their edges. In most cases, the fragments are still attached to the surface, indicating that appreciable fractions of the blistered material were not carried away when the rupturing occurred. In photograph (a) it is seen that large areas of the irradiated surface were covered with this type of fragment. The white areas are somewhat overexposed in this photograph, but are small groups of the fragments. It is interesting that some areas, such as that forming the dark vertical band in (a), have either resisted blister development or were not extensively irradiated because of ion beam spatial inhomogeneities.

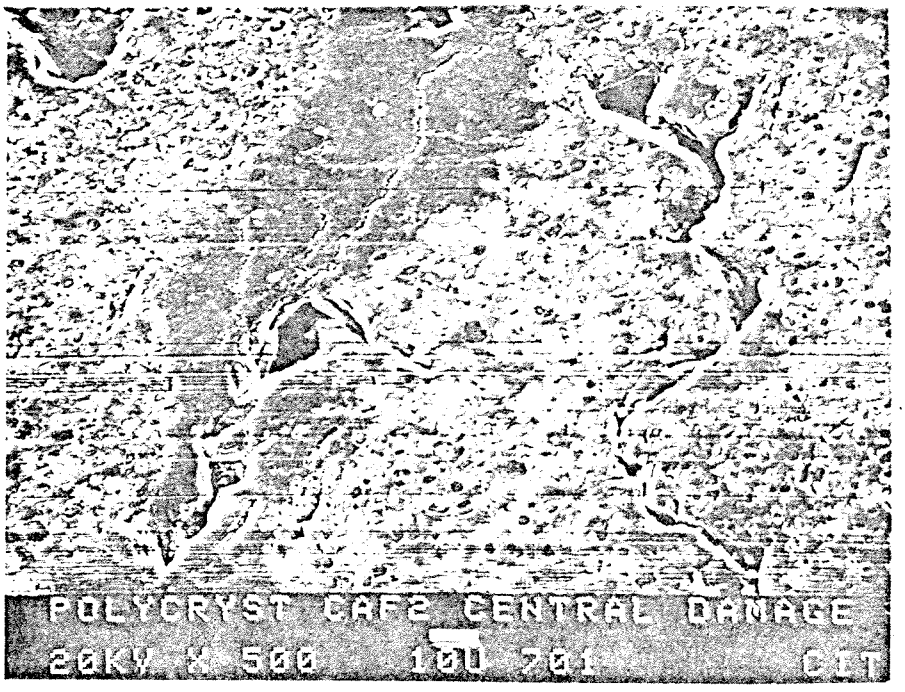

Figure 5-12(a)

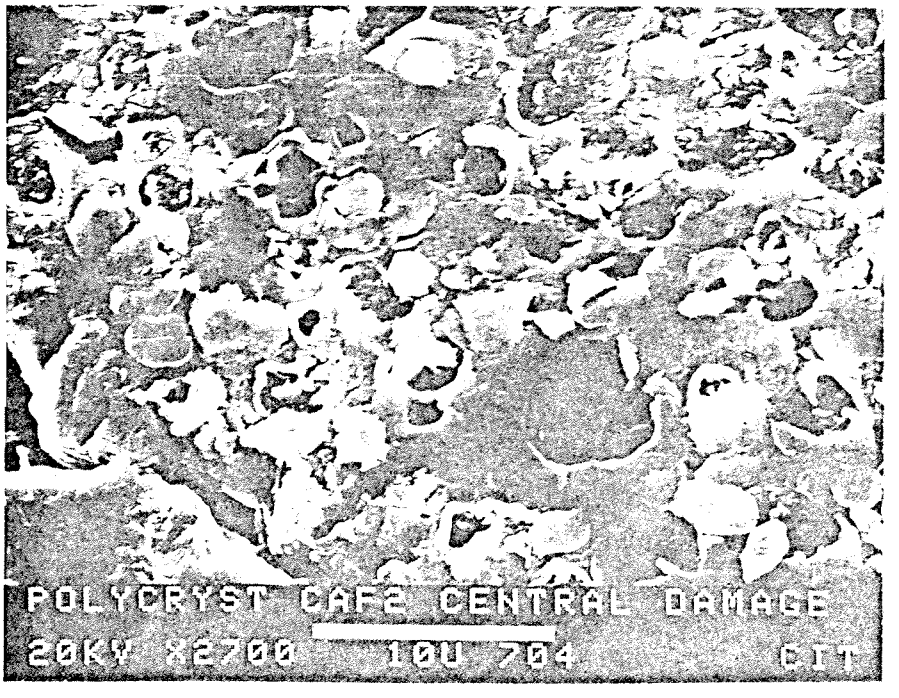

Figure 5-12(b)

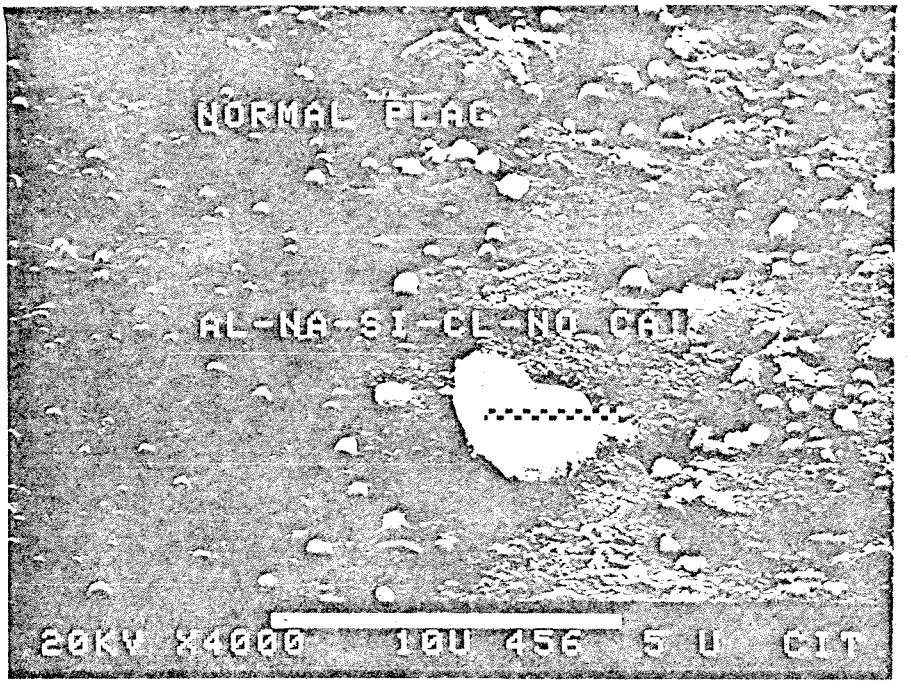

Figure 5-13. Part of the heavily irradiated region of the plagioclase surface (see Table 5-3). The rounded objects seen here were not found in most other locations on the target, which instead had the appearance seen in Figure 5-10(c). These are discussed in the text as being products of possible localized heating by the ion beam. X-ray analysis while in the SEM showed these objects to have been somewhat reduced in Ca relative to the bulk, and to have been significantly enhanced in Na and Cl, the latter possibly originating from HCl vapors in the room in which this sample had been temporarily stored (see text).

Figure 5-14. SEM photographs of the Fluorite-1 monocrystalline sample after the 3B irradiation sequence (Table 5-3). A number of "colonies" of objects such as seen in photograph (a) were observed. The dark circular area at the top which intrudes into this colony is an artifact. The large objects in the middle of the colony may not be attached to the surface. Nearer to the edge though, it appears that some of these objects may be joined to the surface (photograph b). Photograph (b) is a closeup of the lower center of (a). The smallest of these objects, which are around the perimeter of the colony, are clearly joined to the surface. Photograph (c) shows a similar, smaller colony, more examples of which are seen throughout Figure 5-17. In photograph (c), it is clearly seen that these objects are connected to the surface. Many have the appearance of the fragments seen in Figure 5-12(b). However, it is not clear why, if this were the case, such fragments would form only in discrete locations and with an apparent radial distribution of sizes in the larger colonies. No satisfactory explanation for the features seen in (a) is at hand; some possibilities are discussed in the text.

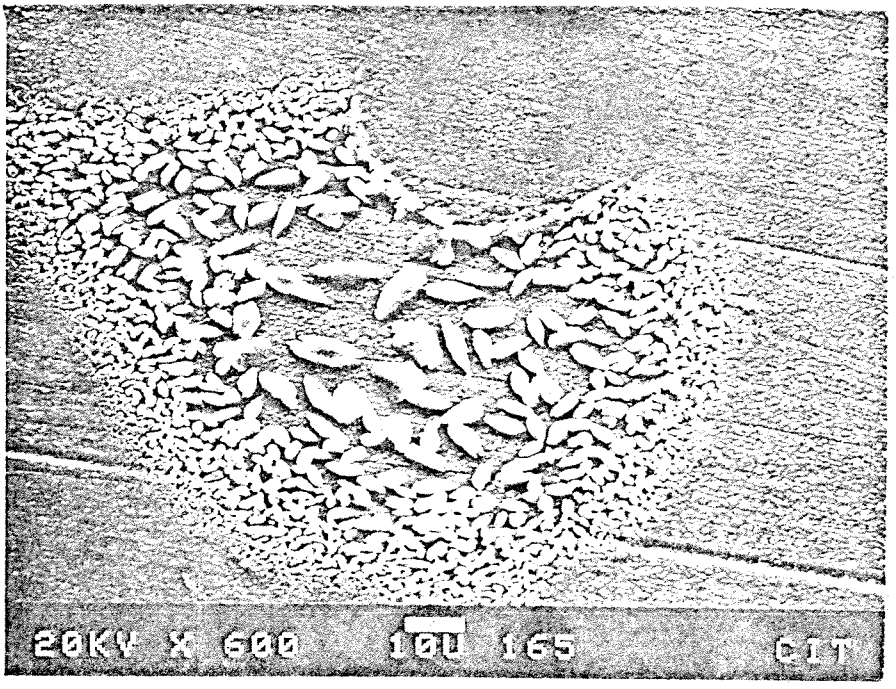

Figure 5-14(a)

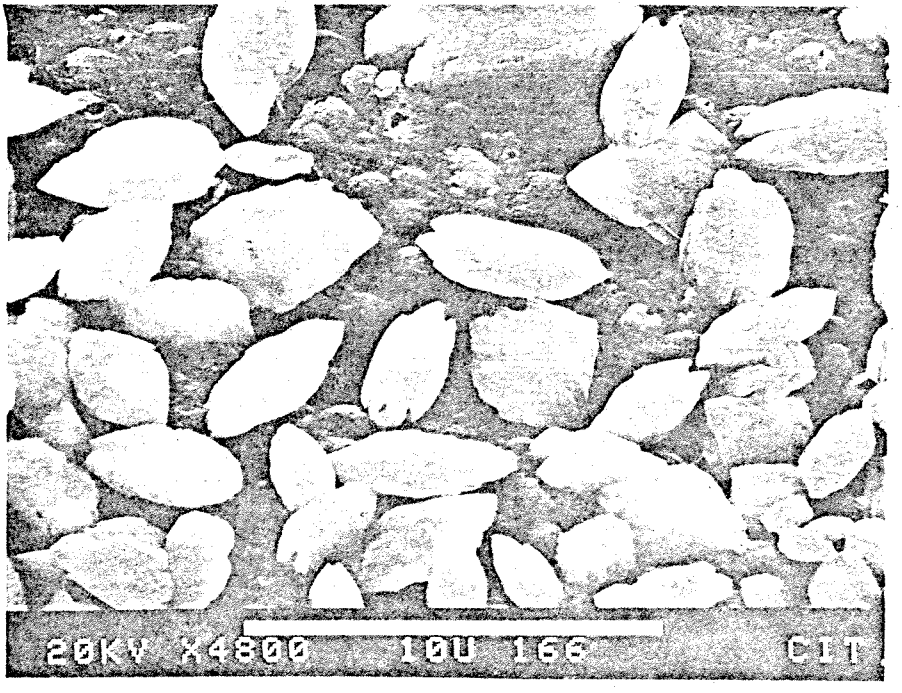

Figure 5-14(b)

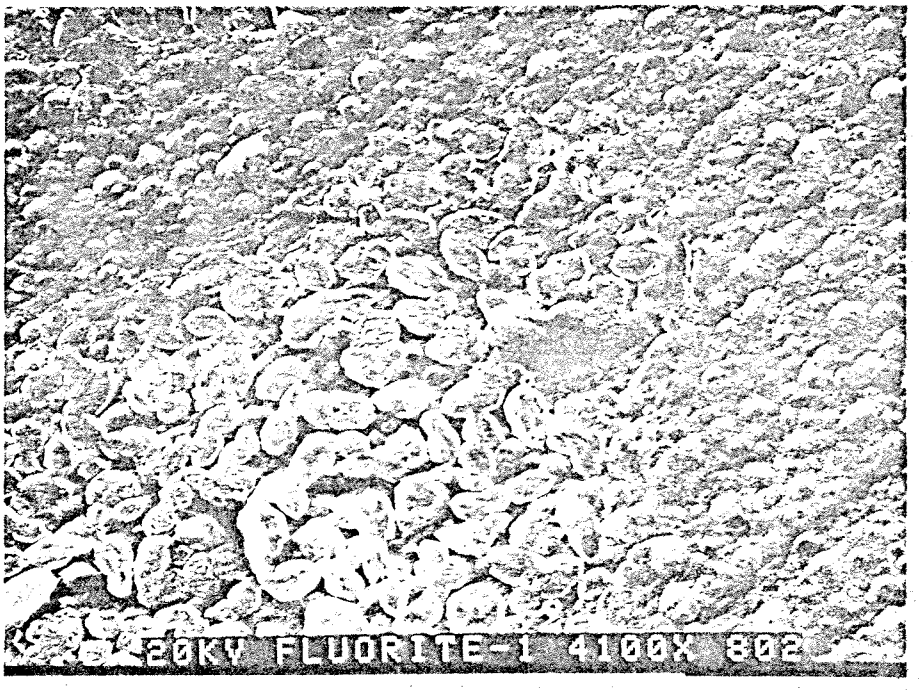

Figure 5-14(c)

Figure 5-15. Two optical micrographs of an area of the Fluorite-1 crystal outside of, but near the apparently heavily irradiated region. The width of each photograph corresponds to 200 μm. These objects were so thin that optical interference patterns were set up between them and the underlying surface. Their thickness is not known, but the maximum separation from the surface is about 2 μm (four wavelengths of light). These objects may be thin pockets of trapped, implanted nitrogen gas or thin layers of material which was melted elsewhere by localized beam heating and then deposited here. The possibility of general, extensive heating by the beam seems to be remote (see text). Momentary concentration of the beam into a smaller area might cause such heating, and cannot be ruled out. A search for these particular features using the SEM proved negative, probably because of the thinness of the material. The observation of highly unstable blisters in the same region (Figure 5-18) supports the suggestion that the objects seen here are large, thin blisters. Their irregular shape remains unexplained.

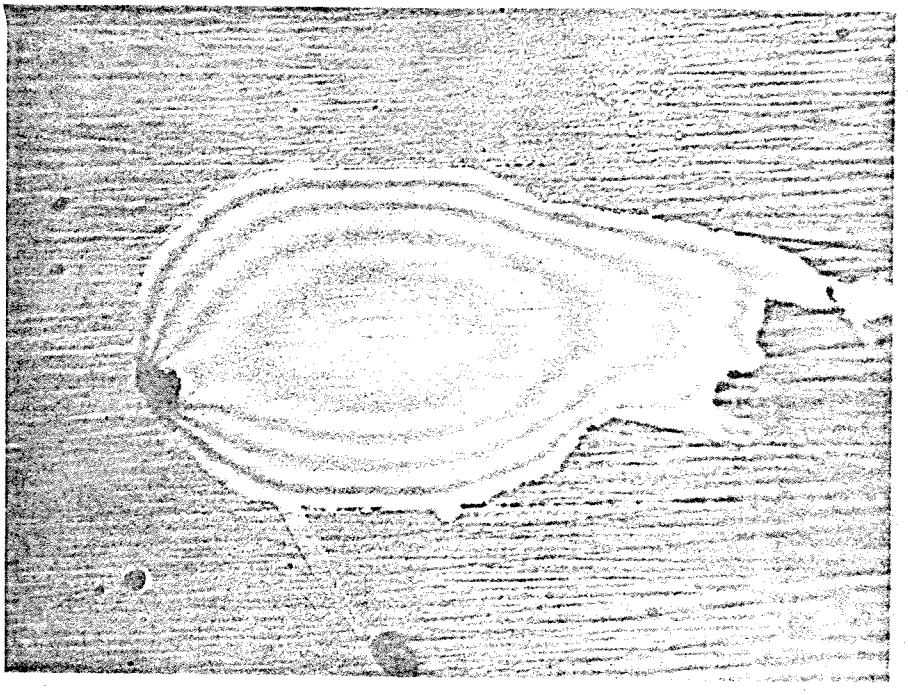

Figure 5-15(a)

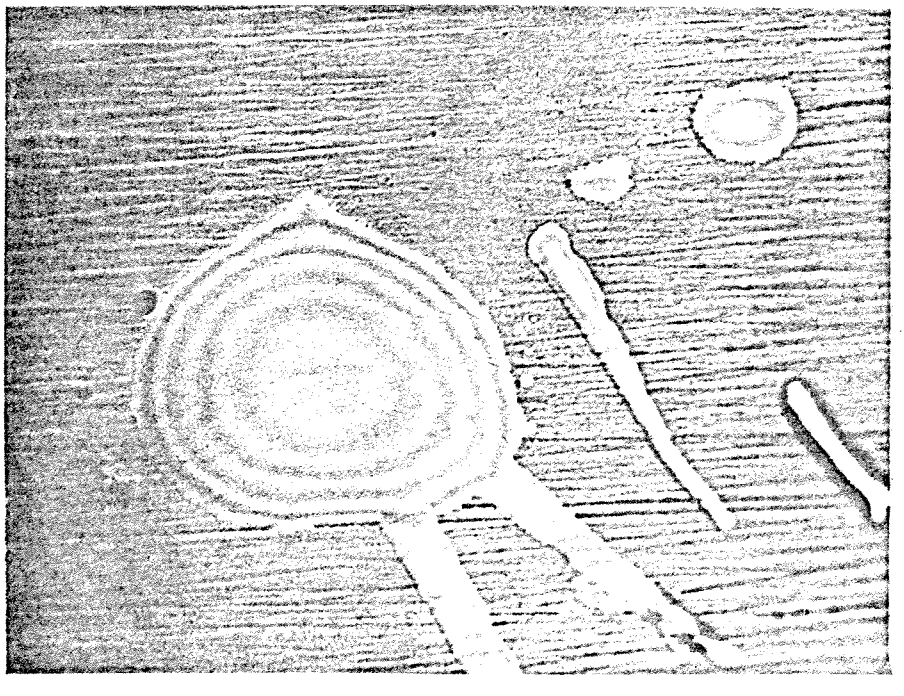

Figure 5-15(b)

Figure 5-16. Two SEM photographs of the general area shown in Figure 5-15. A number of blisters are seen. These are much larger than seen in the heavily irradiated regions (background of Figure 5-14 photographs) and range up to 50 μm or more in diameter. They are somewhat smaller than the objects seen in Figure 5-15, though. The lines running horizontally through each photograph are scratches from the polishing of the surface. It may be that the blisters seen here are fairly deep swellings of the surface, as the scratches appear to run directly through them. However, thin layers of material covering the scratches may not be visible in the SEM. The annular appearance of the feature in photograph (b) is probably caused by several blisters in close proximity to each other.

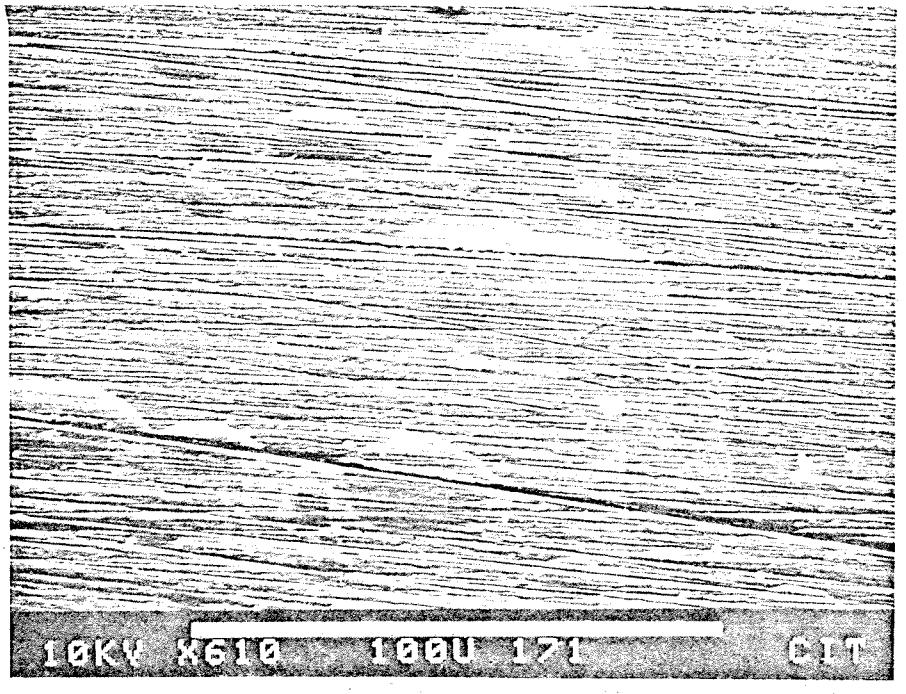

Figure 5-16(a)

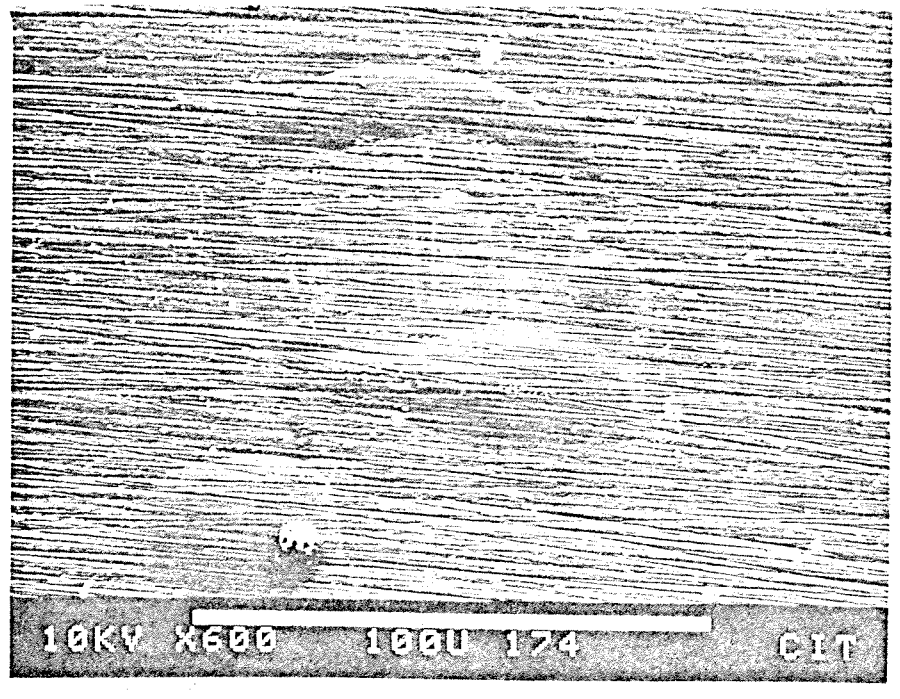

Figure 5-16(b)

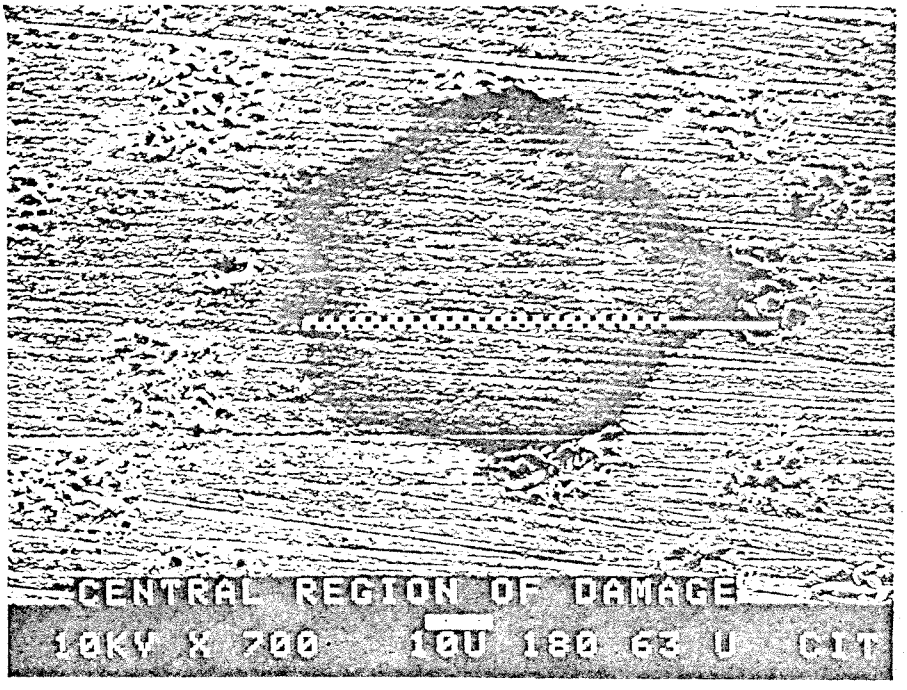

Figure 5-17. The large dark area seen in this SEM photograph of the Fluorite-1 crystal has been proven to be an artifact caused by contamination of the surface after ion bombardment. It may be the result of a small water droplet condensing on this hygroscopic surface. A similar feature is seen at the top of Figure 5-14(a). Also seen here are many small collections of objects similar to those shown in Figure 5-14(c). These were observed throughout the heavily bombarded area of the target.

Figure 5-18. Regions of the Fluorite-1 irradiated surface which were extremely unstable under electron bombardment in the SEM. These areas were observed outside of the area which was heavily irradiated by the nitrogen beam. Comparison of the areas around the edges of photograph (a) with the background in Figure 5-14(a) (also taken at 600 X) shows an absence of the small blisters in this region of the target. Photographs (a) and (b) were taken of the same area, (a) being photographed a few minutes before (b). The blister expanded radially, and left a very bumpy surface in its wake. Photograph (b) was taken at a somewhat lower magnification, accommodating the expanded size of the blister. The unstable nature of the surface was not observed in this one case only, but was seen throughout this region of the target. In the text, the possibility is proposed that significant quantities of the implanted nitrogen were transported out of the heavily irradiated region to peripheral areas and formed thin, unstable pockets of gas. These photographs may be of such pockets of implanted nitrogen.

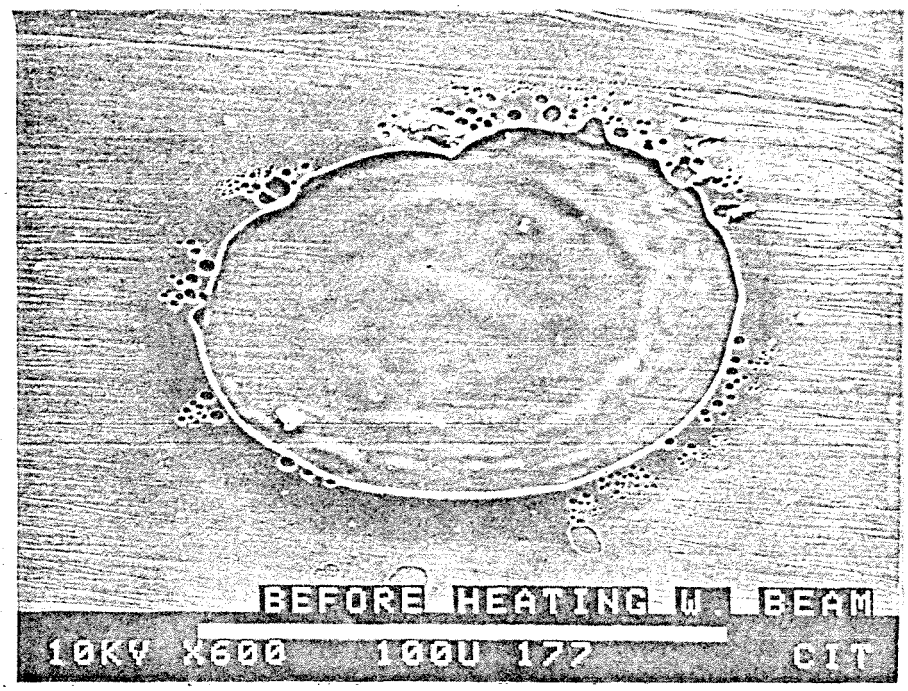

Figure 5-18(a)

Figure 5-18(b)

Figure 5-19. These two SEM photographs of the polycrystalline fluorite target demonstrate the apparent spatial inhomogeneity of the nitrogen ion beam. The white area running diagonally through the center of photograph (a) is seen at higher magnification in (b). Here are seen many objects which appear to be blister fragments, possibly of local origin. It cannot be ruled out that they have been transported from another location on the target, though. The use of extensive video processing to obtain photograph (b) has made it difficult to tell whether these objects are resting on the surface, or are a part of it. The light gray areas seen in the upper and lower left corners of (a) show no structure up to a magnification of 50,000 X. They may be artifacts similar to that seen in Figure 5-17.

Figure 5-19(a)

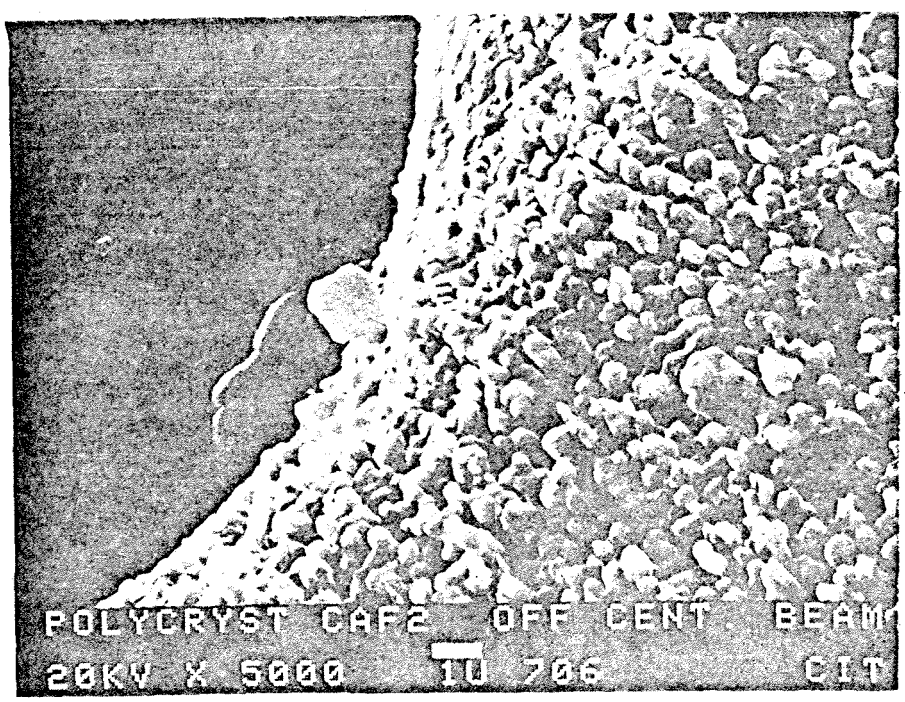

Figure 5-19(b)

Figure 5-20. Fractionation of sputtered calcium as calculated by two models of mixing of unfractionated material into the surface region. The target is treated as containing only calcium isotopes ^{40}Ca and ^{44}Ca. In each case, the relative probability for the sputtering of these isotopes is assumed to be $(44/40)^{1/4} = 1.024$. As material is sputtered, the surface region is restored to its original concentration of atoms by the addition of unfractionated material from an infinite reservoir. This replenishment is carried out continuously on an atom-by-atom basis in one case (solid line), but only whenever the surface concentration falls to half of its original value in the other case (dotted line). The continuous replenishment case is closely similar to that considered by Haff (1977) except that the fractionation of the sputtered material is used, rather than that of the material remaining in the surface layer. The fractionation calculated is analogous to that which would be observed in an experiment with a finite collection interval; it is the net fractionation of all the material sputtered from time zero to a final time T. This is plotted here as a function of T. In this graph it may be seen that both mixing cases give closely similar results which decrease monotonically to $\delta = 0$ for large values of T. Scaling of the abscissa times is done by using equations given by Haff (1977); the time it takes to sputter a given fraction of the surface layer is related to the sputtering yield, beam current, target density, and thickness (Δx) of the surface layer. The abscissa was scaled here according to typical parameters for the present experiments. The time to sputter material to a depth of Δx is here about 400 sec for $\Delta x = 1$ monolayer. Both with and without continuous

mixing, appreciable positive fractionation is observed when T is less than $\sim$1600 sec, the time required to sputter four monolayers. For larger values of T, the integrated fractionation becomes very small. The actual experiments sputtered many more monolayers worth of material, but still led to very large initial positive fractionation. This suggests that either these models or the assumed fractionation factor are inapplicable, or that the mixing depth Δx was appreciably larger.

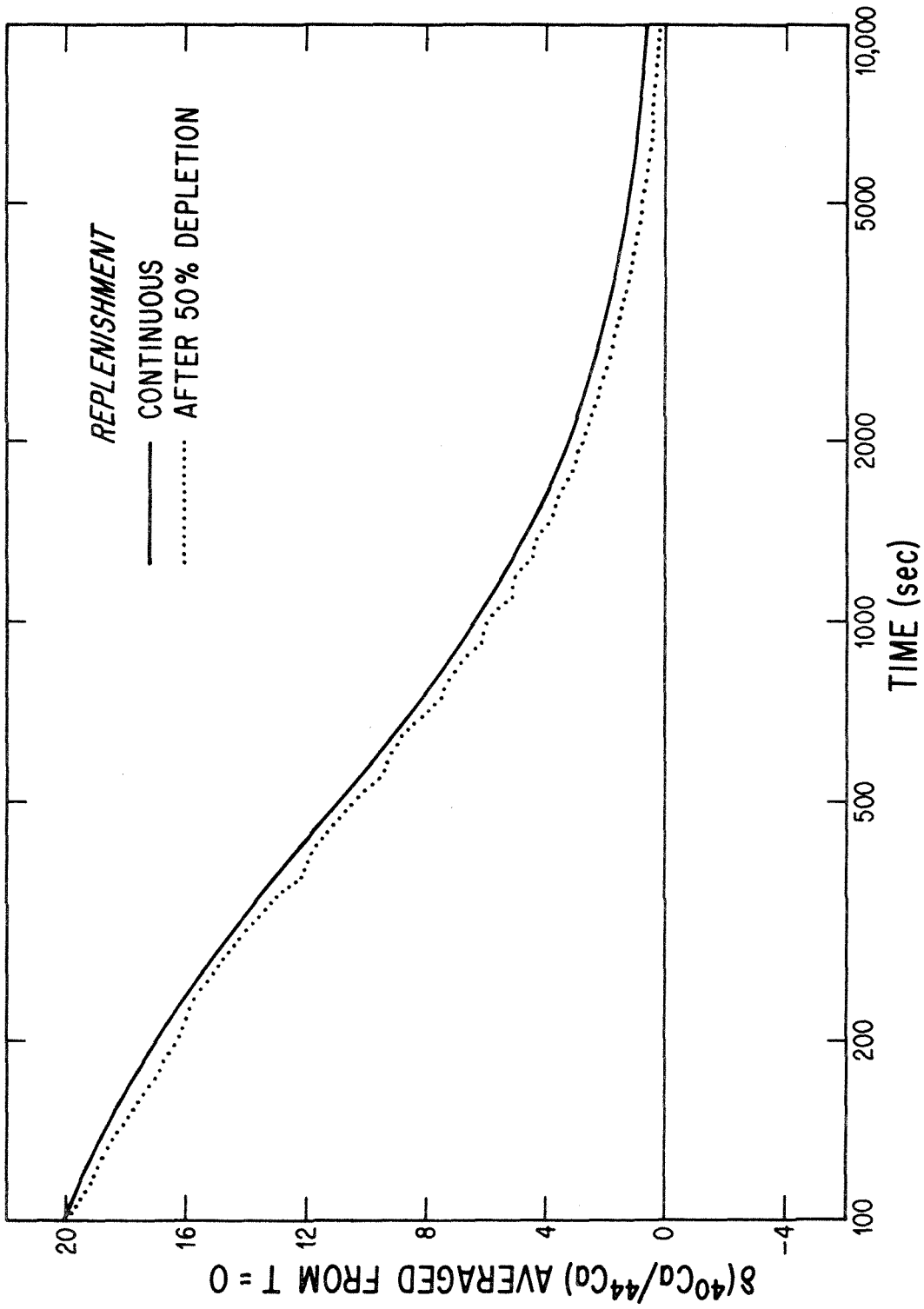
REPLENISHMENT
CONTINUOUS
AFTER 50% DEPLETION
δ(40Ca/44Ca) AVERAGED FROM T = 0
20
16
12
8
4
0
-4
100
200
500
1000
2000
5000
10,000
TIME (sec)

Figure 5-20

Figure 5-21. This graph is useful for finding the fraction of sputtered material which is ejected between the two angles θ_1 and θ_2. It is assumed that $\cos^{\nu}\theta$ angular distributions apply, even though Figure 5-7 indicates that this may not be the case. Zero degrees is defined as ejection perpendicular to the target. To find the fraction of material sputtered, for example, between 20° and 30° with a $\cos^{\frac{1}{4}}\theta$ distribution, simply subtract the two appropriate ordinate values: 0.38 - 0.26 = 0.12, or 12% of all material sputtered.

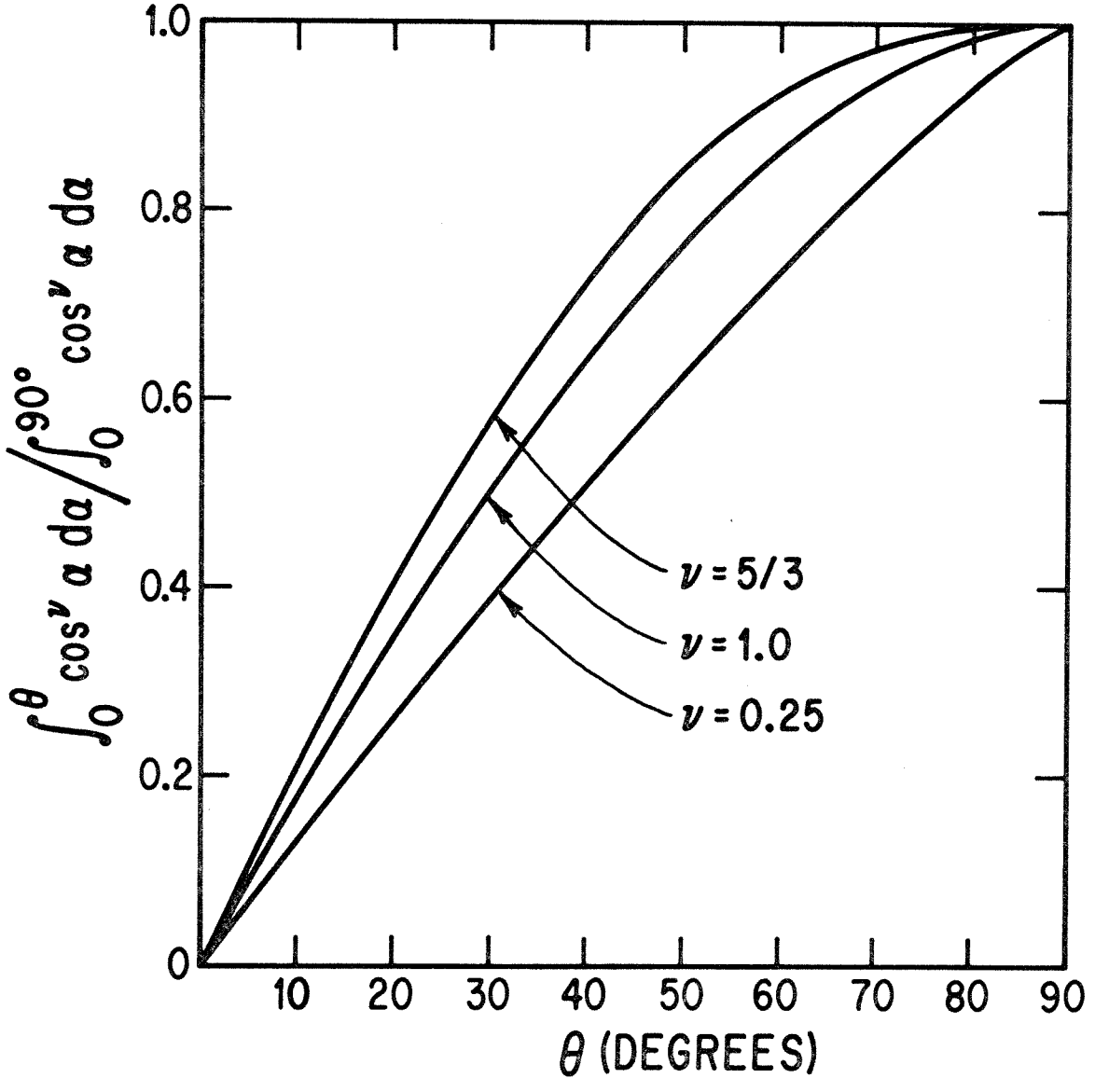
1.0
0.8
0.6
0.4
0.2
0
10
20
30
40
50
60
70
80
90
θ (DEGREES)
$\int_0^\theta \cos^\nu \alpha\, d\alpha / \int_0^{90°} \cos^\nu \alpha\, d\alpha$
ν = 5/3
ν = 1.0
ν = 0.25

Figure 5-21

APPENDIX A. PRELIMINARY SPUTTERING EXPERIMENTS

SiO SPUTTERING

The first attempts to simulate sputtering by the solar wind consisted of the sputtering of 400 $\mu g/cm^2$ evaporated SiO targets using a 40 keV $^{40}Ar^+$ beam. It was desirable to use a binary compound containing Si and O so that isotope data could be obtained for both elements using the techniques employed by Epstein and Taylor (1971) in their lunar sample measurements. SiO was chosen because thick films which adhered to stainless steel substrates without peeling could readily be vacuum evaporated. The main difficulty with this experiment was that large quantities ($\lesssim$ 400 μg) of SiO were required for the O isotope analysis. Without having very large targets, it is not possible to arrange for a large percentage of the SiO remaining on the substrate (the SiO to be isotopically analyzed) to have been close enough to the film surface to be strongly influenced by the sputtering. For example, if a one ion-beam-range film thickness of 100 Å (2 $\mu g/cm^2$) is to be left after sputtering, a sputtered surface area of 200 cm^2 must be produced.

In the experiments actually run, a 0.3 cm^2 area was sputtered. Table A-1 gives the $\delta^{18}O$ results for two sputtered SiO samples, each of which had been evaporated at the same time in a 2×10^{-5} Torr vacuum. Half of each sample was masked from the $^{40}Ar^+$ beam in order to provide non-sputtered controls. The two halves were cut apart after the sputtering and analyzed separately. The minute oxygen gas volumes evolved from each of these samples may have caused some analytical difficulties, resulting in a degradation of normally quite high (0.1‰) precision

attainable for O isotope analyses. This may have contributed at least partially to the observation that the two control samples, which had presumably been identical, had $\delta^{18}O$ values differing by 7‰ (Table A-1). There is an indication of an effect for sample III-2, with the sputtered sample being 14‰ heavier than the control. However, it was decided to pursue other types of solar wind sputtering simulations since, for these O experiments (a) such a small percentage of the SiO remaining in these samples had been disturbed by the sputtering, (b) the large amounts of material required precluded analysis of the SiO sputtered from the target, and (c) the initial SiO results indicated some difficulty in adequately and reliably controlling the experiments.

EVAPORATED CaF_2 SPUTTERING

The difficulties related above with the use of gaseous species for sputtering isotopic fractionation measurements pointed to the need for using an element that could be analyzed in a mass spectrometer in solid form. In such cases where an element can be analyzed in solid form, samples containing orders of magnitude fewer atoms can be precisely measured. This simplifies the sputtering experiments enormously and also opens the way for analysis of the material sputtered off of the target. For these reasons and others listed in Chapter 1, it was decided to pursue fractionation experiments in which calcium, which can be analyzed on solid source mass spectrometers, would be one of the sputtered species.

In the preliminary experiments, thin films of CaF_2 were evaporated onto stainless steel backings. The use of thin films permits a large

fraction of the calcium remaining on the substrate after sputtering to have been within one ion-beam-range of the film surface during the sputtering and thus to have been closely associated with any isotopic fractionation which was occurring. This was important since the material remaining on the substrate after sputtering was that for which isotope analysis would be performed.

Accordingly, calcium fluoride from the same bottle as that used for making the CaF_2 Standard ($\delta \equiv 0$, see Chapter 3) was vacuum evaporated to a 20 $\mu g/cm^2$ thickness onto a series of stainless steel (SS304) strips 1/8" x 3-1/2". The 1/8" width of the strip was comparable to the expected sputtering beam diameter; one strip was mounted in a small ultra-high-vacuum chamber in a holder which permitted the strip to be moved through the beam so that the entire evaporated surface could be irradiated. A second strip or "foil" from the same CaF_2 evaporation batch was not sputtered, but was analyzed separately on the mass spectrometer in order to provide a control. Table A-2 shows that foils from the same evaporation batch have nearly identical δ values, but that these values may be far different from the $\delta = 0$ value of the CaF_2 used as source material for the evaporation. This large fractionation arises from the actual evaporation, and is analogous to the large variable fractionation observed in the ion sources of solid source mass spectrometers. The fact that constancy of δ within a single evaporation batch is observed indicates that the sputtering experiments were well-controlled; the large differences in δ between different batches were caused simply by differences in the intervals during the evaporation sequence during which the targets were unmasked and exposed to the evaporating calcium.

In the sputtering experiment, the evaporated CaF_2 was sputtered with a normally incident 40 keV $^{40}Ar^+$ beam. The range of these ions in CaF_2 is calculated to be 75 ± 80 Å. The measured beam current was 2.5 - 3 μA, but was considered to be overestimated by a factor of 2 - 5 because of current integration problems arising from the unshielded geometry used. The sputtering dose measured from the current integration was 4.6×10^{17} ^{40}Ar atoms, and so was probably about $0.9 - 2.3 \times 10^{17}$ (i.e. about $3 - 8 \times 10^{16}$ cm^{-2}). (The target was stepped through the beam in 1/8" increments.) During the sputtering, a vacuum chamber pressure of 6×10^{-7} Torr was maintained. The Ca remaining on the sputtered foil was subsequently washed off using 1N HNO_3. The experimental results are shown in Table A-3. From the evaporation chamber thickness monitor, the CaF_2 was evaporated to a thickness of 20 - 22 μg/cm^2, in excellent agreement with the value of 21 μg/cm^2 subsequently measured by isotope dilution. This indicates that the evaporated calcium was efficiently removed by the dilute acid washing technique used. Also, additional rinsings of the foils indicated that no further Ca above blank levels was removed. The difference, Δ, in δ values between the sputtered and control foils of 1.0‰ seems to be real and is in the direction expected for sputtering. (Preferential removal of the lighter isotopes would leave a target isotopically heavy, that is, with $\Delta(^{40}Ca/^{44}Ca) < 0$.)

However, it is not possible to use a material balance calculation to confidently determine from this the fractionation in the top 75 Å of the thin film remaining after the sputtering. This is because it is not known how deep into the film a fractionated layer might extend. In the present experiment, ∿ 55 Å was sputtered from the film which was

originally 660 Å thick. Assuming that depths greater than 75 Å have $\Delta = 0$, then the average $\Delta(^{40}Ca/^{44}Ca)$ of the top 75 Å would have been:

$$(-1‰) \quad x \quad (660 - 55)/75 \quad = \quad -8‰ \qquad (A1)$$

At the time of this preliminary experiment, such a calculation could only provide a weak indication that a substantial fractionation might be present. Even with the results of Chapter 5 in hand, it seems unsafe to trust such a calculation to closer than a factor of 2 to 4 since thicknesses of such fractionated layers are not yet well characterized.

Although this first sputtering measurement gave an indication that some fractionation might indeed be caused by sputtering, this type of experiment was not considered to be the preferred way of attacking the problem; large fractions of the evaporated sample have to be sputtered off in order to obtain Δ values large enough to be demonstrably significant, thereby limiting careful investigation into the initial fractionation behavior. Additionally, this technique precludes the possibility of studying any variations of the fractionation of the sputtered calcium as a function of the angle of its ejection from the target. Material balance uncertainties also cause difficulties, interfering with the precise quantification of the results to a degree dependent on the thickness of the remaining film in relation to the unknown thickness of the fractionated layer. Because of these factors, subsequent experiments were designed to allow the fractionation of the calcium sputtered from targets to be measured, an approach which seems more direct with regard to the problem of whether isotopic fractionation accompanies sputtering. For future work aimed however at determining directly the thickness and

fractionation of isotopically heavy surficial layers, it might prove beneficial to run a series of carefully controlled, identical bombardment experiments on CaF_2 thin films of different thicknesses (perhaps 2 $\mu g/cm^2$ to 20 $\mu g/cm^2$ if argon beams are used).

Table A-1. Sputtering of SiO with 40 keV Ar^+

Sample[a]	Vacuum[b] (Torr)	SiO Removed[c] (%)	$\delta^{18}O$
III-1	$2x10^{-6}$	0.6	-30‰[d]
III-1 control	$2x10^{-6}$	0	-30‰
III-2	$3x10^{-6}$	1.2	-23‰[d]
III-2 control	$3x10^{-6}$	0	-37‰

[a] The two samples were evaporated simultaneously with nearly identical geometries with respect to the evaporation boat.

[b] Sputtering chamber vacuum with beam on target.

[c] Estimated percentage of the SiO removed by the Ar sputtering. Estimate used a sputtering yield of S = 3.0 calculated from Sigmund theory.

[d] $\delta^{18}O$ relative to SMOW of the SiO film remaining after sputtering.

Table A-2. Vacuum evaporation of CaF_2 Standard onto foils

Sample	$\left(^{40}Ca/^{44}Ca\right)_C$ [a]	$\delta\left(^{40}Ca/^{44}Ca\right)$
Batch-A[b]		
Foil-1	46.822±4	-7.0±0.1
Foil-2	46.834±4	-6.8±0.1
Batch-B[b]		
Foil 1	47.363±4	+4.5±0.1
Foil-2	47.364±4	+4.5±0.1

[a] Corrected for instrumental mass fractionation. The errors correspond to the last figures shown and are $2\sigma_{mean}$.

[b] Foils in each batch were adjacent, with nearly identical geometries with respect to the evaporation cell.

Table A-3. Sputtering of Evaporated CaF_2 with 40 keV Ar^+

Sample	Ion Range (Å)	Beam Current (μA)	Sample Area (cm^2)	# Ranges Sputtered	S_{Ca}[a]	$\delta(^{40}Ca/^{44}Ca)$
Sputtered Foil	75±80[b]	0.5-1.5[c]	2.8	0.75[d]	0.3-0.8	1.2±0.2[e]
Control Foil	-	-	2.8	-	-	2.2±0.1

[a]Ratio of number of Ca atoms sputtered to number of incident Ar atoms.

[b]Estimated from LSS theory (Lindhard et al., 1963; Schiøtt, 1966).

[c]Apparent current of 3μA corrected by estimated factor of 2-5 to account for secondary electron escape from target.

[d]Computed from comparison of Ca amounts on each target foil, as measured by isotope dilution.

[e]Value for Ca left on target after sputtering.

APPENDIX B. BINDING ENERGY DIFFERENCES OF CALCIUM ISOTOPES IN CALCIUM FLUORIDE

The Sigmund (1969) sputtering yield formula, eq. 4 in Chapter 5, predicts that the yields are inversely proportional to the surface binding energy. It is natural then to inquire into what differences might exist in the surface binding energies of different isotopes of an element. Such differences, if large enough, could cause in part any isotopic fractionation occurring during sputtering. In this appendix, an estimate will be presented which shows that isotopic binding energy differences of calcium in the ionically-bound fluorite lattice are but a negligible fraction of the binding energy. In order to address the problem, certain simplifying assumptions are made. The estimate will be of the difference in binding energies within the lattice rather than at the surface. It is considered reasonable to assume that if significant differences exist at the surface, they will be also present in the lattice interior. (Jackson [1972] provides a discussion about handling problems where surface potential energies are to be calculated.) Secondly, the lattice will be treated as if it is at 0°K so that only the zero point vibrational states are populated. The energy of this zero point motion above the bottom of the interatomic potential, computed and then approximated with a parabolic fit, will then be found for different isotope masses. This will lead directly to the binding energy differences. In computing the interatomic potential,

the zero point motion of all lattice atoms will be ignored. Since zero point vibrations are of very small amplitude, this is a satisfactory assumption.

The calculation of the interatomic potential near a Ca lattice site will now be described. This potential consists of two parts: the Coulomb interactions between the Ca cation, which has charge +2, and the other lattice ions: the other Ca cations and the charge -1 fluorines. To this will be added a Born repulsion energy (which arises from the Pauli exclusion principle) between the Ca cation and its eight nearest neighbors, which are fluorine anions. The next nearest neighbors, 12 calcium cations, are far enough away that the decaying exponential form of the Born potential (cf. Kittel, 1971) yields a negligible contribution to the potential energy.

In computing the Coulomb potential at positions slightly removed from the mean calcium position, one proceeds in a fashion analogous to that used in computing the Coulomb (Madelung) contribution to the cohesive energy of a crystal. It is well known that the series of Coulomb terms between a fixed lattice site and all others is very slowly convergent. Evjen (1932) described a method which is equivalent to rearranging the terms of this conditionally convergent series into a quickly converging one. His method may be used in the present calculation. To do this, the Coulomb energy will be computed numerically between the 126 nearest neighbors and the calcium atom at the origin of a cartesian coordinate system. These 126 lattice sites are those in the eight face-centered cubic

fluorite cells nearest the origin. Now, following the Evjen method, all atoms in the interior of this large cube (whose dimensions are 2 cell-lengths on a side) have their normal +2 or -1 charges. Those on the boundary of the cube, all of which are calcium atoms, are considered to have fractional charges: +2/8 for those on the 8 corners, +2/4 for those 12 on the edges, and +2/2 for those 30 on the cube faces. This yields a net charge for the cube of zero (including the cation at the origin). A feeling for the general magnitude of the accuracy of this calculation comes from evaluating the Madelung constant α, that is, the Coulomb potential at the origin per unit charge, as expressed in units of elementary charge e = 1 and lattice spacing $a_o = 1$. The result is $\alpha = 10.668$, which is 8% lower than the true value $\alpha = 11.637$.

The calculation of the Born contribution to the total potential energy assumes the commonly used form

$$B \exp(-r/\rho) \qquad \text{(B1)}$$

where r is the distance between the two atoms and B and ρ are parameters. Appropriate values for B and ρ are found during cohesive energy calculations from elastic constant data. For CaF_2, Reitz et al. (1961) give

$$B = 3.09 \times 10^{-9} \text{ erg}$$

$$\rho = 0.28 \text{ Å}$$

The total Born potential energy is then taken in the present

calculation to be the sum of the eight terms of the form of eq. B1 arising from the interaction of the eight F anions nearest to the Ca cation vibrating about the origin. Since the Ca cation at the origin has charge +2, the Coulomb potential energy is multiplied by 2 before being added to the Born energy to find the total potential energy.

The potential energy change away from that at the origin is not independent of direction. Hence, for this calculation, the variations were computed in two directions, one along the line between the origin and one of the nearest F anions, and the other along the line between the origin and one of the nearest Ca cations. These will be referred to as Case (a) and Case (b), respectively. The total potential U is tabulated in Table B-1. For each case, this may be fit quite well by a quadratic, although a better fit can be obtained with a power slightly greater than 2. The results are

$$\begin{aligned} \Delta U &= \frac{1}{2}\, 11.96\ r^2 \quad -- \quad \text{Case (a)} \\ \Delta U &= \frac{1}{2}\, 11.83\ r^2 \quad -- \quad \text{Case (b)} \end{aligned} \tag{B2}$$

where ΔU is measured in eV and r, the magnitude of the displacement from the origin, in Å. Here ΔU is defined as the change in potential at r away from the value at the origin, and is given in the last column of Table B-1.

The constants in equations B2 are quite close to each other. Therefore, take their average as the restoring force constant:

$$K = 11.90 \text{ eV } \text{Å}^{-2} = 1.91 \times 10^{5} \text{ erg cm}^{-2} \qquad \text{(B3)}$$

The zero point energy for ^{40}Ca is then

$$3/2\ \hbar\sqrt{K/(40 \times 1.66 \times 10^{-24} \text{ gm})} = 8.43 \times 10^{-14} \text{ erg}$$

$$= 0.053 \text{ eV} \qquad \text{(B4)}$$

Therefore the ratio of the volume binding energies of ^{40}Ca and ^{44}Ca is

$$\frac{U(r=0) + 0.053}{U(r=0) + 0.053\ \sqrt{40/44}} = 1 - 4.7 \times 10^{-5} \qquad \text{(B5)}$$

This calculation indicates that one can only expect a few parts in 10^5 fractionation to occur during sputtering because of binding energy differences. If one wishes to approximately account for the effect of the surface, the value U(r=0) = -53.053 eV used above can be divided by two, thus yielding a fractionation of 9.3 parts in 10^5, still a very small number. The difference between room temperature and 0°K is insufficient to greatly alter these results by diminishing still further the isotopic differences. This is because the first vibrational state has an energy $3\hbar\omega = 0.11$ eV, which is greater than $kT \approx 1/40$ eV.

The value for the zero point energy found in eq. B4 can be used to find the mean vibrational amplitude of the Ca atom at 0°K. Setting

$$\frac{1}{2}\ 0.053\ \text{eV} = \frac{1}{2}\ K\ r^2$$

implies r = 0.067 Å, where r is the mean amplitude. The 1/2 on the left side of the above equation comes from the virial theorem.

In closing, it should be noted that Hamza and Broecker (1974) found oxygen isotopic fractionation between the surfaces and interiors of naturally or artifically grown calcite, dolomite, and witherite crystals. The fewer contributions to the interatomic potential at a free surface increases the lattice spacing (D.L. Goodstein, personal communication) and lowers the frequencies of some or all of the vibrational modes (cf. Hamza and Broecker, 1974). The alteration in the normal mode frequencies altered the isotopic exchange constant between the surface of the calcite and the CO_2 gas used in the experimental procedure, causing fractionation with respect to the isotopic values obtained when measuring the bulk. This is a different phenomenon than that discussed in this appendix, being one related to equilibrium isotopic exchange chemical reactions. The data of Hamza and Broecker therefore provide no reason for suspecting that the calculation of volume binding energies led to an erroneous conclusion about surface binding energies. Equations B4 and B5 indicate that the force constant K would have to be about two orders of magnitude larger before per mil effects could be obtained.

Table B-1. CaF_2 Interatomic Potential

Case[a]	Displacement[b] (r/a_o)	Coulomb Energy(eV)[c]	Born Energy(eV)	Total Potential(eV)	Change in Potential(eV)
a	0	-56.479	3.426	-53.053	≡ 0
	$0.02\sqrt{3}$	-56.480	3.629	-52.851	0.202
	$0.04\sqrt{3}$	-56.494	4.326	-52.168	0.885
	$0.06\sqrt{3}$	-56.562	5.819	-50.743	2.310
	$0.08\sqrt{3}$	-56.763	8.800	-47.963	5.090
	$0.10\sqrt{3}$	-57.240	14.694	-42.546	10.507
b	0	-56.479	3.426	-53.053	≡ 0
	$0.02\sqrt{2}$	-56.479	3.559	-52.920	0.133
	$0.04\sqrt{2}$	-56.481	3.982	-52.499	0.554
	$0.06\sqrt{2}$	-56.489	4.760	-51.729	1.324
	$0.08\sqrt{2}$	-56.506	5.991	-50.515	2.538
	$0.10\sqrt{2}$	-56.530	7.792	-48.738	4.315
	$0.12\sqrt{2}$	-56.545	10.256	-46.289	6.764

[a] See text.

[b] Lattice constant a_o = 5.46 Å.

[c] Coulomb potential per unit charge, multiplied by two since the charge at the origin is +2.

REFERENCES

AIP (American Institute of Physics) Handbook, 3rd edition (1972). D.E. Gray, ed. New York: McGraw-Hill Book Company.

Andersen H.H. (1974) High-energy sputtering. Proc. Seventh Yugoslav Symp. Phys. Ionized Gases, V. Vujnovic, ed., p. 361-426. University of Zagreb, Yugoslavia.

Andersen H.H. and Bay H.L. (1973) Sputtering-yield studies on silicon and silver targets. Radiat. Eff. 19, 139-146.

Andersen H.H. and Bay H.L. (1975) Heavy-ion sputtering yields of gold: Further evidence of nonlinear effects. J. Appl. Phys. 46, 2416-2422.

Andersen N. and Sigmund P. (1974) Energy dissipation by heavy ions in compound targets. Kgl. Danske Videnskab. Selskab, Mat.-Fys. Medd. 39, no. 3.

Arai O., Kobayashi K., Shimamura T. and Tazawa Y. (1976) Variations of isotopic ratios on ion sputtered magnesium. Japan. J. Appl. Phys. 15, 407-408.

Barnes I.L., Garner E.L., Gramlich J.W., Machlan L.A., Moody J.R., Moore L.J., Murphy T.J., and Shields W.R. (1973) Isotopic abundance ratios and concentrations of selected elements in some Apollo 15 and Apollo 16 samples. Proc. Fourth Lunar Sci. Conf., Geochim. Cosmochim. Acta Suppl. 4, 1197-1207. Pergamon Press.

Behrisch R. (1972) First-wall erosion in fusion reactors (review paper). Nucl. Fusion 12, 695-713.

Bibring J.P. Personal communication. Present address: Kellogg Radiation Laboratory, California Institute of Technology.

Bibring J.P., Langevin Y., Maurette M., Meunier R., Jouffrey B., and Jouret C. (1974) Ion implantation effects in "cosmic" dust grains. Earth Planet. Sci. Lett. 22, 205-214.

Bøttiger J., Davies J.A., Sigmund P., and Winterbon K.B. (1971) On the reflection coefficient of keV heavy-ion beams from solid targets. Radiat. Eff. 11, 69-78.

Bøttiger J. and Winterbon K.B. (1973) Reflection of light ions from solid surfaces. Radiat. Eff. 20, 65-67.

Braun P. and Färber W. (1975a) AES studies of surface composition of Ag-Cu alloys. Surface Sci. 47, 57-63.

Braun P. and Färber W. (1975b) Reply to comments on "AES studies of surface composition of Ag-Cu alloys." Surface Sci. 51, 342-343.

Campisano S.U., Foti G. and Rimini E. (1975) Kinetics of phase formation in Au-Al thin films. Phil. Mag. 31, 903-917.

Carslaw H.S. and Jaeger J.C. (1959) Conduction of Heat in Solids, 2nd ed. Oxford University Press.

Chapman G.E., Farmery B.W., Thompson M.W., and Wilson I.H. (1972) The energy distribution of sputtered atoms from gold. Radiat. Eff. 13, 121-129.

Church S.E., Tilton G.R., and Wright J.E. (1976) Volatile element depletion and $^{39}K/^{41}K$ fractionation in lunar soils. Proc. Seventh Lunar Sci. Conf., Geochim. Cosmochim. Acta Suppl. 7, 423-439. Pergamon Press.

Clayton R.N., Mayeda T.K., and Hurd J.M. (1974) Loss of oxygen, silicon, sulfur, and potassium from the lunar regolith. Proc. Fifth Lunar Sci. Conf., Geochim. Cosmochim. Acta Suppl. 5, 1801-1809. Pergamon Press.

Cottrell T.L. (1954) The Strengths of Chemical Bonds. New York: Academic Press.

CRC Handbook of Chemistry and Physics, 53rd edition (1972). R.C. Weast, ed. Cleveland: The Chemical Rubber Company Press.

Epstein S. and Taylor H.P., Jr. (1971) O^{18}/O^{16}, Si^{30}/Si^{28}, D/H, and C^{13}/C^{12} ratios in lunar samples. Proc. Second Lunar Sci. Conf., Geochim. Cosmochim. Acta Suppl. 2, 1421-1441. M.I.T. Press.

Epstein S. and Taylor H.P., Jr. (1972) O^{18}/O^{16}, Si^{30}/Si^{28}, C^{13}/C^{12}, and D/H studies of Apollo 14 and 15 samples. Proc. Third Lunar Sci. Conf., Geochim. Cosmochim. Acta Suppl. 3, 1429-1454. Pergamon Press.

Epstein S. and Taylor H.P., Jr. (1974) Oxygen, silicon, carbon, and hydrogen isotope fractionation processes in lunar surface materials (abstract). Lunar Science V, 212-214. Houston: The Lunar Science Institute.

Epstein S. and Taylor H.P., Jr. (1975) Investigation of the carbon, hydrogen, oxygen, and silicon isotope and concentration relationships on the grain surfaces of a variety of lunar soils and in some Apollo 15 and 16 core samples. Proc. Sixth Lunar Sci. Conf., Geochim. Cosmochim. Acta Suppl. 6, 1771-1798. Pergamon Press.

Erents K. and McCracken G.M. (1969) Trapping and re-emission of fast deuterium ions from nickel. Brit. J. Appl. Phys. (J. Phys. D) 2, 1397-1405.

Erents S.K. and McCracken G.M. (1973) Blistering of molybdenum under helium ion bombardment. Radiat. Eff. 18, 191-198.

Evjen H.M. (1932) On the stability of certain heteropolar crystals. Phys. Rev. 39, 675-687.

Fluitt J.M., Friedman L., Boerboom A.J.H. and Kistemaker J. (1961) Isotopic fractionation of lithium in sputtering. J. Chem. Phys. 35, 1143-1144.

Frocht M.M. (1951) Strength of Materials. New York: Ronald Press.

Garner E.L., Machlan L.A., and Barnes I.L. (1975) The isotopic composition of lithium, potassium, and rubidium in some Apollo 11, 12, 14, 15, and 16 samples. Proc. Sixth Lunar Sci. Conf., Geochim. Cosmochim. Acta Suppl. 6, 1845-1855. Pergamon Press.

Geiss J., Eberhardt P., Bühler F., Meister J. and Signer P. (1970) Apollo 11 and 12 solar wind composition experiments: fluxes of He and Ne isotopes. J. Geophys. Res., Space Phys. 75, 5972-5979.

Goodstein D.L. Personal communication. Present address: Sloan Laboratory, California Institute of Technology.

Gregg R. (1977) Sputtering of uranium. Ph.D. Thesis, California Institute of Technology, Pasadena.

Griffith J.E., Weller R.A. and Tombrello T.A. (1978) Trapping efficiency for sputtered uranium atoms on aluminum oxide. Bull. Am. Phys. Soc. 23, 32-33.

Gschneider K.A., Jr. (1964) Physical properties and interrelationships of metallic and semimetallic elements. Solid State Phys. 16, 275-426.

Haff P.K. (1977) A model for surface layer composition changes in sputtered alloys and compounds. Appl. Phys. Lett. 31, 259-260.

Haff P.K., Switkowski Z.E., Burnett D.S., and Tombrello T.A. (1977a) Gravitational and recoil contributions to surface mass fractionation by solar wind sputtering. Proc. Eighth Lunar Sci. Conf., Geochim. Cosmochim. Acta Suppl. 8, 3807-3815. Pergamon Press.

Haff P.K., Switkowski Z.E. and Tombrello T.A. (1977b) Ion-beam-induced atomic mixing. J. Appl. Phys. 48, 3383-3386.

Hamza M.S. and Broecker W.S. (1974) Surface effect on the isotopic fractionation between CO_2 and some carbonate minerals. Geochim. Cosmochim. Acta 38, 669-681.

Heumann K.G. and Lieser K.H. (1973) Untersuchung von Isotopenfeinvariationen des Calcium in der Natur an rezenten Carbonaten und Sulfaten. Geochim. Cosmochim. Acta 37, 1463-1471.

Hirt B. and Epstein S. (1964) A search for isotopic variations in some terrestrial and meteoritic calcium. Trans. Am. Geophys. Union 45, 113.

Housley R.M. and Grant R.W. (1977) An XPS (ESCA) study of lunar surface alteration profiles. Proc. Eighth Lunar Sci. Conf., Geochim. Cosmochim. Acta Suppl. 8, 3885-3899. Pergamon Press.

Hurkmans A., Overbosch E.G., Olander D.R., and Los J. (1976a) The trapping of potassium atoms by a polycrystalline tungsten surface as a function of energy and angle of incidence. Surface Sci. 54, 154-168.

Hurkmans A., Overbosch E.G. and Los J. (1976b) Trapping probabilities and desorption energies of alkali atoms on a clean and an oxygen covered tungsten (110) surface. Surface Sci. 59, 488-508.

Jackson D.P. (1972) Approximation of lattice sums of exponential interatomic potentials near crystal surfaces. J. Chem. Phys. 56, 3178-3180.

Kittel C. (1971) Introduction to Solid State Physics, 4th edition. New York: John Wiley & Sons.

Kobayashi K., Arai O. and Shimamura T. (1975) An ion counting method with multichannel pulse height analyser for high sensitive mass spectrometry. Japan. J. Appl. Phys. 14, 1361-1370.

Kornelsen E.V., Brown F., Davies J.A., Domeij B., and Piercy G.R. (1964) Penetration of heavy ions of keV energies into monocrystalline tungsten. Phys. Rev. 136, A849-A858.

Lee T., Papanastassiou D.A. and Wasserburg G.J. (1977) Mg and Ca isotopic study of individual microscopic crystals from the Allende meteorite by the direct loading technique. Geochim. Cosmochim. Acta 41, 1473-1485.

Lee T., Papanastassiou D.A. and Wasserburg G.J. (1978) Calcium isotopic anomalies in the Allende meteorite. Ap. J. 220, no. 1, part 2, p. L21-L25.

Liau Z.L., Brown W.L., Homer R. and Poate J.M. (1977) Surface layer composition changes in sputtered alloys and compounds. Appl. Phys. Lett. 30, 626-628.

Lindhard J. (1965) Influence of crystal lattice on motion of energetic charged particles. Kgl. Dnaske Videnskab. Selskab, Mat.-Fys. Medd. 34, no. 14.

Lindhard J., Scharff M. and Schiøtt H.E. (1963) Range concepts and heavy ion ranges. Kgl. Danske Videnskab. Selskab, Mat.-Fys. Medd. 33, no. 14.

Maurette M. Unpublished results presented at a Kellogg Radiation Laboratory seminar, California Institute of Technology, July, 1978.

Mitchell J.B., Davies J.A., Howe L.M., Walker R.S., Winterbon K.B., Foti G. and Moore J.A. (1975) The use of molecular ions for implantation studies in Si and Ge. Proc. Fourth Intern. Conf. on Ion Implantation in Semiconductors and Other Materials, S. Namba, ed. Plenum Press.

Oechsner H. (1975) Sputtering — a review of some recent experimental and theoretical aspects. Appl. Phys. 8, 185-198.

Olson R.R. and Wehner G.K. (1977) Composition variations as a function of ejection angle in sputtering of alloys. J. Vac. Sci. Technol. 14, 319-321.

Patterson H. and Tomlin D.H. (1962) Experiments by radioactive tracer methods on sputtering by rare-gas ions. Proc. Roy. Soc. 265, 474-488.

Poate J.M. and Tisone T.C. (1974) Kinetics and mechanism of platinum silicide formation on silicon. Appl. Phys. Lett. 24, 391-393.

Rees C.E. and Thode H.G. (1972) Sulfur concentrations and isotope ratios in lunar samples. Proc. Third Lunar Sci. Conf., Geochim. Cosmochim. Acta Suppl. 3, 1479-1485. Pergamon Press.

Rees C.E. and Thode H.G. (1974) Sulfur concentrations and isotope ratios in Apollo 16 and 17 samples. Proc. Fifth Lunar Sci. Conf., Geochim. Cosmochim. Acta Suppl. 5, 1963-1973. Pergamon Press.

Reitz J.R., Seitz R.N. and Genberg R.W. (1961) Closed-shell ion-ion interactions in calcium fluoride. J. Phys. Chem. Solids 19, 73-78.

Robbins D.E., Hundhausen A.J. and Bame S.J. (1970) Helium in the solar wind. J. Geophys. Res., Space Phys. 75, 1178-1187.

Samsonov G.V., ed. (1968) Handbook of Physicochemical Properties of the Elements. Translated from the Russian. New York: IFI/Plenum Data Corp.

Schiøtt H. (1966) Range-energy relations for low-energy ions. Kgl. Danske Videnskab. Selskab, Mat.-Fys. Medd. 35, no. 9.

Schneider E., Storzer D., Hartung J.B., Fechtig H. and Gentner W. (1973) Microcraters on Apollo 15 and 16 samples and corresponding cosmic dust fluxes. Proc. Fourth Lunar Sci. Conf., Geochim. Cosmochim. Acta Suppl. 4, 3277-3290. Pergamon Press.

Sigmund P. (1969) Theory of sputtering. I. Sputtering yield of amorphous and polycrystalline targets. Phys. Rev. 184, 383-416.

Silsbee R.H. (1957) Focussing in collision problems in solids. J. Appl. Phys. 28, 1246-1250.

Switkowski Z.E., Haff P.K., Tombrello T.A. and Burnett D.S. (1977) Mass fractionation of the lunar surface by solar wind sputtering. J. Geophys. Res. 82, 3797-3804.

Taylor H.P., Jr. and Epstein S. (1973) O^{18}/O^{16} and Si^{30}/Si^{28} studies of some Apollo 15, 16, and 17 samples. Proc. Fourth Lunar Sci. Conf., Geochim. Cosmochim. Acta Suppl. 4, 1657-1679. Pergamon Press.

Taylor S.R. (1975) Lunar Science: A Post-Apollo View. Oxford: Pergamon Press.

Thode H.G. and Rees C.E. (1971) Measurement of sulphur concentrations and the isotope ratios $^{33}S/^{32}S$, $^{34}S/^{32}S$, and $^{36}S/^{32}S$ in Apollo 12 samples. Earth Planet. Sci. Lett. 12, 434-438.

Thode H.G. and Rees C.E. (1976) Sulphur isotopes in grain size fractions of lunar soils. Proc. Seventh Lunar Sci. Conf., Geochim. Cosmochim. Acta Suppl. 7, 459-468. Pergamon Press.

Townsend P.D., Kelly J.C. and Hartley N.E.W. (1976) Ion Implantation, Sputtering, and Their Applications. New York: Academic Press.

Van Vliet D. (1973) The continuum model of directional effects. Channelling: Theory, Observation and Applications, D.V. Morgan, ed., p. 37-78. New York: John Wiley & Sons.

Wada Y., Usui H. and Ashikawa M. (1975) Substrate temperature measurement during ion implantation. Japan. J. Appl. Phys. 14, 1351-1356.

Wasserburg G.J., Papanastassiou D.A., Nenow E.V. and Bauman C.A. (1969) A programmable magnetic field mass spectrometer with on-line data processing. Rev. Sci. Instrum. 40, 288-295.

Watson, Charles. Personal communication. Present address: Wright Nuclear Structure Laboratory, Yale University.

Wehner G.K. (1955) Sputtering of metal single crystals by ion bombardment. J. Appl. Phys. 26, 1056-1057.

Wehner G.K. (1977) Isotope enrichment in sputter deposits. Appl. Phys. Lett. 30, 185-187.

Wehner G.K., Olson R.R. and King M.E. (1977) Composition and isotope variations in sputtering as a function of the ejection angle. Proc. Seventh Intern. Vac. Congr. & Third Intern. Conf. Solid Surfaces, p. 1461-1463.

Wehner G.K. and Rosenberg D. (1960) Angular distribution of sputtered material. J. Appl. Phys. 31, 177-179.

Weller M.R. Personal communication. Present address: Kellogg Radiation Laboratory, California Institute of Technology.

Weller R.A. (1978) The energy spectra of uranium atoms sputtered from uranium metal and uranium dioxide targets. Ph.D. Thesis, California Institute of Technology, Pasadena.

Weller R.A. Personal communication. Present address: Kellogg Radiation Laboratory, California Institute of Technology.

Winterbon K.B. (1972) Heavy-ion range profiles and associated damage distributions. Radiat. Eff. 13, 215-226.

Winterbon K.B., Sigmund P. and Sanders J.B. (1970) Spatial distribution of energy deposited by atomic particles in elastic collisions. Kgl. Danske Videnskab. Selskab, Mat.-Fys. Medd. 37, no. 14.